

Alkali Metal Aluminate Chemistry: Advances in Hydroelementation Catalysis

Victoria Alison Pollard

Department of Pure and Applied Chemistry

University of Strathclyde

A thesis submitted to the Department of Pure and Applied Chemistry, University of Strathclyde, in part fulfilment of the requirements for a degree of *Doctor of Philosophy*

2019

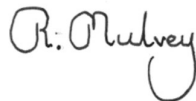
This thesis incorporates published work which is the result of the author's original research. It has been composed by the author and has not been previously submitted for examination which has led to the award of a degree.

Signed (Author):



Date: 25th March 2019

Signed (Supervisor)*:



Date: 25th March 2019

*Confirming the author was primarily responsible for the composition of the published material within the thesis.

Dedicated to my mother and father:

Joan and Nigel

Acknowledgements

Undertaking a PhD is by no means a one-person act. The work reported in this thesis would not have been possible without the support, encouragement and friendship of many people, from around the globe. I would like to take this opportunity to thank those who have helped, encouraged and supported me, in any way, throughout the past three and half years.

Firstly, I must acknowledge my PhD supervisor, Prof. Robert Mulvey, for allowing me the opportunity to be a part of his research team. His project ideas, support, help and guidance have been instrumental to the successes of this project and invaluable to my time at Strathclyde. Thank you for trusting me to represent the group at the various conferences I have had the privilege of attending. Furthermore, I must also thank the other inorganic academics, Prof. Eva Hevia, Dr Charlie O'Hara and Dr Stuart Robertson for all their great suggestions during group meetings and ready availability to discuss anything chemistry. A special thank you to Dr Alan Kennedy for all his time and patience spent fixing up my X-ray structures. Thanks to Dr Chris Dodds for allowing me the opportunity to demonstrate in the inorganic teaching labs, and for always having a supportive word to say when things weren't going as planned in my research. Much of the work in this thesis would not have been possible without Craig Irving. Thank you for your friendship over the past three years, all the pieces of cake you kept for me, and teaching (and trusting!) me to fix problems with the NMR machines. Finally, thank you to Janie-Anne for all the help and glassware, and for ensuring the smooth running of the lab day-to-day.

It is not my intention to omit anyone from these acknowledgements, so I would like to take this opportunity to collectively thank all the members of the Mulvey/Hevia/O'Hara/Robertson research groups between 2015 – 2019: Alberto, Ana, Andy, Antonio, Callum, Etienne, Laia, Leonie, Lewis, Marco, Marina, Michael F., Michael W., Pasquale, Richard, Ross, Sam, Scott, and Stephen. Whether it was Friday group lunches; group trips to Largs/Rothesay; attending the WestCHEM ball; that one time we all went subcrawling; Michael's birthday trip paintballing; sitting to eat lunch together; or even just a Friday pint in the Ark, you guys made the PhD all the more enjoyable and I incredibly am grateful to you all for your friendship. I must thank Dr Ross McLellan for his friendship and for always being willing to answer any question I had – I am sorry for all the weekend texts when I was at X-ray! The work in this thesis was helped enormously by the knowledge and

insight that Ross offered me, and I am grateful to have had the opportunity to work alongside such a talented chemist and fellow cat-lover! Thank you to Laia and Lewis for allowing me to join in their yoga trips. Thank you to Sonia for all the advice during the writing of this thesis and for becoming a good friend. Thank you to Etienne, Andy, Richard, Callum and Stephen for always having the ability to make me laugh, even on the days when I just wanted to cry! During my time at Strathclyde we have had many visiting scholars and it has been a privilege to work with so many different people. In particular, I would like to acknowledge Katharina, who became my Iceland trip buddy, along with Jana. Lastly I would like to acknowledge my fellow 2015 PhD-start, Michael F. I couldn't have imagined a better person to travel this PhD journey alongside. Thank you for helping me get around campus when I first started and for becoming a good friend as the years have passed. Thank you for all the help with running columns and GC-MS. I will never forget the day you told me about your pet chickens! Through all the ups and downs it has been comforting to know I wasn't in this alone!

A huge thank you to my family: my mother, Joan; father, Nigel; and sister, Karen, for their unwavering support and encouragement throughout this PhD. This PhD would not have been possible without all three of you. From sitting with me every night to teach me to read "*Toe by Toe*" when school couldn't; to buying our first computer so I could learn to touch-type; to trailing around behind me every Easter at the Edinburgh International Science Festival – I am incredibly grateful for everything you have ever done for me, and everything you have sacrificed for me. It is a debt I will never be able to repay but I hope the dedication in this thesis goes some way to doing so. Karen, I promise we will get our Sri Lankan holiday together. Thank you all for everything.

Thank you to my partner, David, for coping with me while I perused this PhD. David has been my rock over the past six years and I could not have got to the end of this PhD without him by my side. He saw first-hand all the ups and downs, shared my joys when things were going well, and dealt with all the tears and stresses when chemistry was not going my way. Thank you for always being willing to discuss chemistry with me, and for finding the positives when I couldn't see them. Thank you for your moral support; all the cups of tea you made, and glasses of wine and gin you poured to get me through the writing of this thesis. Finally, thank you to Max for all the help trying to write this thesis, even although you have worse spelling than I do(!); and to both Max and Erwin for providing comic relief over the past three years.

August 2016



November 2018



Abstract

Applying main group compounds, especially aluminium hydride complexes, as catalysts for hydroelementation reactions is gaining momentum. This project develops the application of heterobimetallic lithium aluminates to the catalytic regime. Five lithium aluminates of general formula $(\text{HMDS})_2\text{Al}(\text{H})_2\text{Li}(\text{donor})_x$, **1 – 6**, were prepared and characterised by X-ray crystallography and multinuclear NMR spectroscopy. Subsequently, **1 – 6** were applied as catalysts for hydroboration of aldehydes and ketones. An alkali metal effect was observed upon changing the donor at lithium, indicating that lithium plays a role in catalysis. A catalytic cycle is proposed whereby the carbonyl substrate is initially hydroaluminated; then the boronic ester product forms, with regeneration of the lithium aluminium hydride complex. A postulated intermediate, $(\text{HMDS})_2\text{Al}(\mu\text{-OCH}_2\text{Ph})_2\text{Li}(\text{THF})_2$, **8**, was isolated and characterised.

A comparative study between charged bimetallic lithium aluminate complexes and neutral monometallic aluminium counterparts was undertaken. Lithium aluminates were generally observed to exhibit superior catalytic reactivity for hydroboration of aldehydes, ketones, imines and alkynes. A novel catalyst initiation pathway was uncovered for pre-catalyst $i\text{Bu}_2\text{Al}(\text{TMP})$ *via* β -hydride transfer from *iso*-butyl ligands, generating the characterised aluminium benzyloxide complex, $[(\text{TMP})\{\text{Ph}_2(\text{H})\text{CO}\}\text{Al}\{\mu\text{-OC}(\text{H})\text{Ph}_2\}]_2$, **15**.

The reactivity of aluminium compounds towards boranes was examined, to try to uncover potential aluminium catalyst decomposition pathways. Novel structures were crystallographically characterised resulting from cleavage of a B – O bond in pinacolborane resulting in a new aluminium complex. Less active catalytically than the parent aluminium complex, this represents a possible catalyst decomposition product.

Finally, the concept of lithium aluminate hydroelementation catalysis was extended to hydrophosphination, representing the first reported example of aluminium catalysed hydrophosphination of alkynes, alkenes and carbodiimides. The active catalyst, lithium aluminium phosphide, $i\text{Bu}_3\text{AlPPh}_2\text{Li}(\text{THF})_3$, **22**, was successfully isolated. Analysis of the reaction mechanism by kinetic studies shows that this reaction is inhibited by excess phosphine. Moreover, postulated intermediates were identified *via* stoichiometric reactions, and their reactivity probed, further supporting the mechanism proposed.

Peer Reviewed Publications

- “*Lithium diamidodihydridoaluminates: bimetallic cooperativity in catalytic hydroboration and metalation applications*” – V. A. Pollard, S. A. Orr, R. McLellan, A. R. Kennedy, E. Hevia, R. E. Mulvey, *Chemical Communications*, 2018, **54**, 1233 – 1236
- “*Comparing neutral (monometallic) and anionic (bimetallic) aluminium complexes in hydroboration catalysis: influences of lithium cooperation and ligand set*” – V. A. Pollard, M. Á. Fuentes, A. R. Kennedy, R. McLellan, R. E. Mulvey, *Angewandte Chemie International Edition*, 2018, **57**, 10651 – 10655

Conference Presentations

Oral presentations:

- V. A. Pollard, R. E. Mulvey; *“Heteroleptic lithium aluminium hydrides: synthesis, characterisation and applications.”* Universities of Scotland Inorganic Chemistry Conference 2017 (USIC-51), University of St Andrews, St Andrews, 29 – 30th August **2017**.

Poster presentations:

- V. A. Pollard, M. A. Fuentes, A. R. Kennedy, R. McLellan, R. E. Mulvey; *“Comparing anionic and neutral organoaluminium catalysts for hydroboration reactions.”* University of Strathclyde Doctoral School Launch Event, University of Strathclyde, Glasgow, 5th October **2018**.
- V. A. Pollard, M. A. Fuentes, A. R. Kennedy, R. McLellan, R. E. Mulvey; *“Comparing anionic and neutral organoaluminium catalysts for hydroboration reactions.”* Universities of Scotland Inorganic Chemistry Conference 2018 (USIC-52), University of Edinburgh, Edinburgh, 3 – 4th September **2018**. **Prize Awarded**
- V. A. Pollard, E. Hevia, A. R. Kennedy, R. McLellan, R. E. Mulvey, S. A. Orr; *“It’s AI in the design: heteroleptic aluminium amides as homogenous catalysts for hydroboration.”* RSC Dalton Division Joint Interest Group Meeting 2018, University of Warwick, 3rd – 5th April **2018**.
- V. A. Pollard, S. A. Orr, R. McLellan, A. R. Kennedy, E. Hevia, R. E. Mulvey; *“New lithium aluminium hydride complexes: synthesis, structural characterisation and applications in catalysis.”* Anglo-German Inorganic Chemistry Conference (AGICHEM 2017), Goettingen, Germany, 6 – 9th August **2017**.
- V. A. Pollard, M. A. Fuentes, A. R. Kennedy, E. Hevia, R. E. Mulvey; *“Reaction of nitriles with an aluminium/carbene frustrated Lewis pair.”* Universities of Scotland Inorganic Chemistry Conference 2016 (USIC-50), University of Strathclyde, Glasgow, 11 – 12th August **2016**. **Prize Awarded**

Abbreviations

12-crown-4	1,4,7,10-tetraoxacyclododecane
15-crown-5	1,4,7,10,13-pentaoxacyclopentadecane
9-BBN	9-borabicyclo[3.3.1]nonane
AMMM	Alkali metal mediated <i>metalation</i>
Ar	Generic aryl group
B ₂ pin ₂	Bis(pinacolato)borane
B ₂ pin ₃	2,2'-[1,4-butanediylbis(oxy)]bis[4,4,5,5-tetramethyl-1,3,2-dioxaborolane]
bar	Bar (unit of pressure, 1 bar = 0.987 atm)
Bn	Benzyl group
Bz	Benzoyl group
Et	Ethyl group
EuChemS	European Chemical Society
CIP	Contacted ion pair
Cp	Cyclopentadienyl
Cp*	Pentamethylcyclopentadienyl
Cp ^{3t}	1,3,5-tri- <i>tert</i> -butylcyclopentadienyl
Cy	Cyclohexyl group
d ₈ -toluene	Deuterated toluene
DABCO	1,4-diazabicyclo[2.2.2]octane
DG	Directing group

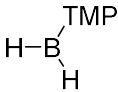
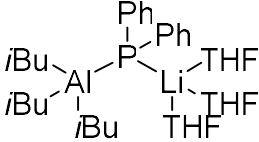
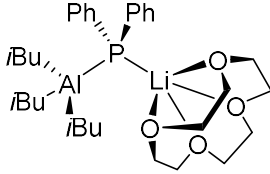
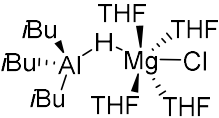
DIBAL	Diisobutylaluminium hydride
DIPP	2,6-diisopropyl phenyl group
DFT	Density functional theory
DMP	Dimethylpiperidide
DoM	Directed <i>ortho</i> metalation
DOSY	Diffusion ordered NMR spectroscopy
dppe	Diphenylphosphino ethane
FLP	Frustrated Lewis pair
HBpin	Pinacolborane (4,4,5,5-tetramethyl-1,3,2-dioxaborolane)
HBcat	Catecholborane
HMDS / HMDS(H)	1,1,1,3,3,3-hexamethyldisilazide / 1,1,1,3,3,3-hexamethyldisilazane
HOMO	Highest Occupied Molecular Orbital
<i>i</i> Bu	<i>Iso</i> -butyl group
<i>i</i> Pr	<i>Iso</i> -propyl group
IR	Infra-red
K	Kelvin
KIE	Kinetic Isotope Effect
LUMO	Lowest Unoccupied Molecular Orbital
Me	Methyl group
Me ₆ TREN	Tris[2-(dimethylamino)ethyl]amine
Mes	Mesityl group; 1,3,5-trimethylphenyl
MPV	Meerwein-Ponndorf-Verley
Nacnac	β -diketiminato ligand

<i>n</i> Bu	<i>n</i> -butyl group
<i>n</i> BuLi	<i>n</i> -butyl lithium
NMR	Nuclear Magnetic Resonance
	s – singlet
	d – doublet
	br – broad
	m – multiplet
	quat. – quaternary carbon
OTf	Triflate group; (O ₂ (CF ₃)SO ⁻)
Ph	Phenyl group
ppm	Parts per million
PMDETA	<i>N,N,N',N'',N'''</i> -pentamethyldiethylenetriamine
R	Generic alkyl group
RT	Room temperature
SSIP	Solvent separated ion pair
<i>t</i> Bu	<i>Tertiary</i> -butyl group
THF	Tetrahydrofuran
TMEDA	<i>N,N,N',N'</i> -tetramethylethylenediamine
TMP / TMP(H)	2,2,6,6-tetramethylpiperidide / 2,2,6,6-tetramethylpiperidine
TMS	Trimethylsilane
TOF	Turnover frequencies
VTNA	Variable Time Normalisation Analysis
X	Halide

Table of Numbered Compounds

No.	Compound	No.	Compound
1		2	
3		4	
5		6	
7		8	
9		10	

No.	Compound	No.	Compound
11		12	
13		14	
15		16	
17		18	
19		20	

No.	Compound	No.	Compound
21a	 $\begin{array}{c} \text{TMP} \\ \\ \text{H}-\text{B} \\ \\ \text{H} \end{array}$	22	 $\begin{array}{c} \text{Ph} \quad \text{Ph} \\ \quad \\ \text{iBu}-\text{Al}-\text{P}-\text{Li} \\ \quad \quad \quad \\ \text{iBu} \quad \text{iBu} \quad \text{THF} \quad \text{THF} \\ \\ \text{THF} \end{array}$
23	LiPPh_2	24	iBu_3Al
25	$\text{iBu}_2\text{AlPPh}_2$	26	 $\begin{array}{c} \text{Ph} \quad \text{Ph} \\ \quad \\ \text{iBu}-\text{Al}-\text{P}-\text{Li} \\ \quad \quad \\ \text{iBu} \quad \text{iBu} \quad \text{Crown Ether} \end{array}$
27	 $\begin{array}{c} \text{iBu} \quad \text{THF} \quad \text{THF} \\ \quad \quad \\ \text{iBu}-\text{Al}-\text{H}-\text{Mg}-\text{Cl} \\ \quad \quad \\ \text{iBu} \quad \text{THF} \quad \text{THF} \end{array}$		

Contents

Acknowledgements	IV
Abstract	VII
Peer Reviewed Publications	VIII
Conference Presentations	IX
Abbreviations	X
Table of Numbered Compounds	XIII
Contents	XVI
Chapter 1: Introduction	1
1.1 Aluminium Chemistry	1
1.1.1 Properties of Aluminium.....	1
1.1.2 Fundamental chemistry of organoaluminium compounds	3
1.1.3 Synthesis, structure and reactivity of Al(I) compounds	5
1.1.4 ²⁷ Al NMR spectroscopy.....	10
1.2 Main group catalysis	11
1.2.1 Broad overview of main group catalysis	11
1.2.2 Homogeneous aluminium catalysis	15
1.3 Synergic main group chemistry.....	24
1.3.1 Development of heterobimetallic metallating agents.....	24
1.3.2 Synergistic reactivity of alkali metal aluminates.....	30
1.4 Overall Aims of the PhD Project.....	34
Chapter 2: Lithium diamidodihydrido aluminates: bimetallic cooperativity in catalytic hydroboration and metallation applications	36
2.1 Abstract	37
2.2 Introduction	37
2.2.1 Hydroboration.....	37
2.2.2 Catalytic examples of hydroboration.....	39
2.2.3 Hydroboration of carbonyls	40
2.3 Project Aims	41
2.4 Introduction from the Manuscript.....	42
2.5 Results and Discussion	43

2.6 Extended Discussion	51
2.6.1 Structure activity relationships for catalytic competence	51
2.6.2 Related unpublished work	58
2.7 Conclusions	60
Chapter 3: Comparing Neutral (Monometallic) and Anionic (Bimetallic) Aluminium Complexes in Hydroboration Catalysis: Influences of Lithium Cooperation and Ligand Set	61
3.1 Abstract	62
3.2 Introduction	62
3.2.1 Hydroboration of more challenging substrates: Imines, and C – C unsaturated bonds	62
3.2.2 Bimetallic systems in catalysis	66
3.3 Project Aims	68
3.4 Introduction from the Manuscript.....	68
3.5 Results and Discussion	71
3.6 Extended Discussion and Future Work	78
3.6.1 Solid state and solution phase structures of 11 , 14 and synthesis of compound 17	78
3.6.2 Hydroboration of imines and acetylenes.....	83
3.6.3 Related unpublished work and future work	86
3.7 Conclusions	88
Chapter 4: Decomposition Studies in Aluminium Catalysed Hydroboration Reactions	90
4.1 Abstract	91
4.2 Introduction	91
4.3 Project Aims	96
4.4 Results and Discussion	97
4.5 Extended Discussion and Future Work	106
4.5.1 Solution phase studies of compounds 19 , and 20	106
4.5.2 Insight into the composition of compound 21b	108
4.5.3 Presence of aluminium borohydride compounds in hydroboration catalysis.....	110
4.6 Conclusions	112
Chapter 5: Lithium Aluminate Catalysed Hydrophosphination	114
5.1 Abstract	115
5.2 Introduction	115
5.2.1 Hydrophosphination	115

5.2.2 Metal-catalysed examples of hydrophosphination	116
5.3 Project Aims	121
5.4 Introduction from the Manuscript	121
5.5 Results and Discussion	123
5.6 Extended Discussion and Future Work	130
5.6.1 Extension to other substrates	130
5.6.2 Structure activity relationships	130
5.6.3 Elucidation of the reaction mechanism by kinetic studies	134
5.6 Conclusions	142
Chapter 6: Conclusions and Outlook	144
6.1 Conclusions	144
6.2 Outlook and Future Perspectives.....	146
Chapter 7: Experimental	151
7.1 General experimental techniques.....	151
7.1.1 Solvent and reagent purification	151
7.1.2 Analytical techniques	151
7.2: Experimental data for Chapter 2	153
7.3: Experimental data for Chapter 3	164
7.4: Experimental data for Chapter 4	171
7.5: Experimental data for Chapter 5	174
7.6: Experimental data for Chapter 6	186
7.7: Crystal structure data and refinement details for compounds reported in this thesis	187
References	193

Chapter 1: Introduction

1.1 Aluminium Chemistry

1.1.1 Properties of Aluminium

In 2019 the chemical community celebrates the “*International Year of the Periodic Table of Chemical Elements*” as designated by the United Nations, in recognition of 150 years of the current depiction of the periodic table, which was first introduced by Mendeleev in 1869.¹ The periodic table in Figure 1.1 was released by the European Chemical Society (EuChemS) to celebrate the occasion, which attempts to provide a visual representation of the natural abundances of the elements, and also highlight the elements at risk of running out.² From this periodic table it is clear to see the significantly greater natural abundance of aluminium in particular, but also many of the elements in group 1 and group 2, compared with many of the transition metals. It is this large natural abundance which attracts chemists to working with and developing the chemistry of aluminium. In fact, aluminium is the third most abundant element in the Earth’s crust, and the most prevalent metal in the Earth’s crust (8.3% by weight).^{3, 4}

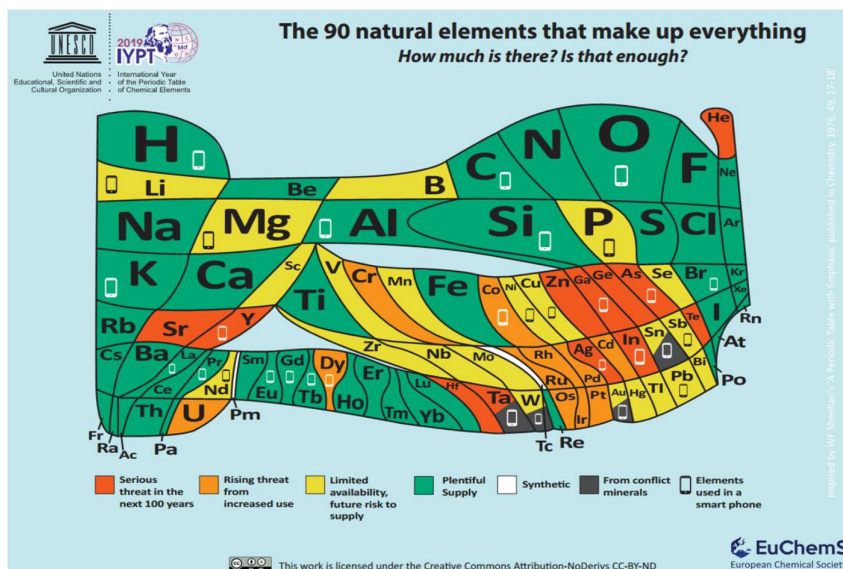


Figure 1.1: Alternative depiction of the periodic table, displaying natural abundance of the elements and highlighting those elements considered ‘endangered’.²

Aluminium is therefore inexpensive in comparison with transition metals, which makes the use of its compounds in stoichiometric or catalytic applications appealing. Indeed, aluminium compounds were among the first metal catalysts to be discovered and applied in synthetic chemistry.^{5,6} Examples include the use of aluminium halides as strong Lewis acid catalysts in Friedel Crafts acylation,⁷ and alkyl aluminium compounds as co-catalysts in the Nobel prize winning chemistry of Ziegler-Natta alkene polymerisation (*vide infra*).^{8,9} Today, a large proportion of the world’s polyolefins are still prepared *via* Ziegler-Natta polymerisation.¹⁰ Consequentially, organoaluminium compounds are prepared on a huge scale globally, with Me_3Al holding the record for the largest tonnage of any organometallic reagent.¹¹ Overlooked for decades in favour of the highly successful transition metals, the study and application of organoaluminium compounds is now, once again, thriving. Driven by curiosity as well as the need to supplement precious transition metals (Figure 1.1), the discovery of stable compounds containing Al – Al bonds, the synthesis of stable subvalent Al(I) compounds, and the application of organoaluminium compounds as catalysts for hydroelementation reactions are all areas where significant progress has been made, and undoubtedly there is much more development to come.^{5,6,11-18}

1.1.2 Fundamental chemistry of organoaluminium compounds

Alkylaluminium (empirically formulated as R_3Al , though R can be different ligands) compounds have a strong tendency to form dimeric units (R_6Al_2) in the solid state and solution phase (Figure 1.2). This results in a combination of bridging Al – R – Al bonds and terminal Al – R bonds. Terminal Al – R bonds can be successfully described by conventional bonding theory as 2-centre-2-electron bonds (covalent bonding though slightly polar, Pauling electronegativity (χ) Al: 1.61, C: 2.55).¹⁹⁻²¹ However, this leaves each aluminium centre with only one electron with which to bond to the bridging R groups, of which there are two. Rundle remarked that “*there is no such thing as electron deficient compounds, only theory deficient chemists*”, and as such a new theory was developed and implemented to explain this phenomenon.²² Originally proposed to explain the electron deficient bonding in borane chemistry, the concept of 3-centre-2-electron bonds can also be applied to these Al – R – Al bridges. These bridging bonds are weaker than the terminal Al – R bond and can be readily cleaved, for example in donor solvents such as THF Me_3Al exists as a monomer rather than dimer. The association of such R_3Al units to dimeric or higher aggregates (for example, trimeric) can be hindered by the use of bulky ‘R’ ligands. Cryoscopic molecular weight measurements and NMR spectroscopy have been used to suggest that *i*Bu₃Al exists as a trimeric species with a six-membered Al_3H_3 core.²³

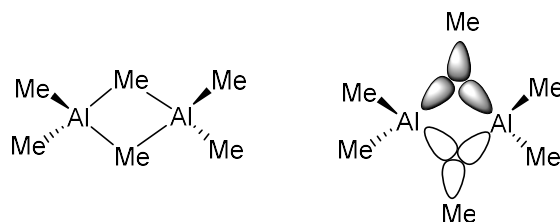
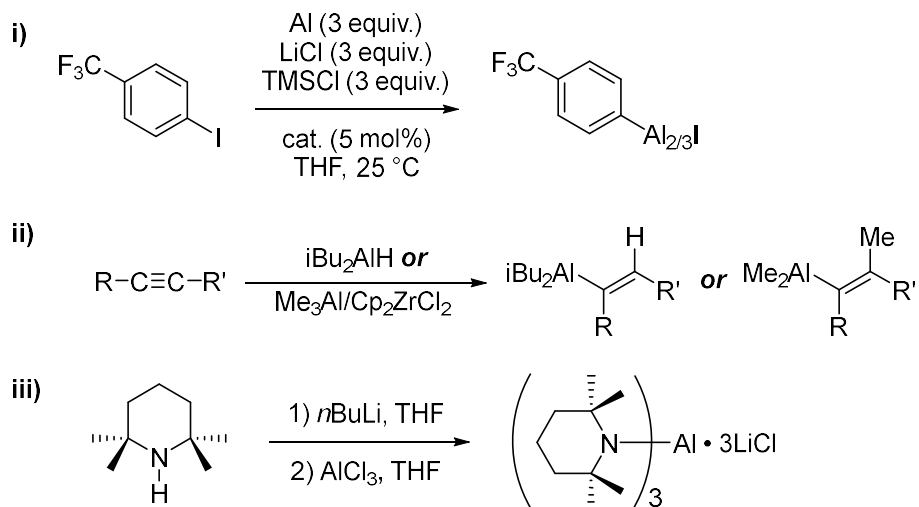


Figure 1.2: Molecular structure of crystalline dimeric Me_3Al depicting bonding model for 3-centre-2-electron bonding.

That the majority of routinely employed organoaluminium reagents (e.g., *i*Bu₃Al, Me_3Al , *i*Bu₂AlH) are commercially available is another reason why it is so desirable to use such aluminium reagents in synthesis. However, there are also numerous methods for the

preparation of organoaluminium compounds in the laboratory.²⁴ Three such methods discussed here are depicted in Scheme 1.1.

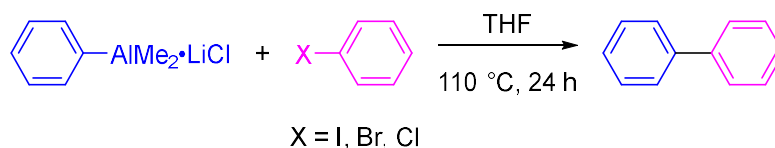


Scheme 1.1: Selection of common laboratory preparative routes to organoaluminium compounds.

Knochel has reported the direct insertion of aluminium powder into aryl halides in the presence of LiCl and catalytic amounts of selected metal chloride salts [Scheme 1.1; i)].²⁵ Surface activation of aluminium powder is required to remove the kinetically inactive oxide layer before any reaction can take place. Catalysts employed include TiCl_4 , BiCl_3 , InCl_3 and PbCl_2 . The arylaluminium reagents prepared by this oxidative addition of the metal exist in complex equilibria with many potential products, and as such the sesquihalide structure ($\text{Ar}_3\text{Al}_2\text{X}_3 = \text{ArAl}_{2/3}\text{X}$) is only one potential product. However, these new arylaluminium reagents have been shown to smoothly undergo palladium catalysed C – C cross couplings giving the desired product in good to excellent yields without an intermediary purification step. One of the most useful methods of forming new Al – C bonds is hydroalumination (or carboalumination), [Scheme 1.1 ii)].⁶ This method is used industrially for the synthesis of R_3Al from the corresponding α -alkene, powdered aluminium metal and H_2 gas. In the laboratory the reaction of alkynes with $i\text{Bu}_2\text{AlH}$ results in hydroalumination, whilst reaction with Me_3Al in the presence of Cp_2ZrCl_2 yields the carboalumination product (Cp = cyclopentadienyl).

Often the resulting alkenyl aluminium reagents can be used for onward cross coupling reactions.²⁶⁻²⁹ Hydroalumination reactions benefit from being stereoselective (*syn*-periplanar addition), and also can exhibit regioselectivity. Lastly, classical transmetallation reactions with more electropositive organometallics (typically, organolithium or organomagnesium reagents) leads to efficient salt metathesis reaction with aluminium halides (Scheme 1.1; iii)).³⁰ In non-polar solvents such as hexane this lithium-aluminium transmetallation reaction is driven by the formation and precipitation of LiCl salt and so purification by filtration is generally all that is required to obtain the pure organoaluminium product. This method, sometimes referred to as salt metathesis, is one of the most widely used methods for the preparation of new organoaluminium compounds.^{31, 32}

In 1976 Negishi reported the first application of organoaluminium compounds in nickel- or palladium-catalysed cross couplings with aryl halides or alkenyl halides.^{26, 27} In the past eight years, Nakamura has reported a Negishi cross-coupling variant using cheaper iron catalysts and arylaluminium reagents.^{33, 34} It was shown that the active aluminium reagent is an aluminium ate species (*vide infra*). Furthermore, Uchiyama has recently reported the direct cross-coupling using arylaluminium reagents and organic halides in the absence of an external catalyst (Scheme 1.2).³⁵ This system was tolerant of a wide range of functional groups situated on the aryl ring including ester, amide, tosylate, triflate and carbamate groups.



Scheme 1.2: Direct cross-coupling of a salt-supported arylaluminium compound with an aryl halide.

1.1.3 Synthesis, structure and reactivity of Al(I) compounds

In organoaluminium compounds, the aluminium centre most often exists in the +3 oxidation state. However, it is possible to obtain aluminium compounds in the +1 oxidation state, and

these compounds can exhibit interesting reactivity. $[\text{Cp}^*\text{Al}]_4$ was the first reported Al(I) compound which is stable at room temperature and could be characterised by X-ray diffraction crystallography (Figure 1.3) [Cp^* = pentamethylcyclopentadienyl].³⁶ Initially the reaction of AlCl and Cp^*_2Mg was used to generate $[\text{Cp}^*\text{Al}]_4$. However, formation of AlCl from elemental aluminium and HCl at 1200 K is challenging and so Roesky reported a more facile method. Thus, reaction of $[\text{Cp}^*\text{AlCl}_2]_2$ with elemental potassium in refluxing toluene generated $[\text{Cp}^*\text{Al}]_4$ in good yields.³⁷ In the crystal $[\text{Cp}^*\text{Al}]_4$ exists as a tetramer in which each aluminium centre occupies a tetrahedral site, bonding to three other aluminium atoms, and coordinating to the Cp^* ligand in an η^5 -fashion. The tetramer undergoes dissociation to the monomer, Cp^*Al , at high temperatures but the monomer cannot be isolated. Very recently the group of Braunschweig have reported the synthesis and isolation of the monomeric $\text{Cp}^{3t}\text{Al}(\text{I})$ (Cp^{3t} = 1,3,5-tri-*tert*-butylcyclopentadienyl), representing a landmark first example of a monomeric Cp-based Al(I) species to be isolated.³⁸

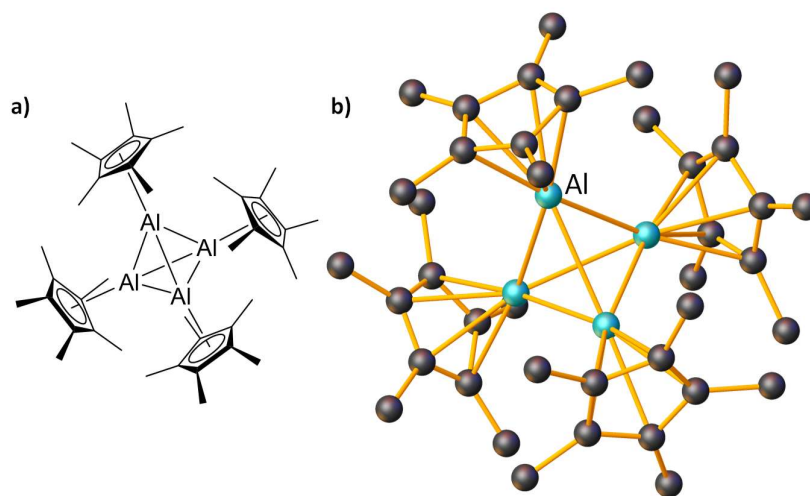
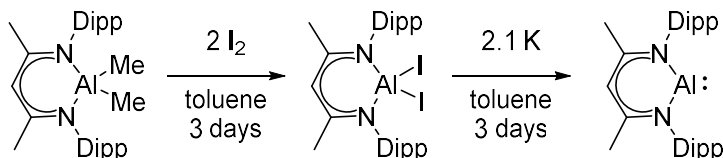


Figure 1.3: a) ChemDraw representation of $[\text{Cp}^*\text{Al}]_4$. b) tetrameric molecular structure of $[\text{Cp}^*\text{Al}]_4$, with hydrogen atoms omitted for clarity.

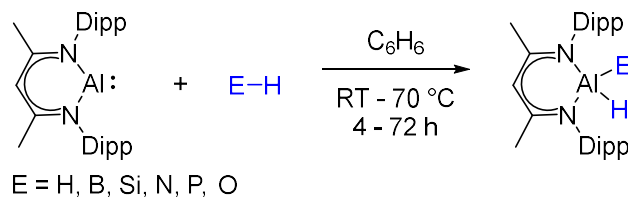
The application of more sterically demanding, chelating ligands has been used to impart kinetic stability to Al(I) compounds, thus facilitating their isolation. Roesky reported the first

example of a monomeric Al(I) compound which could be structurally characterised by X-ray crystallography, by employing a bulky β -diketiminato ligand [nacnac ligand] (Scheme 1.4).³⁹



Scheme 1.4: Synthesis of the monomeric Al(I) compound $^{\text{DIPP}}\text{nacnacAl(I)}$.

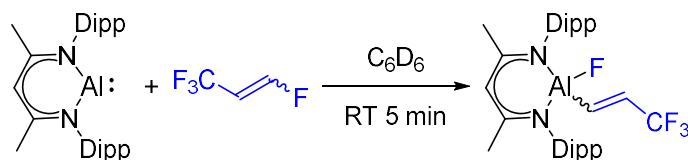
That $^{\text{DIPP}}\text{nacnacAl(I)}$ has an Al-located lone pair and accessible empty 3p orbital on aluminium makes it reminiscent of transition metal complexes (DIPP = 2,6-diisopropyl phenyl). Transition metal complexes make use of similar properties to undertake oxidative addition reactions, an important first step in many transition metal-catalysed reactions (*vide infra*). As a result of this observation, Nikonov employed the $^{\text{DIPP}}\text{nacnacAl(I)}$ compound in oxidative addition reactions of a range of E–H bonds (E = for example H, B, Si, N, P, or O) (Scheme 1.5). In all cases the Al(III) product was characterised using X-ray crystallographic studies.



Scheme 1.5: Oxidative addition of E–H bonds to $^{\text{DIPP}}\text{nacnacAl(I)}$.

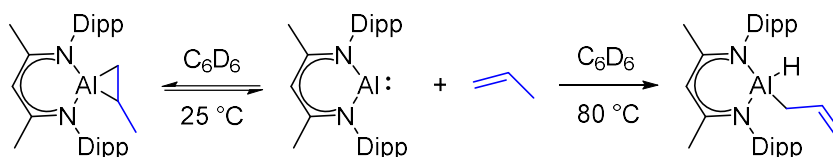
Expanding upon the reactivity portfolio available to the monomeric Al(I) $^{\text{DIPP}}\text{nacnacAl(I)}$ compound, Crimmin has very recently reported the C–F bond activation of a series of fluoroalkanes, fluoroarenes and fluoroalkenes.⁴⁰⁻⁴² With regard to the C–F bond activation of fluoroalkenes, retention of the alkene stereochemistry was not observed (Scheme 1.6). Two possible mechanisms are proposed, backed up by experimental observations and DFT calculations.⁴¹ One reaction pathway is suggested to proceed *via* direct oxidative addition of

the C – F bond to the aluminium centre. This pathway allows retention of the starting alkene stereochemistry. The alternative reaction pathway requires reaction of the alkene to yield a metallocyclopropane intermediate which can then undergo α -fluoride elimination *via* a concerted transition state to generate the product. As the C = C bond is destroyed and reconstructed during the formation and decomposition of the metallocycle, the inversion of stereochemistry is possible.



Scheme 1.6: Representative reaction of DIPPnacnacAl(I) with a fluoroalkene.

Highlighting the potential of DIPPnacnacAl(I) to form metallocyclopropane complexes with alkenes, Crimmin subsequently examined the reactivity towards terminal and strained alkenes, such as 1-propene or norbornene.^{41, 42} Using several examples Crimmin was able to demonstrate that the formation of the metallocyclopropane was reversible under mild conditions (Scheme 1.7). This reversible, reductive elimination step provides a proof of principle for reductive elimination occurring from an aluminium centre, which is rare to observe. Reductive elimination is an important step observed frequently in transition-metal catalysed reactions (*vide infra*).



Scheme 1.7: Reversible alkene binding and allylic C – H activation.

Furthermore, under forcing conditions it was possible to induce irreversible allylic C – H bond activation and generate an Al(III) allyl hydride complex (Scheme 1.7). Interestingly, it was

shown that in order to obtain these allyl hydride complexes alkene dissociation from the metallocyclopropane intermediate was required. This was justified by DFT and MO calculations which showed that the frontier molecular orbitals of the Al(I) compound required for alkene binding are the same as those required for C – H bond activation. This observation has particular implications for the future development of main group catalysts.

Aluminium compounds are known for their Lewis acidity and electrophilicity, but in a remarkable recent development Aldridge has reported the synthesis of a nucleophilic aluminyl anion (Figure 1.4).⁴³ This centrosymmetric dimer consists of two formally anionic [Al(NON)]⁻ units held together through flanking K⁺ --- Ar contacts [NON = 4,5-bis(2,6-diisopropylanilido)-2,7-di-*tert*-butyl-9,9-dimethylxanthene].

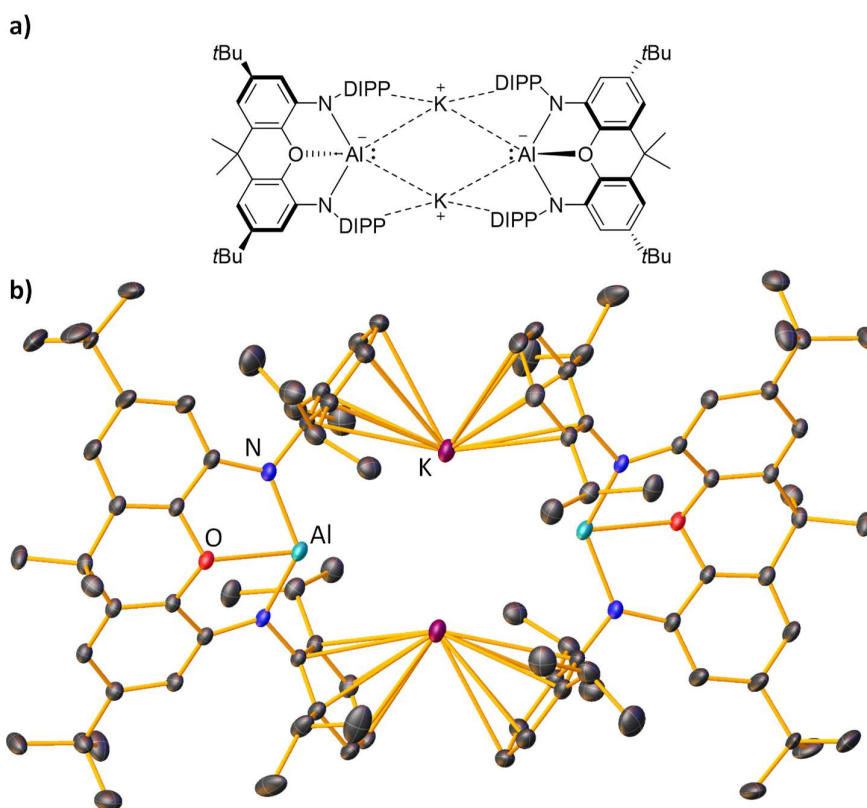
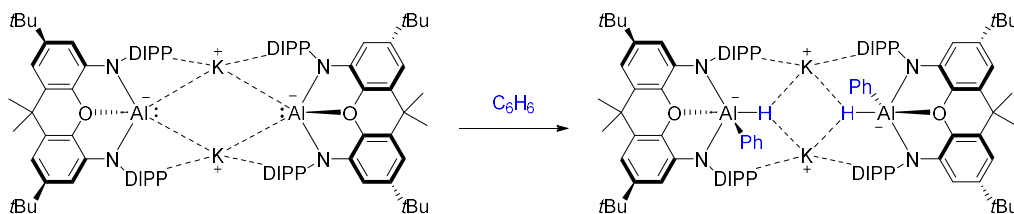


Figure 1.4: a) ChemDraw representation of [K{Al(NON)}]2; b) ball-and-stick molecular structure of [K{Al(NON)}]2, hydrogen atoms have been omitted for clarity.

DFT calculations on this compound suggest that the HOMO has a particularly high energy, suggesting it should be capable of acting as an aluminium nucleophile with a range of electrophilic partners. Thus, reaction of $[K\{Al(NON)\}]_2$ with MeI or MeOTf generated (NON)AlMe and KI (or KOTf), providing a new method for the synthesis of aluminium alkyls. Furthermore, $[K\{Al(NON)\}]_2$ was shown to be capable of undertaking oxidative addition to benzene to yield $[K\{Ph(H)Al(NON)\}]_2$ which represents the first example of oxidative addition of a C – H bond in benzene at a single, well-defined, main group centre (Scheme 1.8).



Scheme 1.8: Oxidative addition of C – H bond from benzene with $[K\{Ph(H)Al(NON)\}]_2$.

1.1.4 ^{27}Al NMR spectroscopy

Aluminium benefits from an NMR active nuclide, ^{27}Al , which has a natural abundance of 100%. However, ^{27}Al is a quadrupolar nucleus ($I = 5/2$), and also has an incredibly large chemical shift window (-100 to 300 ppm).⁴⁴ As a result, ^{27}Al NMR spectroscopy is hampered by incredibly broad signals, the line-width (ω) of which increases with ligand asymmetry about the metal centre. In spite of this, the use of ^{27}Al NMR spectroscopy is still beneficial and can be used to confirm the coordination environment of the aluminium centre in a compound including ligand type and coordination number. Generally, a tri-coordinate R_3Al complex will exhibit a ^{27}Al NMR signal in the region 225 – 300 ppm, whilst a four-coordinate R_4Al centre will have a chemical shift in the region 50 – 225 ppm.⁴⁵ Examples of ^{27}Al NMR signals of common alkyl aluminium compounds are reported in Table 1.1.⁴⁴⁻⁴⁸

Table 1.1: ^{27}Al NMR signals for selected alkylaluminium compounds:

	^{27}Al NMR δ/ppm	$\omega_{1/2}/\text{Hz}$	Coord. No.
$i\text{Bu}_3\text{Al}$	276	6300	3
Me_3Al	153	850	4
Et_2AlH	154	2550	4
Et_2AlCl	167	3300	4

1.2 Main group catalysis

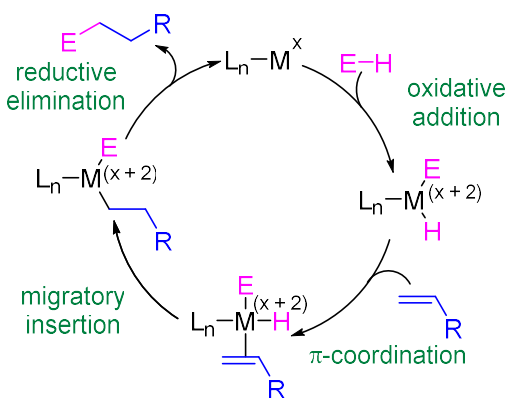
1.2.1 Broad overview of main group catalysis

Catalysis is important industrially and accounts for approximately 20% of the gross domestic product (GDP) of the USA.⁴⁹ Catalysts can be defined as either homogeneous or heterogeneous systems. In a heterogeneous system the catalyst (typically a solid) is in a different phase from the reactants (typically a gas, liquid, or a solution); in homogeneous reactions the catalyst is in the same phase as the reactants. The majority of homogeneous catalysis reactions are mediated through the reactivity of precious transition metals such as platinum, palladium, rhodium or iridium. These metals are associated with high cost, toxicity concerns (particularly with a view to applications in the medicinal-pharmaceutical sector) and potential supply restrictions due to geological scarcity. Thus, in response to these concerns there has been a global effort to identify more sustainable catalysts, including first row transition metal catalysts, organocatalysts and main group catalysts. In 2010 Power commented that the idea of main group catalysis was an “*exciting prospect*”.⁵⁰ Now, nearly 10 years later, the field of main group catalysis has expanded enormously from an initial concept to a flourishing area of research. This is indicated by the numerous book chapters, review articles and journal papers which have recently been published on this topic.^{15-18, 49, 51,}

52

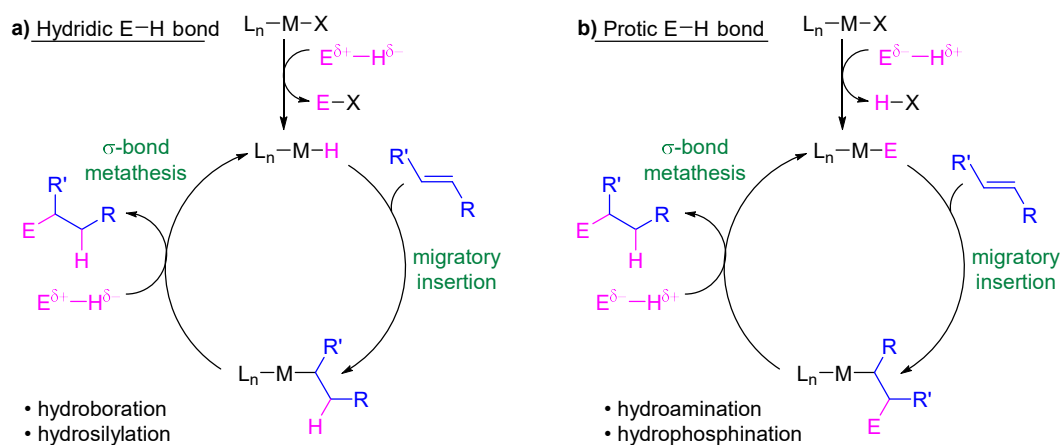
Catalytic cycles for transition metals are typically based upon their redox processes, owing to the ease with which they can change oxidation state. Scheme 1.9 depicts typical key

reaction steps which are often observed in transition metal catalysed hydroelementation. The key features are the oxidative addition and reductive elimination steps with concomitant change in metal oxidation state.



Scheme 1.9: General mechanism for transition metal catalysed hydroelementation of an alkene substrate.³

Conversely, the redox inactivity of main group complexes generally precludes such reaction steps which can hamper their ability to mimic the catalytic performances of transition metals. As such, main group catalysis typically relies upon σ -bond metathesis and migratory insertion steps in order to build up catalytic cycles.⁴⁹ In the literature two general catalytic cycles are proposed for main group catalysed hydroelementation which diverge as a result of the polarisation of the $E-H$ substrate (Table 1.2 and Scheme 1.10). Thus, hydroelementation reactions employing an $E-H$ substrate with a hydridic hydrogen will generally follow the catalytic cycle depicted in Scheme 1.10 (a), such as hydroboration or hydrosilylation. Hydroelementation reactions such as hydroamination or hydrophosphination, where the substrate has a protic hydrogen in the $E-H$ fragment, will often follow the catalytic cycle in Scheme 1.10 (b).



Scheme 1.10: General mechanism for main group catalysed hydroelementation reactions of an alkene with **a)** addition of an E – H fragment with polarisation of the E – H bond yielding a hydridic hydrogen; **b)** addition of an E – H fragment with polarisation of the E – H bond yielding a protic hydrogen.

Table 1.2: Pauling electronegativity values for selected main group elements.²¹

	H	B	Si	N	P
χ (Pauling units)	2.20	2.04	1.90	3.04	2.19

The application of well-defined complexes of s-block metals as catalysts has received considerable attention in the literature.^{49, 51} Notable examples include the popular β -diketiminate ligated magnesium complexes, $\text{DIPP}^{\text{nacnacMg}}(\text{R})$ ($\text{R} = n\text{Bu}, \text{Me}, \text{H}$), employed by Hill which have been shown to be active for a range of different hydroelementation reactions including hydroboration, hydroamination and hydrosilylation (Figure 1.5).⁵³⁻⁶¹ Harder reported the family of metal silylamides $\text{M}(\text{HMDS})_2$ ($\text{M} = \text{Ca}, \text{Sr}, \text{Ba}$) for the hydrogenation of imines and alkenes, in all cases with catalytic activity increasing with increasing metal size (Figure 1.5).⁶²⁻⁶⁴ Examples of catalysts from group one include the use of a lithium dihydropyridine pre-catalyst as a soluble LiH surrogate for diamine borane cyclisation, dehydrocoupling of Me_2NHBH_3 , and hydroboration reactions (Figure 1.5).^{65, 66}

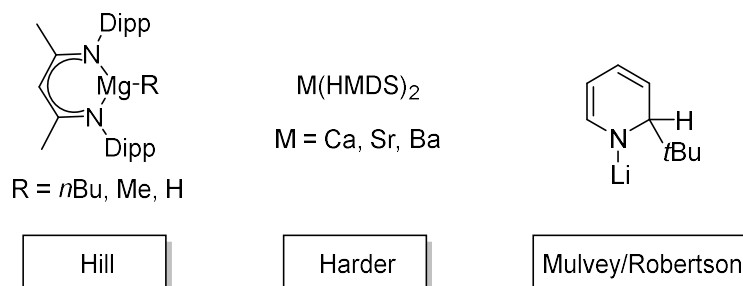
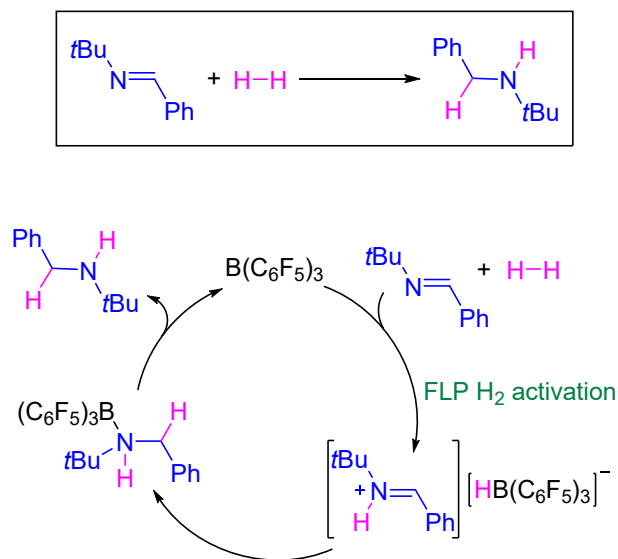


Figure 1.5: Selected examples of s-block main group catalysts.

Within the p-block the concept of Frustrated Lewis Pairs (FLPs) has attracted a lot of attention since Stephan's first report of heterolytic H_2 cleavage in 2006.⁶⁷ A FLP can be described as a combination of Lewis acid and Lewis base which, as a result of high steric demands, are incapable of forming the classical Lewis acid-base adducts. These FLP systems continue to be studied in detail and now can be applied as catalysts for hydrogenation reactions of a range of unsaturated substrates.⁶⁸⁻⁷¹ For example, combining imine substrates with a catalytic amount of $\text{B}(\text{C}_6\text{F}_5)_3$ (5 mol%) under 4 bar H_2 resulted in the hydrogenation of the imine to the corresponding amine (Scheme 1.11).⁷² In this example, the imine reagent acts as both substrate and Lewis base partner in the FLP, generating an activated iminium species *via* heterolytic splitting of H_2 by the imine and borane.



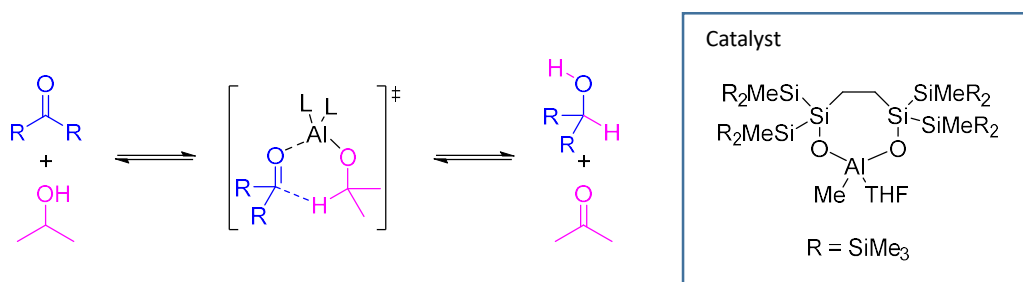
Scheme 1.11: FLP-catalysed imine hydrogenation.

1.2.2 Homogeneous aluminium catalysis

In the 1950s Ziegler employed alkyl aluminium reagents as co-catalysts in polymerisation reactions. The use of a $\text{TiCl}_4/\text{AlEt}_3$ catalyst/co-catalyst system allowed the polymerisation of alkenes; specifically ethylene and propylene were transformed into polyethylene and polypropylene, respectively.^{8,11} In 1963 the Nobel Prize was awarded to Ziegler and Natta for this work with the citation “for their discoveries in the field of chemistry and technology of high polymers”.⁹ In contrast to the extensive use of aluminium compounds as polymerisation co-catalysts there are surprisingly few historical examples of aluminium reagents acting as catalysts themselves in bond forming reactions. However, in this main group renaissance, the use of aluminium compounds as homogeneous catalysts for the reduction of unsaturated organic molecules *via* hydrogenation or hydroelementation reactions has accelerated in recent times.¹⁵⁻¹⁸ A brief overview of some key examples of aluminium catalysed hydroelementation will be discussed below.

The Meerwein-Ponndorf-Verley (MPV) process proceeds *via* hydride transfer from a secondary alcohol to a carbonyl compound, mediated by coordination to a Lewis acidic metal centre. Aluminium alkoxide complexes, such as $\text{Al}(\text{O}i\text{Pr})_3$, were the first reported catalysts for transfer (de)hydrogenation in the MPV process; however, often stoichiometric equivalents

of aluminium were required. More recently the application of well-defined aluminium compounds bearing sterically demanding ligands has allowed for a decrease in catalyst loading as well as milder reaction conditions. Krempner employed an aluminium bis(siloxide) as a catalyst for the MPV reduction of a range of aldehydes and ketones with low catalyst loadings (0.05 – 0.5 mol%) and low temperatures (25 – 50 °C) under solvent free conditions (Scheme 1.12).⁷³ The efficiency of this system is attributed to the large steric bulk of the ligand which prevents aggregation of the aluminium compound in solution, and also facilitates product dissociation from the aluminium centre at the end of the reaction.

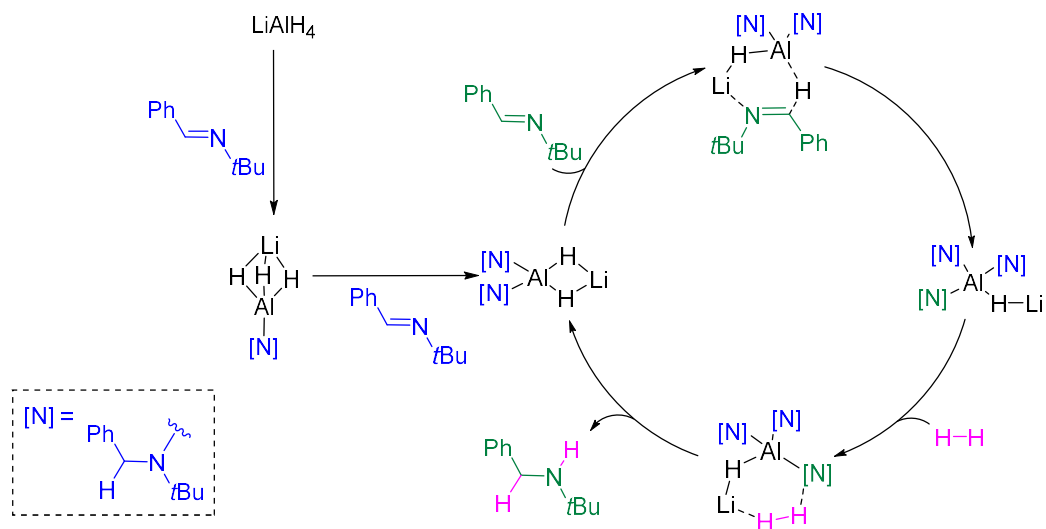


Scheme 1.12: LHS: Typical MPV reaction scheme showing the proposed transition state;

RHS: Catalyst system developed by Krempner.

Aluminium complexes have also been shown to be capable of catalysing hydrogenation processes of unsaturated substrates *via* a series of hydroalumination and H – H / X – Al σ -bond metathesis steps. In 2014, Stephan reported the hydrogenation of imines employing either commercial *i*Bu₂AlH (5 mol%) or *i*Bu₃Al (10 mol%) as the catalyst.⁷⁴ However, harsh reaction conditions (102 bar H₂, 100 °C) and long reaction times of 24 hours were required to obtain the desired amine products. A similar reaction mechanism is realised in the *i*Bu₂AlH catalysed hydrogenation of alkynes; although this process operates under even harsher conditions (>100 bar H₂, >200 °C).⁷⁵ In 2018, Harder reported the hydrogenation of imines to amines under milder reaction conditions than Stephan, by employing LiAlH₄ as a pre-catalyst.⁷⁶ The effects of temperature, H₂ pressure, solvent and catalyst modifications were examined and optimal reaction conditions of 5 mol% LiAlH₄, 1 – 7 bar H₂, 85 °C were chosen. Crucially the authors observed the reaction to be faster in the absence of solvents, presumably as a result of dilution. On the basis of experimental evidence and DFT calculations

Harder proposes a reaction mechanism in which the imine is first hydroaluminated, then in a second step Al – N / H – H σ -bond metathesis is observed, generating the amine product and regenerating the active lithium diamidoaluminate, which appears to be the true catalyst (Scheme 1.13).



Scheme 1.13: Proposed reaction mechanism for the LiAlH₄ pre-catalysed hydrogenation of imines.

The splitting of H₂ is a challenging chemical reaction, and the handling of gaseous and explosive H₂ has important safety implications. On a small scale, such as in the academic laboratory, the substitution of gaseous H₂ for solid or liquid polar reductants (E – H) is often much more convenient. To this end, aluminium catalysed hydroelementation reactions of unsaturated substrates have been investigated with a range of different polar reductants (E – H, where E = B, Si, or N). The aluminium catalysed addition of H – B across an unsaturated bond (hydroboration) has been reported for a range of substrates such as aldehydes, ketones, imines, alkynes and alkenes, amongst others.¹⁵⁻¹⁸ The concept of hydroboration catalysis, and specifically aluminium catalysed hydroboration reactions will be discussed in more detail in Chapters 2 and 3.

Hydrosilylation, the addition of $H^{\delta-} - Si^{\delta+}$ across an unsaturated bond, is another such hydroelementation process. Earlier examples employed simple Lewis acidic aluminium salts, such as $AlCl_3$, but more recently the focus has shifted to well-defined molecular compounds.^{16, 18} Such aluminium compounds include the more strongly Lewis acidic compounds $[^{DIPP}nacnacAl(H)]^+[B(C_6F_5)_4]^-$, and $Al(C_6F_5)_3$ (Figure 1.6).^{77, 78}

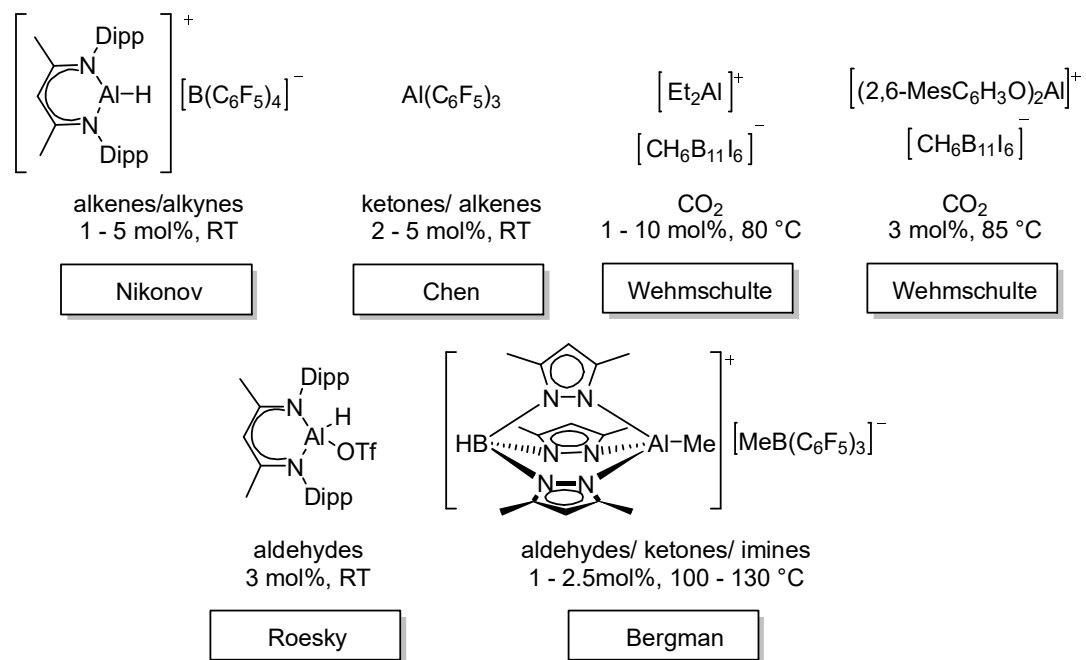
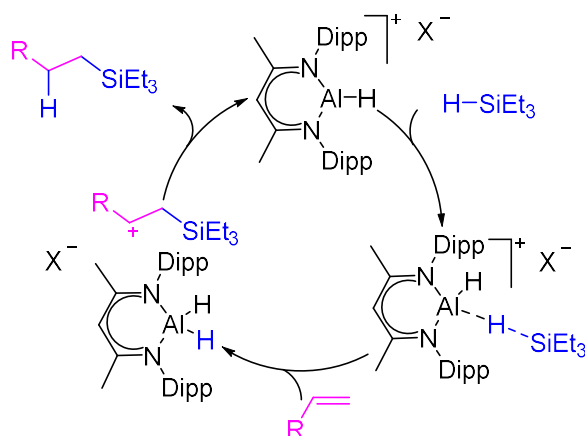


Figure 1.6: Reported well-defined organoaluminium catalysts for hydrosilylation.

In these systems the reaction is believed to proceed through the formation of an $[R_nAl \cdots H \cdots SiR'_3]^+$ adduct which delivers a silylium ion to the alkene substrate to generate a carbocation. Hydride transfer from the aluminium to the cation then usually leads to the anti-Markovnikov product (Scheme 1.14).^{16, 18, 77} However, the true reaction mechanism has yet to be unequivocally determined.



Scheme 1.14: Lewis acid promoted hydrosilylation [$X^- = B(C_6F_5)_4$].

Of these cationic aluminium complexes, the $[^{DIPP}nacnacAl(H)]^+[B(C_6F_5)_4]^-$ system is the most active and is successful in the hydrosilylation of terminal alkenes and aliphatic alkynes at room temperature, with low catalyst loadings (1 – 5 mol%) and short reaction times.⁷⁷ Comparatively, the neutral analogue $^{DIPP}nacnacAl(OTf)(H)$ was reported to catalyse the hydrosilylation of aldehydes at room temperature within 6 hours.⁷⁹ In this instance, the authors proposed a catalytic cycle based on the hydridic main group cycle in Scheme 1.10 (a) in which the aldehyde substrate first inserts into the Al – H bond. Hydrosilylation of polar unsaturated substrates such as aldehydes, ketones, imines and CO_2 has also been reported with other aluminium catalysts (Figure 1.6).⁸⁰⁻⁸² For example, $[Tp^*AlMe]^+[MeB(C_6F_5)_3]^-$ displayed good activity for hydrosilylation of carbonyls, imines and lactones [$Tp^* =$ hydrotris(1,3-dimethylpyrazol-1-yl)borate].⁸¹

Hydroamination reactions provide atom economical routes to the synthesis of new amine containing compounds by formal addition of a $N^{\delta-} - H^{\delta+}$ bond across an unsaturated substrate. The first example of aluminium catalysed intramolecular hydroamination was reported by Bergman in 2010.⁸³ Though a phenylenediamine aluminium complex (Figure 1.7) was shown to be active in the intramolecular hydroamination of aminopentenes, high catalyst loadings (10 mol%) and harsh reaction conditions (150 °C, 12 – 90 hours) were required. Intramolecular hydroamination of aminoalkenes presents a convenient approach for the construction of cyclic amines which are of interest to those chemists working in pharmaceutical and natural products chemistry.⁸⁴ The use of an OCO pincer complex of

aluminium required similarly harsh reaction conditions (10 mol%, 150 °C) and also extended reaction times (100 hours).⁸⁵

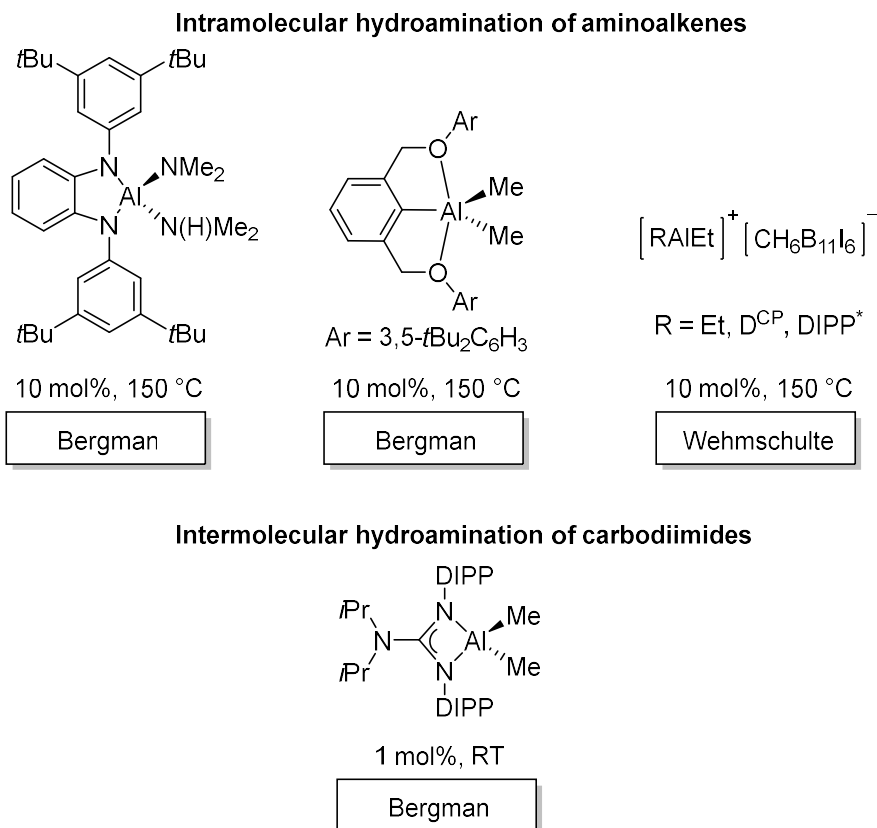
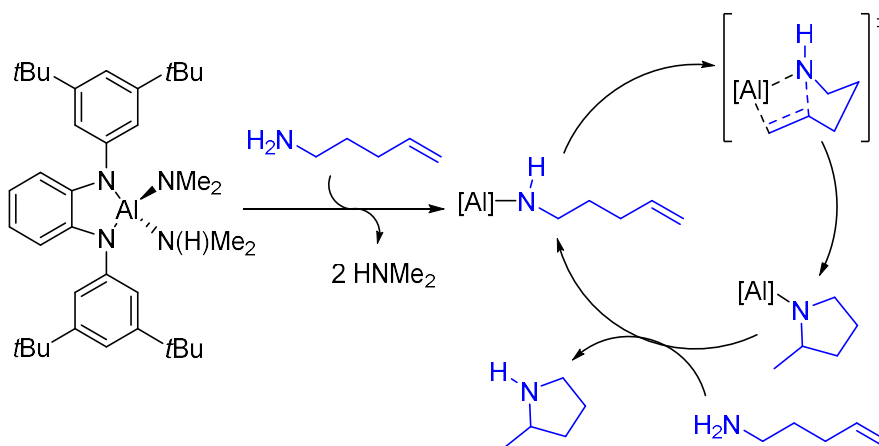


Figure 1.7: Reported aluminium catalysts for selected hydroamination reactions.

In contrast, low coordinate cationic aluminium complexes were shown to be more active catalysts for intramolecular hydroamination reactions (Figure 1.7).⁸⁶ A series of four $[\text{RAIEt}]^+[\text{X}]^-$ complexes were tested: $[\text{Et}_2\text{Al}]^+[\text{CH}_6\text{B}_{11}\text{I}_6]^-$, $[\text{Et}_2\text{Al}]^+[\text{CH}_6\text{B}_{11}\text{Cl}_6]^-$, $[\text{D}^{\text{CP}}\text{AlEt}]^+[\text{CH}_6\text{B}_{11}\text{Cl}_6]^-$ [$\text{D}^{\text{CP}} = 2,6-(2,6\text{-ClC}_6\text{H}_3)_2\text{C}_6\text{H}_3$], and $[\text{DIPP}^*\text{AlEt}]^+[\text{CH}_6\text{B}_{11}\text{Cl}_6]^-$ [$\text{DIPP}^* = 2,6-(2,6\text{-}i\text{Pr}_2\text{C}_6\text{H}_3)_2\text{C}_6\text{H}_3$]. In each case, these cationic aluminium complexes were employed at 10 mol% catalyst loading, and a marginally lower reaction temperature of 135 °C. Overall $[\text{DIPP}^*\text{AlEt}]^+[\text{CB}_{11}\text{H}_6\text{Cl}_6]^-$ was found to be the most active aluminium precursor for this intramolecular hydroamination reaction. In comparison with the neutral aluminium

analogues (Et_3Al , $\text{D}^{\text{CP}}\text{AlEt}_2$ and $\text{DIPP}^*\text{AlEt}_2$), the cationic complexes were up to 25 times more catalytically active.

DFT calculations on the aluminium phenylenediamine system favour a stepwise reaction mechanism in preference to a concerted reaction process. The proposed mechanism starts from an initially formed amide/amine adduct, followed by 1,2-insertion of the alkene and subsequently Al – N protonolysis (Scheme 1.15).⁸⁷



Scheme 1.15: Proposed catalytic cycle for intramolecular hydroamination of aminoalkenes.

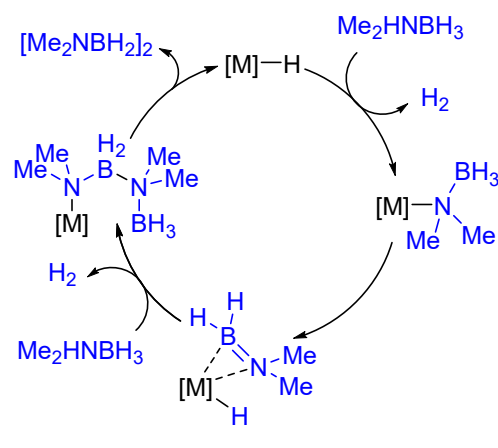
Aluminium catalysed intermolecular hydroamination has been significantly less well studied. To date, only one example of intermolecular hydroamination performed by aluminium catalysts has been reported. Bergman prepared aluminium guanidinate-supported complexes which were capable of efficient catalysing of the intermolecular hydroamination of carbodiimides with anilines (Figure 1.7).⁸⁸ Low catalyst loadings (1 mol%) and mild reaction conditions (room temperature, 30 minutes) were required to generate the substituted guanidine products in good yields. The solution structure of the catalyst was shown to be important, with only monomeric three coordinate aluminium complexes being active catalysts. The catalytic cycle was proposed to proceed *via* a similar mechanism to that proposed in Scheme 1.10 (b), namely the formation of an aluminium amide complex that can then add across the C = N unsaturated bond of the carbodiimide. In the second step a second

equivalent of aniline protonates the guanidine, forming the product and regenerating the active aluminium amide catalyst.

Other organic transformation methodologies which have been catalysed by aluminium complexes include dehydrocoupling.^{52, 89} Dehydrocoupling reactions provide a convenient route to the formation of new E – E bonds [forming either homoatomic E – E bonds (homo-dehydrocoupling), or heteroatomic E – E' bonds (hetero-dehydrocoupling)] *via* elimination of H₂ gas. The resultant products have found widespread interest including in H₂ storage applications for greener fuels, in organic synthesis, and in materials chemistry.⁵² Roesky reported that ^{Ar}nacnacAlH₂ was a catalyst for the dehydrocoupling of boranes with amines, thiols and phenols at room temperature in the presence of 5 mol% catalyst (Ar = 2,6-Et₂C₆H₃).⁹⁰ Reaction of the aluminium dihydride pre-catalyst with one equivalent of RE – H (amine E = N, thiol E = S, or phenol E = O) generated the active catalytic species, ^{Ar}nacnacAl(H)ER *via* elimination of one equivalent of H₂ gas, which was observed experimentally. The mechanism was proposed on the basis of DFT calculations and experimental observations to follow a catalytic cycle similar to that depicted in Scheme 1.10 (b). In a subsequent step a second equivalent of RE – H is deprotonated by the remaining Al – H bond. Following this, the H^{δ-} – B^{δ+} bond of HBpin (HBpin = 4,4,5,5-tetramethyl,1,3,2-dioxaborolane) interacts with one of the Al – E bonds to form a four membered transition state. At the end of the catalytic cycle the hydride is transferred to the aluminium centre with formation of the dehydrocoupled product and regeneration of the active aluminium species. Note that subsequently Bertrand reported that this reaction can proceed under catalyst- and solvent-free conditions.⁹¹

Ammonia borane, (H₃NBH₃), contains 19.6 wt% of hydrogen which makes it an interesting compound for the chemical storage of hydrogen in future applications such as fuel cells.⁹²⁻⁹⁴ As such, the dehydrocoupling of ammonia borane and related secondary amine boranes, (RH₂NBH₃ or R₂HNBH₃), is an important catalytic reaction which has received a good deal of interest, with the use of aluminium catalysts for such processes pioneered by Wright.⁹⁵⁻⁹⁸ As such a range of aluminium pre-catalysts have been employed (Scheme 1.16). In all cases, the presence of an aluminium hydride appears critical in the catalytic cycles, and consequently aluminium hydride species are implicated as the true active species for these reactions. The use of Al(NMe₂)₃ for the dehydrocoupling of Me₂HNBH₃ showed the clean formation of dimeric [Me₂NBH₂]₂ within 48 hours at 50 °C with 5 mol% catalyst.⁹⁵ It was

proposed that the structurally defined aluminium hydride complex $[(\text{Me}_2\text{N})_2\text{BH}_2]_2\text{AlH}$ could be one of the active species in the catalytic cycle. A similar aluminium hydride complex, $[\text{iPr}_2\text{NAlH}_2]_2$, has been isolated from the reaction between $\text{Al}(\text{NiPr}_2)_3$ and $\text{iPr}_2\text{HNBH}_3$ and has also been shown to be catalytically active in dehydrocoupling reactions.⁹⁶ In light of these observations, the catalytic application of LiAlH_4 for the dehydrocoupling of Me_2HNBH_3 was also examined by Wright.⁹⁷ It was reasoned that LiAlH_4 was expected to perform the catalysis faster than $\text{Al}(\text{NR}_2)_3$ ($\text{R} = \text{Me}$ or iPr) due to the presence of $\text{Al} - \text{H}$ bonds in the pre-catalyst removing any induction period, but due to solubility problems the catalysis was relatively slow. The main product arising from this catalytic system is dimeric $[\text{Me}_2\text{NBH}_2]_2$. *In situ* NMR spectroscopic studies on this LiAlH_4 catalysed reaction reveal a complicated system which involves a combination of deprotonation, $\text{B} - \text{N}$ bond formation and $\text{B} - \text{N}$ cleavage. Lastly, Wright employed a series of mixed alkoxide-hydride complexes $[(\text{tBuO})_x\text{AlH}_{3-x}]$ ($x = 1, 2$) and $(\text{L})\text{Li}[(\text{tBuO})_2\text{AlH}_2]$ ($\text{L} = \text{THF}, 1,4\text{-dioxane}$) as catalysts for Me_2HNBH_3 dehydrocoupling.⁹⁸ It was found that the monoalkoxide $(\text{tBuO})\text{AlH}_2$ was the best catalyst from this series, in terms of catalytic activity and product selectivity, observing quantitative formation of dimeric $[\text{Me}_2\text{NBH}_2]_2$ after 16 hours at 110°C with 10 mol% catalyst. The crystal structure of $(\text{tBuO})\text{AlH}_2$ is dimeric, which reflects the similar structures obtained in initial reactivity screening of $\text{Al}(\text{NR}_2)_3$. A proposed catalytic cycle is provided for the generation of the main dehydrocoupled product (Scheme 1.16).



Aluminium catalysts:

$Al(NMe_2)_3$
5 mol%, 50 °C, 48 h

$LiAlH_4$
10 mol%, 110 °C, 16 h

$(tBuO)AlH_2$
10 mol%, 110 °C, 16 h

Scheme 1.16: General mechanism proposed for the dehydrocoupling of amine borane Me_2HNBH_3 with different aluminium catalysts.

1.3 Synergic main group chemistry

1.3.1 Development of heterobimetallic metallating agents

First introduced over 100 years ago by the pioneering work of Schlenk and Holtz,^{99, 100} alkyllithium $(LiR)_n$ and lithium amide $(LiNR_2)_n$ reagents today are near ubiquitous in metallation reactions.¹⁰¹⁻¹⁰³ Highlighting the significance of organolithium reagents Collum commented that at least 95% of natural products rely upon the use of organolithium reagents at some point in their synthesis.¹⁰⁴ The widespread utility of alkyllithium reagents comes as a result of the high reactivity of these reagents due to the high polarity of the Li – C bond (Table 1.3).²¹ However, this high reactivity comes at the price of low functional group tolerance, and the incompatibility with ethereal solvents such as THF.⁸ Often the use of cryogenic reaction temperatures are employed in an attempt to mitigate side reactions.

Lithium amides are one of the most commonly used polar organometallic reagents in synthesis. The combination of high Brønsted basicity (though not as high as that of alkyllithium compounds) and poor nucleophilicity enables them to be used for selective deprotonation reactions, and renders them good rivals to alkyllithium reagents.¹⁰⁵ As a result, they are less likely to participate in nucleophilic type side reactions, such as addition across

a C = O bond, than alkyllithium reagents. The most synthetically important amides are the sterically demanding secondary amides LiTMP, LiDA, and LiHMDS, which are popular due to their ease of handling, and good hydrocarbon solubility (TMP = 2,2,6,6-tetramethylpiperidide, DA = diisopropylamide, HMDS = 1,1,1,3,3,3-hexamethyldisilazide).¹⁰⁶

In some instances, Grignard reagents (“RMgX”) can be used instead of organolithium reagents. The use of Grignard reagents can provide better functional group tolerance and exhibit greater selectivity at higher temperatures than organolithium reagents.⁸ However, Grignard reagents can have decreased reactivity as a result of the less polar Mg – C bond (Table 1.3), poor solubility in hexane solvents and solution complexity as a result of Schlenk equilibria.⁸

Table 1.3: Pauling electronegativity values for H, C and selected metal elements.

	H	C	N	Li	Mg	Zn	Al
χ (Pauling units)	2.20	2.55	3.04	0.98	1.31	1.65	1.61

The application of heterobimetallic reagents, which combine two metals with distinct polarities, can provide important benefits such as improved functional group tolerance and the ability to be used under milder reaction conditions.¹⁰⁷⁻¹⁰⁹ In these bimetallic systems the two metals work together, with the appropriate ligands, to create a unique synergistic effect, executing a reactivity that the distinct metals cannot display individually. The combination of an alkali metal (AM: for example lithium, sodium or potassium) with a less electropositive metallating agent (*M*: for example, magnesium, zinc or aluminium), either with homoleptic (all R) or heteroleptic anionic ligands (R, R' etc.), results in the formation of mixed metal “ate” species of the general formula [(AM)MR_x].¹⁰⁷ It is the moiety containing the less electropositive metal that carries the negative charge, the so-called metallate. The presence of the alkali metal is crucial for synergic reactivity as it activates the less reactive metal, and as such the term “alkali metal mediated *metallation* (AMMM)” is often applied to metallation reactions with these bimetallic systems.^{107, 110} The ratio of alkali metal (AM) to metal (*M*) can often be varied, giving rise to lower order ates (1:1) or higher order ates (2:1) with the number of charge balancing ligands changing appropriately (Figure 1.8).

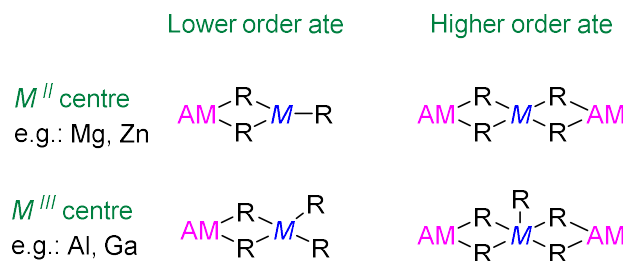


Figure 1.8: Schematics of lower order and higher order metallate compounds.

The simplest and best-known lithium aluminate is the commercially available LiAlH_4 . First prepared by Schlesinger in the 1940s from the reaction of lithium hydride (LiH) with aluminium chloride, AlCl_3 , it is one of the most widely utilised reducing agents in the synthetic laboratory today.¹¹¹⁻¹¹³ As a result of its high lattice energy (920 kJ mol^{-1}) LiH exists as an inert and air-stable salt. However in combination with AlH_3 , it becomes a very efficient reducing agent capable of reducing almost all organic functional groups, under mild reaction conditions and in good yields.^{114 113, 115} In fact, LiAlH_4 is such a powerful reductant that it cannot be employed in the presence of sensitive functional groups. This enhanced reactivity compared with homometallic LiH can be attributed in part to the enhanced solubility of LiAlH_4 in ethereal solvents. Comparatively, homometallic AlH_3 reacts more slowly with these substrates and is less easy to handle and purify than its lithium derivative LiAlH_4 .^{111, 115, 116} As LiAlH_4 is capable of reactivity not available to its monometallic components, its reducing capabilities are therefore a result of metal-metal bimetallic cooperativity.¹¹⁶

The first reported example of an ate species, “ NaZnEt_3 ”, was reported by Wanklyn in 1858.¹¹⁷ Wittig later introduced the term “ate” in 1951 to describe his lithium triphenylmagnesiato complex $[\text{LiMgPh}_3]$, which refers to compounds where the metal centre is part of the anionic moiety.¹¹⁸ The preparation of ate species is easily performed using one of two common methodologies: i) the co-complexation of Lewis acidic and Lewis basic components, or ii) through salt metathesis of a metal halide with an organoalkali metal reagent. The application of heterobimetallic reagents allows for the deprotonation and stabilisation of challenging and/or sensitive substrates, and has been achieved using heterobimetallic bases such as alkali metal magnesiates, zincates and aluminates.^{109, 119} Today, the application of heterobimetallic chemistry to metallation chemistry is vast, and for

brevity it would not be feasible to discuss here all the breakthroughs which have been observed. Instead, selected notable examples of heterobimetallic bases have been chosen in an attempt to provide examples of the sorts of reactivity benefits attainable by employing such synergistic reagents.

A classical example of heterobimetallic chemistry is the application of the Lochmann-Schlosser superbases for deprotonations which generally $n\text{BuLi}$ cannot effect on its own. The Lochmann-Schlosser superbases usually comprise an equimolar mixture of $n\text{BuLi}$ and $\text{KO}t\text{Bu}$, and exhibits an attractive reactivity intermediate between less reactive (but often controllable) $n\text{BuLi}$ and more reactive (but often uncontrollable) $n\text{BuK}$, implying the formation of a co-complexed reagent.^{120, 121} As such, the Lochmann-Schlosser superbase is capable of deprotonating benzene, at $-50\text{ }^\circ\text{C}$ in THF solvent.¹²² Benzene represents a challenging substrate to metallate due to its low acidity, with a $\text{p}K_{\text{a}}$ value of 44.7.¹²³ The exact molecular structure(s) of this prototypical superbase is currently unknown. However, in 2016 Klett prepared and structurally defined the crystal structure of the *neopentyl* (Np) analogue from the reaction of NpLi and $\text{KO}t\text{Bu}$, with the approximate composition of $[\text{Li}_4\text{K}_3\text{Np}_4(\text{O}t\text{Bu})_3]$ (Figure 1.9).¹²⁴

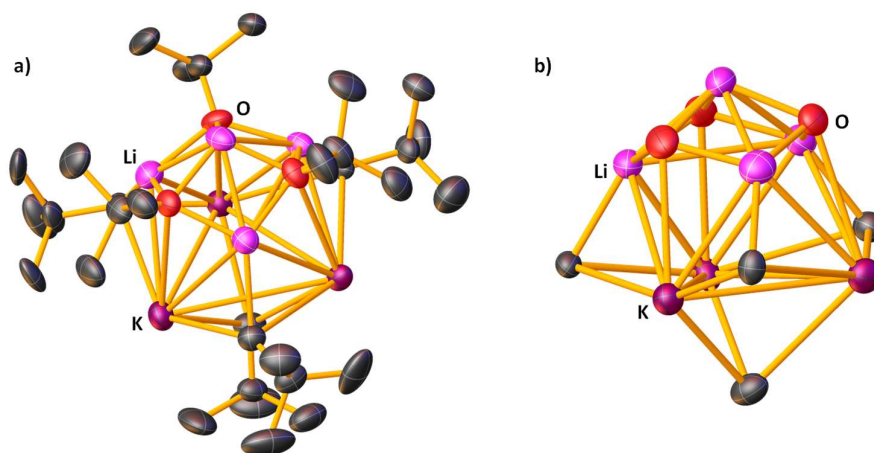
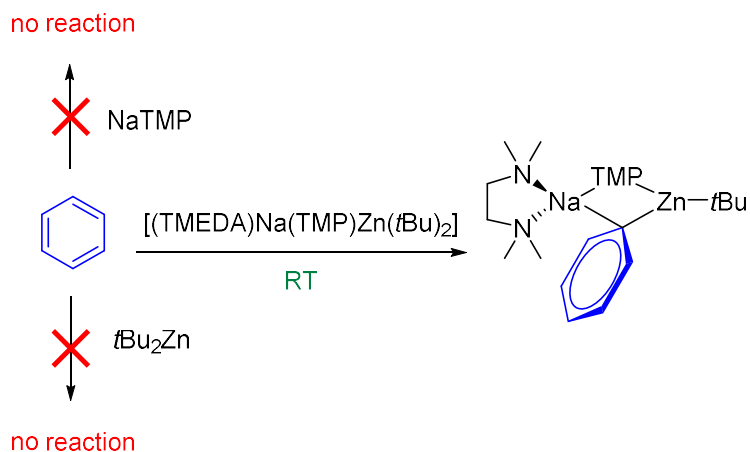


Figure 1.9: **a)** Molecular structure of Klett's *neopentyl* variant of the Lochmann-Schlosser superbase; **b)** Framework with Np^- and $t\text{BuO}^-$ ligands omitted for clarity.

Mulvey has also exploited bimetallic cooperative reactivity to deprotonate benzene (Scheme 1.17). Reaction of NaTMP and $t\text{Bu}_2\text{Zn}$ in the presence of TMEDA yields the sodium zincate, $(\text{TMEDA})\text{Na}(\mu\text{-TMP})(\mu\text{-}t\text{Bu})\text{Zn}(t\text{Bu})$, which performs this deprotonation of benzene ($\text{TMEDA} = N,N,N',N'$ -tetramethylethylenediamine).¹²⁵ Comparatively, neither NaTMP, nor $t\text{Bu}_2\text{Zn}$ are capable of instigating such a deprotonation independently, reaffirming the idea that the observed reactivity occurs as a result of cooperative AMM Zn . In comparison with the Lochmann-Schlosser superbases (*vide supra*), the deprotonation of benzene with $(\text{TMEDA})\text{Na}(\mu\text{-TMP})(\mu\text{-}t\text{Bu})\text{Zn}(t\text{Bu})$ has the advantage that it is performed at room temperature.



Scheme 1.17: Contrasting reactivities of NaTMP, $t\text{Bu}_2\text{Zn}$, and heterobimetallic $[(\text{TMEDA})\text{Na}(\text{TMP})\text{Zn}(t\text{Bu})_2]$.

The regioselectivity of deprotonation reactions of substituted arene substrates is usually governed by “directed *ortho* metallation” (DoM), a seminal concept in organolithium chemistry.^{126, 127} Gilman and Wittig independently observed that the presence of a “directing group” (DG) on the aromatic cycle activates an adjacent (*ortho*) C – H bond towards metallation either by providing the incoming Lewis acidic metallation agent with a Lewis basic coordination site, and/or weakening the C – H bond *via* electron-withdrawing inductive properties.^{128, 129} Groups can exhibit weak (e.g.: alkyl), moderate (e.g.: alkoxy, trifluoromethyl) or strong directing effects (e.g.: amide $[\text{R}_2\text{N}(\text{C}=\text{O})]$). The DoM concept

generally applies irrespective of the choice of metallating agent. However, an example of templated metallation by Mulvey and O'Hara allows for directed *ortho-meta'* and *meta-meta'*-dimetallation reactions of arene substrates using the mixed-metal magnesiate base $[\text{Na}_4\text{Mg}_2(\text{TMP})_6(n\text{Bu})_2]$ (Figure 1.10 and Figure 1.11).¹³⁰

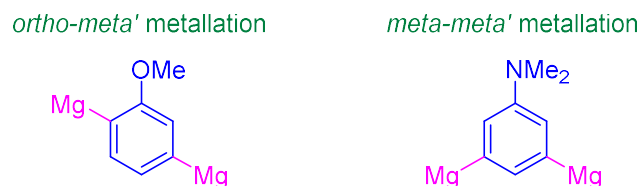


Figure 1.10: Example deprotonations by inverse crown base showing *ortho-meta'* and *meta-meta'* selectivities. Note only the Mg atoms of the host rings are shown.

The primary driving force for these dimetallation reactions is the pre-organisation of the bimetallic metallating agent, $[\text{Na}_4\text{Mg}_2(\text{TMP})_6(n\text{Bu})_2]$, into a spectacular inverse crown topology which instigates a template mechanism. The pre-inverse crown is held in a 12-membered cycle with TMP anions bridging the metal centres. The magnesium centres oppose each other across the open pocket of the crown structure, and the deprotonation proceeds *via* loss of the *n*Bu ligands as butane gas. The orientation of the substrate within the inverse crown thus dictates the positions on the aromatic ring which are deprotonated (In Figure 1.11 the substrate is *N,N*-dimethylaniline). Subsequently it has been shown that this template methodology can be used to dimetallate polyaryl substrates lacking a directing group, including biphenyl, an important molecular scaffold in pharmaceutical agents and host materials for organic light-emitting diodes (OLEDs).¹³¹ Such substrates can be troublesome to metallate with conventional deprotonating agents, and so this template mixed-metal base presents an elegant solution to this challenge.

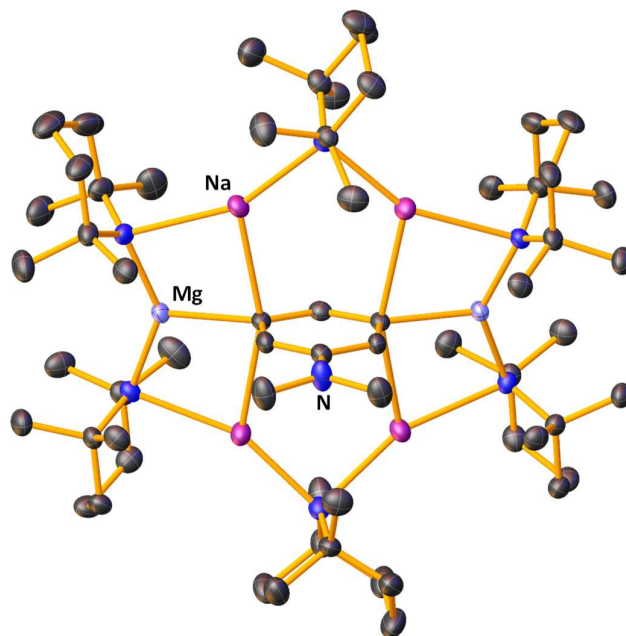


Figure 1.11: Molecular structure of $[\text{Na}_4\text{Mg}_2(\text{TMP})_6(\text{C}_6\text{H}_3\text{NMe}_2)]$, showing *meta-meta'* dimetallation of the aniline. Thermal ellipsoids are drawn at 40% probability; hydrogen atoms have been omitted for clarity.

1.3.2 Synergistic reactivity of alkali metal aluminates

The application of lithium aluminates for metallation reactions was first introduced by Uchiyama and Kondo. The heteroleptic complex $[i\text{Bu}_2\text{Al}(\mu\text{-}i\text{Bu})(\mu\text{-TMP})\text{Li}(\text{THF})]$ (Figure 1.12) was found to be an excellent metallating agent for aromatic substrates with sensitive substituents such as halogens.^{132, 133}

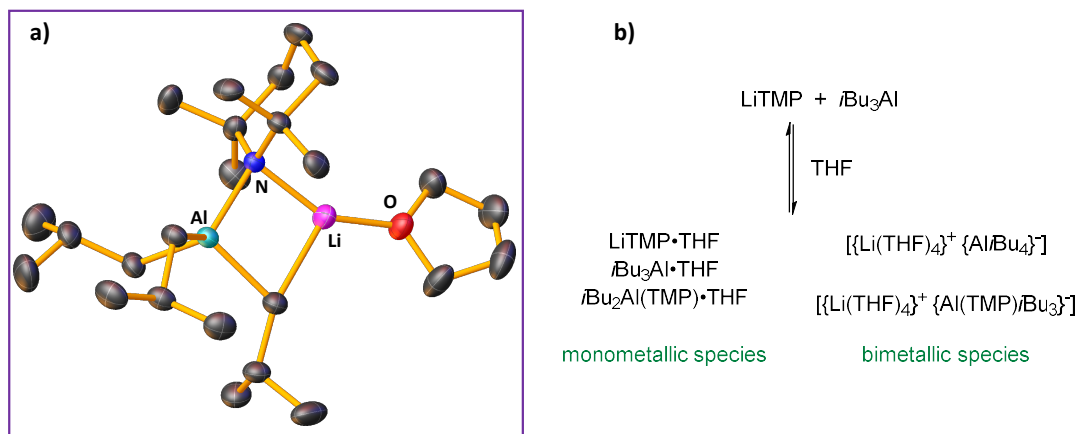
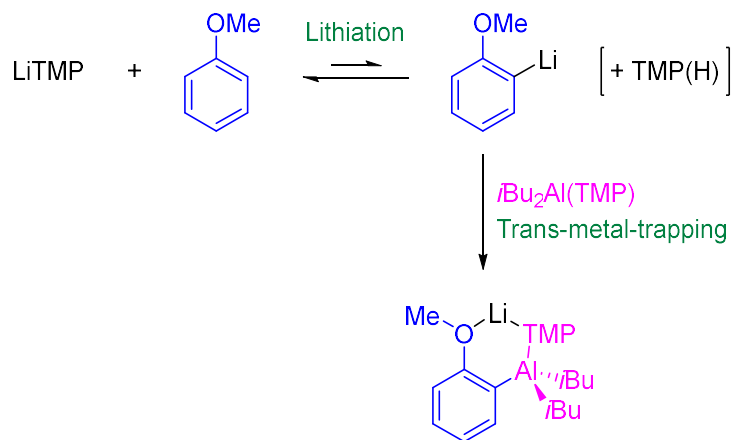


Figure 1.12: **a)** Molecular structure for the proposed active metallating agent from the co-complexation of $i\text{Bu}_3\text{Al}/\text{LiTMP}$. **b)** Species formed upon mixing $\text{LiTMP}/i\text{Bu}_3\text{Al}$ in THF solution.

Mulvey subsequently introduced the related bis-amido system $\text{LiTMP}/i\text{Bu}_2\text{Al}(\text{TMP})$ as an alternative AMMA/ reagent.¹³⁴ Further systematic studies by Mulvey provided an in-depth investigation into how these reagents operate and revealed some remarkable observations.¹³⁵ Firstly, on the basis of detailed NMR spectroscopic studies it was concluded that Uchiyama's $\text{LiTMP}/i\text{Bu}_3\text{Al}$ system was in fact an equilibrium mixture of up to five different species in THF solution, (Figure 1.12). In fact, the only species from this complicated mixture which was shown to have any deprotonation reactivity was LiTMP ; that is to say, the structurally characterised lithium aluminate reported by Uchiyama is in fact not the active species under these reaction conditions. Detailed investigations into the mode of reactivity of the bis-amido system comprising $i\text{Bu}_2\text{Al}(\text{TMP})/\text{LiTMP}$ revealed that this system actually operates *via* a two-step mechanism. This pathway is highlighted in Scheme 1.18 with anisole as an exemplar substrate. On its own, LiTMP is a very poor metallating agent for anisole, with the equilibrium for this reaction lying heavily towards the starting materials. That notwithstanding, addition of the Lewis acidic, carbophilic, aluminium reagent $i\text{Bu}_2\text{Al}(\text{TMP})$ leads to a rapid reaction with the lithio-carbanion and drives the equilibrium of the metallation towards the wanted products. This then allows for almost quantitative metallation of anisole, which formally has been *ortho*-aluminated. Importantly, LiTMP and $i\text{Bu}_2\text{Al}(\text{TMP})$ do not react with each other to form a lithium aluminate, as a result of steric

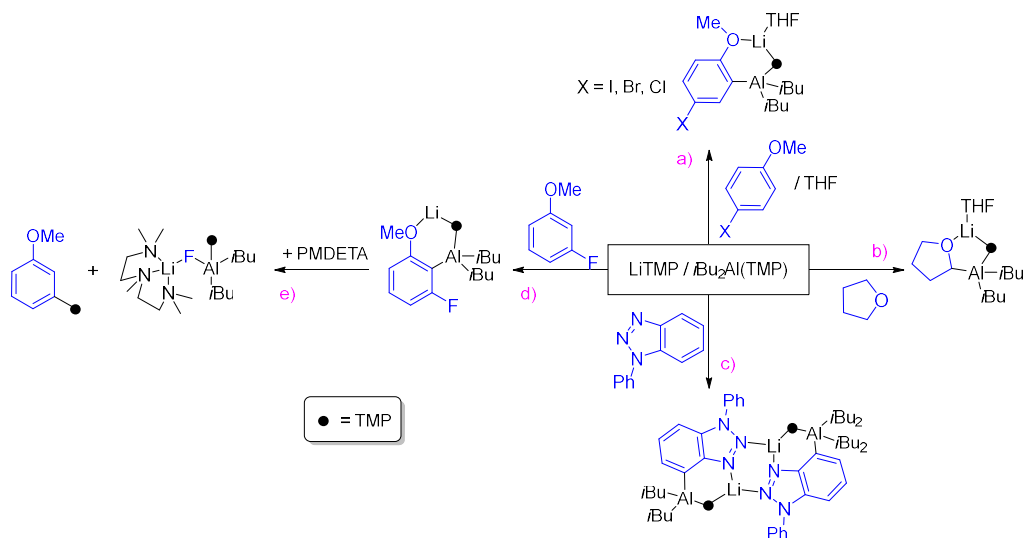
incompatibility, hence this process represents an example of stepwise cooperation between two metal reagents. Critically, in the final metallated products, which can be isolated and characterised by X-ray crystallography, the lithium remains part of the structure. As a result of this two-step pathway, and given that the lithium is not dispelled from the metallated product the name “trans-metal-trapping” was coined, and is deemed more appropriate and more accurate than the common denotation “transmetalation”.^{135, 136}



Scheme 1.18: Proposed two-step pathway for the trans-metal trapping methodology illustrated here with anisole.

Trans-metal-trapping is attractive due to the possibility to transform failed lithiations into successful metallation reactions and can also stabilise sensitive carbanions formed *via* metallation due to the decreased polarity of the C – Al bond *versus* C – Li. To this end, the concept of trans-metal-trapping has been applied to a number of useful and/or sensitive substrates including the metallation of 4-haloanisoles, THF, phenyl-substituted benzotriazoles and fluorinated aromatics, amongst several other substrates (Scheme 1.19).^{134, 137-141} In reactions with fluoroarenes, the fluorophilicity of aluminium is too high, and as a result the fluoride anion is removed from the arene, generating a lithium aluminium fluoride complex (Scheme 1.19 (d), (e)). The fluoride anion is replaced by the TMP anion at the arene. This reactivity can be circumvented by employing a gallium trap instead,

$\text{Ga}(\text{CH}_2\text{SiMe}_3)_3$, which is less fluorophilic than aluminium, and so the resulting metallated (gallated) fluoroarene is stable.¹⁴⁰



Scheme 1.19: Examples of trans-metal-trapping with a range of substrates.

Reports of other alkali metal mixed-alkyl(amide)aluminate combinations have been rather limited. Mulvey reported the first example of a sodium aluminate, as an alkali metal variant of Uchiyama's lithium aluminate system, $[(\text{TMEDA})\text{Na}(\mu\text{-TMP})(\mu\text{-}i\text{Bu})\text{Al}/i\text{Bu}_2]$ [Figure 1.13 (a)].¹⁴² This sodium aluminate was reported to deprotonate phenylacetylene forming an alkynyl sodium aluminate complex, $[(\text{TMEDA})\text{Na}(\mu\text{-}i\text{Bu})(\mu\text{-C}\equiv\text{CPh})\text{Al}/i\text{Bu}_2]$, however the exact reaction mechanism has not yet been elucidated. Examples of potassium aluminates containing different secondary amide ligands of the type, $(\text{PMDETA})\text{K}(\mu\text{-NR}_2)(\mu\text{-}i\text{Bu})\text{Al}/i\text{Bu}_2$, have also been structurally characterised but no metallation reactivity has been reported ($\text{NR}_2 = \text{TMP}$, DMP , or HMDS) [$\text{PMDETA} = N,N,N',N'',N''$ -pentamethyldiethylenetriamine; $\text{DMP} = 2,6$ -dimethylpiperidine], (Figure 1.13 (b)).¹⁴³ In a related study, Mulvey reported the "self-metallation" of the TMP anion from a reaction mixture containing KTMP , $i\text{Bu}_2\text{Al}(\text{TMP})$ and TMEDA (Figure 1.13 (c)).¹⁴⁴ Thus it is clear to see that the application of alkali metal aluminates to metallation chemistry is still very much at an early stage; however, the initial results are promising.

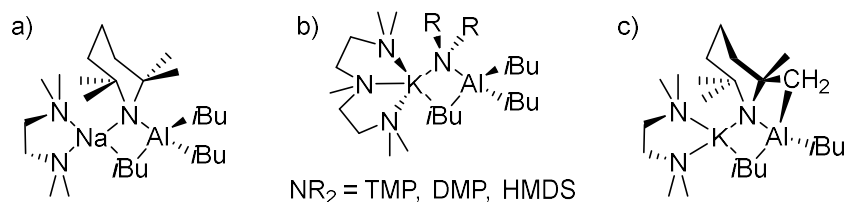


Figure 1.13: Examples of heavier alkali metal mixed alkyl-amido aluminate complexes.

1.4 Overall Aims of the PhD Project

As discussed in Section 1.2, the use of aluminium complexes as catalysts for hydroelementation reactions is an interesting and developing area of research. Investigation into the application of well-defined aluminium compounds as catalysts for such reactions for the purpose of identifying structure-activity relationships is important in order to target new, ideally more catalytically active, aluminium compounds in the future. It is noteworthy that the application of LiAlH₄ as a catalyst for such catalytic reductions has only been examined in a few instances given its prominence as a stoichiometric reducing agent. Furthermore, with the exception of the cationic aluminium complexes discussed for hydrosilylation and hydroamination, the aluminium complexes employed as hydroelementation catalysts have been monometallic, neutral complexes. In Section 1.3, it was observed that the application of heterobimetallic ate complexes often leads to synergistic reactivity allowing new reactivity unattainable to either of the monometallic precursors alone. The enhanced catalytic reactivity of cationic aluminium complexes for hydroamination catalysis was attributed to high Lewis acidity and coordinative unsaturation. Therefore, the application of heterobimetallic aluminate complexes as potential catalysts where the aluminium centre is protected by four anionic ligands may seem counter-intuitive. However, the presence of the cationic alkali metal present in the alkali metal aluminate may still allow for catalytic rate enhancement, because this cationic metal can play a role in the catalysis. Hence changing the alkali metal from lithium to sodium or potassium may induce pronounced alkali metal effects. The Mulvey group has a strong interest in the applications of heterobimetallic complexes and as such it was decided to investigate the applicability of such aluminate complexes as candidates for homogeneous catalysis. Consequently, the overall aims of this PhD were:

- To prepare and characterise new lithium aluminate complexes bearing hydride ligands, for application as (pre)-catalysts in hydroelementation reactions. Full characterisation would be achieved where appropriate by techniques including single crystal X-ray diffraction and IR spectroscopy in the solid state; and in the solution phase by multinuclear NMR spectroscopy including ^{27}Al and ^7Li NMR spectroscopy and 2D NMR studies including ^1H DOSY NMR measurements.
- To determine whether employing heterobimetallic aluminate complexes imparts superior (synergistic) or inferior catalytic activity compared with neutral aluminium complexes and with other monometallic main group catalysts currently reported.
- To identify any structure-activity relationships relating catalyst structure to catalyst efficiency.
- To investigate the reaction mechanisms operating in these hydroelementation reactions employing lithium aluminate (pre)-catalysts by identifying key reaction intermediates, and key reaction steps in the catalytic cycle.

Chapter 2: Lithium diamidodihydrido aluminates: bimetallic cooperativity in catalytic hydroboration and metallation applications

This chapter is based upon a published article:

Chemical Communications, 2018, **54**, 1233 – 1236

Putting the results in context with the literature extended introduction, discussion and conclusion sections are provided in addition to the published manuscript.

Contributing authors to the paper and their roles:

Victoria A. Pollard – Designed and performed the experiments; analysed the data; drafted the manuscript

Samantha A. Orr – Obtained the preliminary crystal structures of compounds **1** and **9**

Ross McLellan – Ran and solved the X-ray diffraction data for compounds **1** and **9**; helped with data processing; contributed to drafting of the manuscript

Alan R. Kennedy – Checked the accuracy of X-ray diffraction data processing

Eva Hevia – Collaborator and secondary PhD supervisor of Victoria A. Pollard

Robert E. Mulvey – Principal investigator

The supporting information can be found in Chapter 7: Experimental; Section 7.2 and Table

7.7.1

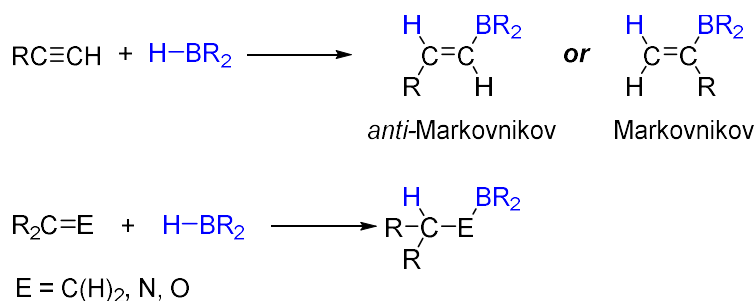
2.1 Abstract

Cooperativity between the lithium and aluminium centres is implicated in catalytic hydroboration reactions of aldehydes and ketones with pinacolborane *via* heteroleptic lithium diamidodihydroaluminates. In addition to implementing hydroalumination, these versatile heteroleptic aates can also perform as amido bases as illustrated with an acidic triazole.

2.2 Introduction

2.2.1 Hydroboration

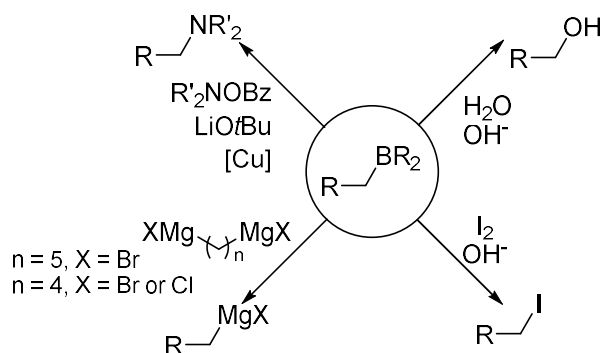
Hydroboration can be defined as the addition of a H – B unit across an unsaturated bond, for example carbon – carbon (e.g.: alkynes and alkenes), carbon – oxygen (e.g.: aldehydes and ketones) or carbon – nitrogen (e.g.: imines, pyridines) bonds, ideally in a regioselective (Markovnikov or *anti*-Markovnikov) and stereoselective (*cis*-addition) manner (Scheme 2.1).⁸



Scheme 2.1: General hydroboration reactions showing typical regio- and stereo-selectivity.

Hydroboration was first introduced by H. C. Brown in 1939 in the uncatalyzed reaction of diborane (B₂H₆) with aldehydes and ketones, resulting in the reduction of the carbonyl bond.¹⁴⁵ This work was subsequently expanded to other unsaturated substrates such as alkenes.¹⁴⁶ Today, hydroboration is one of the most versatile methods in organic synthesis, and the resulting organoborane products can be converted by numerous synthetic transformations to generate the required, value added products.¹⁴⁷ For example, a hydroboration step is utilised in the natural product synthesis of the antibiotic monensin.¹⁴⁸ Scheme 2.2 provides some synthetic

methodology exemplars employed in the transformation of organoboranes, including halogenation, oxidation, amination as well as the synthesis of new organometallic reagents.^{8, 149, 150} The products of hydroboration are also important intermediates in the formation of new carbon – carbon bonds *via* Suzuki-Miyaura cross coupling with an aryl halide and a palladium catalyst.¹⁵¹⁻¹⁵³ As such, organoboranes find widespread application in pharmaceutical synthesis, in the production of agrochemicals as well as advancing asymmetric synthesis and enhancing the development of new organic molecules with novel electronic, optical or mechanical properties.¹⁵⁴



Scheme 2.2: Representative onward functionalisation reactions from hydroboration products

The importance of hydroboration was recognised when Brown was awarded the Nobel Prize in 1956, jointly with Wittig, the citation reading, “*for their development of the use of boron- and phosphorus-containing compounds, respectively, into important reagents in organic synthesis.*”¹⁵⁵

A toxic and pyrophoric gas, the simplest borane, B_2H_6 , also suffers from poor regioselectivity in hydroboration reactions. As such there was a drive to find more user-friendly borane sources, that also exhibited better regioselectivity. A selection of possible hydroborating reagents are depicted in Figure 2.1. Boranes with sterically demanding ligands such as the dimeric 9-borabicyclo(3.3.1)nonane (9-BBN) were shown to have improved regioselectivities over diborane and having the additional benefit of being easy to manipulate solids.¹⁵⁶

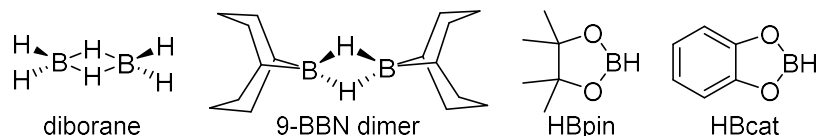


Figure 2.1: A selection of borane reagents employed in hydroboration reactions.

Boronic esters such as pinacolborane (HBpin), which was first prepared by Knochel in 1992, and catecholborane (HBcat) are now widely used as hydroborating reagents.^{157, 158} These reagents have lower Lewis acidities as a result of oxygen lone pair donation into boron's vacant p-orbital and so often higher reaction temperatures, or the use of a catalyst, are required. However, the resulting products tend to be more stable and often can withstand column chromatography allowing for purification and isolation of the target borane products.¹⁵⁷

2.2.2 Catalytic examples of hydroboration

Transition metal catalysed hydroboration has allowed for the preparation of useful boranes under milder conditions than was previously possible. A breakthrough came in 1985 when Männig and Nöth reported the first example of rhodium catalysed hydroboration of alkenes and alkynes with HBcat using Wilkinson's catalyst (RhCl(PPh₃)₃).¹⁵⁹ Since then, a series of metals from across the d-block have been shown to be competent catalysts for hydroboration reactions.¹⁵⁴ This includes examples of catalysts based on Ti,¹⁶⁰ Zr,¹⁶¹ Mn,¹⁶² Fe,^{163, 164} Ru,¹⁶⁵ Co,¹⁶⁶ Rh,¹⁶⁷ Ir,¹⁶⁸ Cu,¹⁶⁹ and Zn.¹⁷⁰

There are also many examples of main group compounds capable of catalysing hydroboration reactions.¹⁷¹ These include: compounds of s-block metals such as Li,^{65, 172} Na,¹⁷³ K,¹⁷⁴ and Mg;⁵³⁻⁵⁸ p-block compounds including B,^{175, 176} Al,^{79, 90, 177-183} Si,¹⁸⁴ Ge,¹⁸⁵ P,¹⁸⁶ As;¹⁸⁷ and even f-block compounds, for example La.¹⁸⁸ Through this vast selection of catalysts it has been proved possible to hydroborate an impressive range of different substrates including carbonyls, alkenes, alkynes, imines, pyridines, isonitriles and even CO₂. As this chapter deals solely with the hydroboration of carbonyls a more in-depth discussion of these particular substrates is provided.

2.2.3 Hydroboration of carbonyls

The selective reduction of carbonyl bonds by hydroelementation processes is a useful synthetic route to industrially important alcohols that avoids the use of explosive and flammable hydrogen gas.¹¹² Of the main group based catalysts listed above the most ubiquitous is undoubtedly Hill's β -diketiminato supported $\text{D}^{\text{IPP}}\text{nacnacMg}n\text{Bu}$ species which has been shown to catalyse the hydroboration of a wide selection of different substrates under relatively mild conditions, including aldehydes and ketones, but it has also been applied to imines, isonitriles and pyridines.⁵³⁻⁵⁸ Okuda has reported the hydroboration of carbonyls using the very active charge-separated s-block metal catalyst $[\text{LiMe}_6\text{-TREN}][\text{HBPPH}_3]$ ($\text{Me}_6\text{-TREN}$ = Tris[2-(dimethylamino)ethyl]amine), in 0.01 mol% catalyst loading, and achieved turnover frequencies (TOF) of over $66,600 \text{ h}^{-1}$.¹⁷⁴ Examples from the p-block include low valent Ge(II) and Sn(II) hydride catalysts which are also notably active for the hydroboration of aldehydes and ketones with TOF values in the range $17 - 13300 \text{ h}^{-1}$.¹⁸⁵ The catalytic hydroboration of aldehydes and ketones has also been reported for several aluminium-based catalysts, such as **I – V** (Figure 2.2)^{79, 178-181} Roesky reported the first aluminium hydride complex, stabilised by a β -diketiminato ligand, **I** (Figure 2.2) that is an active catalyst for the hydroboration of carbonyls.¹⁵ In comparison to **I – IV**, catalyst **V** represents the first example of a tri-coordinate, cationic aluminium complex employed for the hydroboration of aldehydes and ketones, published as recently as 2018.¹⁸¹ Catalyst **V** represents an incredibly Lewis acidic compound, more so even than AlCl_3 or $\text{B}(\text{C}_6\text{F}_5)_3$, as determined by the Gutmann-Beckett method.¹⁸⁹⁻¹⁹¹ Employed in the hydroboration of aldehydes and ketones (with HBcat rather than HBpin) excellent yields were obtained within 5 hours.

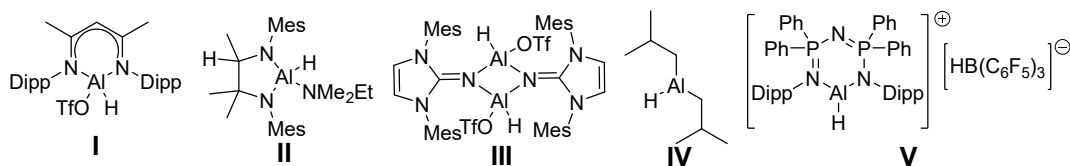
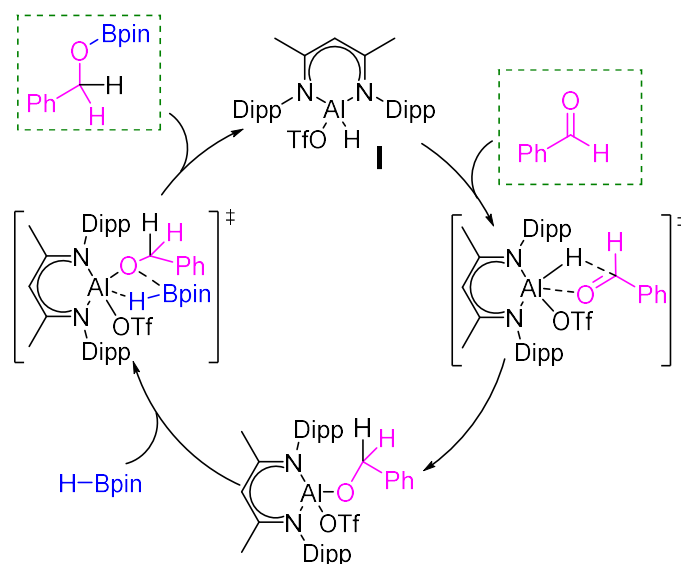


Figure 2.2: Selected reported aluminium hydride catalysts for hydroboration applications.

Based upon the results of DFT calculations, Roesky proposes a catalytic cycle for catalyst **I**, which involves the insertion of the carbonyl group into the Al – H bond, followed by a σ -bond metathesis step with HBpin to generate the product and regenerate the Al – H bond, (Scheme 2.3).⁷⁹ The

insertion step is calculated to have the greatest kinetic energy barrier and so is considered the rate determining step in this particular catalytic cycle. Similar catalytic cycles are proposed for catalysts II, III and V.



Scheme 2.3: Proposed catalytic cycle for the hydroboration of carbonyl groups with catalyst I.

2.3 Project Aims

The aims of this part of the project are summarised below.

- To attempt to synthesise a series of new lithium aluminate complexes bearing hydride ligands.
- To endeavour to grow crystals of these new lithium aluminate complexes to enable full characterisation in the solid state (by single crystal X-ray diffraction, and IR spectroscopy) and in the solution phase (by multinuclear NMR spectroscopy, including ²⁷Al NMR spectroscopy, and DOSY NMR measurements).
- To test these lithium aluminates as catalysts for the hydroboration of aldehydes and ketones.

- To try and gain a good understanding of the relationship between catalyst structure and catalyst reactivity.

2.4 Introduction from the Manuscript

The application of main group complexes in homogeneous catalysis is currently gaining momentum, driven by a quest to supplement expensive and low abundant precious transition metals by more earth abundant sustainable alternatives. Aluminium is the most abundant metal in the Earth's crust and has low toxicity. Its compounds have therefore been the focus of an increasing number of studies and find application in a range of chemical processes including as catalysts for dehydrocoupling, hydrosilylation and hydroboration,^{15, 16, 90} as well as small molecule activation by frustrated Lewis pairs (FLP)¹⁹²⁻¹⁹⁴ and trans-metal-trapping.¹³⁵ Catalytic hydroboration of aldehydes and ketones has been reported for several aluminium-based catalysts, such as I – IV (Figure 2.2).^{79, 178-180} Roesky reported one of the first aluminium hydride complexes stabilised by a β -diketiminato ligand, I (Figure 2.2) that is an active catalyst for hydroboration of terminal alkynes and organic carbonyls.¹⁵ Notably, Cowley and Thomas utilised DIBAL, IV (Figure 2.2), and Et₃Al·DABCO for alkyne hydroboration (DABCO = 1,4-diazabicyclo[2.2.2]octane).¹⁷⁸

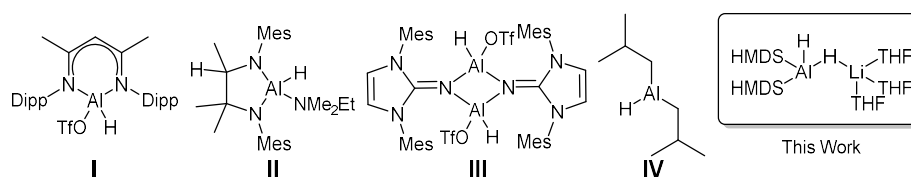


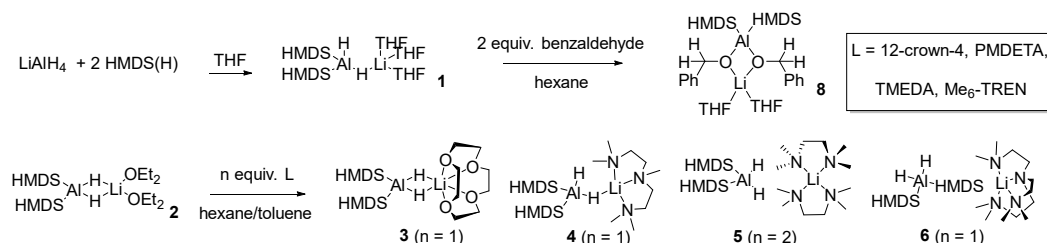
Figure 2.2: Selected reported aluminium hydride catalysts for hydroboration reactions.

It is significant that to date most aluminium-based catalysts for such hydroboration reactions involve neutral complexes. Given our interest in bimetallic systems that can function synergistically under stoichiometric regimes,¹⁰⁷ and recent advances suggesting that borates are crucial reaction intermediates in hydroboration,^{173, 176} we propose that aluminates would exhibit even greater reactivity. In this contribution we introduce anionic complexes to this important emerging area through a series of heteroleptic lithium diamidodihydridoaluminate complexes

with the bulky 1,1,1,3,3,3-hexamethyldisilazide ligand [HMDS, (Me₃Si)₂N⁻]. We show that: (i) the performance of the anionic [(HMDS)₂Al(H)₂]⁻ moiety in hydroboration reactions of aldehydes and ketones can be influenced by the nature of Lewis donor solvation of the lithium centre; (ii) an intermediate from a stoichiometric reaction with benzaldehyde retains both metal centres following hydride transfer; and (iii) while HMDS acts as a stabilising spectator in the hydroboration reactions, it can operate as a base with a suitably acidic aromatic substrate, establishing the dual functionality of these ates.

2.5 Results and Discussion

Reaction of LiAlH₄ with two equivalents of HMDS(H) in THF yielded the heteroleptic diamidodihydride (HMDS)₂AlH(μ-H)Li(THF)₃, **1**, as colourless crystals in 61% yield. Figure 2.3(a) shows the molecular, contacted ion pair (CIP) structure of **1**. A Cambridge Structural Database search identified a similar compound, (HMDS)₂Al(μ-H)₂Li(OEt)₂, **2**, prepared by Stalke.¹⁹⁵ Complex **1** contains one terminal hydride and one bridging hydride ligand between the aluminium and lithium centres, whereas both hydrides bridge in **2**. Towards obtaining a solvent-separated ion pair (SSIP) variant, donor ligand exchange was performed on **2** with 12-crown-4 (1,4,7,10-tetraoxacyclododecane), PMDETA, TMEDA, and Me₆-TREN (Scheme 2.4).



Scheme 2.4: Synthesis of heteroleptic lithium diamidodihydridoaluminate complexes **1** – **6**, and of bis-benzyloxy complex, (HMDS)₂Al(μ-OCH₂Ph)₂Li(THF)₂, **8**.

The products (HMDS)₂Al(μ-H)₂Li(L) (L = 12-crown-4, **3**), (HMDS)₂AlH(μ-H)Li(L) (L = PMDETA, **4**) and [(HMDS)₂AlH₂][Li(L)] [L = (TMEDA)₂, **5** or Me₆-TREN, **6**] were obtained. Figure 2.3 depicts the crystallographically determined structures of **1**, **3**, and **5**, with those of **4** and **6** in Section 2.5: Extended discussion. In **3** both hydrides bridge and 12-crown-4 binds to lithium in a κ⁴ manner. Compound **4** has only one bridging hydride, with the second bonded solely to aluminium. TMEDA

and Me₆-TREN, generated solvent separated ion pairs (SSIPs) **5** and **6** respectively. In **5** and **6** the hydrides reside on aluminium centres. The lithium centre in **5** is in a distorted tetrahedral environment, while in **6** the Me₆-TREN chelates lithium leaving one face of it open for contacts between lithium and hydrogen atoms on a HMDS on the neighbouring Al centre [Li...H-CH₂ distance 2.41(1) Å and 2.99(1) Å].

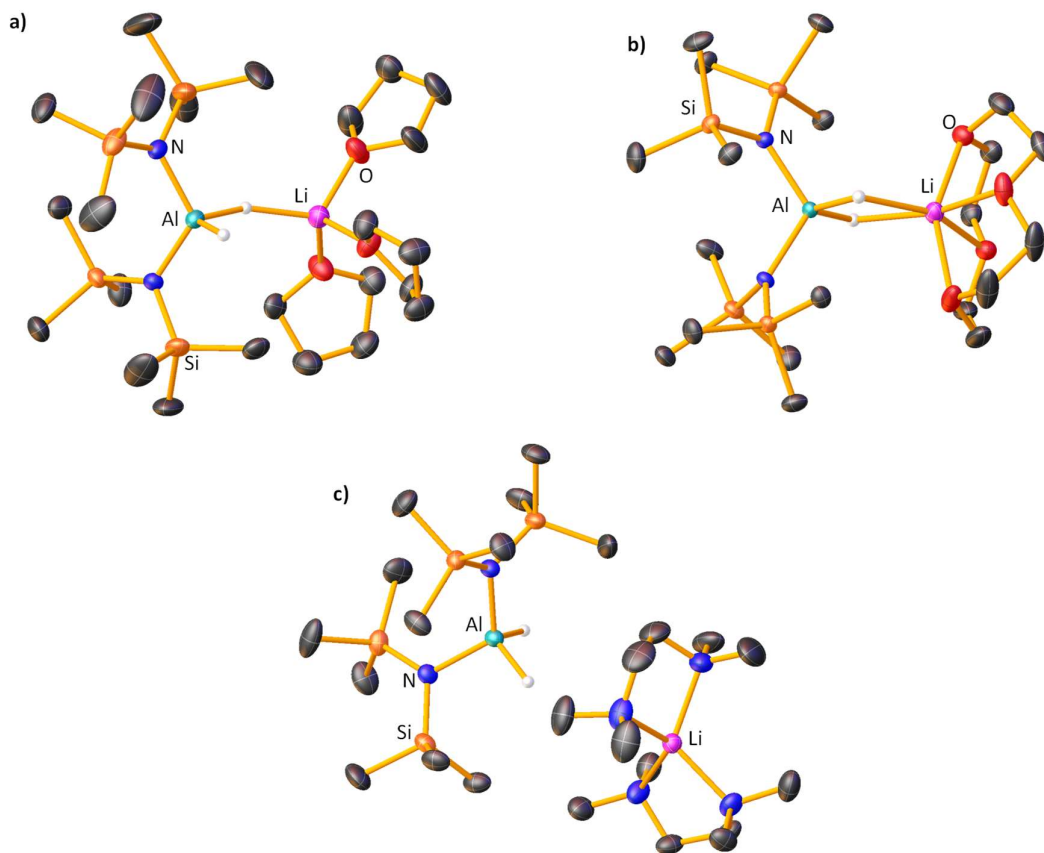


Figure 2.3: Molecular structures of (a) **1**, (b) **3** and (c) **5**. Hydrogen atoms except hydrides, and disordered THF in **1** and TMEDA in **5**, and co-crystallised toluene in **3** have been omitted.

Thermal ellipsoids are drawn at 40% probability.

Note Okuda studied ligand effects on the rate of hydroboration catalysis with [(L)Li][HBPh₃], finding Me₆-TREN to be superior to other ligands tested.¹⁹⁶ A sodium analogue of **1** made using NaAlH₄ generated **7**, (HMDS)₂AlH(μ-H)Na(THF)₄ (see 2.5 Extended discussion). For complexes **1** and **4** – **6** terminal Al–H bond lengths lie in the range 1.54(2)–1.61(5) Å, while the Al – μH range

[1.57(2)–1.61(2) Å] is similar. Li – H bond lengths for **1** and **4** are 1.83(2) Å and 1.81(2) Å, respectively. These compare to those in **2** (Al–H 1.62(2)/1.55(2) Å, Li – H 1.89(2)/1.97(2) Å). In comparison, **3** has longer Li – H bond lengths of, 2.13(2) Å and 2.11(2) Å.

In all cases, it was not possible to observe the hydride signals in the ^1H NMR spectrum. This is unsurprising since both ^{27}Al and ^7Li are quadrupolar nuclei. However, a $^1\text{H}\{^{27}\text{Al}\}$ NMR experiment revealed a new, broad singlet at approximately 3.8 ppm in each case. Integrating to two, this signal lies in the expected chemical shift range for an Al – H signal. In crystalline **1** and **4** the hydrides are inequivalent, and so the broad singlet in $^1\text{H}\{^{27}\text{Al}\}$ NMR indicates that the exchange of the inequivalent hydrides is fast on the NMR time scale. However, a variable temperature $^1\text{H}\{^{27}\text{Al}\}$ NMR experiment with **1** (–40 °C to 70 °C) did not give a sharp singlet, or the resolution of two signals. In comparison, the ^1H NMR chemical shifts for the hydride signals in $\text{LiAlH}_4 \cdot \text{Me}_6\text{-TREN}$ appear as a broad singlet at 3.86 ppm.¹⁹⁷ A high temperature ^{27}Al NMR experiment on **3** shows that as the temperature is increased the signal becomes sharper, and at 70 °C a triplet is resolved ($^1J_{\text{Al-H}}$, 173.6 Hz) (Figure 2.4). This is consistent with reported $^1J_{\text{Al-H}}$ couplings (e.g., for $[\text{AlH}_2(\text{NEt}_2)_2]^-$, 175 Hz).⁴⁴

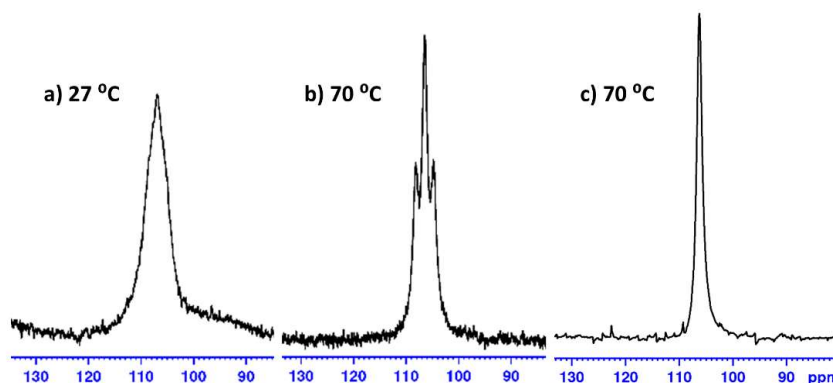


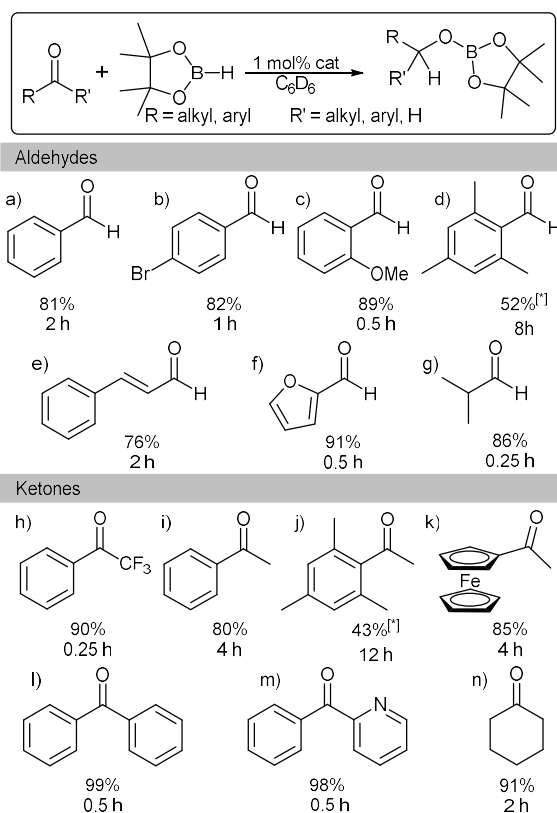
Figure 2.4: (a) and (b) ^{27}Al NMR spectra of **3**; a triplet resolves at 70 °C, $^1J_{\text{Al-H}} = 173.6$ Hz. (c) $^{27}\text{Al}\{^1\text{H}\}$ NMR experiment shows the triplet has collapsed to a singlet. NMR spectrum recorded in C_6D_6 solution.

Despite the SSIP structures in solid **5** and **6**, DOSY (Diffusion Ordered Spectroscopy) NMR studies for **1** – **6** indicate that all species are contacted ion pairs (CIP) in C_6D_6 solution (See 2.5 extended

discussion). Thus, the level of solvation on the lithium centre appears to play a key role in the resulting catalytic performance (see below).

Several examples exist of aluminium hydrides that can act as catalysts for hydroboration of carbonyls.¹⁵ Encouraged by these studies we screened **1** for catalytic activity. Benzaldehyde, pinacolborane (HBpin), and a catalytic loading of **1** (1 mol%) in C₆D₆ were placed in a J. Young's NMR tube and the ¹H and ¹¹B NMR spectra were monitored over time. After 2 hours, 81% of the hydroborated product was obtained. (Table 2.1; entry a). The substrate scope includes a range of functional groups (Table 2.1; a – g). Notably, halides are compatible with this system; 4-bromobenzaldehyde was cleanly converted to the borate ester in 82% yield in 2 hours. The α,β -unsaturated cinnamaldehyde was selectively hydroborated at the carbonyl group in 76% yield. The bulky mesitaldehyde required heating to 70 °C for 8 hours to obtain 52% yield, with no further conversion observed over 16 hours.

Table 2.1: Catalytic hydroboration of aldehydes and ketones using **1** in C₆D₆.



Catalysis performed in C₆D₆, at room temperature, 1 mol% pre-catalyst. ¹H NMR yields relative to internal standard hexamethylcyclotrisiloxane. [*] heated to 70 °C.

In comparison to **1**, Nembenna used 0.5 – 1 mol% of **II** (Figure 2.1) to achieve good to excellent yields at room temperature in 0.33 hours with a range of aldehydes.¹⁷⁹ Hydroboration of ketones was examined next, using 1 mol% of **1** in C₆D₆ at room temperature. Reaction times were generally found to be longer than with aldehydes. Again, a range of different functionalities were tolerated (Table 2.1; h – n). Heteroaromatics are compatible: 2-benzoylpyridine is hydroborated cleanly at the carbonyl. As with mesitaldehyde, bulky 2,4,6-trimethyl acetophenone required heating at 70 °C. Deprotonation of the acidic (C=O)Me group could possibly be interfering in this case, though NMR data did not show any significant amounts of the corresponding Bpin enolate.

Alkyl ketones are also tolerated with cyclohexanone requiring 2 hours to reach 91% yield. These results are in keeping with those with other aluminium catalysts: for example, Nembenna used 2 mol% of **II** (Figure 2.3) to hydroborate a range of ketones in high yields in 3 – 4 hours,¹⁷⁹ while Roesky used 2 mol% of **I** for hydroboration of acetophenone (51% in 6 hours).⁷⁹ **1** achieves 80% yield in 4 hours with acetophenone.

The stoichiometric reaction of **1** with two equivalents of benzaldehyde yielded crystals of hydrometallated product **8**, (HMDS)₂Al(μ-OCH₂Ph)₂Li(THF)₂ (Scheme 2.4 and Figure 2.5).

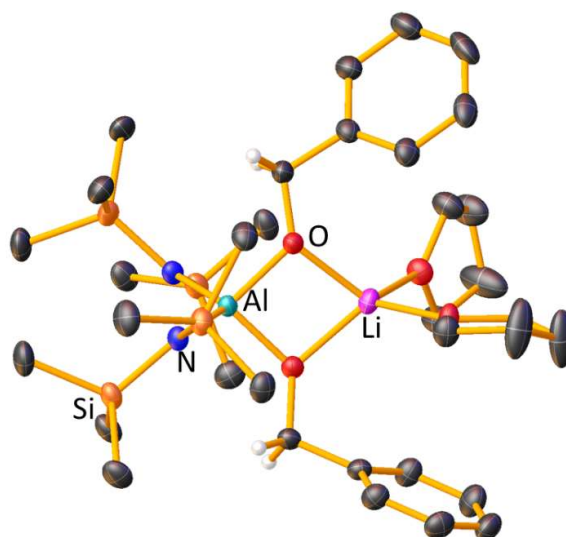


Figure 2.5: Molecular structure of **8**, disordered THF ligands and hydrogen atoms (except benzyloxy CH₂) omitted for clarity. Thermal ellipsoids drawn at 40% probability.

Roesky used DFT calculations to propose that the rate determining step of carbonyl hydroboration by aluminium catalyst, **1**, is hydroalumination to give a benzyloxy product.⁷⁹ Compound **8**, as the hydrometallated product, is in keeping with this postulate, though here the substrate initially binds to lithium not aluminium. Significantly, applying **8** in a catalytic quantity (1 mol%) for hydroboration of benzaldehyde with HBpin generates the desired product in 80% yield after 2 hours. This result is akin to that using catalytic **1**, proving that **8** is catalytically competent. The catalysis with sodium analogue **7** was found to be less efficient than **1**, suggesting a possible alkali metal effect. LiAlH₄ was also tested for catalytic activity using solid LiAlH₄ in 10 mol% (for ease of weighing owing to its lower molecular weight), and for comparison the catalysis with **1** was repeated using 10 mol% (0.05 mmol). It was found the catalysis with 10 mol%

of **1** reached 81% within 0.25 hours before the reaction plateaued out, whereas using catalytic LiAlH_4 gave 94% within 0.25 hours. Catalyst deactivation may be responsible for the yield of product plateauing out. While this result is slightly better, unlike LiAlH_4 , **1** hydrolyses slowly, is easily employed in known lower catalyst loadings, and has a well-defined molecular structure that provides insights into the tandem hydroalumination process (*e.g. via 8*). Surprisingly, LiAlH_4 has only been used catalytically in a few instances including the hydrosilylation of olefins and dehydrocoupling of amine boranes.^{97, 198-200}

Next, the Lewis donor effect on the catalysis was probed using acetophenone as substrate. Table 2.2 shows a perceptible trend in catalysis efficiency. For example, **1**, bearing three labile THF ligands outperforms **4**, containing the non-labile chelating PMDETA ligand. This fact may be due to the ease of displacement of THF compared with one arm of the PMDETA ligand, which would inhibit access of substrate to the active metal centre(s) in a catalytic regime. Expanding upon this idea we repeated hydroboration of acetophenone with **1** and **4** in bulk d_8 -THF, rationalising that catalysis would proceed in similar rates, since excess THF replaces the PMDETA ligand from **4**. In each case the NMR yield after 4 hours is *ca.* 95%, giving credence to the dramatic solvent effects displayed in these systems in C_6D_6 . These data imply the catalysts operate through bimetallic cooperation with the hydride transfer emanating from aluminium, but the initial substrate coordination occurring at lithium, the ease of which depends on the relative lability of the donor ligands. This idea is supported by the structure of **8** where the reduced substrate bridges both aluminium and lithium centres.

Table 2.2: Effect on rate of hydroboration of acetophenone by changing the catalyst.

Pre-catalyst	X-ray structure	DOSY structure	% Yield at 4 h
1	CIP	CIP	80
2	CIP	CIP	60
3	CIP	CIP	50
4	CIP	CIP	29
5	SSIP	CIP	55
6	SSIP	CIP	15
7	CIP	CIP	57
1 ^[a]	CIP	CIP	81 ^[b]
LiAlH ₄ ^[a]	-	-	94 ^[b]
1 ^[c]	CIP	CIP	95 ^[d]
4 ^[c]	CIP	CIP	99 ^[d]

Reactions performed in C₆D₆, room temperature, 1 mol% of pre-catalyst, all yields relative to internal standard hexamethylcyclotrisiloxane. ^a 10 mol% pre-catalyst. ^b Yield obtained within 0.25 hours. ^c Catalysis performed in d₈-THF, 1 mol% pre-catalyst, room temperature. ^d Yield obtained within 2 hours.

Hydroboration relies on **1** donating a hydride to the carbonyl substrate, however we envisaged other reactivity modes may be available to it. Roesky demonstrated hydroboration of terminal alkynes with HBpin to yield boronate esters with deprotonation a pivotal step.⁹⁰ In that case hydride was the base, but we pondered whether **1** could also exhibit amido basicity. Preliminary investigations with 1-methyl-1,2,4-triazole gave (HMDS)AlH(μH)[C₃H₄N₃]Li(THF), **9** (yield, 55%) in which the triazole has been aluminated at C5 (Figure 2.6).

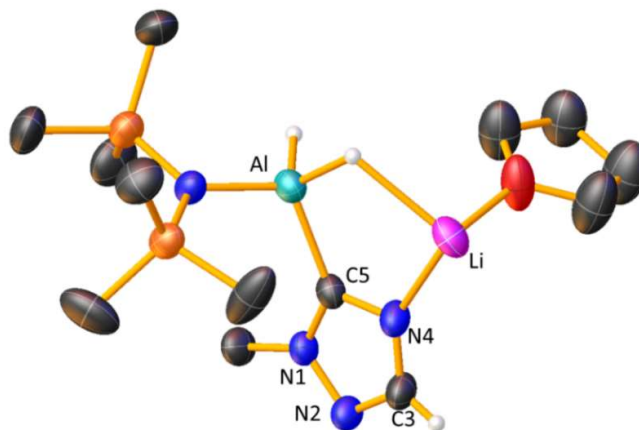


Figure 2.6: Asymmetric unit of polymeric structure **9** with triazole ring atoms labelled. Hydrogen atoms (except hydride and C3 – H) and disordered THF molecules have been omitted for clarity. Thermal ellipsoids are drawn at 40% probability.

Here one HMDS ligand acts as an internal base. Conforming to the cooperativity between the two metals, the lithium also remains within **9**, coordinated to N4 on the triazole ring. Crystalline **9** exists as a one-dimensional polymeric chain propagating *via* Li–N2 bonds between asymmetric units (see ESI). Metallation of triazoles typically requires careful control of reaction conditions, with the metallated intermediates fragmenting at ambient temperature,²⁰¹⁻²⁰³ so it is significant this reaction occurred at room temperature.

In conclusion, this first application of anionic aluminates for hydroboration of aldehydes and ketones establishes that coordination of lithium plays a part though hydride transfer occurs from aluminium, signifying a bimetallic process.

2.6 Extended Discussion

2.6.1 Structure activity relationships for catalytic competence

Figure 2.7 shows the molecular structures of compounds **4**, $\text{HMDS}_2\text{AlH}_2\text{Li}(\text{PMDETA})$, and **6**, $[\text{HMDS}_2\text{AlH}_2][\text{Li}(\text{Me}_6\text{-TREN})]$. In the solid state **4** exhibits a contacted ion pair structure, while

6 has a solvent-separated ion pair structure. However, in C_6D_6 solution both compounds appear to be contacted ion pairs, as determined by 1H DOSY NMR measurements.

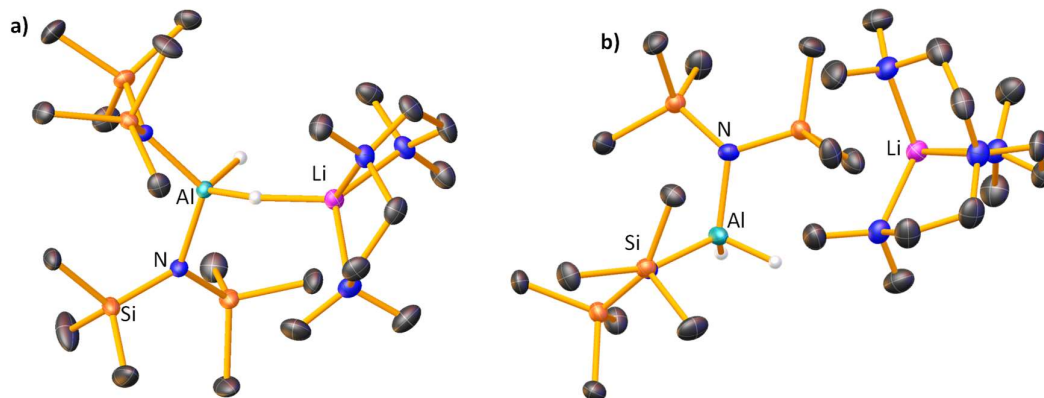


Figure 2.7: Molecular structures of aluminate a) **4** and b) **6**. Hydrogen atoms except hydrides have been removed for clarity. Thermal ellipsoids drawn at 40% probability.

DOSY NMR spectroscopy is a 2D technique which correlates 1H NMR chemical shift data with the separation of species by their diffusion coefficient.²⁰⁴ This method has been applied in several different areas of chemistry with the purpose of estimating molecular volumes, determining the degree of aggregation of compounds, and studying host-guest interactions.²⁰⁵ Recently, Stalke has reported a new methodology to determine the molecular weight of small molecules using external calibration curves (ECC), with normalised diffusion coefficients.^{206, 207} This method takes into account the shape of the molecules and is independent of temperature, viscosity and NMR spectrometer differences.

In this instance, 1H DOSY NMR is applied to provide an estimation of molecular weights of the lithium aluminates employing either tetramethylsilane (TMS) or 1,2,3,4-tetraphenyl-naphthalene as internal standards, in line with Stalke's ECC method. From these estimated molecular weights, it is possible to determine if the lithium cation and anionic aluminium moiety are diffusing together or separately; and thereby, establish whether the lithium aluminate exists as a contacted ion pair or a solvent-separated ion pair, in C_6D_6 solution. As Figure 2.8; Table 2.3, and Figure 2.9; Table 2.4 display, both compounds **4** and **6** diffuse as contacted ion pairs in C_6D_6 solution.

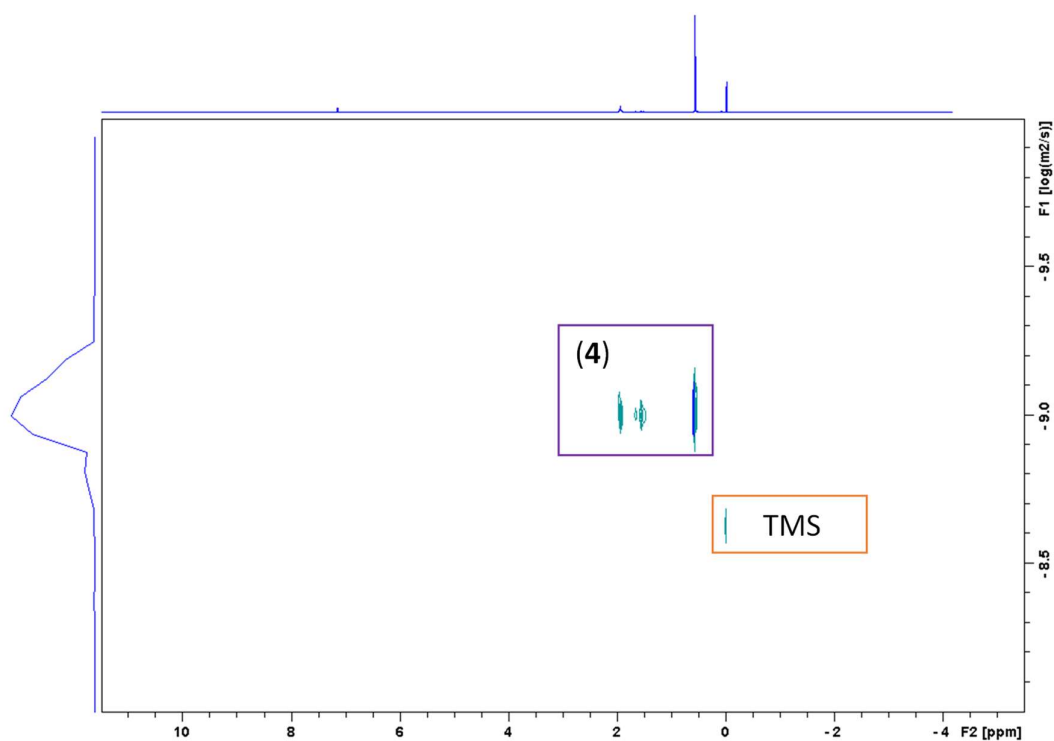


Figure 2.8: ^1H DOSY NMR spectrum of **4**, in C_6D_6 solution.

Table 2.3: Diffusion coefficient data from ^1H DOSY NMR spectrum of **4**, in C_6D_6 solution.

Signal	D [m^2s^{-1}]	MW_{calc} [g mol^{-1}]	MW_{est} [g mol^{-1}]	Error [%]
PMDETA	7.87×10^{-10}	530.02	535	-1 (HMDS ₂ AlH ₂ LIPMDETA) (4)
HMDS	8.07×10^{-10}	530	530	0 (HMDS ₂ AlH ₂ LiPMDETA) (4)
TMS	1.667×10^{-9}	88.23	90	-2 (TMS)

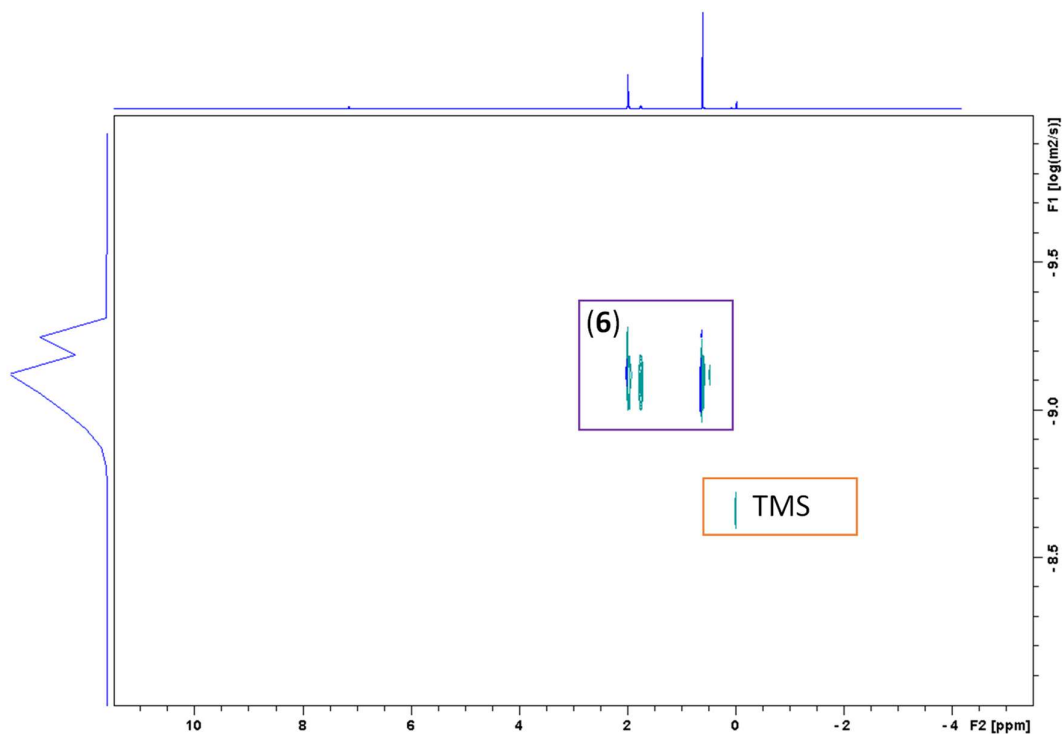


Figure 2.9: ^1H DOSY NMR spectrum of **6**, in C_6D_6 solution.

Table 2.4: Diffusion coefficient data from ^1H DOSY NMR spectrum of **6**, in C_6D_6 solution.

Signal	D [m^2s^{-1}]	MW_{calc} [g mol^{-1}]	MW_{est} [g mol^{-1}]	Error [%]
$\text{Me}_6\text{-TREN}$	6.724×10^{-10}	586.48	638	-8 [HMDS ₂ AlH ₂ Li(Me ₆ -TREN)] (6)
HMDS	6.776×10^{-10}	586.48	653	-10 [HMDS ₂ AlH ₂ Li(Me ₆ -TREN)] (6)
TMS	1.189×10^{-9}	88.07	90	-2 (TMS)

A similar scenario is observed for the related aluminate compounds **1** – **3** and **5**. However, when a ^1H DOSY NMR spectrum is recorded for **4** in $d_8\text{-THF}$ the PMDETA signals appear to be diffusing separately from the rest of the molecule; and also the chemical shifts of the PMDETA signals agree with a standard of the free ligand in $d_8\text{-THF}$ (Figure 2.10 and Table 2.5). Meanwhile the diffusion coefficient associated with the HMDS ligands corresponds to a

molecular weight similar to that of **1**. Thus, it can be surmised that the PMDETA ligand has been displaced by the bulk THF solution. That the degree of, and type of solvation at the lithium centre have an effect on the rate of the hydroboration of acetophenone suggests that the lithium has a role to play and that it is not solely the Al – H that contributes to the catalytic process (Table 2.2).

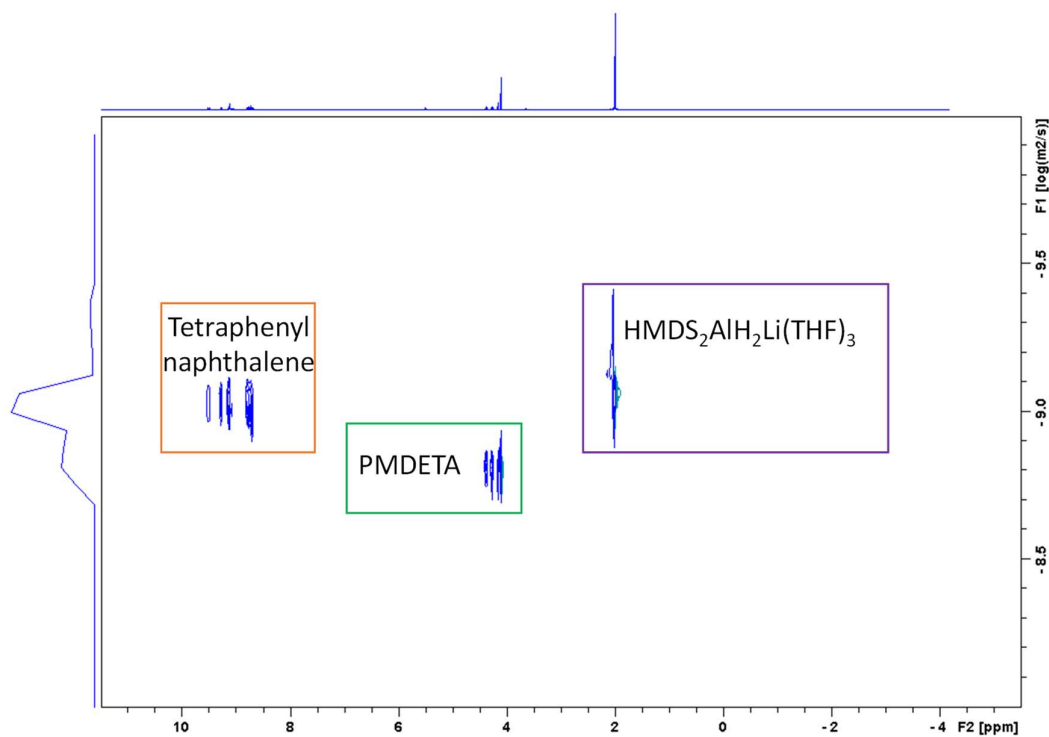


Figure 2.10: ¹H DOSY NMR spectrum of HMDS₂AlH₂Li(PMDETA), **4**, in d₈-THF solution.

Table 2.5: Diffusion coefficient data from ^1H DOSY NMR spectrum of $\text{HMDS}_2\text{AlH}_2\text{Li}(\text{PMDETA})$, **4**, in d_8 -THF solution.

Signal	D [m^2s^{-1}]	MW _{calc} [g/mol]	MW _{est} [g/mol]	Error [%]
PMDETA	1.218×10^{-9}	173.3	196	14 ['free' PMDETA]
HMDS	6.944×10^{-10}	569.36	562	-1 [$\text{HMDS}_2\text{Al}(\mu\text{-H})_2\text{Li}(\text{THF})_3$] (1)
1,2,3,4-Tetra phenylnaphthalene	7.63×10^{-10}	432.55	437	-1 [tetraphenylnaphthalene]

A selection of substrates and catalytic conditions for catalysts **I**–**III** are provided in Table 2.6 and compared with the results for aluminate **1** from this study (Figure 2.11). Catalyst **III** required a higher catalyst loading (4 mol%) than **I** (1 mol%), **II** (0.5 – 1 mol%) or catalyst **1** (1 mol%) for both aldehydes and ketones. With regards to the ketones, catalyst **III** also required elevated temperatures (50 °C) in contrast to the other catalysts (room temperature). Note that Nembenna made use of solvent-free conditions for liquid substrates with catalyst **II**. A recent study on catalyst-free hydroboration of aldehydes and ketones showed that to achieve good yields of boronic ester products solvent-free conditions were necessary.²⁰⁸ Running the same catalyst-free reaction of benzaldehyde in toluene solvent significantly reduced the yield of product from 95% within 1 hour to only traces observed. However, with the solid substrate benzophenone catalyst **II** still achieves an excellent yield (92%) with a short reaction time (4 hours). In comparison with **1**, Roesky's catalyst **I** provides better yields and reaction times with aldehydes. Substrates with increased steric bulk at the aldehyde are challenging for catalyst **1** and require elevated temperatures to achieve good yields within short reaction times. Catalysts **II** and **III** are more efficient catalysts than **1** for this mesitaldehyde substrate, as they are able to catalyse this substrate at room temperature. With respect to ketones, compound **1** was employed in a lower catalytic loading (1 mol%) than catalysts **I**–**III** (2 mol% for **I** and **II**, and 4 mol% for **III**) and achieves similar yields within similar reaction times.

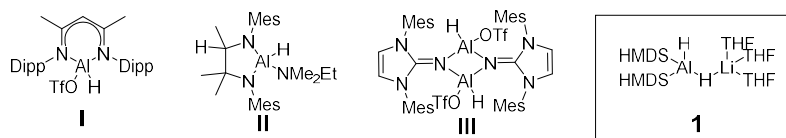


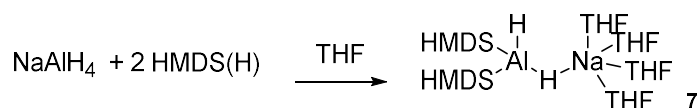
Figure 2.11: Selected reported Al – H hydroboration catalysts for key substrates, and compound **1**.

Table 2.6: Summary of hydroboration capabilities of selected reported Al – H catalysts for key substrates.

Catalyst	I	II	III	Compound 1
Aldehydes	1 mol%, C ₆ D ₆ , RT	0.5 – 1 mol%, RT	4 mol%, C ₆ D ₆ , RT	1 mol%, C ₆ D ₆ , RT
Benzaldehyde	99%, 1 h	99%, 0.33 h (neat)	91%, 24 h	81%, 2 h
Mesitaldehyde	n/a	99%, 0.33 h (neat)	85%, 24 h	52%, 8 h (70 °C)
Cinnamaldehyde	99%, 6 h	n/a	n/a	76%, 2 h
Ketones	2 mol%, C ₆ D ₆ , RT	2 mol%, RT	4 mol%, C ₆ D ₆ , RT	1 mol%, C ₆ D ₆ , RT
Benzophenone	n/a	92%, 4 h (C ₆ D ₆)	7%, 6 h (60 °C)	99%, 0.5 h
Acetophenone	51%, 6 h	93%, 3 h (neat)	53%, 6 h (60 °C)	80%, 4 h
Cyclohexanone	n/a	89%, 3 h (neat)	n/a	91%, 2 h

n/a: data not available for these substrates.

Sodium aluminate **7**, (HMDS)₂AlH(μ-H)Na(THF)₄, (Figure 2.11 and Scheme 2.5) was prepared as a sodium analogue of **1** in order to test for any difference in reactivity as a result of the identity of the alkali metal cation. When **7** is employed as a catalyst for the hydroboration of acetophenone it was found to be slower than when lithium compound **1** was used (57% *versus* 80% after 4 hours). The slower catalysis with **7** (Na) than of **1** (Li) could be due to the larger radius of sodium compared with lithium which will provide a poorer orbital overlap with the oxygen atom of the ketone. Thus, initial coordination of the substrate to the catalyst is less efficient.



Scheme 2.5: Synthesis of sodium analogue, $\text{HMDS}_2\text{Al}(\mu\text{-H})_2\text{Na}(\text{THF})_4$, **7**.

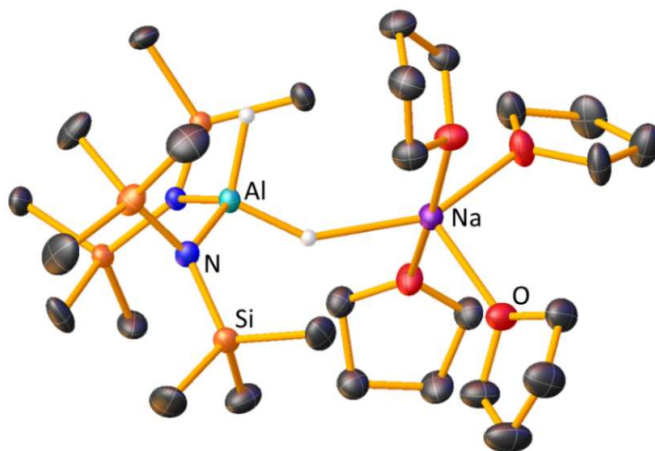


Figure 2.11: Molecular structure of **7**. Hydrogen atoms except hydrides and disordered THF ligands have been removed for clarity. Thermal ellipsoids drawn at 40% probability.

2.6.2 Related unpublished work

The primary objective of this part of the project was to synthesise and characterise a series of lithium aluminate compounds and then apply them as catalysts for the hydroboration of aldehydes and ketones. Aluminate **1** possesses the ability of reacting *via* hydridic mechanisms in the reaction with aldehydes, yielding $(\text{HMDS})_2\text{Al}(\mu\text{-OCH}_2\text{Ph})_2\text{Li}(\text{THF})_2$, **8**, and this reactivity is what drives the catalytic turnover in the hydroboration catalysis. It was also observed that **1** can alternatively react *via* the amido ligands, demonstrated in the deprotonation of the acidic substrate 1-methyl-1,2,4-triazole. Further work was undertaken with the hope of crystallising the metallated product of a range of other acidic substrates such as phenyl acetylene, benzoxazole and benzothiazole (Figure 2.12).

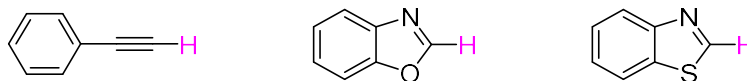
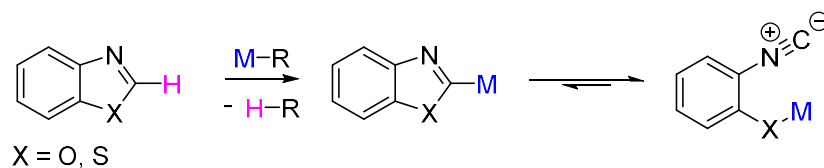


Figure 2.12: Other substrates employed for metallation with **1**.

However, despite repeated attempts no crystallisation of a metallated product was possible for any of the three substrates. Turning to NMR scale reactions, reaction of **1** with phenyl acetylene in C_6D_6 solution within 1 hour at room temperature caused the disappearance of the terminal C – H signal in the 1H NMR spectrum (δ 2.73 ppm) with the concomitant formation of extra signals in the region of the HMDS ligand signals. Crucially there was no indication of the formation of H_2 (δ 4.47 ppm). This is indicative of deprotonation *via* amide basicity rather than hydridic deprotonation. Further, reaction of phenyl acetylene by the closely related lithium aluminate [*i*Bu₂Al(TMP)(H)Li] is proposed to occur *via* TMP deprotonation, however as is the case here it was not possible to isolate any crystals from this reaction mixture.²⁰⁹ Reaction of **1** with both benzoxazole and benzothiazole were inconclusive, leading to a complex mixture of products; but again no signals for H_2 were observed in the 1H NMR spectrum. Deprotonation of benzoxazole and benzothiazole at the acidic C2 position often leads to ring opening of the heterocycle (Scheme 2.6).²¹⁰ It is therefore possible that ring opening is occurring in these reactions with **1**. Examples of metallation of 1,3-benzazoles with main group metals is scarce in the literature, with examples known only with Mg,²¹¹ Sn,²¹² and Ga.²¹³



Scheme 2.6: Equilibrium of C2 deprotonated 1,3-benzazoles and their ring opened isomers.

2.7 Conclusions

This part of the research project documented the first application of anionic aluminates for hydroboration of aldehydes and ketones establishing that coordination at lithium is one important factor in the rate of the Al – H catalysis. The preparation and structural characterisation of a series of lithium aluminate complexes with different Lewis donor ligands at the lithium centre make this conclusion possible. A diversity of solid-state structures were found for these lithium aluminium hydrides including solvent-separated ion pairs, such as **5** and **6**; as well contacted ion pairs with either one (compounds **1** and **4**) or two (compounds **2** and **3**) bridging hydrides. However, in spite of these structural differences in the solid state, compounds **1**, **3** – **6** all seem to exhibit contact ion pair structures in C₆D₆ solution. The application of these compounds as (pre)-catalysts for the hydroboration of aldehydes and ketones signifies that coordination at the lithium centre is an important factor in the rate of the catalysis. Employing more sterically demanding ligands, or more strongly binding, chelating ligands significantly hinders the speed of catalysis, confirming that the coordination to the lithium centre must play a role at some stage in the catalytic cycle. However, hydride transfer occurs from aluminium, identifying this as a genuine cooperative bimetallic process. The isolation of compound **8** indicated a potential intermediate on the catalytic pathway. That **8** is catalytically active to a similar level as **1** provides further support that **8** could be implicated in the catalysis. The presence of both lithium and aluminium centres, with bridging benzyloxy units strengthens the hypothesis that the hydroboration catalysed by **1** is a bimetallic process. That sodium analogue **7** exhibits decreased catalytic activity compared with the lithium analogue **1** adds more credence to the view that the alkali metal cannot be ignored for a full understanding of this novel catalytic system.

In comparison with the aluminium-based catalysts for hydroboration of aldehydes and ketones reported in the literature, our charged, bimetallic system is comparable with previously published neutral aluminium catalysts. The work outlined in this chapter represents the first example of a charged bimetallic aluminate catalyst for hydroboration of aldehydes and ketones. Further work within our group on a related lithium aluminate system, *i*Bu₂Al(TMP)(H)Li.L (L = ligand, for example PMDETA, THF, or DABCO) drew similar conclusions, further reiterating the bimetallic nature of these types of catalysts.²⁰⁹ Pinpointing the exact nature of the role each metal centre plays in the catalysis is challenging and will likely need theoretical modelling to unravel the complexity involved.

Chapter 3: Comparing Neutral (Monometallic) and Anionic (Bimetallic) Aluminium Complexes in Hydroboration Catalysis: Influences of Lithium Cooperation and Ligand Set

Published Article:

Angewandte Chemie International Edition, 2018, **57**, 10651 – 10655

Putting the results in context with the literature an extended introduction, discussion and conclusion are provided in addition to the published manuscript.

Contributing authors to the paper and their roles:

Victoria A. Pollard - Designed and performed the experiments; analysed the data; contributed to drafting of the manuscript

M. Ángeles Fuentes – Ran and solved the crystal structure of compound **15**

Ross McLellan – Helped with data processing and drafting of the manuscript

Alan R. Kennedy – Checked the accuracy of X-ray diffraction data processing

Robert E. Mulvey – Principal investigator

The supporting information can be found in Chapter 7: Experimental; Section 7.3 and Table 7.6.2

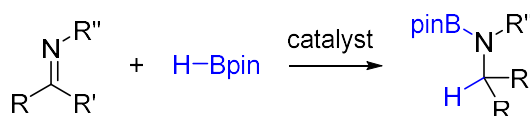
3.1 Abstract

Bimetallic lithium aluminates and neutral aluminium counterparts are compared as catalysts in hydroboration reactions with aldehydes, ketones, imines and alkynes. Possessing Li – Al cooperativity, ate catalysts are found to be generally superior. Catalytic activity is also influenced by the ligand set: alkyl and/or amido. Devoid of an Al – H bond, *i*Bu₂Al(TMP) operates as a masked hydride, reducing benzophenone through a β – H transfer process. This catalyst library therefore provides an entry point into the future design of aluminium catalysts targeting substrate specific transformations.

3.2 Introduction

3.2.1 Hydroboration of more challenging substrates: Imines, and C – C unsaturated bonds

Whilst there has been a huge surge in the catalysed hydroboration of aldehydes and ketones, other important unsaturated substrates such as imines have been less examined (Scheme 3.1). This is surprising as the resulting amines are important precursors in chemicals used in pharmaceutical, agricultural and food chemistry.¹⁵⁴ However, since 2016 there has been a significant increase in reports of the catalytic hydroboration of imines, where the catalyst is based on different transition metals, such as Re,²¹⁴ Ru,²¹⁵ Co,²¹⁶ Ni,²¹⁷ and Zn.²¹⁸ Main group complexes have also been reported as catalysts but to a much more limited extent and research has focused mainly on complexes of Li,²¹⁹ Mg,^{55, 220} B,²²¹ Si,¹⁸⁴ and P^{222, 223} (Figure 3.1).



Scheme 3.1: General reaction scheme for the hydroboration of imines.

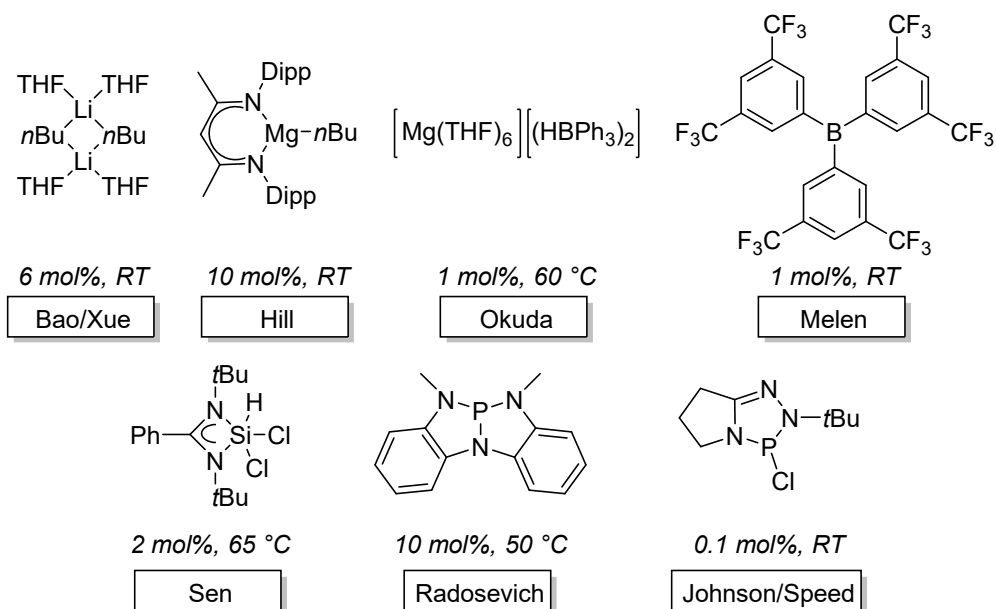
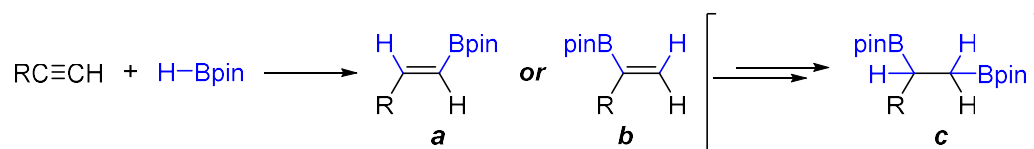


Figure 3.1: Selected examples of main group catalysts for the hydroboration of imines showing catalyst loading employed.

Very recently, *n*BuLi was employed as a catalyst for the hydroboration of imines (Figure 3.1) with a low catalyst loading (6 mol%), at room temperature, in THF solution, achieving good to excellent yields in generally short reaction times (typically 1 hour).²¹⁹ Whilst in hexane solvents *n*BuLi exists as a hexamer at room temperature, Williard has recently shown on the basis of DOSY NMR measurements that in bulk THF solvent *n*BuLi exists as a tetra-solvated dimer.²²⁴ Meanwhile, Hill employed the β -diketiminate ligated ^{DIPP}nacnacMg*n*Bu pre-catalyst for the hydroboration of imines, carbodiimides and isonitriles.^{56, 57} These C – N unsaturated substrates were hydroborated with a 10 mol% catalyst loading (5 mol% for isonitriles) under moderate reaction conditions in good to excellent yields.

The products arising from the hydroboration of alkynes and alkenes are important in organic synthesis. Vinyl borane products are highly desirable intermediates as they can be employed in Suzuki-Miyaura C – C cross coupling reactions.¹⁵¹ As such, both alkynes and alkenes have been extensively studied substrates in transition-metal-catalysed hydroboration processes. However, these substrates have been significantly less well examined for main group catalysed systems. Alkynes and alkenes are more challenging

substrates for hydroboration than aldehydes, ketones or imines, as the C – C unsaturated bond is significantly less polarised than the C = E bond (E = O, N). In particular, alkynes pose specific problems in terms of isomeric mixtures of products, which can be challenging to separate, and have the potential for over-reduction of the C \equiv C triple bond to the alkane product (Scheme 3.2).¹⁵⁴



Scheme 3.2: General reaction scheme for the hydroboration of an alkynes, depicting the possible products: **a)** anti-Markovnikov vinyl borane product; **b)** Markovnikov vinyl borane product; **c)** double hydroboration to alkane product.

Alkyne hydroboration has been catalysed by only a small number of main group compounds (Figure 3.2).^{90, 173, 176-178, 180, 219, 225, 226}

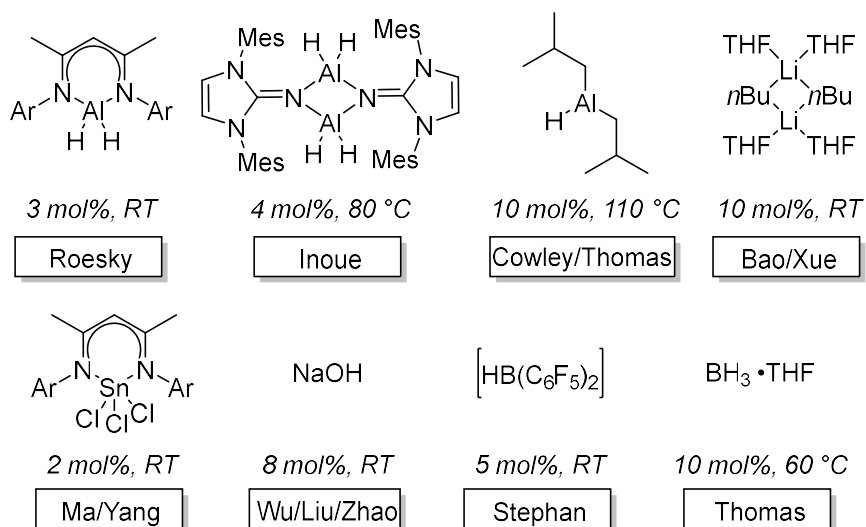
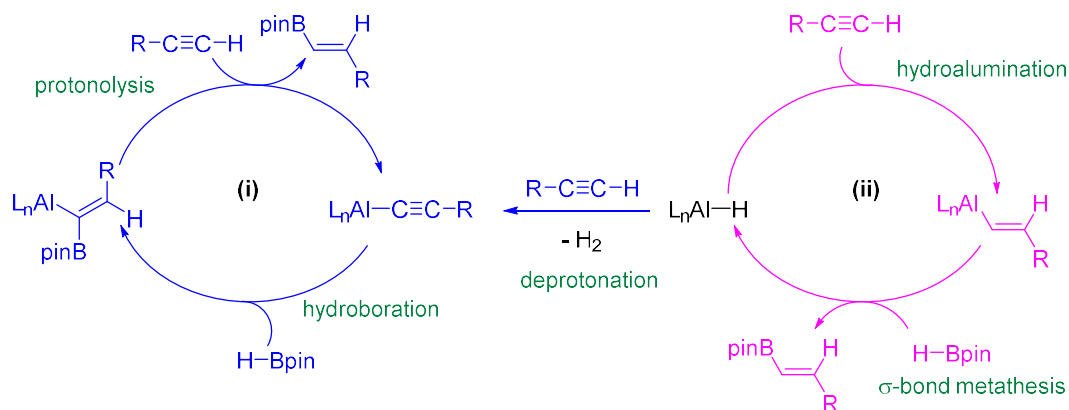


Figure 3.2: Selected main group catalysts for the hydroboration of alkynes.

Roesky utilised his β -diketiminato ligated $^{\text{Ar}}\text{nacnacAlH}_2$ ($\text{Ar} = 2,6\text{-Et}_2\text{C}_6\text{H}_3$) for the hydroboration of terminal alkynes, under very mild conditions (3 mol%, room temperature, 12 hours).⁹⁰ Interestingly, aliphatic alkynes were more easily hydroborated than aryl alkynes with this catalyst system. In the first step of the proposed catalytic cycle (Scheme 3.3), established by DFT calculations, the aluminium hydride deprotonates the terminal alkyne C–H and forms H_2 gas. As a result of this proposed catalytic pathway, both aryl and aliphatic internal alkynes were not compatible. Inoue reported the use of N-heterocyclic imine stabilised aluminium hydrides for the hydroboration of terminal aryl alkynes.¹⁸⁰ Focusing on simple commercially available aluminium reagents, Cowley and Thomas have reported the hydroboration of a large scope of alkynes with $i\text{Bu}_2\text{AlH}$ or $\text{Et}_3\text{Al.DABCO}$ as catalysts.¹⁷⁸ Harsher conditions (10 mol% catalyst, 110 °C, 2 hours) were required to obtain the products in good yields for both terminal and internal aryl and aliphatic alkynes. Yields were similar between both catalysts, which suggests a shared mode of reactivity. The authors showed that for the $\text{Et}_3\text{Al.DABCO}$ system an initiation step with HBpin is required to form the hydride derivative $\text{Et}_2\text{AlH.DABCO}$ which is proposed as the catalytically active system. In contrast to the deprotonation mechanism hypothesised by Roesky, Cowley and Thomas put forward a catalytic cycle based upon hydroalumination/ σ -bond metathesis steps, on the basis of stoichiometric reactions performed in the study. (Scheme 3.3).



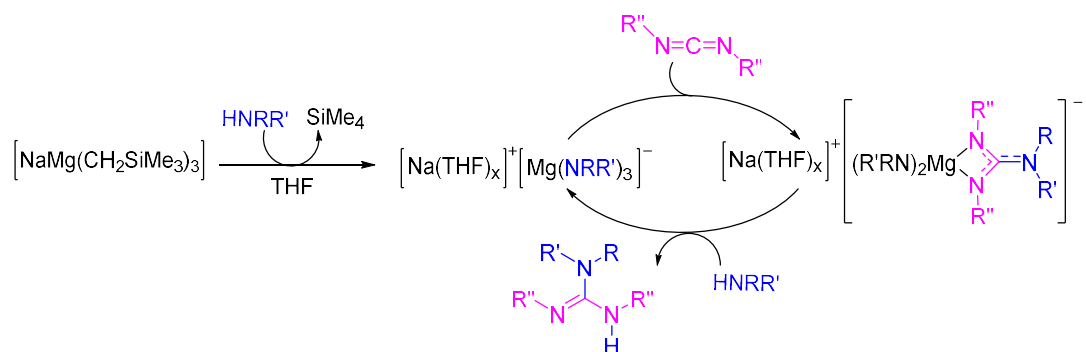
Scheme 3.3: Proposed mechanisms for the aluminium hydride catalysed hydroboration of terminal alkynes. Mechanism (i) was proposed by Roesky; Mechanism (ii) was proposed by Cowley.

Cowley and Thomas subsequently explored the hydroboration of alkenes this time employing the common stoichiometric reducing agent LiAlH_4 , as a catalyst.^{111, 112, 227, 228} Using 10 mol% catalyst, at 110 °C under solvent free conditions, a range of terminal alkene substrates were hydroborated within 3 hours to give the linear boronic ester products in moderate to good yields.¹⁷⁷ Internal alkenes did not react, and terminal alkenes bearing reactive functional groups (for example a keto or nitrile group) did not cleanly react to identifiable products. This methodology was subsequently applied to polarised substrates such as ketones, esters and nitriles giving the desired product in every instance. However, the role of the alkali metal, if any, was not elaborated upon in this study.

3.2.2 Bimetallic systems in catalysis

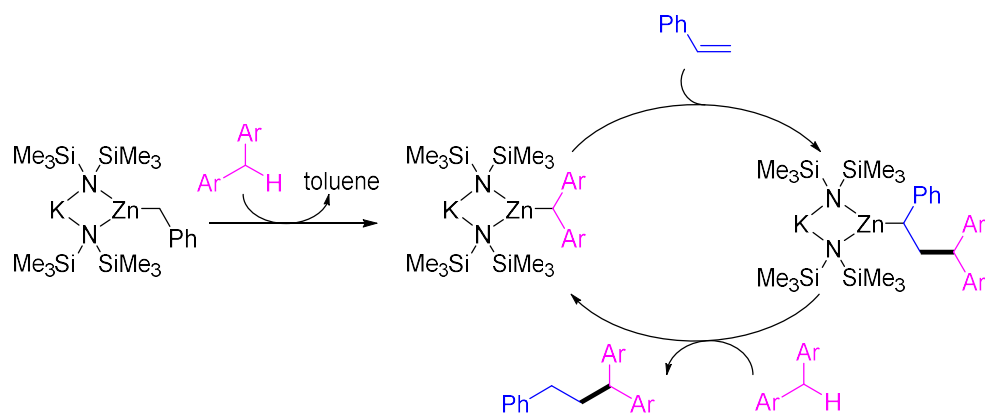
An emerging area of homogeneous catalysis is the use of catalysts featuring two metal centres.^{229, 230} Such bimetallic catalysts can utilise many different combinations of metals spanning alkali metals, transition metals, and lanthanides. The benefit of applying mixed metal systems is the possibility of introducing synergistic effects observed where the two distinct metals cooperate to modulate each other's reactivity, (see Chapter 1; Section 1.3). Thus, bimetallic catalysts represent a complementary approach to traditional single metal catalyst systems. Within main group bimetallic catalysis, Westerhausen has reported potassium calciates such as the higher order complex $\text{K}_2\text{Ca}(\text{Ni}^i\text{PrPh})_4$ for the hydroamination of diphenylbutadiyne by anilines.²³¹ Other mixed metal s-block catalysts include the sodium trisalkylmagnesiates $[\text{NaMg}(\text{CH}_2\text{SiMe}_3)_3]$, disclosed by Hevia, for the selective hydroamination or cyclotrimerisation of isocyanates.²³² It was proposed that the cationic sodium enables further activation of the organic electrophile by bringing it into close proximity with the anionic magnesiates component. Selective hydroamination of isocyanates (RNCO) bearing a bulky R group (such as *t*Bu) was observed, while reducing the steric bulk of the R group (for example to an aryl groups) resulted in selective cyclotrimerisation without formation of oligomeric by-products. In a follow-up publication, Hevia expanded the catalytic scope of $[\text{NaMg}(\text{CH}_2\text{SiMe}_3)_3]$ to the hydroamination (and hydrophosphination) of carbodiimides with a series of amines (Scheme 3.4).²³³ Enhanced catalytic reactivity was observed over the monometallic component parts of the magnesiates $[\text{NaCH}_2\text{SiMe}_3]$ and $[\text{Mg}(\text{CH}_2\text{SiMe}_3)_2]$. Stoichiometric reactions and NMR spectroscopic observations offered insight into the

potential catalytic pathway. The authors conclude that the role of the sodium is essential but secondary only and that the rate enhancement observed with the bimetallic catalysis arises as a result of anionic activation of the magnesium centre, resulting from the presence of the reducing sodium centre.



Scheme 3.4: Proposed mechanism for the guanylation of anilines with $[\text{NaMg}(\text{CH}_2\text{SiMe}_3)_3]$.

Away from hydroamination catalysis, Guan has recently reported the benzylic C – H addition of diarylmethanes to styrenes employing a potassium zincate catalyst, $\text{KZn}(\text{HMDS})_2\text{Bn}$ (Scheme 3.5).²³⁴ A range of styrenes and conjugated dienes as well as different diarylmethanes were tolerated by this system, yielding the desired C – H alkylation products in all cases.



Scheme 3.5: Proposed mechanism for the C – H alkylation of styrenes by diarylmethanes.

To date the majority of the aluminium compounds reported for hydroboration catalysis have been monometallic (neutral) compounds. In Chapter 2 lithium aluminate (HMDS)₂AlH(μ-H)Li(THF)₃, **1**, was introduced as a catalyst for the hydroboration of aldehydes and ketones, representing the first report of a charged lithium aluminate catalyst for this reaction. Further work in our group identified donor-free [*i*Bu₂Al(TMP)(H)Li]₂, **10**, as an alternative lithium aluminate which is also catalytically active.²⁰⁹ The recent report of LiAlH₄ mediated hydroboration of alkenes provided another example of a lithium aluminate catalyst; however, the authors proposed that the active species for this catalysis was AlH₃, arising from the disproportionation of LiAlH₄.¹⁷⁷ The (potential) role of the lithium, or LiH, was never established. The LiAlH₄-catalysed hydrogenation of imines is proposed to proceed *via* a cooperative mechanism in which both lithium and aluminium play a role.⁷⁶ Thus, building on the results of Chapter 2, and other work from our group and from others, it is now pertinent to have a closer examination of the effect the presence of the lithium cation plays on these lithium aluminate systems.

3.3 Project Aims

The aims of this part of the project are summarised below.

- To expand the concept of lithium aluminate catalysed hydroboration to more challenging, and less examined substrates such as imines and alkynes.
- To undertake a comparative study between anionic lithium aluminate catalysts and neutral monometallic aluminium catalysts in order to determine what effect if any the presence of the lithium cation has on the efficiency and rate of catalysis.

3.4 Introduction from the Manuscript

The synthetic value of main group metal complexes aside from the highly reactive and versatile organolithium and organomagnesium reagents have, from a historical perspective, been overshadowed by the illustrious reputation of transition metal (notably precious metals) and lanthanide metal counterparts especially in catalysis.⁵⁰ To a large extent main

group research has been driven by fundamental curiosity and the understanding of the nature of chemical bonding and structure. A step-change occurred when it was realised that such main group metal species can act in homogeneous catalytic roles, previously the exclusive province of transition metal and lanthanide complexes. Emulating the high reactivity, selectivity and versatility of the often toxic and scarce precious metal complexes is a tantalising challenge that needs addressing. In this regard, the pioneering work of Harder, Hill, Jones, Okuda, Power, Roesky, Wright among others, are expanding the vistas of main group complexes in homogeneous catalysis.^{15, 49, 50, 62, 98, 171, 185, 196} Since aluminium is the most abundant metal in the Earth's crust, and also benefits from low toxicity, harnessing its reactivity is given high prominence in this main group uprising with longer term sustainability being a key issue. Thus, recently aluminium complexes have made significant strides forward in important stoichiometric and catalytic transformations.¹⁶ For example, they are utilised in C – C cross coupling chemistries, and in deprotonative metallation.^{35, 136} Catalytic hydroelementation reactions have also witnessed impressive progress in the past few years. Roesky demonstrated that a β -diketiminato stabilised aluminium hydride complex is an excellent catalyst for hydroboration of alkynes and carbonyl groups.^{79, 90} More recently, Cowley and Thomas revealed that DIBAL(H), and Et₃Al·DABCO can catalyse hydroboration of alkynes.¹⁷⁸

Our group's interests lie in exploiting the synergistic reactivity imparted by two distinct metal centres²³⁵ installed within a bimetallic complex. In this regard we introduced ate complexes (Figure 3.3), detailing that heteroleptic lithium diamido-dihydridoaluminates and lithium monoamido-monohydrido-dialkylaluminates implicate that the alkali metal influences the ensuing "aluminium reactivity" in the hydroboration of aldehydes, ketones and terminal alkynes.^{209, 236}

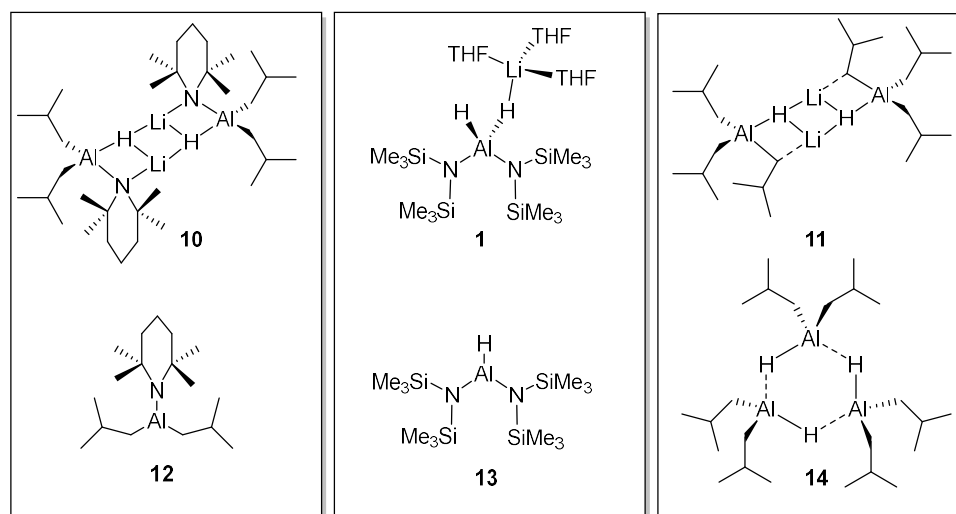
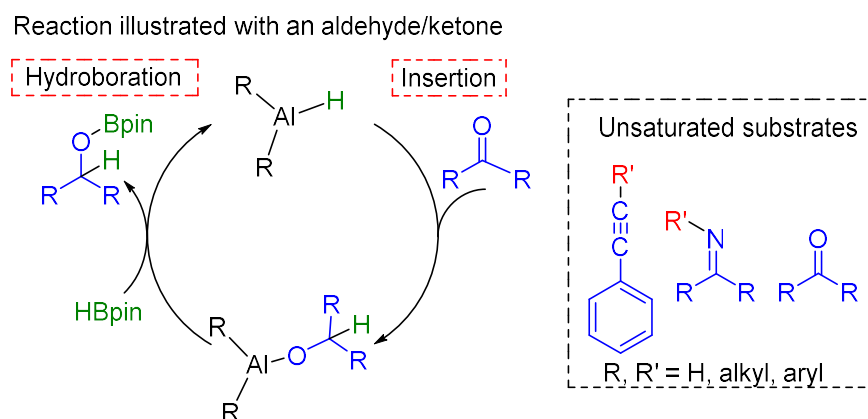


Figure 3.3: Aluminium complexes, **1**, **10** – **14** assessed in this study: ate complexes **1**, **10**, **11**; neutral complexes **12** – **14**.

Further, the catalytic chemistry of LiAlH_4 has recently been explored by Cowley and Thomas in the challenging hydroboration of alkenes, however the role of the alkali metal was not elaborated.¹⁷⁷ Thus, the current state of the field dictates that a systematic analysis of the secondary metal cooperative effects and various ligand factors that contribute to efficient hydroboration, is required in order to establish empirical rules for a *posteriori* design of future catalysts.

Hydroboration of unsaturated substrates under aluminium catalysis is gaining a foothold in the literature, and a variety of neutral aluminium complexes are displaying excellent potential in this role.^{15, 16, 18, 172, 179-181} Previously, we reported that bimetallic lithium $[\text{iBu}_2\text{AlTMP}(\text{H})\text{Li}]_2$, **10** and $[(\text{HMDS})_2\text{AlH}(\mu\text{-H})\text{Li}(\text{THF})_3]$, **1**, are both efficient bimetallic (pre)catalysts in the hydroboration of aldehydes and ketones.^{209, 236} However, any synthetic advantages/disadvantages of using ate complexes are yet to be fully uncovered, despite their potential. Thus, here, for the first time ate complexes are compared with their neutral aluminium counterparts to fully quantify their value in synthesis, and to glean understanding of their *modus operandi*. Moreover, the complexes chosen vary in their ligand constitution, i.e., alkyl versus amido constituents, providing further comparison. Mechanistically a frequently postulated two-step reaction pathway is: i) insertion of an unsaturated substrate into an $\text{Al} - \text{H}$ bond; ii) σ -bond metathesis with a borane, regenerating an active species and liberating product (Scheme 3.6).



Scheme 3.6: Postulated insertion mechanism in aluminium-catalysed hydroboration.

3.5 Results and Discussion

Catalytic activities were screened with aldehydes, ketones, imines and alkynes, providing reaction scope to determine key divergences in catalyst reactivity. We previously reported **1** and **10** in catalytic hydroboration and these are compared with the neutral analogues **12** and **13**, which differ by formal removal of LiH. We prepared new complex **11**, an all alkyl variant of **10**, by a simple co-complexation procedure (see 3.4 Extended discussion). **11** can be considered an ate version of DIBAL(H), **14** and was characterised *via* NMR characterisation, including DOSY. Our results from comparative studies (reaction conditions are identical between different catalysts) are summarized in Table 3.1. Complexes **1**, **10** – **14** (5 mol%) were all tested in hydroboration reactions with benzophenone and pinacolborane (HBpin) at room temperature in J. Young's tubes in C₆D₆. Each bimetallic complex exhibits superior activity to its monometallic counterpart, affording quantitative conversion after 30 minutes, apart from **12**, which is 94% complete after 30 minutes. This is surprising since **12** does not possess an Al–H bond. Rationalising that an Al–H bond must form *in situ* during the catalysis we performed a stoichiometric reaction between **12** and benzophenone in hexane and C₆D₆, where clear, facile quantitative reaction occurs rapidly at room temperature (isobutene, the coproduct of β-hydride elimination, is seen in the ¹H NMR spectra). X-ray diffraction studies of colourless crystals grown from the hexane solution revealed formation of [(TMP){Ph₂(H)CO}Al{μ-OC(H)Ph₂}]₂, **15** in a 45% isolated yield (Scheme 3.7). It is germane to

note that $\text{Et}_3\text{Al}\cdot\text{DABCO}$ can catalyse hydroboration of alkynes due to a redistribution reaction with HBpin generating the active Et_2AlH species.¹⁷⁸ The structure of **15** (Figure 3.4 LHS) reveals a dimer wherein both *t*Bu⁻ groups of **12** have been replaced, by $\text{Ph}_2(\text{H})\text{CO}^-$ ligands, formed by apparent β -hydride elimination from the parent complex. β -Hydride elimination is known in alkyl-aluminium chemistry with carbonyls,^{237, 238} but to our knowledge this is the first example in hydroboration catalysis used to generate a transient aluminium hydride. Thus **12** may be considered a masked hydride complex in hydroboration of ketones.

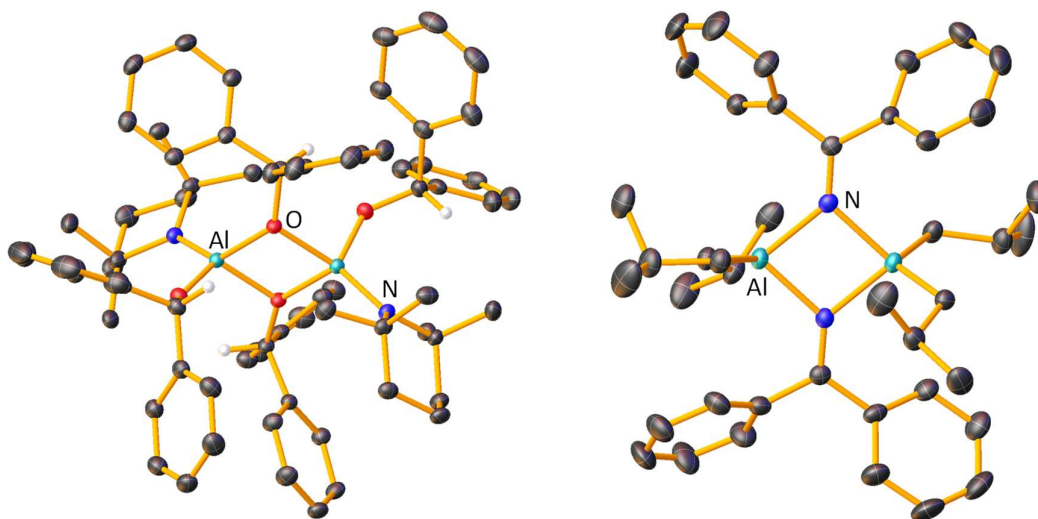
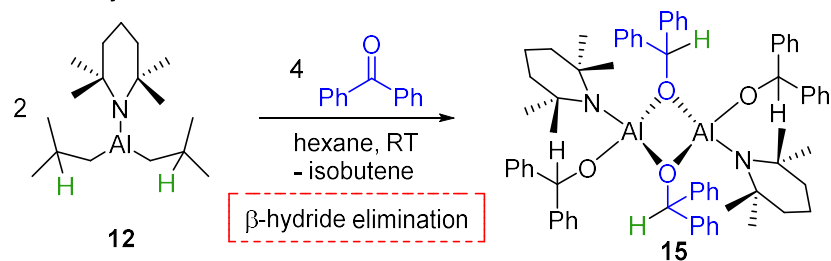


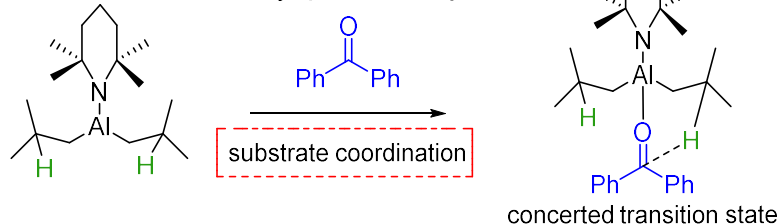
Figure 3.4: Molecular structures of **15** (LHS) and **16** (RHS). All hydrogen atoms are omitted for clarity except those on the reduced benzophenone anions. Thermal ellipsoids are drawn at 40% probability.

Elaborating this step further, it is pertinent to consider the Meerwein-Ponndorf-Verley (MPV) reduction,^{237, 239-241, 242} employing aluminium alkoxides as the hydride source to reduce ketones. Two competing mechanisms have been studied *in silico*.²⁴² The first involves β -hydride transfer from the alkoxide ligand giving a high energy Al – H intermediate, which can then follow the pathway represented in Scheme 3.6. The second pathway is much lower in energy and describes a concerted process containing a 6-membered transition state, facilitating direct hydride transfer to the substrate (Scheme 3.7).

Pre-catalyst activation



Meerwein-Ponndorf-Verley type reactivity



Scheme 3.7: (Top) Reaction between **12** and benzophenone, revealing formation of the active catalytic species **15** via β -hydride elimination. (Bottom) Reaction between **12** and benzophenone proceeding via a possible Meerwein-Ponndorf-Verley type reaction.

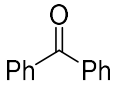
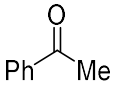
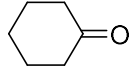
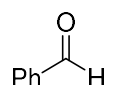
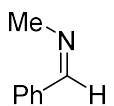
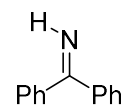
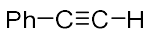
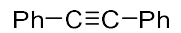
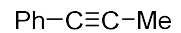
15 (2.5 mol%) is shown to be catalytically active in a reaction with benzophenone and HBpin, where quantitative hydroboration occurs after 3 hours. Since **12** seems a reactivity outlier, showing comparable reactivity to **10**, they were both screened catalytically with one aldehyde and two further ketones. In each case the bimetallic complex **10** showed far superior activity.

Furthermore, a control reaction employing LiH as a catalyst (5 mol%) for hydroboration of benzophenone gave a yield of only 10% after 4 hours. This illustrates that, in this regard, the neutral aluminium or lithium reagents in isolation deliver markedly reduced reactivities compared with the bimetallic formulations. Importantly, for the first time direct comparison experiments reveal the synthetic superiority of lithium aluminate complexes in the context of hydroboration.

Hypothesising that any “ate effect” would be magnified with more challenging substrates we turned our attention to imines, which hitherto have not been catalytically hydroborated with aluminium complexes. That said, examples exist of main group complexes catalysing this transformation, and of aluminium complexes catalysing hydrosilylation or

hydrogenation of imines,^{18, 55, 62, 74, 76, 81, 184} suggesting that imine hydroboration is a viable synthetic target.

Table 3.1: Hydroboration catalysis results for carbonyls, imines and acetylenes using **1**, **10** – **14** as catalysts.

		
10 ^[a] 99% 0.5 h 12 94% 0.5 h	10 ^[a] 97% 2 h 12 40% 6 h	10 ^[a] 93% 2.5 h 12 53% 2 h
1 ^[b] 99% 0.5 h 13 69% 5 h	1 ^[b] 80% 3 h 13 55% 5 h	1 ^[b] 91% 2 h 13 57% 1 h
11 79% 0.5 h 14 17% 4 h	11 99% 0.5 h	11 98% 0.25 h
		
10 ^[a] 99% 0.25 h 12 79% 1 h	10 42% 2 h 12 3% 2 h	10 73% 0.5 h 12 34% 5 h
1 ^[b] 81% 2 h 13 88% 0.25 h	1 35% 2 h 13 22% 2 h	1 78% 0.75 h 13 56% 4 h
11 99% 0.25 h	11 53% 2 h 14 5% 2 h	11 80% 0.5 h 14 33% 4 h
		
10 71% 2 h 12 0% 17 h	10 0% 2 h	11 60% 2 h (2.2:1 ratio)
11 83% 2 h 14 ^[c] 85% 2 h	11 10% 2 h 14 ^[c] 40% 2 h	14 ^[c] trace

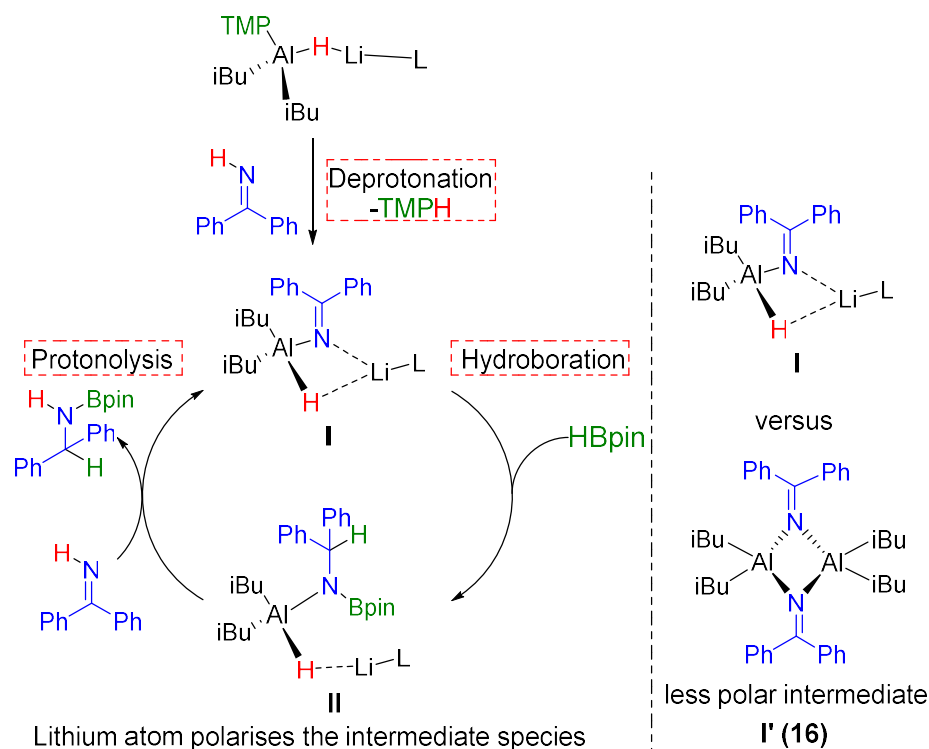
Aldehydes/ketones: 5 mol% [Al] catalyst loading, C₆D₆, room temperature. Imines: 10 mol% [Al] catalyst loading, C₆D₆, room temperature. Alkynes: 10 mol% [Al] catalyst loading, in d₈-toluene at 110 °C/ [a] data for **10** from reference 209. [b] data for **1** (1 mol% catalyst) from reference 236. [c] data for **14** from reference 178. All yields against ¹H NMR internal standard hexamethylcyclotrisiloxane.

Catalytic hydroboration reactions of N-benzylidenemethylamine, using **1**, **10** – **14** showed lower reactivity at room temperature than with aldehydes and ketones, however the same reactivity pattern emerges, in that the bimetallic complexes are superior to monometallic counterparts. After two hours, conversions are with **10** (42%), **1** (35%), **11** (53%), **12** (3%), **13** (22%) and **14** (5%). Nevertheless, these results with **1**, **10** – **12** constitute the first use of aluminium complexes in imine hydroboration. Stoichiometric reactions between **10**, **11**, **12** and **14** with the imine provide further insight. **12** forms only a coordination adduct with the

imine in contrast to the β -hydride elimination product with benzophenone, whereas, **10**, **11** and **14** add across the C = N double bond, with **14** displaying higher insertion reactivity. Notably Stephan reported a dimeric structure of an analogous reaction between **14** and a related imine.⁷⁴ However, faster substrate insertion does not translate into fast catalytic transformation. Thus, we infer that the σ -bond metathesis step with HBpin is greatly facilitated by the additional polarity imposed by the bimetallic ate constitution. Reinforcing this hypothesis, Harder's imine hydrogenation using catalytic LiAlH₄ illuminates the important role of the alkali metal, *via* DFT studies, wherein Al – H – Li interactions are retained throughout the proposed catalytic cycle.⁷⁶

We next screened benzophenone imine in the catalysis with **10**, **11**, **12** and **14** (10 mol%), since this substrate has an acidic N – H atom amenable to deprotonation and therefore provides the possibility of reaction proceeding *via* an alternative deprotonation pathway. Furthermore, amido groups in **10** and **12** can be directly compared with alkyl groups in **11** and **14**. **10** and **11** achieve 73% and 80% conversion after 2 hours or 30 minutes respectively. **12** and **14** perform poorly, showing no catalytic activity at room temperature, prompting further consideration. Two stoichiometric reactions between benzophenone imine and **10**, and **12** were conducted, wherein both exhibit amido basicity. In the latter case [*i*Bu₂Al(μ -N=CPh₂)]₂, **16** (Figure 3.4 RHS), was isolated as single crystals in a 24% yield (¹H NMR yield of 86% against hexamethylcyclotrisiloxane as internal standard). In contrast to the benzophenone case where catalysis proceeds after a β -hydride elimination step, the reactivity here ceases after an initial deprotonation by the TMP basicity. Interestingly, both **11** and **14** display trace amounts of H₂ evolution as evidenced by a low intensity singlet resonance in the respective ¹H NMR spectra at δ 4.47 ppm.

The catalytic results with benzophenone imine merit further comment. Both **10** and **12** exhibit deprotonation, suggesting that in a catalytic regime, reaction (using **10**) may proceed in the pathway outlined in Scheme 3.8, that is, deprotonation followed by hydroboration then protonolysis to liberate product and generate a catalytically active species.



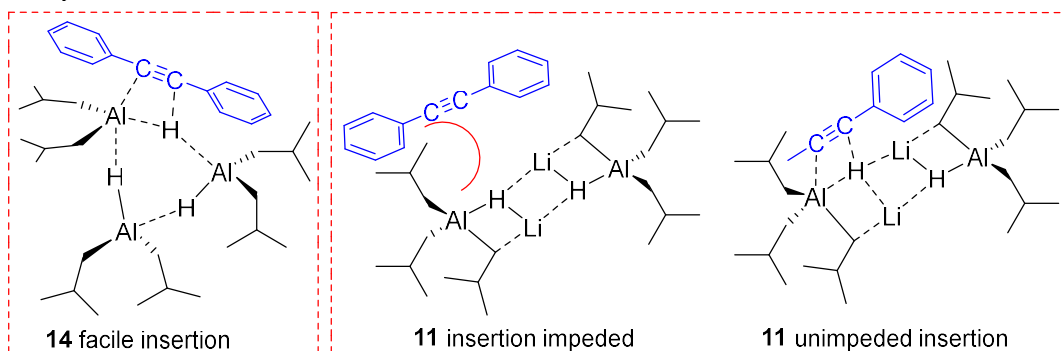
Scheme 3.8: Suggested mechanism for hydroboration of benzophenone imine catalysed by **10**. RHS – Alternative intermediate for catalytic profile using **11**.

That **10** is active and **12** is not, may be assigned to the nature of deprotonation products, which clearly demonstrates the key role of bimetallic (Li – Al) cooperativity. **I** is the proposed deprotonation intermediate using **10** and **I'** using **12**, which corresponds to the crystallographically authenticated **16**. In **I** the alkali metal would instil a different molecular charge distribution to that in **I'**. This scenario clearly facilitates the hydroboration step, which is not the case with **I'**. A final comment on benzophenone imine hydroboration is that **10** (73% 0.5 hours) offers marginally less reactivity than **11** (80% 0.5 hours). This difference may describe a subtle alkyl *versus* amido effect, whereby the replacement of one TMP anion for an *i*Bu anion imparts greater nucleophilicity onto the hydride, priming it for addition across the unsaturated substrate. Alternatively, the increased steric demand of TMP may slow reactivity. Moreover, it is apparent that even when the deprotonation pathway is available (catalyst **10** with benzophenone imine), the pathway that follows, insertion (catalyst **11** with benzophenone imine) is favoured, albeit marginally.

Finally, we turned to acetylene hydroboration comparing reactivity once more between **10**, **11**, **12** and **14**. Stoichiometric reactions of TMP-containing **10** and **12** with terminal alkyne phenylacetylene (PhCCH) in C_6D_6 , reveal deprotonation of PhCCH at room temperature, in agreement with the fact that hydroboration of PhCCH with **10** implicated deprotonation as a key step.²⁰⁹ Alternatively **11** is unreactive with PhCCH, and **14** only very slowly hydroaluminates PhCCH, at room temperature. Catalysis, using 10 mol% loadings in d_8 -toluene at 110 °C, in line with the reported reaction conditions using **14** (85% conversion after 2 hours),¹⁷⁸ reveal that **10** and **11** catalyse the transformation to the anti-Markovnikov vinylboronate ester in yields of 71% and 83% respectively. Conversely, **12** as expected, does not function as a catalyst. Thus **11** is comparable to **14** however, for the first time we note that a clear ate effect is not in operation. Furthermore, **11** is a better catalyst than **10** underlying that increased hydride nucleophilicity is more important, mechanistically, than deprotonation, though reduced sterics may also be a factor.

A similar picture is seen with the internal alkyne diphenylacetylene. **14** (10 mol%) is reported to convert diphenylacetylene to the boronic ester in 40% yield after 2 hours at 110 °C in d_8 -toluene,¹⁷⁸ whereas **10** is completely inactive, and **11** only reaches conversions of ca. 10% after 2 hours, which is surprising given our preceding observations. One potential rationale for this marked reduction in ate reactivity with diphenylacetylene may be attributed to a steric effect (Scheme 3.9).

Acetylene insertion



Scheme 3.9: Comparative insertion profiles for reaction of diphenylacetylene with **14** and **11** and 1-phenyl-1-propyne with **11**.

Considering the required initial insertion step at the *sp*-C of diphenylacetylene, insertion into the Al – H bond of **11** (three *i*Bu groups, one hydride) is likely to be slower than for **14** (two *i*Bu groups, one hydride) due to the inherently more sterically demanding ate constitution, even given the trimeric solution constitution of **14** (*via* DOSY NMR see 3.6 Extended Discussion). Clearly, with ketones and imines any insertion step at the *sp*² O/N would be considerably less congested, thus facile insertion would occur, thereby facilitating the ate enhancement seen in the ensuing hydroboration catalysis. Elaborating further, we attempted one further substrate in comparative catalytic experiments with **14** and **11**. With **14**, 1-phenyl-1-propyne is only hydroborated in trace amounts, despite the intrinsically smaller CH₃ group with respect to diphenylacetylene.¹⁷⁸ On the other hand, **11** catalyses the transformation to a mixture of regio-isomers (60% conversion overall) in favour of borylation at the least sterically hindered alkyne carbon atom, demonstrating once more the advantage of ate complexes in these catalytic transformations.

This study into hydroboration of aldehydes, ketones and imines reveals that anionic ate complexes are important additions to the main group catalyst toolbox, providing higher conversions in shorter timescales. We attribute this superiority to the greater polarisation of key reaction intermediates induced by the heterobimetallic complexes. Moreover, a novel new catalytic activation pathway was elucidated for ketone hydroboration involving β -hydride elimination. With internal alkynes the scenario is different and mononuclear species are the catalysts of choice when steric constraints override the ate effect. Overall this study illuminated that while ate complexes are beneficial in most cases, the mononuclear species are more effective in others. Thus, in the field of aluminium-catalysed hydroelementation, there is a high degree of substrate dependence, governing the appropriate choice of catalyst.

3.6 Extended Discussion and Future Work

3.6.1 Solid state and solution phase structures of **11**, **14** and synthesis of compound **17**

¹H DOSY NMR spectroscopic studies were performed on *i*Bu₃AlHLi, **11**, in order to determine its composition in the solution phase, in C₆D₆ solvent.²⁰⁶ In the absence of any donor ligands, and on the basis of DOSY NMR studies, **11** exists as a dimer (Figure 3.5 and Table 3.2). The

diffusion coefficient corresponding to the *i*Bu ligands of **11** indicates a molecular weight of 465 g mol⁻¹, consistent with the dimeric structure, [iBu₃AlHLi]₂ (412.44 g mol⁻¹), with a 7% error.

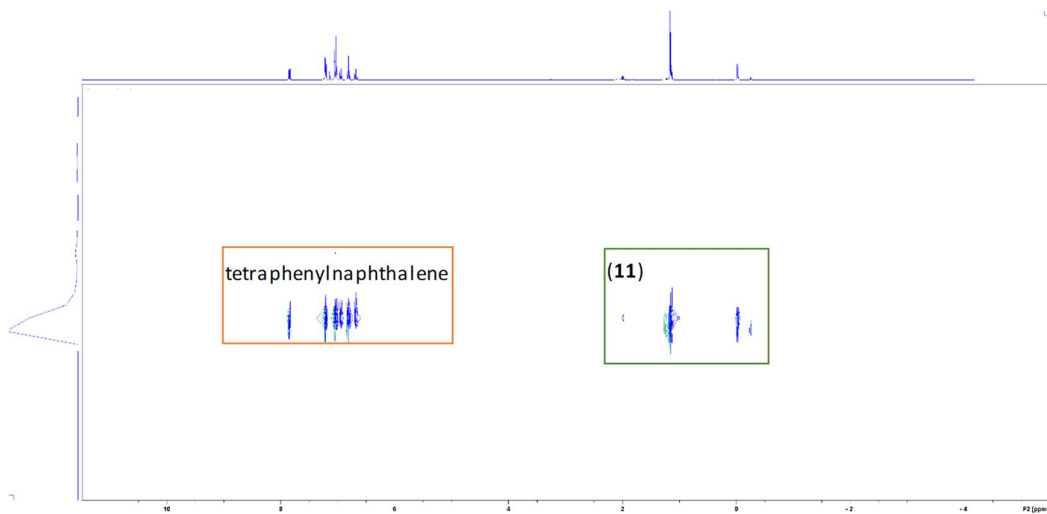
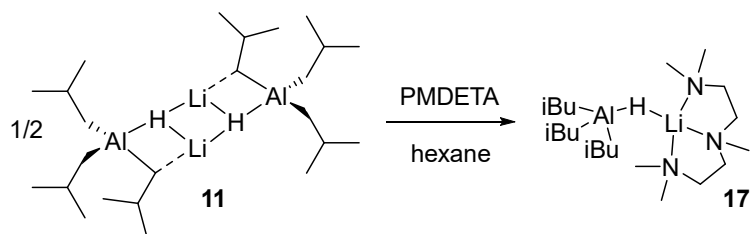


Figure 3.5: ¹H DOSY NMR spectrum for **11** with internal standard tetraphenyl-naphthalene, in C₆D₆.

Table 3.2: Diffusion coefficient data from ¹H DOSY NMR spectrum of **11**, in C₆D₆ solution.

Compound	D [m ² s ⁻¹]	MW _{calc} [g mol ⁻¹]	MW _{est} [g mol ⁻¹]	Error %
[iBu ₃ AlHLi] ₂	1.217 x 10 ⁻⁹	412.44	465 (dimeric structure)	-7
Tetraphenyl-naphthalene	1.211 x 10 ⁻⁹	432.55	465	-11

However, in the presence of powerful Lewis donors such as PMDETA, the solvated monomeric complex *i*Bu₃AlHLi(PMDETA), **17**, is obtained (Scheme 3.10 and Figure 3.6). Compound **17** was crystallised from a hexane solution at -15 °C as colourless crystals which were suitable for single crystal X-ray diffraction. The isolated yield of crystalline **17** was 71%.



Scheme 3.10: Synthesis of $i\text{Bu}_3\text{AlHLi}(\text{PMDETA})$, **17** from the unsolvated parent compound.

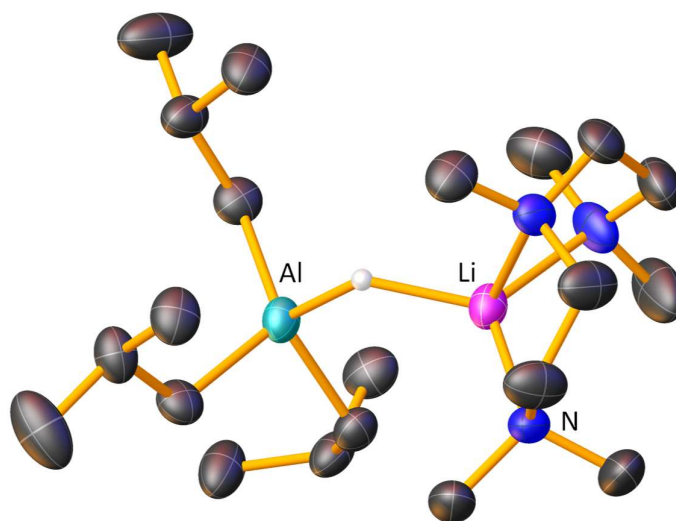


Figure 3.6: Molecular structure of $i\text{Bu}_3\text{AlHLi}(\text{PMDETA})$, **17**. Disordered $i\text{Bu}$ and PMDETA ligands and hydrogen atoms, except for hydride, have been omitted for clarity. Thermal ellipsoids are drawn at 40% probability.

Compound **17** crystallises in a relatively high symmetry (orthorhombic, $Pnma$) space group and also has the added complexity of atoms lying on special positions within the unit cell. This crystal structure determination revealed a monomeric, contacted ion pair structure. All of the organic ligands are disordered which precludes a discussion of geometries but, nevertheless, the structure provides proof of connectivity for **17**. As commonly found in other structures the PMDETA ligand coordinates to lithium *via* its three nitrogen atoms.²⁴³⁻²⁴⁵ The aluminium centre is coordinated to three $i\text{Bu}$ ligands. In compound **17**, the hydride was not disordered and was able to be located in the electron density map and refined isotropically.

The lithium and aluminium centres both bond to the bridging hydride with bond lengths of 1.76(2) Å and 1.68(2) Å, respectively. In the ^1H NMR spectrum no signal is visible for the hydride, which is not surprising as the hydride couples to both ^7Li ($I = 3/2$) and ^{27}Al ($I = 5/2$) nuclei.

Next, the solution state structure of *i*Bu₂AlH (DIBAL, **14**) was examined in both C₆D₆ and d₈-toluene by ^1H DOSY NMR. These studies suggest that **14** adopts a trimeric structure at room temperature in both of these solvents. The diffusion coefficient in C₆D₆ corresponds to a proposed molecular weight of 401 g mol⁻¹ which fits with a 6% error for the trimeric [*i*Bu₂AlH]₃ (426.4 g mol⁻¹) (Figure 3.7 and Table 3.3). Meanwhile, in d₈-toluene solution the diffusion coefficient also corresponds to a trimeric structure with a very small -1% error (Figure 3.8 and Table 3.4). Monomeric *i*Bu₂AlH has a molecular weight of 142.1 g mol⁻¹ while dimeric [*i*Bu₂AlH]₂ has a molecular weight of 282.2 g mol⁻¹, both of which are too low to fit the observed diffusion coefficient. Aluminium compounds are well known for their 3-centre-2-electron bonding (for example, in dimeric AlMe₃)¹⁹ and so it is not surprising that *i*Bu₂AlH is capable of existing in this higher aggregate state.²³

The ^1H DOSY NMR investigations probing the solution structures of **11** and **14** allow some insight into the difference in catalytic reactivity between these two compounds, which differ by formal removal of an *i*BuLi unit. That **14** is active for the hydroboration of diphenylacetylene but **11** is not, is proposed to be due to the increased steric profile of **11** which has three *i*Bu ligands, and so may impede the initial coordination of substrate. Conversely, for 1-phenyl-1-propyne, **11** is more active than **14** showing the benefit of employing such ate species as catalysts. At this point it is clear that the correct matching of substrate to the catalyst may be necessary to achieve optimum yields.

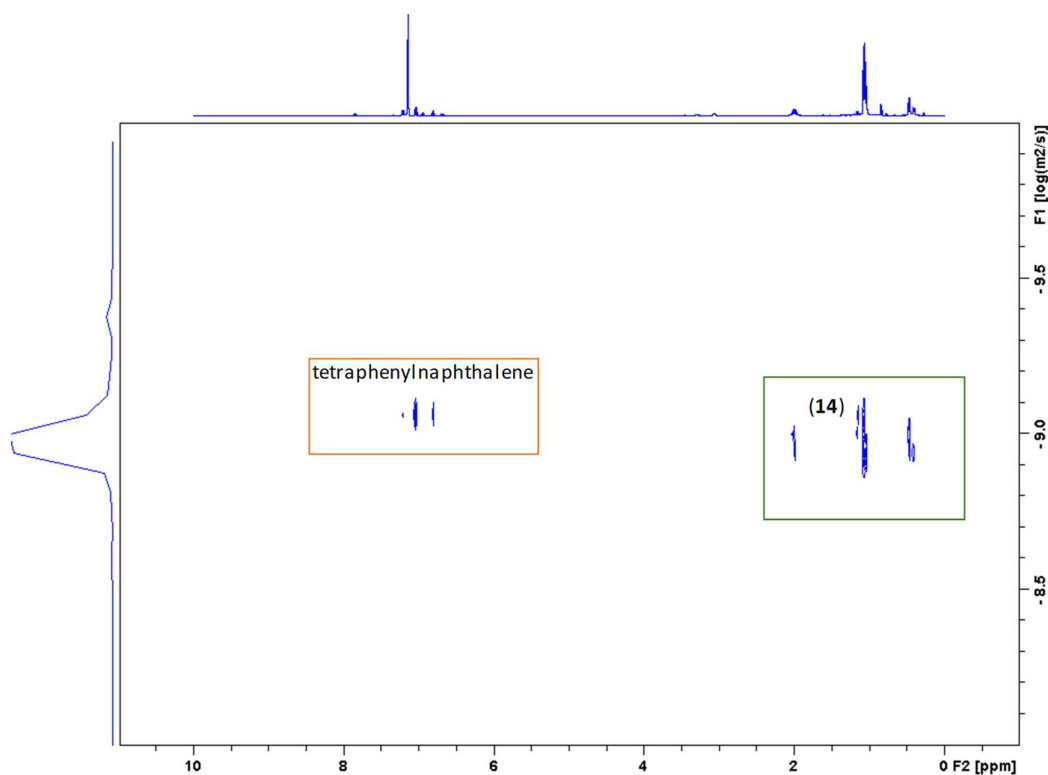


Figure 3.7: ¹H DOSY NMR spectrum for **14**, in C₆D₆.

Table 3.3: Diffusion coefficient data from ¹H DOSY NMR spectrum of **14**, in C₆D₆ solution.

Compound	D [m ² s ⁻¹]	MW _{calc} [g mol ⁻¹]	MW _{est} [g mol ⁻¹]	Error %
<i>i</i> Bu ₂ AlH	8.981 × 10 ⁻¹⁰	142.13 (monomer) 426.39 (trimer)	431	-1% (for trimer)
1,2,3,4-Tetraphenyl naphthalene	8.162 × 10 ⁻¹⁰	432.55	433	0%

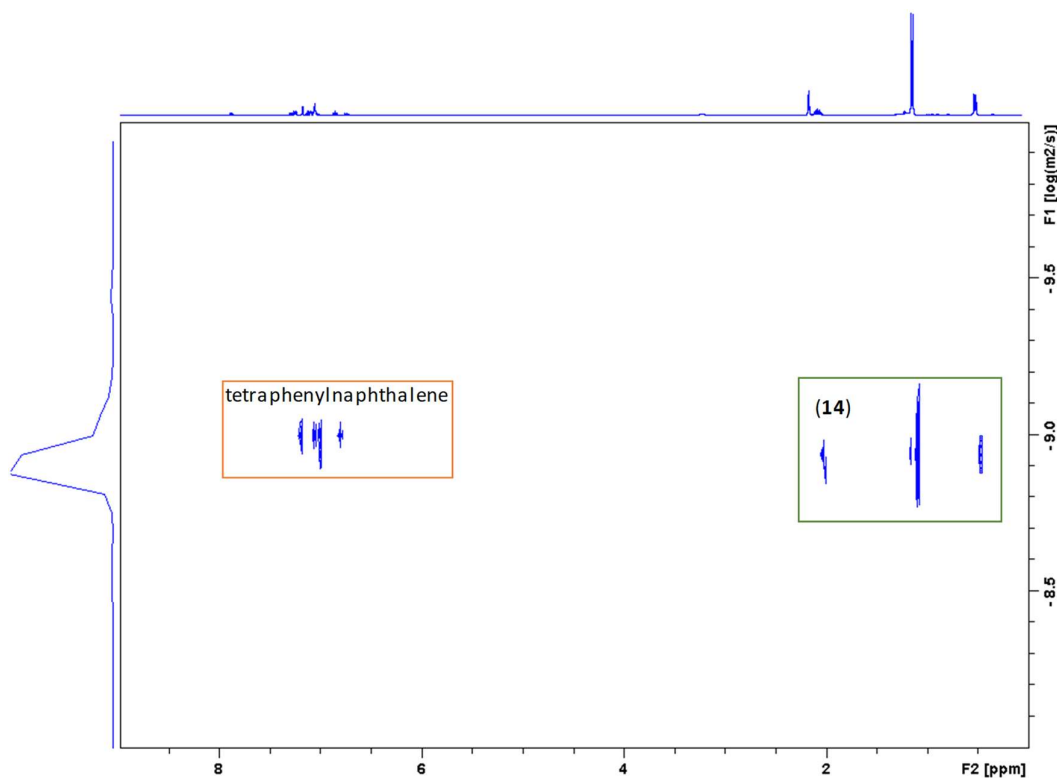


Figure 3.8: ^1H DOSY NMR spectrum for **14**, in d_8 -toluene.

Table 3.4: Diffusion coefficient data from ^1H DOSY NMR spectrum of **14**, in d_8 -toluene solution.

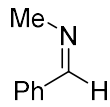
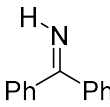
Compound	D [m^2s^{-1}]	MW _{calc} [g mol^{-1}]	MW _{est} [g mol^{-1}]	Error %
<i>i</i> Bu ₂ AlH	1.0897×10^{-9}	142.13 (monomer) 426.39 (trimer)	401	6 % (for trimer)
1,2,3,4-Tetraphenyl naphthalene	8.778×10^{-10}	432.55	433	0%

3.6.2 Hydroboration of imines and acetylenes

A selection of main group catalysts which have been reported to catalyse the hydroboration of imines is provided in Table 3.5 and compared with the best catalyst from this study, namely [*i*Bu₃AlHLi], **11**. Of the main group catalysts reported in the literature, only two have been shown to hydroborate the imines used in this study. *n*BuLi has recently been shown to catalyse the hydroboration of imines (6 mol%, THF solvent) and both

N-benzylidenemethylamine (99%, 3 hours, 70 °C) and benzophenone imine (99%, 1 hour, room temperature) were well tolerated by this system.²¹⁹ Compared with **11**, *n*BuLi requires much higher reaction temperatures for the hydroboration of *N*-benzylidenemethylamine (70 °C *versus* room temperature). Sodium hydroxide, NaOH, has also been reported to catalyse the hydroboration of a range of substrates including *N*-benzylidenemethylamine which achieved 91% yield after 6 hours at room temperature.¹⁷³ Catalyst **11** catalyses the hydroboration of benzophenone imine much more efficiently than *N*-benzylidenemethylamine, achieving a greater yield, and in a shorter reaction time.

Table 3.5: Summary of hydroboration capabilities of selected reported main group catalysts for key imine substrates.

Catalyst	<i>n</i> BuLi	NaOH	[<i>i</i> Bu ₃ AlHLi] ₂ , 11
	6 mol%, RT, THF	5 mol%, 90 °C, C ₆ D ₆	10 mol%, RT, C ₆ D ₆
	99%, 3 h, 70 °C	91%, 6 h	53%, 2 h
	99%, 1 h, RT	n/a	80%, 0.5 h

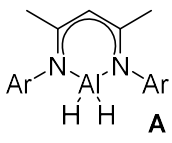
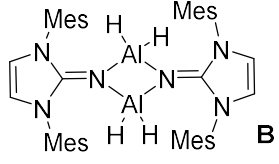
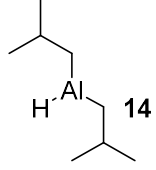
n/a – data not reported for this substrate.

Other research groups have focused on hydrogenation or hydrosilylation of imines with aluminium-based catalysts. The first aluminium catalysed hydrogenation of imines was reported by Stephan in 2014.⁷⁴ *i*Bu₂AlH (5 mol%) or *i*Bu₃Al (10 mol%) were employed as catalysts under harsh conditions (102 bar H₂, 100 °C, 24 hours) to generate the corresponding amine products in low to excellent yields (16 – 100%). High conversions were noted for imines with small electron-donating groups (for example Me or SiMe₃) on the nitrogen atom. Conversely, bulky groups (*t*Bu) or electron-withdrawing groups resulted in a low yield of product. The authors propose that the mechanism for this reaction proceeds *via* hydroalumination of the imine and then hydrogenolysis to liberate the product and regenerate the catalyst.

More recently, Harder has reported the LiAlH_4 (pre)-catalysed hydrogenation of imines. Employing significantly less harsh conditions than Stephan (5 – 10 mol%, 85 °C, 1 bar H_2 , solvent free), a range of different imines could be reduced.⁷⁶ Neither LiH or AlH_3 independently catalyse this reaction, whilst the use of NaAlH_4 provides less product than LiAlH_4 (NaAlH_4 : 5 mol%, 85 °C, 6 bar H_2 , 6 hours, 77% yield *versus* LiAlH_4 : 5 mol%, 85 °C, 5 bar H_2 , 6 hours, 99% yield). As such the authors propose a mechanism in which both the lithium and aluminium are involved. Elucidated *via* stoichiometric reaction and DFT calculations it was shown that the active species in this reaction is $[\text{N}-(t\text{Bu})\text{CH}_2\text{Ph}]_2\text{AlH}_2\text{Li}\cdot\text{L}$ (L = THF, PMDETA, or TMEDA), a structure which is reminiscent of the lithium aluminate complexes **1 – 6** prepared and discussed in Chapter 2.

Turning next to the hydroboration of alkynes, Table 3.6 summarises the results from a selection of published main group catalysts, and compares them with compound **11** in this study. For both catalyst **A**, $^{\text{Ar}}\text{nacnacAlH}_2$ (Ar = 2,6- $\text{Et}_2\text{C}_6\text{H}_3$), and **B**, *N*-heterocyclic imine supported aluminium hydride, only terminal alkynes were able to be hydroborated, as during the catalytic cycle there is a step where the terminal alkynes are deprotonated to form an aluminium alkynide, which then undergoes hydroboration with an equivalent of HBpin.^{90, 180} Contrastingly, internal alkynes without a terminal acidic hydrogen atom cannot be activated by this system. Similarly, *n*BuLi (10 mol%, RT, solvent free) is only successful as a catalyst for the hydroboration of terminal alkynes, achieving a yield of 90% for phenylacetylene within 16 hours.²¹⁹ With 1-phenyl-1-propyne the *n*BuLi-catalysed system generates only traces of product. Alternatively, Cowley and Thomas propose *i*Bu₂AlH, **14** as an active catalyst for the hydroboration of both terminal and internal alkynes. In this work they suggest an alternative mechanism in which the alkyne inserts into the Al – H bond and undergoes hydroalumination. In a second step the borane product is generated and the active Al – H species is regenerated *via* σ -bond metathesis (Scheme 3.3).

Table 3.6: Summary of hydroboration capabilities of selected reported main group catalysts for acetylene substrates.

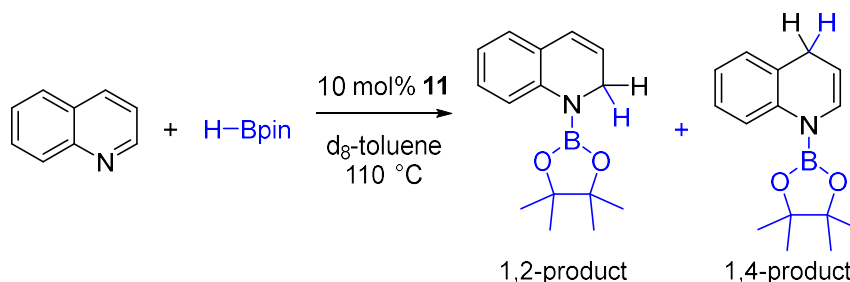
Catalyst	 A	 B	 14	$[i\text{Bu}_3\text{AlHLi}]_2$, 11
	3 mol%, RT, CDCl_3	4 mol%, 80 °C, <i>tol.</i>	10 mol%, 110 °C, <i>tol.</i>	10 mol%, 110 °C, <i>tol.</i>
Ph-C≡C-H	73%, 12 h	80%, 40 h	85%, 2 h	83%, 2 h
Ph-C≡C-Ph	n/a	n/a	40%, 2 h	10%, 2 h
Ph-C≡C-Me	n/a	n/a	traces, 2 h	60%, 2 h

n/a – data not available for these substrates.

Compared with aluminium catalysts **A** and **B**, **11** presented in this chapter is a competitive catalyst. Harsher conditions are required for the hydroboration of phenylacetylene with **11** in contrast to catalyst **A** (10 mol%, 110 °C *versus* 3 mol%, room temperature) but at the advantage of shorter reaction times (2 hours *versus* 12 hours). In comparison with catalyst **B**, catalyst **11** is significantly faster for the hydroboration of phenylacetylene generating the vinyl boronic ester product in 83% yield after only 2 hours, a significantly shorter time than the 40 hours required by catalyst **B**.

3.6.3 Related unpublished work and future work

The use of more challenging substrates, such as imines and acetylenes, in this study has highlighted the benefits available by the application of lithium aluminate complexes as hydroboration catalysts. It was also interesting to try to employ the most active lithium aluminate, **11**, as a catalyst in the hydroboration of pyridine substrates (Scheme 3.11). These substrates are especially challenging as hydroboration requires disruption of the aromaticity of the ring, and the resulting dearomatised N-heterocycles are important scaffolds in organic synthesis and chemical biology; for example, they are present in nicotinamide adenine dinucleotide (NADH).²⁴⁶



Scheme 3.11: Hydroboration of quinoline showing 1,2- and 1,4-dihydroquinoline products.

Preliminary investigations into the hydroboration of quinoline by HBpin with 10 mol% catalyst at 110 °C suggests that this catalyst was modestly active for this reaction (52% after 4 hours), but a mixture of 1,2- and 1,4-isomers, the kinetic and thermodynamic products respectively, were obtained (1:1.6). Quinoline was chosen as a test substrate due to the fused ring scaffold, which would off-set the disruption to the aromaticity of the pyridine ring. In contrast, no hydroboration of pyridine was observed after heating at 110 °C for 24 hours in the presence of 10 mol% **11**. These results are in contrast to Hill's ^{DIPP}nacnacMg(*n*Bu) pre-catalyst system (quinoline: 5 mol%, RT, 5 hours, 90% yield, 100:0 1,2:1,4-adduct; pyridine: 10 mol%, 80 °C, 16 hours, 90% yield, 5:95 1,2:1,4-adduct).⁵³ Further work on this system, including reaction optimisation (solvent, temperature, catalyst loading and dihydropyridine selectivity) would be required before a full substrate scope could be examined.

Other challenging substrates such as alkenes or nitriles could also be examined in future work. In 2019 the first example of aluminium catalysed hydroboration of nitriles was reported.¹⁸³ In the literature there is a growing presence of main group catalysed, solvent free hydroboration reactions.^{177, 179, 183} Such reactions are only possible if the catalyst is soluble within the liquid substrate or the HBpin reagent. Solvent-free conditions have not been trialled with the lithium aluminate catalysts discussed herein, as multi-nuclear NMR spectroscopies have been employed for reaction monitoring of these catalytic reactions. However, as solvent-free conditions can often lead to enhanced reaction yields and shorter reaction times, this may be something that is worth pursuing to allow the hydroboration of more taxing substrates using the lithium aluminate catalysts reported in this thesis.

3.7 Conclusions

The aim of this project was to establish if there were any advantages of using lithium aluminate bimetallic catalysts over neutral monometallic aluminium catalysts. By comparing a series of lithium aluminates and aluminium compounds which differ by formal removal of LiH it was possible to determine that generally these lithium aluminate catalysts were capable of providing higher conversions and shorter reaction times. These trends were consistent across aldehyde, ketone and imine substrates. The structural characterisation of $[(\text{TMP})\{\text{Ph}_2(\text{H})\text{CO}\}\text{Al}\{\mu\text{-OC}(\text{H})\text{Ph}_2\}]_2$, **15**, highlighted a new mode of catalyst activation for ketone hydroboration involving β -hydride elimination from the *i*Bu ligands of *i*Bu₂Al(TMP), **12**, reminiscent of Meerwein-Ponndorf-Verley transfer hydrogenation catalysis.

Turning to imines, the advantages of lithium aluminate catalysts started to become more obvious. The benefit of using such catalysts is proposed to be due to the enhanced polarisation of key reaction intermediates by the presence of the lithium cation, which can enhance the σ -bond metathesis step with HBpin. This notion is supported by stoichiometric reactions and the structural characterisation of the mixed alkyl-ketimide complex $[i\text{Bu}_2\text{Al}(\mu\text{-N}=\text{CPh}_2)]_2$, **16**, arising from the deprotonation of benzophenone imine by **12**. In the stoichiometric regime, both **10** and **12** deprotonate benzophenone imine *via* amide basicity. That **12** is not an active catalyst for the hydroboration of imines but lithium aluminate analogue $[i\text{Bu}_2\text{Al}(\text{TMP})(\text{H})\text{Li}]_2$, **10**, implies the significance of the presence of the lithium cation. Stoichiometric reactions of benzophenone imine with either **11** or **14** show deprotonation of the substrate by the hydride, as shown by the formation of H₂ in the ¹H NMR spectrum. However, in spite of this, **14** is not capable of catalyzing the hydroboration of imines. That $[i\text{Bu}_3\text{AlHLi}]_2$, **11**, is more active than **10** for the hydroboration of imines could be due to the enhanced nucleophilicity of the hydride as a result of three *i*Bu ligands coordinated to the aluminium in **11**.

In the case of alkynes, it is again clear that different reaction pathways are available for the aluminium catalysts. In stoichiometric reactions, **10** deprotonates phenylacetylene, and thus is proposed to follow a catalytic pathway akin to that depicted in Scheme 3.3 (i), while **11** is proposed to follow the hydroalumination pathway in Scheme 3.3 (ii). As this project developed it became apparent that solution structure is important and it is not always a case of “one size fits all” in terms of catalysis. Thus, for sterically congested substrates monometallic aluminium complexes (such as *i*Bu₂AlH, **14**), may be a better choice in terms of

product yield and reaction times. This observation was corroborated when the hydroboration of alkynes was considered, in which **14** is the more active catalyst for diphenylacetylene than **11**, but where **11** is the more active catalyst for 1-phenyl-1-propyne than **14**. The current state of the field dictates that a full investigation into the role of the lithium cation is now required. Use of heavier alkali metal aluminates, such as those of sodium or potassium, would help support the so far observed lithium benefit. DFT calculations on these systems are also now required in order to back up experimental observations and help direct the next generation of hetero-bimetallic aluminate catalysts for such hydroelementation reactions.

Chapter 4: Decomposition Studies in Aluminium Catalysed Hydroboration Reactions

Putting the results in context with the literature an extended discussion and conclusion to the manuscript are provided

Contributing authors to this chapter and their roles:

Victoria A. Pollard – Designed and performed the experiments; drafted the manuscript

Ross McLellan – Helped with data processing and data interpretation

Alan R. Kennedy – Checked the accuracy of X-ray diffraction data processing

Robert E. Mulvey – Principal investigator

The supporting information can be found in Chapter 7: Experimental; Section 7.4 and Table

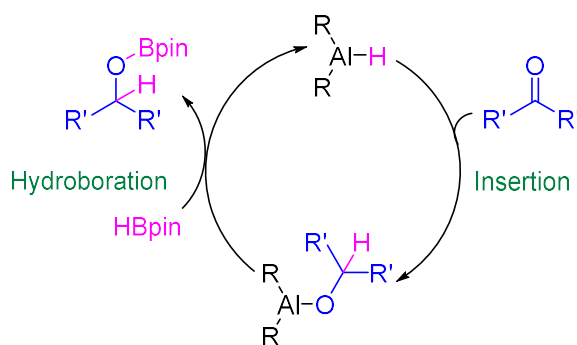
7.7.3

4.1 Abstract

A comparison between bimetallic lithium aluminates and neutral aluminium counterparts is made in a reactivity study with boron reagents that are commonly used in hydroboration studies. Neutral aluminium species are observed to cleave the B – O bond of HBpin, generating novel aluminium complexes. Conversely, bimetallic lithium aluminates are shown to undergo ligand scrambling reactions. The poor performance of these new species as hydroboration catalysts implicates them as potential aluminium catalyst deactivation complexes.

4.2 Introduction

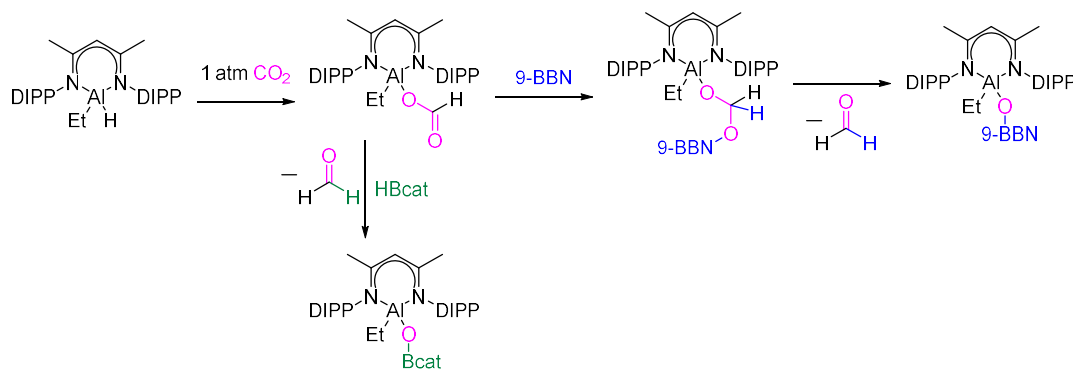
One of the most successful examples of organic transformations catalysed by aluminium is the hydroboration of unsaturated substrates, most notably carbonyls, with pinacolborane, HBpin.^{15, 16} The reagent HBpin was first introduced to synthetic chemistry by Knochel.¹⁵⁷ The reaction mechanism for hydroboration has been studied in considerable depth, and is typically proposed to go *via* a two-step pathway: in the first step an aluminium hydride catalyst hydroaluminates the substrate (for example a ketone), while in the second step a σ -bond metathesis takes place with HBpin yielding the desired boronic ester product and regenerating the catalytic aluminium hydride complex (Scheme 4.1).



Scheme 4.1: Generally proposed catalytic cycle for aluminium-catalysed hydroboration, illustrated with an aldehyde/ketone substrate.

This catalytic cycle is widely postulated as the reaction mechanism for the majority of aluminium-catalysed hydroboration reactions.⁷⁹ Furthermore, there have been several examples in the literature of isolated potential catalytic intermediates.^{76, 177, 178, 181} These “intermediate” compounds can react with HBpin to generate the desired product stoichiometrically, and are themselves catalytically active, which implicates them as having a role in the catalytic cycles. Therefore, it is well established in the literature that this is a viable mechanism in this instance. Examples of such intermediate complexes include the benzaldehyde derivative (HMDS)₂Al(μ-OCH₂Ph)₂Li(THF)₂, **8**, and the benzophenone derivative [(TMP){Ph₂(H)CO}Al{μ-OC(H)Ph₂}]₂, **15**, disclosed in Chapters 2 and 3 of this thesis, respectively.

A recent study by Aldridge on the reduction of CO₂ using a range of nacnac-ligated aluminium hydride complexes has, however, indicated that the required Al–O/B–H σ-bond metathesis is not always viable, thus thwarting the turnover step in the catalytic cycle.²⁴⁷ Investigation of a series of ^{DIPP}nacnacAl(R) compounds highlighted the need for consideration of the choice of spectator ligands, with R = Me or Et weakening the Al–H bond and effectively rendering the system more hydridic and consequently more able to perform hydroalumination. Conversely, when R = Cl or OTf the Al–H bond was stronger and therefore less likely to react. Reaction of ^{DIPP}nacnacAl(Et)H with 1 bar CO₂ at room temperature readily generates the expected formate complex (Scheme 4.2).



Scheme 4.2: Reaction summaries for ^{DIPP}nacnacAl(Et)(H) with HBcat or 9-BBN.

Onward reactivity with HBpin was not observed even under forcing conditions. That notwithstanding, addition of excess HBcat generated a new nacnac-ligated aluminium boryloxy complex (Scheme 4.2). In the presence of excess HBcat, even under forcing conditions, no generation of an Al – H bond was observed, signalling that Al – O/B – H σ -metathesis is not thermodynamically feasible with this system. A similar situation is observed with 9-BBN, however in this instance the authors were able to isolate and characterise the intermediate aluma-bora-acetal (Scheme 4.2). This intermediate complex is much more stable with 9-BBN (it was not observed at all with HBcat) and only very slowly converts to the corresponding aluminium boryloxy complex. The generation of such aluminium boryloxy complexes is proposed to proceed *via* extrusion of formaldehyde, and the significant difference in reaction rates between HBcat and 9-BBN suggests that the aluminium boryloxy complex is generated by a C – O/B – H σ -bond metathesis reaction.

A prevailing feature of organo group-13 hydrides is their ability to form M – H – M bridges, and there are several examples of mixed aluminium boron hydrides in the literature (Figure 4.1). In 1998, Nöth reported the synthesis of $(\text{TMP})_2\text{AlH}_2\text{BR}_2$, from the salt metathesis reaction of $(\text{TMP})_2\text{AlCl}$ with LiH_2BH_2 or $\text{LiH}_2(9\text{-BBN})$.²⁴⁸ Both aluminium borates were characterised in the solid state and solution phase. In the ^{11}B NMR spectrum, the tetrahydroborate complex exhibits a quintet signal at -24.4 ppm ($J = 89$ Hz), while the 9-BBN complex has a broad, unresolved signal at -3 ppm. More recently, the synthesis of $i\text{Bu}_2\text{Al}(\text{BH}_4)$ was reported, from the reaction of $i\text{Bu}_2\text{AlH}$ and $\text{BH}_3\cdot\text{SMe}_2$, with a ^{11}B NMR chemical shift of -36.8 ppm for the borate centre.²⁴⁹ Although not structurally authenticated, $i\text{Bu}_2\text{Al}(\text{BH}_4)$ was reported to be incredibly active for the reduction of tertiary amides to the corresponding amines under ambient conditions, circumventing the harsh reaction conditions required with $i\text{Bu}_2\text{AlH}$ or LiAlH_4 .

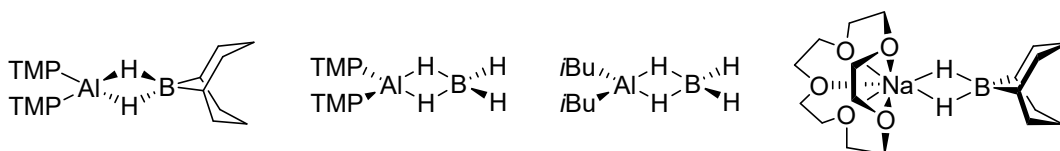
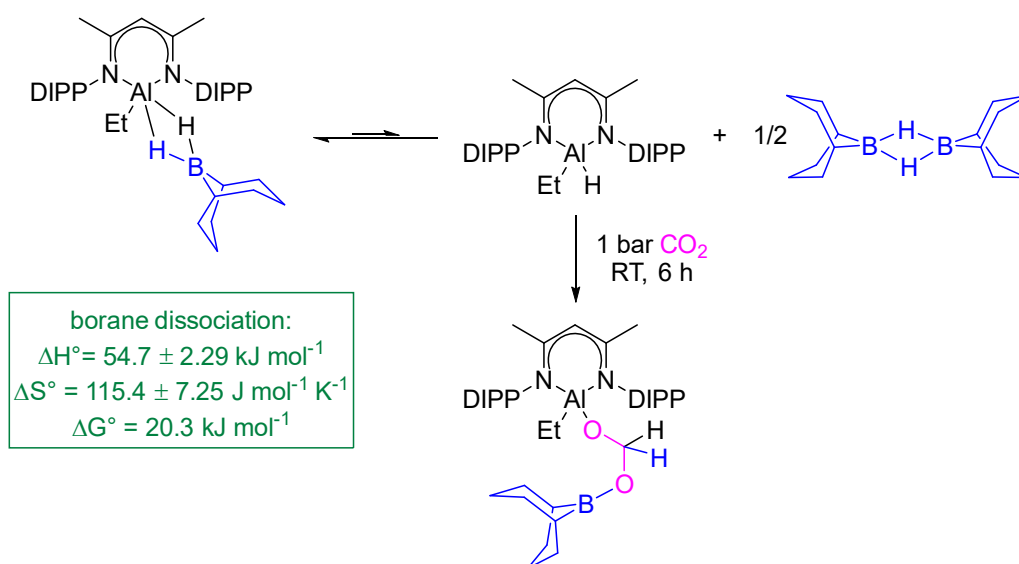


Figure 4.1: Examples of aluminium, and sodium, borate complexes.

A catalytic role for borate complexes in alkene hydroboration has been proposed in titanium- and calcium-catalysed hydroboration of alkenes with HBcat.^{250, 251} Furthermore, Thomas has recently reported the hydroboration of alkynes and alkenes with HBpin employing monomeric $\text{BH}_3 \cdot \text{L}$ (L = THF or SMe_2) as the catalyst (10 mol%, 60 °C, 0.5 – 18 hours).¹⁷⁶ Other recent reports implicate borate complexes as important species in hydroboration catalysis.^{173, 252, 253} For example, the recent publication by Wu, Liu and Zhao has suggested that in NaOH catalysed hydroboration the active catalytic species is in fact a sodium borate.¹⁷³ This sodium borate was crystallographically authenticated upon addition of 15-crown-5 as $(15\text{-crown-5})\text{Na}(\mu\text{-H})_2(9\text{-BBN})$, (Figure 4.1) [15-crown-5 = 1,4,7,10,13-pentaoxacyclopentadecane]. Such adduct formation between boranes and nucleophiles has been calculated to induce a weakening of the B – H bond, and hence lead to enhanced hydridic character which would facilitate the hydroboration processes.¹⁷³ In spite of these observations, and the presence of such aluminium borates in the literature, the application of such complexes to the hydroboration of unsaturated substrates has only recently been examined for the first time by Aldridge.²⁵⁴ Treatment of nacnac-ligated aluminium hydride complexes, $\text{D}^{\text{IPP}}\text{nacnacAl}(\text{R})\text{H}$, (R = H, Me, Et, OTf) with 0.5 equivalents of the 9-BBN dimer at room temperature cleanly yielded the expected aluminium borate complexes (Scheme 4.3). A number of these borates displayed unusual dissociation of the borane from the aluminium hydride in solution at ambient conditions. The lability of the borane was shown to be effected by the nature of the “R” group; electron-withdrawing substituents lead to a greater dissociation of borane. In comparison, the analogous structure $\text{D}^{\text{IPP}}\text{nacnacAl}(\text{Et})(\text{BH}_4)$ does not display any borane dissociation. The differences in borane lability affect the reactivity of the aluminium borates with CO_2 . Thus, the $\text{D}^{\text{IPP}}\text{nacnacAl}(\text{Et})(\text{BH}_4)$ does not react with CO_2 at room temperature. However, in contrast $\text{D}^{\text{IPP}}\text{nacnacAl}(\text{Et})(9\text{-BBN})$ reacts readily with CO_2 to selectively yield, after extended reaction times, $\text{D}^{\text{IPP}}\text{nacnacAl}(\text{Et})\{\text{OCH}_2\text{O}(9\text{-BBN})\}$ (Scheme 4.3). The authors propose that the CO_2 does not react directly with the higher coordinated aluminium borate, but rather with the lower coordinated free aluminium hydride, which is present in low concentrations in solution, due to partial dissociation of the borane. This observation is consistent with observations in the nickel-catalysed hydroborations of CO_2 where the metal borate complex represents a resting state on the catalytic cycle.²⁵⁵



Scheme 4.3: Borane dissociation from aluminium borate complexes, and onward reactivity with CO_2 , for the example where $\text{R} = \text{Et}$.

In a similar vein, examples of elucidated catalyst decomposition pathways in hydroboration are limited. This is surprising as the decomposition pathway of the catalyst employed will determine its maximum lifetime, and thus the required catalyst loading. The compound 2,2'-[1,4-butanediylbis(oxy)]bis[4,4,5,5-tetramethyl-1,3,2-dioxaborolane], B_2pin_3 , is a known, crystallographically-characterised decomposition product of HBpin (Figure 4.2).²⁵⁶

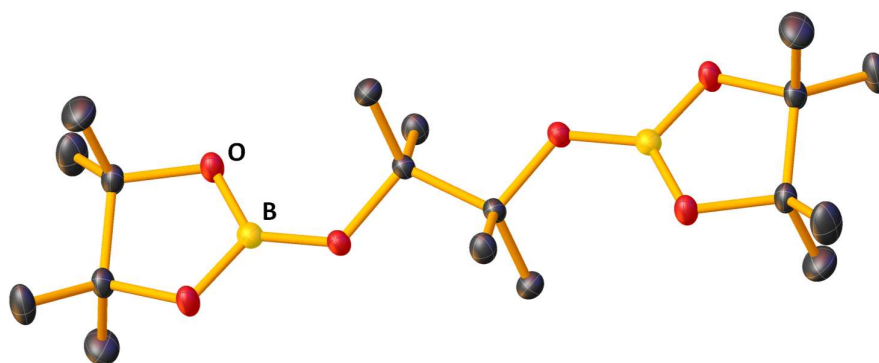


Figure 4.2: Molecular structure of one HBpin decomposition product, B_2pin_3 . Thermal ellipsoids are drawn at 40% probability and hydrogen atoms have been removed for clarity.

Hill reported the formation of trace amounts of B_2pin_3 in the hydroboration of imines, catalysed by a β -diketiminato magnesium alkyl complex, $^{DIPP}nacnacMg(nBu)$, under relatively forcing conditions (60 °C for reactions exceeding 24 hours).⁵⁵ Harder employed a β -diketiminato calcium hydride complex, $[^{DIPP}nacnacCa(H)(THF)]_2$ for hydroboration of diphenylethene with HBcat and determined that the calcium complex was acting as a “Trojan horse” and facilitating the decomposition of HBcat to $B_2(cat)_3$ and B_2H_6 , amongst other boron containing products.²⁵⁰ The authors concluded that it was the borane B_2H_6 rather than the hydride HBcat which was performing the hydroboration in this instance. To find other documented examples of cleavage of one or both of the B – O bonds in HBpin or HBcat one has to turn to transition metal, lanthanide, or actinide complexes.²⁵⁷⁻²⁶⁵ Ligand redistribution reactions between alanes AlX_3 and boranes BY_3 to $AlX_{3-n}Y_n$ and $BY_{3-n}X_n$ are also well documented.^{266, 267} Cowley and Thomas harness this reactivity to generate the active catalyst Et_2AlH from a Et_3Al pre-catalyst and HBpin in their hydroboration of acetylenes.¹⁷⁸ Similarly, $iBu_2Al(H)$ and HBpin also undergo ligand scrambling generating $iBuBpin$ and iBu_3B , amongst other products.¹⁷⁸

Under typical catalytic conditions, for example utilising 10 mol% catalyst, at the start of the reaction there are 10 equivalents of HBpin per aluminium centre, so it is important to understand how these reagents interact with each other. Stoichiometric reactions between popular, widely-utilised boranes, and either monometallic organoaluminium or bimetallic lithium aluminate complexes, were undertaken in order to determine the nature of the product/s involved which might also shed light on potential decomposition pathways in aluminium amide mediated hydroboration catalysis.

4.3 Project Aims

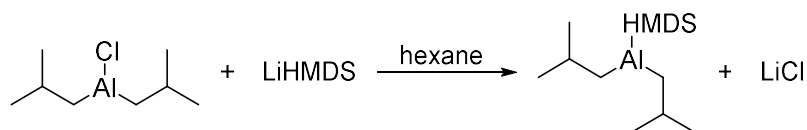
The aims of this part of the project are summarised below.

- To investigate the reactivity of HBpin towards the neutral monometallic dialkylaluminium amide reagents $iBu_2Al(TMP)$ and $iBu_2Al(HMDS)$.
- To determine whether the mode of reactivity found is general for $iBu_2Al(TMP)$ when treated with other common, commercial “utility” borane reagents.

- To understand what differences in reactivity, if any, exist between neutral monometallic aluminium amide reagents and bimetallic lithium aluminate complexes, containing these bulky amide ligands, with common hydroborating reagents.
- To attempt to isolate and characterise any metallo intermediates formed during the course of these reactions.

4.4 Results and Discussion

Previously, $i\text{Bu}_2\text{Al}(\text{TMP})$, **12**, was reported to be able to catalyse the hydroboration of ketones with HBpin *via* a β -hydride transfer mechanism at room temperature.²⁶⁸ Testing the generality of this initiation pathway to other alkyl aluminium amides, $i\text{Bu}_2\text{Al}(\text{HMDS})$, **18**, was prepared by a salt metathesis reaction between $i\text{Bu}_2\text{AlCl}$ and Li(HMDS), isolating the desired compound as a colourless oil in high yield (Scheme 4.4). Note that TMP is more sterically demanding than HMDS and in the case of their lithium complexes, the former is significantly more basic.



Scheme 4.4: Synthesis of $i\text{Bu}_2\text{Al}(\text{HMDS})$, **18**, via a salt metathesis reaction.

A reaction performed in a J. Young's NMR tube between $i\text{Bu}_2\text{Al}(\text{HMDS})$ and benzophenone in C_6D_6 solution with subsequent monitoring by ^1H NMR spectroscopy lead to the observation of signals consistent with *isobutene* [^1H NMR: δ 1.58 (t, $J = 1.20$ Hz, 6H); 4.72 (sept. $J = 1.20$ Hz), 2H], the co-product of β -hydride transfer (Figure 4.3).

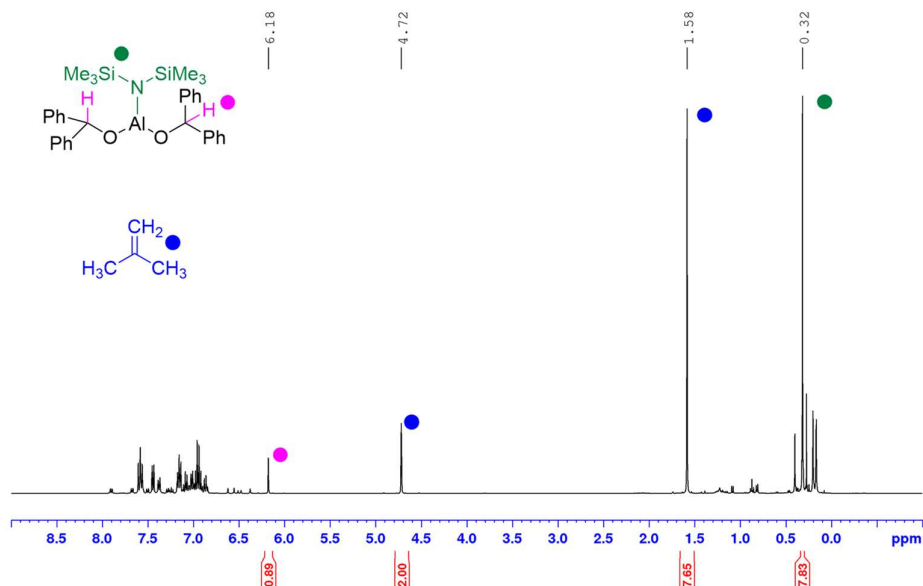
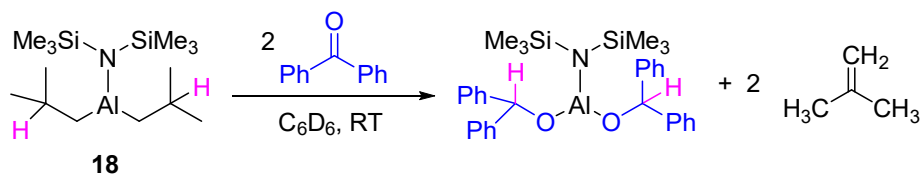


Figure 4.3: ^1H NMR spectrum for the NMR scale reaction of benzophenone with $i\text{Bu}_2\text{Al}(\text{HMDS})$, **18**. Key diagnostic signals have been labelled and colour coded. The spectrum was recorded in C_6D_6 at 400 MHz.

This implies that **18** acts as a masked hydride in the same way as **12** suggesting that the novel catalyst initiation pathway operating for **12** may be general to other such di-*iso*-butyl $i\text{Bu}_2\text{Al}(\text{NR}_2)$ pre-catalyst compounds (Scheme 4.5).

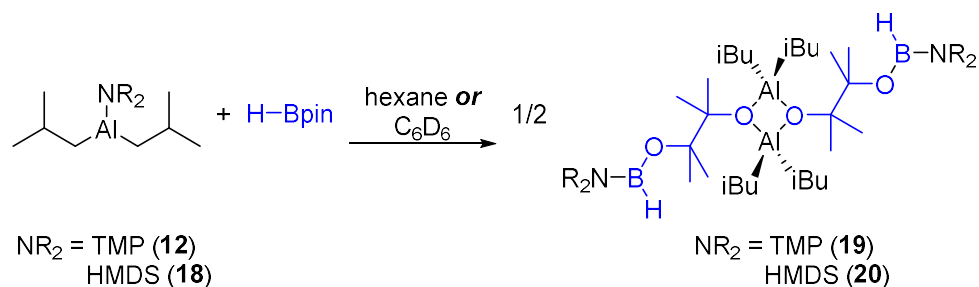
Pre-catalyst activation: β -hydride transfer



Scheme 4.5: Catalyst initiation pathway *via* β -hydride transfer.

In an effort to uncover potential decomposition pathways in hydroboration reactions utilising **12** as the catalyst, we performed a stoichiometric reaction between $i\text{Bu}_2\text{Al}(\text{TMP})$ and HBpin

in C_6D_6 in a J. Young's NMR tube. It was expected that a mixture of products such as *i*BuBpin and (TMP)Bpin would be obtained. Instead, the rapid formation of colourless crystals of compound **19** was observed at room temperature (56% crystalline yield, Scheme 4.6). Subsequent scale up of this reaction and single crystal X-ray diffraction studies of the product revealed the novel molecular structure $[iBu_2Al\{OC(Me)_2C(Me)_2O\}B(H)(TMP)]_2$, **19** (Figure 4.4). Surprisingly, **19** retains the typically more reactive B – H bond (416 kJ/mol dissociation energy), yet cleaves the far stronger B – O bond (890 kJ/mol dissociation energy).²⁶⁹ This is significant as in order for hydroboration catalysis to proceed cleavage of the B – H bond is required. The formula of **19** indicates that the 5-membered BOCCO ring of HBPin has opened during this reaction and inserted into the Al – N bond of the aluminium amide. Comparatively the bond dissociation energy for a B – N bond is 377 kJ/mol, while bond dissociation energies at aluminium have been reported as: Al – H 288 kJ/mol; Al – O 502 kJ/mol; and Al – N 368 kJ/mol.²⁶⁹ Therefore, it is clear to see that a B – H bond is stronger than the corresponding Al – H bond, while the B – N bond is stronger than the Al – N bond. However, a B – O bond is still stronger than the corresponding Al – O bond, which presents some questions as to the driving force in the formation of **19**. One possible driving force could be due to stabilisation as a result of aggregation upon forming the dimeric species.



Scheme 4.6: Synthesis of the dimeric Bpin ring-opening compounds **19** and **20**.

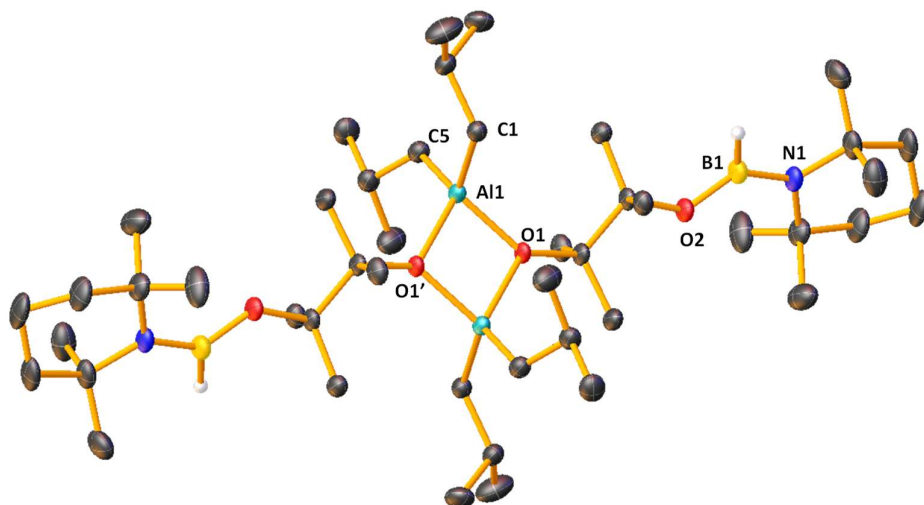


Figure 4.4: Molecular structure of compound **19**. Hydrogen atoms, except B–H hydride have been omitted for clarity. Thermal ellipsoids are drawn at 40% probability. Symmetry operations used to generate equivalent atoms $-x$; $-y$; $1-z$. Selected bond lengths (Å) and angles (°): Al1 – O1, 1.8701(14); Al – O1', 1.8727(13); Al1 – C5, 1.982(2); Al1 – C1, 2.002(2); B1 – O2, 1.377(3); B1 – N1, 1.418(3); B1 – H1, 1.13(3); C5–Al1–O1, 117.16(8); C1–Al1–O1, 113.38(7); C5–Al1–O1', 117.23(7); C1–Al1–O1', 110.96(7); C1–Al1–C5, 112.90(8); O1–Al1–O1', 81.68(6); H1–B1–N1, 117.5(15); H1–B1–O2, 122.8(2); O2–B1–N1, 119.8(15).

Compound **19** exists as a centrosymmetric dimer featuring a planar rhombus Al – O – Al – O core. The aluminium centres exist in a distorted tetrahedral geometry made up of two O and two C atoms with bond angles in the range 110.96(7) – 117.22(7) °, whilst the boron centre is in a slightly distorted trigonal planar environment with bond angles in the range 117(2) – 122.7(2) °. The TMP and aluminium fragments sit at opposite ends of the ring-opened B – pinacol unit. In the ^1H NMR spectrum the resonance of the hydride is observed as a broad singlet at 4.75 ppm in C_6D_6 solution, which sharpens upon applying ^{11}B decoupling. In comparison, the ^1H NMR resonance for the hydride in HBpin exhibits as a broad quartet at 4.17 ppm with a J coupling constant of 171.56 Hz, in C_6D_6 solution at 400 MHz. The ^{11}B NMR spectrum of **19** displays a broad singlet signal at 30.0 ppm, while for HBpin the ^{11}B NMR signal occurs as a doublet at 28.1 ppm ($J = 174$ Hz). The lack of observed splitting in the ^1H and ^{11}B NMR spectra of **19** could be as a result of signal broadening due to

a quadrupolar nucleus (^{11}B) in an asymmetrical environment. Undertaking a ^1H DOSY NMR experiment on **1** in C_6D_6 solution provides an estimated molecular weight of 830 g/mol, which is in agreement with **19** retaining its dimeric structure in solution (818.73 g/mol; -1% error). The $^{13}\text{C}\{^1\text{H}\}$ NMR spectrum displayed all the expected signals. Unfortunately, no signal was observed in the ^{27}Al NMR spectrum.

A similar situation is observed when $i\text{Bu}_2\text{Al}(\text{HMDS})$ and HBpin are reacted together in hexane solution. Crystals of $[\text{iBu}_2\text{Al}\{\text{OC}(\text{Me})_2\text{C}(\text{Me})_2\text{O}\}\text{B}(\text{H})(\text{HMDS})]_2$, **20**, were obtained from the reaction in a low 24% crystalline yield (Scheme 4.6). Determined by X-ray crystallography, the molecular structure of **20** is analogous to that of **19**, in that the five-membered pinacolborane ring has been opened, the B – O bond has been cleaved, the B – H bond retained, and the amide ligand delivered to the boron centre. Decomposition product **20** also exists as a centrosymmetric dimer with a planar Al – O – Al – O core (Figure 4.5). As can be seen in Table 4.1, structurally the core elements of compounds **19** and **20** are essentially identical. For example, the O – Al – O bond angle in **19** is $81.68(6)^\circ$, in **20** it is $81.73(6)^\circ$. Furthermore, key bond lengths such as Al – O [**19**: 1.8701(14) Å and 1.8727(13) Å; **20**: 1.8624(13) Å and 1.8774(13) Å] and B – N (**19**: 1.418(3) Å; **20**: 1.422(3) Å) are essentially indistinguishable. Performing a ^1H DOSY NMR study in C_6D_6 confirms that **20** also exists as a dimeric species in solution with an estimated molecular weight of 915 g/mol (858.64 g/mol; -6 % error). A similar ^1H NMR resonance for the B – H is observed at 4.80 ppm. The ^{11}B NMR signal for **20** is also a broad signal, with a chemical shift of 31.8 ppm.

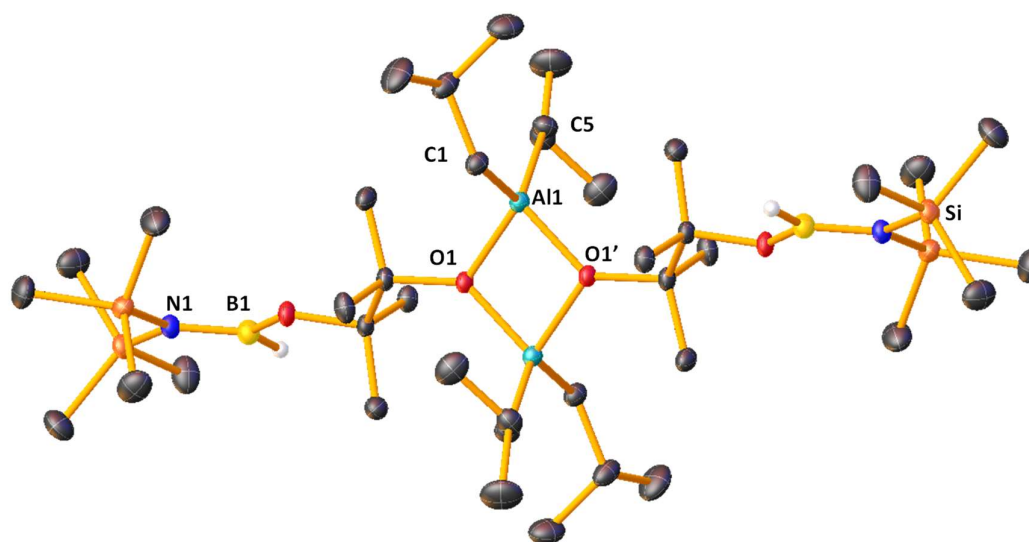


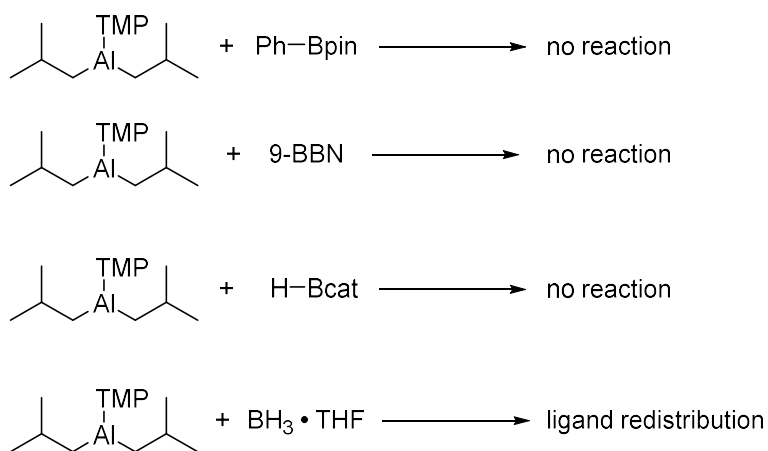
Figure 4.5: Molecular structure of **20**. Hydrogen atoms except B – H hydride have been omitted for clarity. Thermal ellipsoids are drawn at 40% probability. Symmetry operations used to generate equivalent atoms $1 - x$; $1 - y$; $1 - z$. Selected bond lengths (Å) and angles (°): Al1 – O1, 1.8264(13); Al1 – O1', 1.8774(13); Al1 – C1, 1.987(2); Al1 – C5, 1.979(2); B1 – O2, 1.364(3); B1 – N1, 1.422(3); B1 – H1, 1.07(2); C1-Al1-O1, 110.40(7); C1-Al1-O1', 110.59(7); C5-Al1-O1, 115.34(9); C5-Al1-O1', 115.71(7); C5-Al-C1, 115.34(9); O1-Al1-O1', 81.73(6); O2-B1-H1, 115.7(11); N1-B1-H1, 124.0(11); O2-B1-N1, 120.33(9).

Table 4.1: Comparison of selected bond lengths and angles between **19** and **20**.

	Compound 19	Compound 20
Al – O / Å	1.8701(14); 1.8727(13)	1.8624(13); 1.8774(13)
B – N / Å	1.418(3)	1.422(3)
B – O / Å	1.377(3)	1.364(3)
B – H / Å	1.13(3)	1.07(2)
O – Al – O / °	81.68(6)	81.73(6)
Al – O – Al / °	98.32(6)	98.27(6)

Next the reactivity of **12** with other commercially available borane reagents was examined (Scheme 4.7). No reaction is observed with (Ph)Bpin, even at elevated temperatures (70 °C).

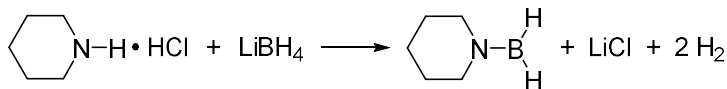
Similarly no reaction is observed with borabicyclo(3.3.1)nonane (9-BBN) or bis(pinacolato)borane (B₂pin₂). Even catecholborane (HBcat) is not observed to react with **12**. It is thought that the increased rigidity of the catechol ligand compared with pinacol is the reason for this lack of reactivity. This is notable however, as generally HBpin, being based on a tertiary alkyl ether, is considered less prone to ring opening than the phenolic ether-based HBcat.²⁷⁰⁻²⁷² Mixing *i*Bu₂Al(TMP) with BH₃·THF in hexane afforded a complex mixture of products as indicated by at least seven signals in the ¹¹B NMR spectrum, indicative of ligand redistribution. This is consistent with the ligand redistribution process noted by Cowley and Thomas between *i*Bu₂AlH and HBpin which forms *i*BuBpin, and the trialkylborane *i*Bu₃B.¹⁷⁸



Scheme 4.7: Attempted reactivity of **12** with a range of common commercial boranes.

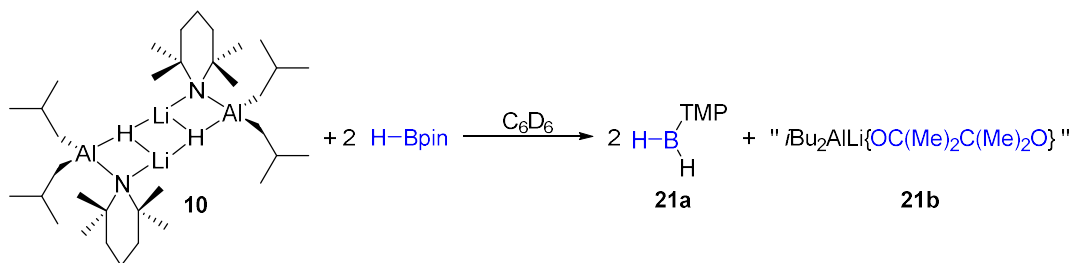
Previously it has been shown that charged bimetallic lithium aluminates tend to show superior catalytic activity in the hydroboration of various unsaturated substrates, compared with the neutral analogues.^{209, 236, 268} It was therefore expected the reactivity of such bimetallic lithium aluminates with HBpin would differ from the observations above with neutral **12**. A NMR scale reaction of [*i*Bu₂Al(TMP)(H)Li]₂, **10**, with HBpin produces a new compound **21a** which displays a triplet in the ¹¹B NMR spectrum at 37 ppm (J = 126 Hz), which collapses to a singlet upon ¹H decoupling. This is indicative of a new BH₂ species. Unfortunately, no isolation by crystallisation was possible for any of the components within this reaction mixture, despite repeated attempts. A search of the literature identifies

H₂B(piperidide) which has a reported ¹¹B chemical shift of 37 ppm,²⁷³ in agreement with the observed signal for **21a** (Scheme 4.8).



Scheme 4.8: Reported literature synthesis of H₂B(piperidide).

Therefore, it is speculated that **10** and HBpin are undergoing a ligand scrambling process which results in transfer of both the hydride and the TMP amide ligands from the lithium aluminate reagent to the borane generating compound **21a**; it is postulated that **21b** is also formed (Scheme 4.9). The formation of a new lithium species is confirmed in the ⁷Li NMR spectrum, where a signal shift is seen from $\delta = -0.10$ ppm (**10**) to 0.59 ppm (**21b**). It should be noted that at the same concentration in C₆D₆ the ⁷Li NMR signal for LiTMP is 2.49 ppm, indicating that in this NMR reaction of **10** and HBpin no LiTMP is liberated. In the ¹H NMR spectrum of this reaction a very broad quartet is apparent at 5.07 ppm ($J = 126$ Hz), indicative of a boron hydride complex. It is notable that in the ¹H NMR spectrum the signal corresponding to the methyl groups of the pinacol ligand appear as one singlet, suggesting they exist in an equivalent chemical environment (see Extended discussion). A lithium aluminate co-product, *i*Bu₂Al{OC(Me)₂C(Me)₂O}Li (**21b**) is tentatively proposed in addition to H₂B(TMP) **21a**.



Scheme 4.9: Reaction of **10** with HBpin showing postulated products **21a** and **21b** arising as a result of ligand redistribution processes.

Next, the analogous reaction between **10** and HBcat was investigated. Interestingly, this reaction also gives rise to a new triplet in the ^{11}B NMR at 37 ppm ($J = 127$ Hz), which also collapses to a singlet in a $^{11}\text{B}\{^1\text{H}\}$ NMR spectrum. Based on these observations in the ^{11}B NMR, it is highly likely that the boron containing product is the same compound **21a** as a result of the identical chemical shift and coupling constant observed in the ^{11}B NMR spectrum. This suggests that the lithium aluminate component of this reaction is similar to that of **21b**, bearing a catechol ligand rather than a pinacol ligand. However, the ^1H NMR spectrum of this reaction was inconclusive due to the broadness of the signals observed and as such no assignments could be performed.

Lastly, the application of **18**, **19**, **20** and **21** as catalysts for hydroboration of benzophenone with HBpin was performed to check the catalytic viability of these new complexes (Table 4.2). The catalysis of benzophenone with 5 mol% of **18** as a catalyst is notably slower than with **12**, requiring 3 hours to reach 97% conversion, compared to 0.5 hours required to achieve quantitative conversion with **12**. This suggests that the β -hydride transfer reaction for the formation of the active aluminium hydride catalyst is significantly faster with **12** than **18**. Note that the insertion and hydroboration steps in the catalytic cycle may also be effected by the change in amide ligand, possibly as a result of steric differences, and this may be contributing to the differences in the efficiency of the catalysis.

Employing 5 mol% of aluminium borane **19** as a catalyst in the hydroboration of benzophenone managed only a low yield of 35%, after 17 hours, in contrast to the quantitative conversion obtained within 0.5 hours when **12** is used as a catalyst. As might be expected from its close similarity to **19**, **20** also performs poorly as a catalyst, with only 24% conversion after 21 hours at room temperature when 5 mol% was used. This suggests that both **19** and **20** exist as off-cycle products from the hydroboration with **12** and **18** as catalysts, respectively. Therefore, **19** and **20** can be considered deactivation products from these monometallic aluminium catalysts. However, it should be noted that when **12** is employed as a catalyst in hydroboration reactions no signals corresponding to **19** are observed in the ^{11}B NMR spectrum. This indicates that in the presence of a ketone substrate the rate of the hydroboration reaction is greater than the rate of B – O cleavage and formation of **19**. Similarly, upon subsequent addition of benzophenone and HBpin to the preformed mixture of **21** (5 mol%), only 61% conversion to borane ester product is obtained after 5 hours. This

significantly lower catalytic rate with **21** compared with **10** (quantitative conversion within 0.5 hours) indicates that **21a** and **21b** are also potential off-cycle products, resulting from catalyst deactivation. However, that **19**, **20**, and **21** still exhibit some catalytic activity suggests that their formation may be reversible.

Table 4.2: Hydroboration of benzophenone catalysed by selected aluminium catalysts, and comparison between different borane sources.

Catalyst (5 mol% [Al])	Yield (%)	Time (h)
$[i\text{Bu}_2\text{Al}(\text{TMP})(\text{H})\text{Li}]_2$, 10	99	0.5
$i\text{Bu}_2\text{Al}(\text{TMP})$, 12	99	0.5
$i\text{Bu}_2\text{Al}(\text{HMDS})$, 18	97	3
$[i\text{Bu}_2\text{Al}\{\text{OC}(\text{Me})_2\text{C}(\text{Me})_2\text{O}\}\text{B}(\text{H})(\text{TMP})]_2$, 19	35	17
$[i\text{Bu}_2\text{Al}\{\text{OC}(\text{Me})_2\text{C}(\text{Me})_2\text{O}\}\text{B}(\text{H})(\text{HMDS})]_2$, 20	24	21
$[\text{H}_2\text{B}(\text{TMP}) / i\text{Bu}_2\text{Al}\{\text{OC}(\text{Me})_2\text{C}(\text{Me})_2\text{O}\}\text{Li}]$, 21a/b mixture	61	5

5 mol% [Al] catalyst loading, C_6D_6 solvent, room temperature. All yields against ^1H NMR internal standard hexamethylcyclotrisiloxane.

4.5 Extended Discussion and Future Work

4.5.1 Solution phase studies of compounds **19**, and **20**

Both compounds **19** and **20** exist as dimers in the solid state. Investigation into their solution phase structures in C_6D_6 solution *via* ^1H DOSY NMR studies confirmed that this dimeric structure is retained in solution. For $[i\text{Bu}_2\text{Al}\{\text{OC}(\text{Me})_2\text{C}(\text{Me})_2\text{O}\}\text{B}(\text{H})(\text{TMP})]_2$, **19**, a molecular weight of 830 g/mol is proposed which agrees with the theoretical molecular weight of the

dimeric complex (818.73 g/mol) with a -1% error, against 1,2,3,4-tetraphenylnaphthalene as a standard (Figure 4.6 and Table 4.3).



Figure 4.6: ^1H DOSY NMR spectrum of **19**, in C_6D_6 solution.

Table 4.3: Diffusion coefficient data from ^1H DOSY NMR spectrum of **19**, in C_6D_6 solution.

Compound	D [m^2s^{-1}]	MW_{calc} [g/mol]	MW_{est} [g/mol]	Error %
$[\text{iBu}_2\text{Al}\{\text{OC}(\text{Me})_2\text{C}(\text{Me})_2\text{O}\}\text{B}(\text{H})(\text{TMP})]_2$	5.356×10^{-10}	818.73 (dimer)	830	-1
1,2,3,4-Tetraphenylnaphthalene	6.883×10^{-10}	432.55	441	-2

Similarly, the ^1H DOSY NMR spectrum for **20**, $[\text{iBu}_2\text{Al}\{\text{OC}(\text{Me})_2\text{C}(\text{Me})_2\text{O}\}\text{B}(\text{H})(\text{HMDS})]_2$, is indicative of retention of the dimeric structure in the solution phase (Figure 4.7 and Table 4.4). A predicted molecular weight of 915 g/mol is in good agreement with the actual molecular weight of the dimer with a -6% error.



Figure 4.5: ^1H DOSY NMR spectrum of **20**, in C_6D_6 solution.

Table 4.4: Diffusion coefficient data from ^1H DOSY NMR spectrum of **20**, in C_6D_6 solution.

Compound	D [m^2s^{-1}]	MW_{calc} [g/mol]	MW_{est} [g/mol]	Error %
$[\text{iBu}_2\text{Al}\{\text{OC}(\text{Me})_2\text{C}(\text{Me})_2\text{O}\}\text{B}(\text{H})(\text{HMDS})]_2$	5.287×10^{-10}	858.64 (dimer)	915	-6
1,2,3,4-Tetraphenylnaphthalene	7.186×10^{-10}	432.55	441	-2

4.5.2 Insight into the composition of compound **21b**

The exact composition of **21b** has not yet been determined conclusively. Two potential compounds have been postulated (Figure 4.8). Compound **21b'** is similar in structure to compounds **19** and **20** and involves a pinacol ligand acting as a bridge between the lithium and aluminium centres. Alternatively, **21b''** proposes the formation of a solvent-separated lithium aluminate.

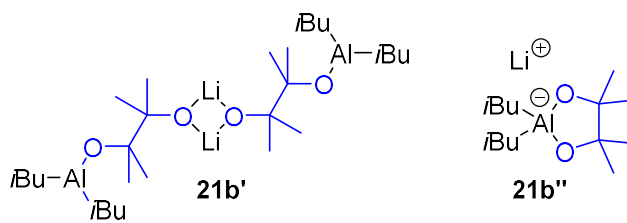
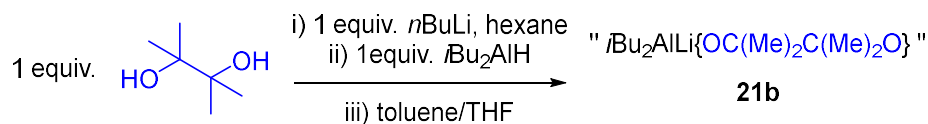


Figure 4.8: Postulated alternative compositions for **21b**, " $\text{iBu}_2\text{AlLi}\{\text{OC}(\text{Me})_2\text{C}(\text{Me})_2\text{O}\}$ ".

Investigations into the composition of **21b** have been undertaken by attempted rational synthesis of **21b**. It was expected that employing the sequential deprotonation of pinacol with $n\text{BuLi}$ and iBu_2AlH might lead to **21b** (Scheme 4.10).



Scheme 4.10: Attempted rational synthesis of **21b**.

The addition of THF as a Lewis donor ligand to a solution of this species has not yet been successful in generating crystals suitable for X-ray diffraction study. As noted above, in the reaction mixture of **21a/21b** the methyl groups of the pinacol ligand are represented by a singlet in the ^1H NMR spectrum, indicative of an equivalent chemical environment. This observation therefore suggests that the formation of **21b''** may be more likely. Whilst analysis of the signals in the ^1H NMR spectrum for the rational synthesis of **21b** are complicated as a result of poor solubility in C_6D_6 , leading to broad signals, it can be said that the signals in both reactions are present at similar chemical shifts (Figure 4.9). Furthermore, no signals consistent with unreacted iBu_2AlH are present. This suggests that the product of this rational synthesis is consistent with the observed product from the reaction of **10** with HBpin. Further investigations into the precise nature of **21b** is required both by crystallisation techniques and multinuclear NMR spectroscopy including DOSY NMR.

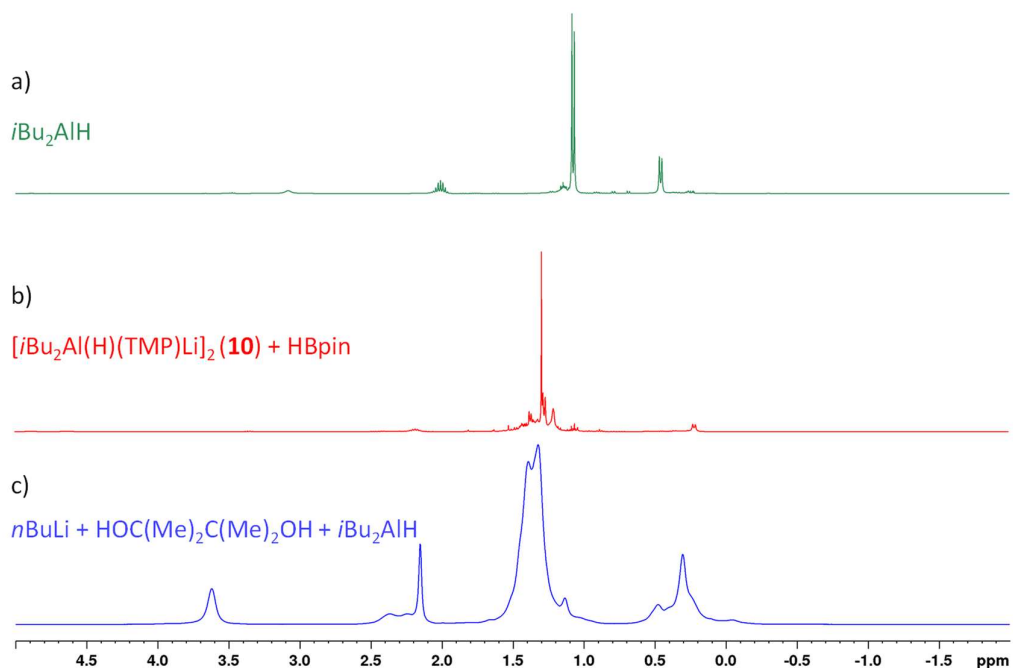
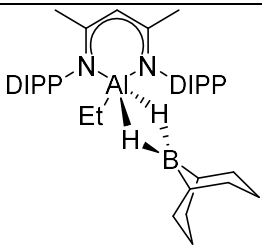
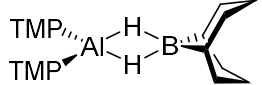
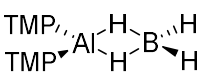
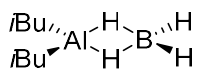
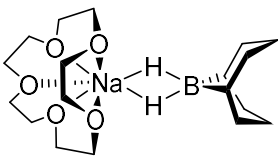


Figure 4.9: ^1H NMR spectra overlay of **a)** $i\text{Bu}_2\text{AlH}$, **b)** reaction of **10** with HBpin, and **c)** the rational synthesis of **21b**. All spectra were acquired in C_6D_6 solvent at 400 MHz.

4.5.3 Presence of aluminium borohydride compounds in hydroboration catalysis

As noted in the introduction to this chapter, metal borate complexes have been implicated as resting states for the catalyst species in hydroboration reactions employing transition metal based catalysts. Aldridge recently reported the first investigation into the reactivity of aluminium borates for the reduction of CO_2 and found them to undergo an unusual borane dissociation.²⁵⁴ The substrate CO_2 was shown to react only with the free aluminium hydride, thus implicating the aluminium borates characterised as potential resting states of a catalytically active species within main group catalysis. Table 4.5 provides a summary of ^{11}B NMR chemical shifts for such aluminium borate complexes.

Table 4.5: Summary of selected $\mu\text{-H}_2\text{BR}_2$ coordinated ligands to main group metal centres reported in the literature.

Compound	^{11}B chemical shift / ppm	Reference
	^{11}B δ : -16 (br. s)	254
	^{11}B δ : -3 (br. s)	248
	^{11}B δ : -24.4 (quintet)	248
	^{11}B δ : -36.8 (quintet)	249
	^{11}B δ : - 17.88 (t)	173

Crucially, no signals are observed in the ^{11}B NMR spectrum in the region -3 to -37 ppm in any of the stoichiometric reactions reported in this chapter, or in any of the hydroboration reactions undertaken in the course of this PhD project in Chapters 2 and 3. This implies that the formation of an aluminium borohydride species is not involved at any stage of the hydroboration catalysis. It is of note that $(15\text{-crown-5})\text{Na}(\mu\text{-H})_2(9\text{-BBN})$ is proposed to be the active species in the NaOH catalysed hydroboration of aldehydes, ketones, alkynes and alkenes, in the presence of 15-crown-5.¹⁷³ Furthermore, cationic aluminium complexes are reported to be up to 25 times more active than their neutral analogues in hydroamination catalysis (Chapter 1).⁸⁶ Therefore, further investigation into the application of aluminium borates as hydroboration (pre)-catalysts may be of interest.

4.6 Conclusions

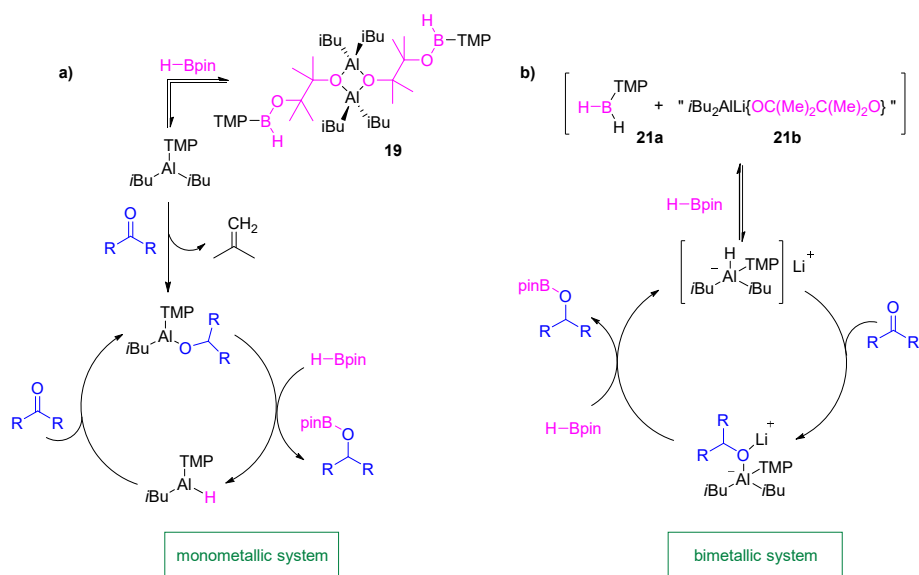
The study of decomposition products and deactivation pathways of aluminium catalysts for hydroelementation reactions is of interest for the development of next-generation aluminium catalysts which would, theoretically, exhibit enhanced catalytic activities over the current state of the art. The ligand scrambling reactions between alanes and boranes are well documented and whilst they can also be utilised, as shown by Cowley and Thomas,¹⁷⁸ often they are detrimental to catalytic reactivity. An understanding of the key reaction steps involved in the catalytic cycle is central to perfecting these catalytic applications. As shown by Aldridge, in certain circumstances these reaction steps are no longer thermodynamically viable and thus the reaction is not able to turn over, either stoichiometrically or catalytically.²⁴⁷ It is interesting that a catalyst system which is active for the hydroboration of aldehydes and ketones is not capable of undertaking the Al – O/B – H σ -metathesis step in the hydroboration of CO₂. This observation further emphasises the lack of a universal aluminium catalyst for a range of hydroelementation reactions.

As a result of these literature reports, stoichiometric reactions were employed with a view to uncovering potential deactivation pathways for a selection of aluminium based catalysts examined throughout this project. For neutral, monometallic aluminium complexes, *i*Bu₂Al(TMP), **12** and *i*Bu₂Al(HMDS), **18**, reaction with HBpin leads to ring-opening of the pinacolborane 5-membered ring, with retention of the B – H bond. Conversely, no reaction was seen between **12** or **18** and PhBpin, MeOBpin, 9-BBN or HBcat. With regards to HBcat the lack of reactivity is proposed to be due to the increased rigidity of the ligand which prevents it from opening to form a similar geometry as is observed in the crystal structures of **19** and **20**. With regard to the lithium aluminate system examined ligand redistribution processes are proposed whereby H₂B(TMP), **21a**, is formed as determined *via* ¹¹B NMR spectroscopy. The co-product of this reaction, [*i*Bu₂Al{OC(Me)₂C(Me)₂O}Li]₂, **21b**, was never structurally characterised despite repeated attempts. Preliminary attempted synthesis of an authentic sample of **21b** has been undertaken but as yet no conclusive evidence as to the true identity of **21b** has been obtained.

Lastly, **19**, **20** and **21** were all tested for catalytic activity in the hydroboration of benzophenone. In every instance these compounds were less catalytically active than their parent aluminium complexes. Whilst no indication of such compounds was observed in the

hydroboration reactions with **10** or **12** as catalysts, the results presented here implicate **19** and **21** as potential deactivation products arising as a result of off-cycle pathways within hydroboration reactions (Scheme 4.11).

Further investigation into the reaction pathways leading to these products by DFT calculations would be beneficial. This is particularly true for the lithium aluminate complex **10** where no products were able to be crystallographically authenticated. Furthermore, further experimentation should be performed in order to unequivocally determine the true identities of compounds **21a** and **21b**. It would also be beneficial to expand this reactivity study to other aluminium systems, such as $[\text{iBu}_3\text{AlHLi}]_2$, **11**, which has also been used as a hydroboration catalyst throughout this PhD project.



Scheme 4.11: Proposed potential off-cycle reactions with **a)** monometallic aluminium amide catalysts, and **b)** bimetallic lithium aluminate catalysts.

Chapter 5: Lithium Aluminate Catalysed Hydrophosphination

Preliminary drafted manuscript.

Putting the results in context with the literature an extended introduction, discussion and conclusion to the paper are provided.

Contributing authors to the manuscript and their roles:

Victoria A. Pollard – Designed and performed the experiments; analysed the data; drafted the manuscript

Allan Young – Performed the computational calculations

Ross McLellan – Helped with data processing; contributed to drafting of the manuscript

Alan R. Kennedy – Checked the accuracy of X-ray diffraction data processing

Tell Tuttle – Collaborator and academic supervisor of Allan Young

Robert E. Mulvey – Principal investigator

Alberto Hernan Gomez - For help with the interpretation of the kinetic data

David J. Nelson – For help with the interpretation of kinetic data

The supporting information can be found in Chapter 7: Experimental; Section 7.5 and Table 7.7.4

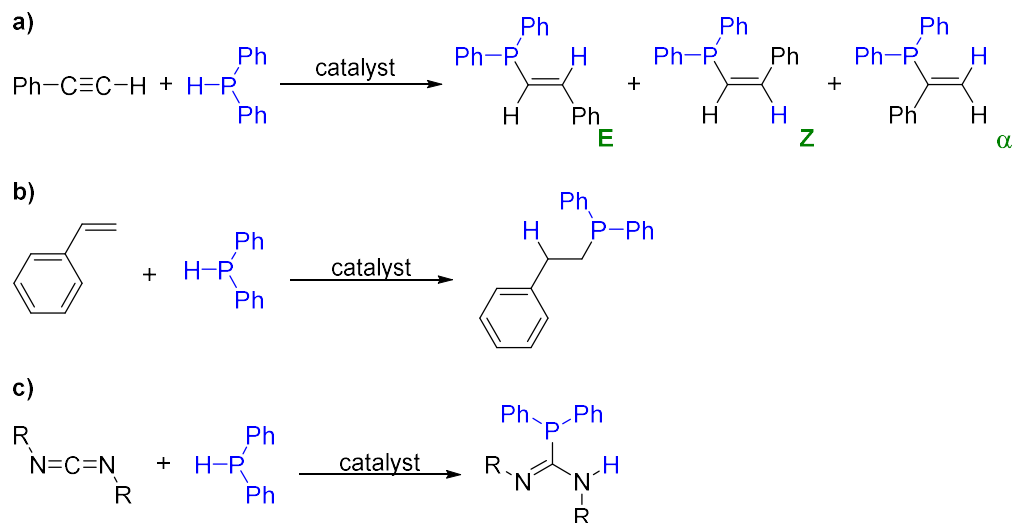
5.1 Abstract

The first examples of lithium aluminate-catalysed hydrophosphination is reported herein. Employing lithium aluminate complexes as catalysts, the hydrophosphination of alkynes, alkenes and carbodiimides is achieved. The proposed active species has been isolated and structurally characterised. Preliminary investigations into the reaction mechanism for the hydrophosphination of alkynes, using stoichiometric reactions, Kinetic Isotope Effect (KIE) measurements and reaction kinetics, are presented.

5.2 Introduction

5.2.1 Hydrophosphination

Hydrophosphination can be defined as the addition of H – P across an unsaturated bond, ideally in a regio-selective and stereo-selective manner (Scheme 5.1). Thus, it is an important reaction that offers an atom economical approach for the preparation of new phosphines. The resultant phosphine products can find application in a range of different sectors including agrochemicals and pharmaceuticals, can be applied as catalysts in organocatalysis, or employed as ligands for transition metal complexes.²⁷⁴



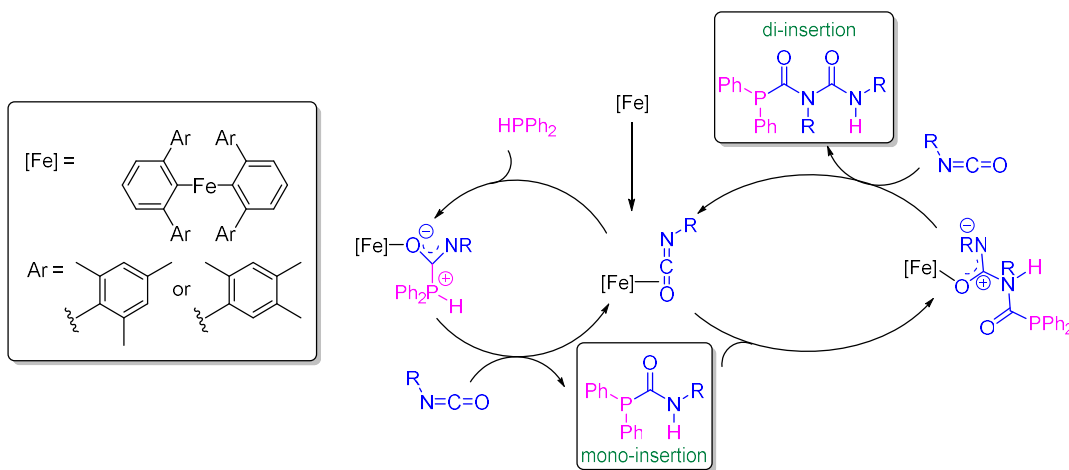
Scheme 5.1: General reaction scheme for the hydrophosphination of: **a)** phenylacetylene showing different stereo- (*E*, *Z*) and regio-selectivities (α) attainable in the vinyl phosphine product; **b)** styrene showing the alkyl phosphine product; and **c)** carbodiimides showing the phosphaguanidine product.

Whilst the majority of the examples of hydrophosphination in the literature make use of the secondary diphenylphosphine (HPPH₂), other secondary phosphines such as dicyclohexylphosphine (HPCy₂) can also be used. Similarly, there are examples of hydrophosphination employing primary phosphines, such as phenylphosphine (H₂PPh). Throughout this chapter, unless stated otherwise, the phosphine in discussion will be HPPH₂.

5.2.2 Metal-catalysed examples of hydrophosphination

Whilst it has been shown that thermally induced hydrophosphination of alkyne and alkene substrates can proceed under certain catalyst- and solvent-free conditions,²⁷⁵ recently there has been a surge of activity in the study of metal-catalysed hydrophosphination reactions.²⁷⁶⁻²⁷⁸ This has been driven by curiosity and more importantly by the need to find more efficient synthetic protocols: phosphorus is an element in danger of becoming scarce or unaccessible,²⁷⁹ and therefore the synthesis of phosphorus containing compounds needs to be as efficient as possible. Metals from the d-block employed as catalysts for hydrophosphination catalysis include Zr,²⁸⁰ Co,²⁸¹ Ni,²⁸² and Pd.²⁸³ Examples from the

lanthanides include La, Sm, and Yb.²⁸⁴⁻²⁸⁶ Of the transition metals, iron-based systems are by far the most well developed.²⁸⁷⁻²⁹⁰ As such there are numerous iron based-catalysts capable of catalysing the hydrophosphination of alkenes and alkynes, however heterocumulenes have been less examined. Notably, Kays reported the first example of transition metal catalysed hydrophosphination of isocyanates as recently as 2017.²⁹⁰ By performing the reactions in C₆D₆ solvent it was possible to selectively favour the formation of the di-inserted phosphinocarboxamide products (Scheme 5.2).

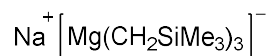
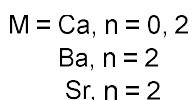
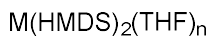


Scheme 5.2: Proposed reaction mechanism for hydrophosphination of isocyanates.

Examples of s-block catalysts for the hydrophosphination of alkynes, alkenes and carbodiimides include complexes of Li,²⁹¹ K,^{291, 292} Mg,^{233, 293} Ca,^{286, 294-296} as well as Sr and Ba,^{285, 297} (Figure 5.1). Hill reported the efficient hydrophosphination of a range of moderately activated alkenes and dienes by employing 10 mol% ^{DIPP}nacnacCa(HMDS)(THF) as a catalyst (75 °C, 13 – 24 hours).²⁹⁴ One example of an alkyne, diphenylacetylene, was considered, and required 20 mol% catalyst at 75 °C for 13 hours. The reaction was exceptionally sensitive to the steric demands of the substrate, and therefore particularly hindered substrates such as α -methyl styrene, 1,2-diphenylethene and *trans*-stilbene were not tolerated. However, in terms of carbodiimides the homoleptic silylamide M(HMDS)₂(THF)_n (M = Ca, n = 0 or 2; Sr, n = 2; Ba, n = 2) complexes were found to be more active catalysts than ^{DIPP}nacnacCa(HMDS)(THF), with catalytic rates increasing with increasing metal radius

(2 – 10 mol%, 25 – 60 °C, 0.25 – 16 hours).²⁹⁷ Harder recently reported the hydrophosphination of phenylacetylene by $[\text{DIPPnacnacMg} \cdot \text{C}_6\text{D}_6]^+ [\text{B}(\text{C}_6\text{F}_5)_4]^-$ (10 mol%, 60 °C, 20 hours) achieving a 72% conversion.²⁹³ However, only a very small substrate scope was reported: internal alkynes did not react at all, and terminal trimethylsilylacetylene only yielded trace amounts of product. An example of a heterobimetallic sodium magnesiate pre-catalyst, $[\text{NaMg}(\text{CH}_2\text{SiMe}_3)_3]$ has been shown by Hevia to be active in the hydrophosphination of a range of carbodiimides (2 mol%, room temperature, 0.5 – 1 hours).²³³

hydrophosphination of carbodiimides

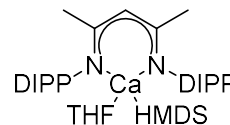
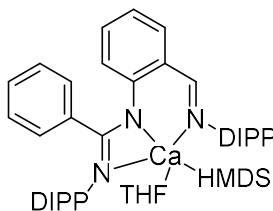
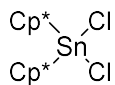


Hill

Hou

Hevia

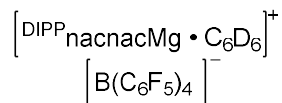
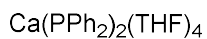
hydrophosphination of alkenes/alkynes



Waterman

Cui

Hill



Westerhausen

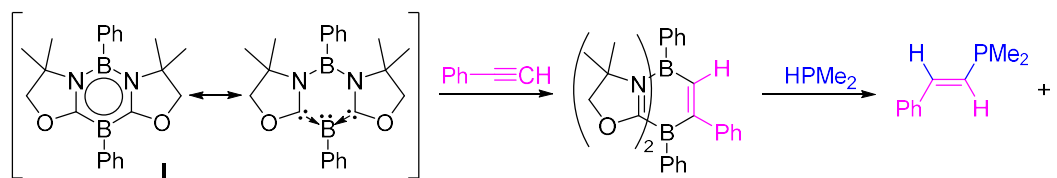
Webster

Harder

Figure 5.1: Literature examples of main group catalysts for hydrophosphination reactions of carbodiimides, alkenes and alkynes.

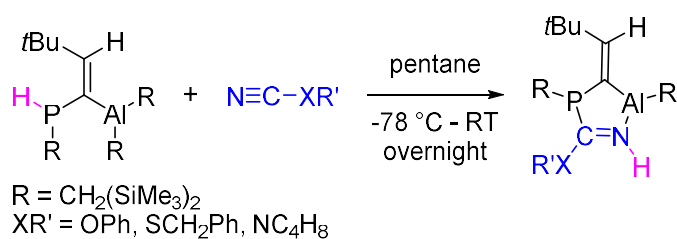
In comparison, there are significantly fewer examples of hydrophosphination catalysts from the p-block. Investigation of tin compounds, such as $\text{Cp}^*_2\text{SnCl}_2$, required a hydrogen

atmosphere to inhibit phosphine dehydrocoupling of HPPH_2 .^{298, 299} Other examples of p-block catalysts are limited to theoretical studies. The hydrophosphination of phenylacetylene by dimethylphosphine, Me_2PH , catalysed by the boron-boron FLP system 1,3,2,5-diazadiborinine has been examined by DFT calculations (Scheme 5.3).³⁰⁰ The results of this investigation concluded that experimentally this reaction should be feasible, and identified the insertion of the alkyne into the H–P bond as the rate determining step with an activation barrier of 31.7 kcal/mol.



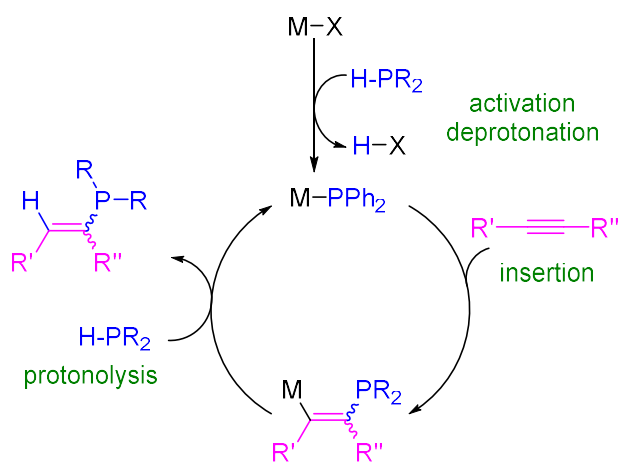
Scheme 5.3: Theoretically calculated hydrophosphination of phenylacetylene by HPMe_2 , catalysed by the boron-boron FLP 1,3,2,5-diazadiborinine, I.

The paucity of p-block catalysed hydrophosphination studies is surprising given that stoichiometric hydrophosphination processes have been reported with such compounds.³⁰¹⁻³⁰⁴ Notably, Uhl reports the stoichiometric hydrophosphination of heteroatom substituted nitriles by a P/Al-based FLP system.^{301, 302} The room temperature hydrophosphination of the $\text{C}\equiv\text{N}$ bonds affords imines which are incorporated into AlCPCN heterocycles (Scheme 5.4).



Scheme 5.4: Stoichiometric hydrophosphination of heterosubstituted nitriles by a P/Al FLP system.

Mechanistically, main group catalysed hydrophosphination reactions are proposed to proceed in a similar manner to that depicted in Scheme 5.5. In the first instance, the main group pre-catalyst undergoes an activation step through a deprotonation reaction with the phosphine reagent HPR_2 , in order to generate the active metal phosphide species. Subsequently, the unsaturated substrate can insert into the polarised $\text{M} - \text{P}$ bond. Finally, the product can be liberated *via* protonolysis by a second equivalent of HPR_2 , which also regenerates the active metal phosphide complex to complete the catalytic cycle. Crucially, this reaction mechanism differs from that of hydroboration as a result in the differing polarisation of the $\text{E} - \text{H}$ bond ($\text{E} = \text{B}$ or P). As such, for $\text{H}^{\delta-} - \text{B}^{\delta+}$ the hydrogen is hydridic [Pauling electronegativity (χ) B: 2.04; H 2.20]; whereas for $\text{H}^{\delta+} - \text{P}^{\delta-}$ the hydrogen atom is protic [Pauling electronegativity (χ) P: 2.19].²¹ As a result of this, different reactivity is required from the catalyst in order for it to catalyse hydroboration or hydrophosphination. In spite of the renaissance of aluminium-catalysed hydroelementation reactions no report of aluminium-catalysed hydrophosphination has yet been published. That notwithstanding, it should be noted that aluminium catalysed hydrophosphonylation (phosphorus in +V oxidation state rather than the +III oxidation state) is known.³⁰⁵ With a view to determining how general the application of lithium aluminate complexes as catalysts for hydroelementation reactions could be, **11** was employed as a catalyst for the hydrophosphination of a range of substrates.



Scheme 5.5: General catalytic cycle for hydrophosphination catalysed by a $\text{M} - \text{X}$ catalyst (X = for example, amide or hydride).

5.3 Project Aims

The aims of this part of the project are summarised below.

- To investigate whether the concept of lithium aluminate catalysed hydroelementation reactions can be extended to processes other than hydroboration.
- To introduce and refine aluminium catalysed hydrophosphination reactions and compare them with existing examples of main group catalysed systems.
- To gain insight into the mechanism of these aluminium-catalysed hydrophosphination reactions by studying the kinetics of these reactions *via* reaction monitoring and deuterium labelling studies as well as in collaboration with computational chemists.
- To establish the scope and limitation of aluminium-catalysed hydrophosphination reactions.

5.4 Introduction from the Manuscript

Phosphines are utilized in a range of applications spanning agriculture (e.g., in fertilizers), medicinal chemistry (e.g., in antibiotics), and organocatalysis, in addition to their ubiquity as ligands in transition metal catalysis.²⁷⁴ Hydrophosphination, the addition of a P – H bond across an unsaturated C – E (E = e.g., C, N) bond, offers an atom economical approach for the preparation of phosphines. Recently there has been growing interest in developing new metal-catalysed hydrophosphination reactions.²⁷⁶⁻²⁷⁸ A plethora of different transition metal catalysts has been used for this purpose, with examples across the d-block including iron,

nickel, palladium and zirconium.^{277, 278, 280, 282, 287, 290} Rare earth metal systems based on lanthanum, samarium, and ytterbium have also been shown to be catalytically active.²⁸⁴⁻²⁸⁶ Solvent and catalyst free hydrophosphinations can be thermally induced under certain circumstances.²⁷⁵

A sea change currently taking place in homogeneous catalysis including hydrophosphination,^{49, 50} is the introduction of catalysts based on main group metals. Importantly, these new arrivals can promote catalytic dehydrocoupling of phosphines which can compete with hydroelementation.⁵² s-Block potassium, calcium and magnesium compounds have been reported as hydrophosphination catalysts for alkene, alkyne and carbodiimide substrates with diphenyl phosphine (HPPH₂), forming alkyl phosphines, vinyl phosphines and phosphaguanidines, respectively.^{233, 285, 286, 291-295, 297} p-Block compounds, predominantly of tin, are capable of catalysing hydrophosphination reactions,^{278, 298, 299} though Cp*₂SnCl₂ required a hydrogen atmosphere to inhibit competing phosphine dehydrocoupling reactions of HPPH₂.²⁹⁹

Attractive industrially due to its high natural abundance and low toxicity, aluminium is gaining prominence in this main group homogeneous catalysis enlightenment.¹⁵⁻¹⁸ Recent work by Roesky, Wright, Cowley/Thomas, Harder, Stephan, and others, have successfully employed aluminium compounds as catalysts in hydroboration and hydrogenation applications.^{74, 76, 79, 90, 98, 177, 178} Uhl has also demonstrated that a P/Al geminal frustrated Lewis pair (FLP) is capable of stoichiometrically hydrophosphinating heteroatom substituted nitriles at room temperature, generating imines incorporated into five-membered AlCPCN heterocycles.³⁰² Examples also exist of aluminium-catalysed hydrophosphonylation (using P(V) reagents).³⁰⁵ However, to our knowledge no examples of aluminium catalysed hydrophosphination (using P(III) reagents) of alkynes, alkenes or carbodiimides are currently known.

The study of bimetallic ate complexes which can exhibit synergistically enhanced stoichiometric reactivities over their neutral monometallic components has been a central theme of our research.¹⁰⁷ Recently we have expanded this work into the catalytic regime, by employing lithium aluminate complexes as catalysts for hydroboration of aldehydes, ketones, imines and acetylenes.^{209, 236, 268} Comparing the neutral monometallic components

with their charged bimetallic counterparts showed that, generally, the bimetallic species were the more active catalysts.²⁶⁸

Herein, we investigate the ability of our most active lithium aluminate, $[i\text{Bu}_3\text{AlHLi}]_2$, **11**, as a catalyst in hydrophosphination reactions of alkynes, alkenes, and carbodiimides.

5.5 Results and Discussion

Initially, phenylacetylene was reacted with HPPH_2 and 5 mol% of dimeric $[i\text{Bu}_3\text{AlHLi}]_2$, **11**, in d_8 -toluene at 110 °C. The reaction yielded 72% conversion (1:8 *E/Z* ratio, Figure 5.2) within 24 hours, to the anti-Markovnikov product consistent with *syn* addition of H – P across the $\text{C} \equiv \text{C}$ bond. Changing the solvent to d_8 -THF (65 °C) lowered the *E/Z* selectivity of the reaction, while using CD_2Cl_2 (40 °C) poisoned the catalyst and resulted in no product formation. Satisfied this system is a capable hydrophosphination catalyst, a range of alkynes were screened (Table 5.1). Internal alkynes, diphenylacetylene and 1-phenyl-1-propyne reacted faster than terminal alkynes. However, more challenging unactivated alkynes, 1-hexyne and 3-hexyne did not react, in common with other reports of main group catalysed hydrophosphination.²⁹⁹

To gain further insight a stoichiometric reaction between $[i\text{Bu}_3\text{AlHLi}]_2$ and HPPH_2 , with three equivalents of THF, resulted in complete consumption of the hydridoaluminate generating a solution, which deposited crystals of the lithium aluminium phosphide, $i\text{Bu}_3\text{AlPPh}_2\text{Li}(\text{THF})_3$, **22**, (isolated yield, 41%) [Figure 5.2 a)]. Phosphidoaluminate **22** is the result of deprotonation of HPPH_2 by **11**, and importantly, implies this process is the first step in catalytic hydrophosphination. In the crystal, **22** [Figure 5.2 b)] is monomeric, with three THF molecules solvating the lithium. Its Al–P bond length is 2.4698(13) Å and Li – P bond length is 2.596(6) Å. ¹H DOSY NMR studies confirm that its monomeric state is retained in d_8 -toluene solution. Alternatively, **22** can be prepared *via* simple co-complexation of LiPPh_2 with $i\text{Bu}_3\text{Al}$ and THF.

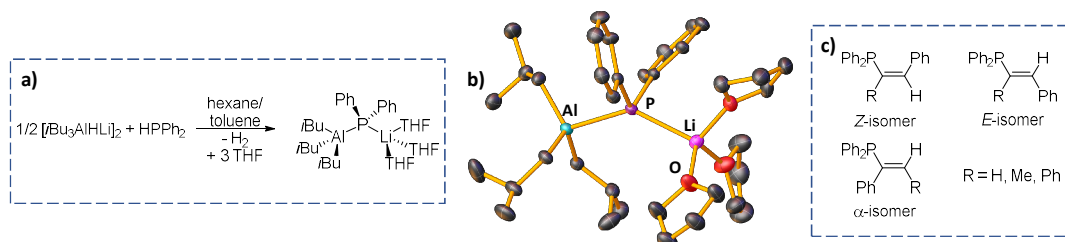
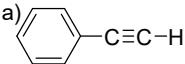
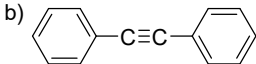
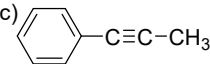
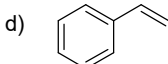
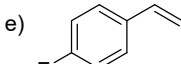
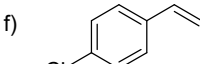
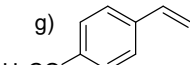
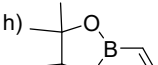
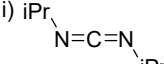
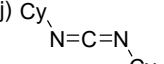


Figure 5.2: a) Synthesis of $\text{iBu}_3\text{AlPPh}_2\text{Li}(\text{THF})_3$, **22**; b) molecular structure of **22**, H atoms and disordered THF molecules omitted for clarity, and thermal ellipsoids drawn at 40% probability; c) depiction of *E*-, *Z*- stereoisomers and α -regioisomer arising from hydrophosphination of alkyne substrates.

Knowing that dehydrocoupling can compete with hydrophosphination, a control reaction between HPPH_2 and 10 mol% of **22** in d_8 -toluene was heated at 110 °C for 20 hours. Less than 15% of HPPH_2 had undergone dehydrocoupling to form 1,1,2,2-tetraphenyl diphosphine (determined by ^{31}P NMR spectra) signifying that this is unlikely to be a significant problem in this system. Subsequently **22** was tested as a catalyst for the hydrophosphination of alkynes, under the previously optimised conditions (10 mol% [Al], d_8 -toluene, 110 °C), (Table 5.1). For phenylacetylene a 95% conversion (1:3 *E/Z* ratio) of the anti-Markovnikov product was obtained after 20 hours (cf. 72% using **11**), albeit with reduced *E/Z* stereoselectivity. By contrast, Waterman's tin catalyst Cp^*SnCl_2 is poorly active for phenylacetylene (10 mol% catalyst, 18 hours, 65 °C, 4% yield).²⁹⁹ Using **22**, hydrophosphination is much faster with internal alkynes than terminal alkynes, with a 99% yield (10:1 *E/Z* ratio) for diphenylacetylene being obtained within just 1 hour (using **11** takes 5 hours). Similarly, 1-phenyl-1-propyne is converted fully to the anti-Markovnikov vinyl phosphine product within 1 hour. The catalytic activity of **22** with diphenylacetylene compares favourably with the β -diketiminato calcium amide catalyst $\text{DIP}^{\text{P}}\text{nacnacCa}(\text{HMDS})(\text{THF})$ which required extended reaction times (10 mol% catalyst, 75 °C, 13 hours, 94% yield).²⁹⁴ However, heteroleptic $[\text{Ca}(\text{PPh}_2)_2(\text{THF})_4]$ was able to successfully catalytically hydrophosphinate diphenylacetylene after 2 hours at room temperature.²⁹⁵ Cui employed a tridentate imino-amidinate ligated calcium complex as a catalyst for hydrophosphination of 1-phenyl-1-propyne and observed quantitative conversion after 5 hours at 60 °C, using 5 mol% [Ca].²⁸⁶ Adding a catalytic amount (30 mol%) of THF to 10 mol% of **11** resulted in hydrophosphination of diphenylacetylene within the same time as that using pre-formed **22**, suggesting that deaggregation of dimeric **11** by THF

is advantageous in catalysis. Again attempted catalysis with unactivated 1-hexyne or 3-hexyne and HPPH₂ by **22** proved unsuccessful.

Table 5.1: Hydrophosphination of alkynes, alkenes and carbodiimides using **11**, **14**, **22** – **25** as catalysts.

Alkynes		
a) 	b) 	c) 
Cat. yield(%) E/Z/ α , time(h)		
11 72%, 1:8:0*, 20 h	11 98%, 10:1, 5 h	11 99%, 1:1:0, 6 h
22 95% (78%), 1:3:0, 20 h	22 99% (80%), 10:1, 1 h	22 99% (79%), 1:1:0, 1 h
23 86%, 1:3:0, 20 h	23 98%, 10:3, 3 h	23 95%, 1:3:0, 10 h
24 72%, 1:8:8, 20 h		
14 62%, 1:12:4, 20 h		
25 62%, 1:12:4, 20 h		
Alkenes		
d) 	e) 	f) 
11 89%, 6 h	22 84%, 20 h	22 86%, 18 h
22 84% (60%), 6 h		
23 72%, 6 h		
g) 	h) 	
22 87%, 20 h	22 93%, 4 h	
Carbodiimides		
i) 	j) 	
22 99% (80%), 0.25 h	22 86%, 20 h	

General conditions: 0.6 mmol substrate, 0.5 mmol HPPH₂, d₈-toluene Alkynes/Alkenes: 10 mol% [Al] catalyst, 110 °C Carbodiimides: 5 mol% [Al] catalyst, RT. *E/Z/ α -selectivity.

Conversions based on ³¹P NMR spectra ratios, and against ¹H NMR internal standard hexamethylcyclotrisiloxane. Selected isolated yields in parenthesis.

Next, the more challenging hydrophosphination of alkenes was examined using **22** (Table 5.1). Styrene undergoes hydrophosphination in 6 hours, at 110 °C, yielding 84% of the anti-Markovnikov product. Halo-substituted styrenes are also tolerated

(Table 5.1, entries e – f). 4-Vinyl anisole undergoes hydrophosphination to the alkyl phosphine product in 87% yield after 20 hours at 110 °C. More sterically demanding substrates such as α -methyl styrene, *trans*- β -methyl styrene, as well as less activated alkenes such as 1-hexene did not undergo hydrophosphination with **22** as the catalyst. Similar failures with both calcium and tin based catalysts have been noted for these more defiant substrates.^{294, 299} Hydrophosphination of vinyl boronic acid pinacol ester (vinyl Bpin) achieved a 93% yield after 4 hours at 110 °C, producing linear phosphine boronic ester $\text{Ph}_2\text{P}(\text{CH}_2)_2\text{Bpin}$. To our knowledge this is the first time $\text{Ph}_2\text{P}(\text{CH}_2)_2\text{Bpin}$ has been prepared via a hydrophosphination route, since earlier published methods required hydroboration of diphenyl vinyl phosphine.^{306, 307}

Phosphidoaluminate **22** is also an able catalyst for hydrophosphination of carbodiimides at room temperature. Thus, using 5 mol% catalyst loading (Table 5.1, entries i – j), diisopropylcarbodiimide is converted fully to the phosphaguanidine product within 15 minutes; while the more sterically demanding dicyclohexylcarbodiimide required 20 hours, to achieve 86% conversion. Hill reports quantitative yields for diisopropyl- (iPr) and dicyclohexyl- (Cy) carbodiimides within 1 hour and 4 hours, respectively, using 2 mol% $\text{Ca}(\text{HMDS})_2$ as catalyst, also at room temperature. Significantly longer reaction times were seen when employing $\text{D}^{\text{IPP}}\text{nacnacCa}(\text{HMDS})(\text{THF})$ as a catalyst (1.5 mol%) (iPr – 6 hours, 99%; Cy – 28 hours, 85%).²⁹⁷ KHMDs is also reported to be a competent catalyst for carbodiimides requiring low catalyst loadings and short reaction times.²⁹¹ Hevia described a sodium magnesiate pre-catalyst that also catalysed hydrophosphination of carbodiimides.²³³

Attempting to pinpoint the catalytically active species a series of different compounds – LiPPh_2 (**23**), $i\text{Bu}_3\text{Al}$ (**24**), $i\text{Bu}_2\text{AlH}$ (**14**) and $i\text{Bu}_2\text{AlPPh}_2$ (**25**)³⁰⁸ – were screened for catalytic viability using phenylacetylene as a model substrate (Table 5.1). Using LiPPh_2 as a catalyst yields 86% conversion to the vinyl phosphine after 20 hours, with anti-Markovnikov regioselectivity, similar to that of **22**. $i\text{Bu}_3\text{Al}$ (**24**), $i\text{Bu}_2\text{AlH}$ (**14**) and $i\text{Bu}_2\text{AlPPh}_2$ (**25**) afford different product regio- and stereo-selectivities as well as lower yields for hydrophosphination of phenylacetylene. Interestingly when $i\text{Bu}_3\text{Al}$ (**24**) is used as the catalyst (72%; 1:8:8 *E/Z*/ α) the major isomer products are the *Z*- anti-Markovnikov isomer, and equally the Markovnikov [α – isomer; $\text{Ph}(\text{Ph}_2\text{P})\text{C}=\text{CH}_2$]. In contrast, **22** does not generate any appreciable amounts of the α -isomer, suggesting that **22** is not disproportionating in solution at high temperatures into LiPPh_2 and $i\text{Bu}_3\text{Al}$.

In order to ascertain whether LiPPh_2 is implicated in the catalytic profile we conducted a further stoichiometric reaction (Figure 5.3). Monitoring a reaction of **22** and diphenylacetylene, in d_8 -toluene, by ^{31}P NMR spectroscopy shows that after 2 hours at 110°C full consumption of **22** occurs with concomitant growth of two new signals at 3.4 and -16.5 ppm. We were unable to isolate these species after several attempts; thus, we tentatively assign them as two isomers resulting from insertion of diphenylacetylene into **22**. Subsequent addition of HPPH_2 and further heating at 110°C allows for product formation [8.9 ppm (*E*-isomer) and -7.3 ppm (*Z*-isomer)] and regeneration of **22** (-49.3 ppm). We rationalise the intermediate species (at 3.4 ppm) reacts onwards to form the *E*-stereoisomer as it is consumed faster than the other intermediate. Significantly there are no resonances corresponding to LiPPh_2 present in the spectrum (-52 ppm) further reinforcing that **22** is the catalytically active species.

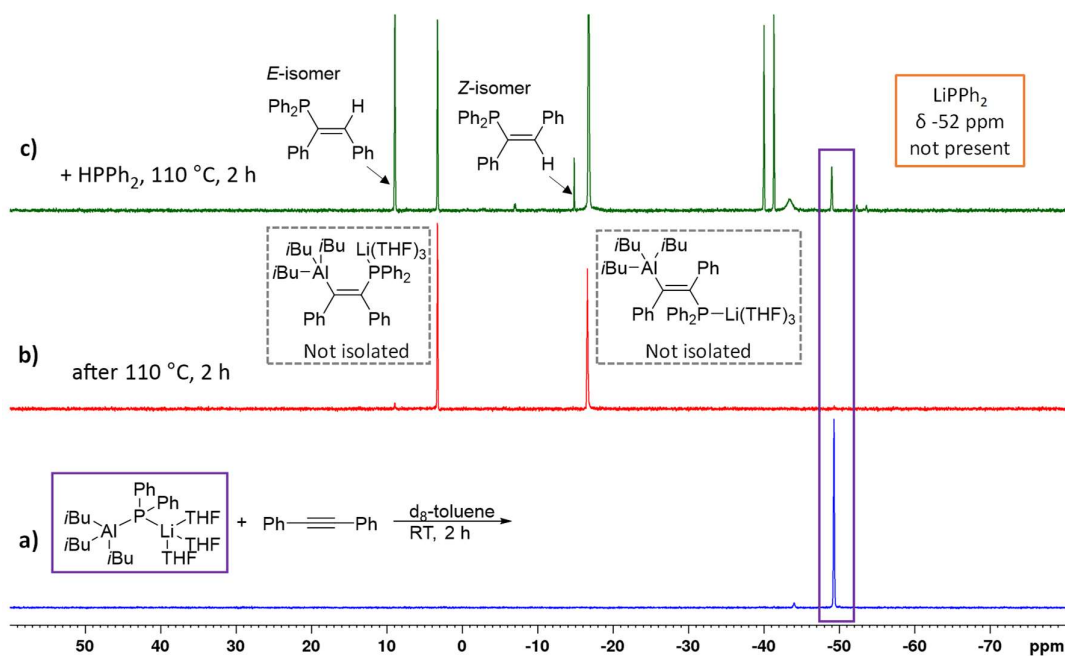
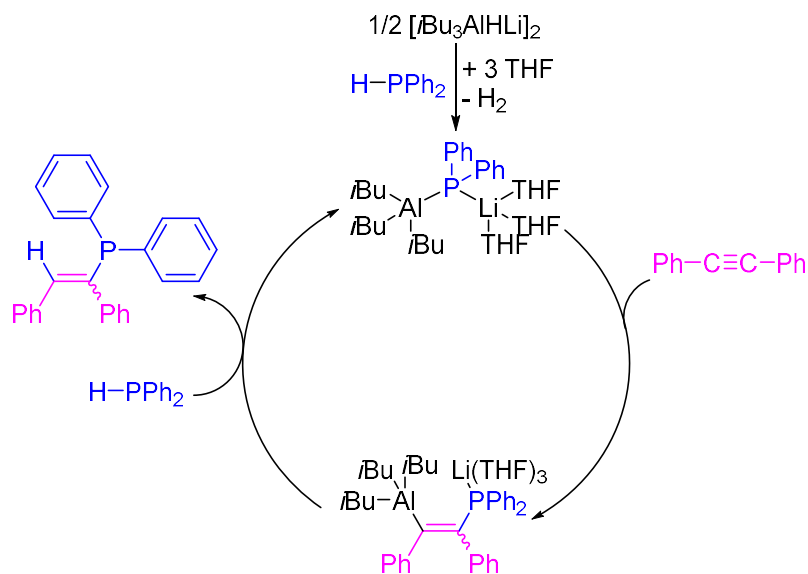


Figure 5.3: ^{31}P NMR spectra: a) mixture of diphenylacetylene and **22** at RT; b) after heating for 2 h at 110°C ; c) after adding excess HPPH_2 and heating at 110°C – formation of *E*- and *Z*-vinyl phosphines and regeneration of **22**.

Drawing these observations together, a catalytic cycle is proposed as shown in Scheme 5.6. The cycle begins by deprotonation of HPPh_2 by $[\text{iBu}_3\text{AlHLi}]_2$, releasing H_2 gas and forming compound **22**. Next, a substrate molecule inserts into the Al – P bond. Subsequent protonolysis by a second equivalent of HPPh_2 accesses the hydrophosphinated product whilst regenerating the active catalytic species **22**.



Scheme 5.6: Proposed reaction mechanism for hydrophosphination of diphenylacetylene by pre-catalyst **11**, showing formation of active species **22**.

Since after the facile room temperature deprotonation step, alkyne insertion and protonolysis are the other key steps, we decided to perform a deuterium labelling study to investigate the cycle more fully. Catalytic hydrophosphination between diphenylacetylene and DPPh_2 favoured formation of the *E*- stereoisomer and deuterium was incorporated into the vinyl phosphine product, $\text{Ph}(\text{Ph}_2\text{P})\text{C}=\text{C}(\text{D})\text{Ph}$, as confirmed by ^2H NMR spectroscopy and GC-MS (see experimental section). Furthermore, in a stoichiometric reaction between $[\text{iBu}_3\text{AlHLi}]_2$ and DPPh_2 the presence of HD was detected in the ^1H NMR spectrum (triplet at 4.45 ppm, $^1J = 42.8$ Hz), confirming the initial deprotonation step. A kinetic isotope effect (KIE) experiment was conducted for hydrophosphination of diphenylacetylene by recording the reaction profile in duplicate for HPPh_2 and DPPh_2 at 100°C , in d_8 -toluene, with 10 mol% of **22**. By monitoring the rate of consumption of phosphine by ^{31}P NMR spectroscopy, rates

were obtained, and in each case the overall reaction rate is pseudo-first order. From the rates observed a KIE of 1.38 ± 0.13 was determined (see extended discussion). This is a small value, compared with other literature reports, and suggests the cleavage of the P – H bond is only involved to a small extent in the rate determining step.²⁹⁹ Furthermore, this indicates that alkyne insertion into **22** is rate determining, which given the rather congested structure of **22** and bulky nature of the alkyne is not surprising.

Finally, in order to reinforce our experimental insight, we turned to theoretical DFT calculations. The calculations were performed on the full system with the internal alkyne, diphenylacetylene used as the model substrate. The calculations were performed at the B3LYP-D3/³⁰⁹⁻³¹⁵6-311G(d,p)³¹⁶⁻³¹⁸ level of theory employing a continuum solvent with the dielectric constant of toluene within the IEFPCM model.³¹⁹ The relative stability of the formation of **22** from $[\text{iBu}_3\text{AlHLi}]_2$ with 2 HPPH₂ and 6 THF molecules was initially investigated. The formation of the catalyst (**22**) is thermodynamically favourable despite the entropic penalty associated with the coordination of THF, with a calculated $\Delta G = -63.8$ kcal/mol ($\Delta H = -130.8$ kcal/mol). In contrast to the induction step, the first step in the catalytic cycle (the addition of diphenylacetylene to **22**) is mildly endergonic for both the *E* and *Z* isomers of the intermediate shown in Scheme 5.6. However, the *E* isomer is more stable in the intermediate state of the reaction ($\Delta G = 6.9$ kcal/mol), with the *Z*-isomer ($\Delta G = 8.3$ kcal/mol) being further destabilised by 1.4 kcal/mol, relative to the *E*-isomer. Finally, generation of the product and the reformation of the catalytic species takes place in an exergonic reaction. In this step, the formation of the *Z*-isomer ($\Delta G = -25.3$ kcal/mol) is favoured over the *E*-isomer ($\Delta G = -20.4$ kcal/mol). The reversal of the relative stabilities of the isomers in the intermediate state versus the product state suggests that the formation of the intermediate is deterministic for the final product distribution, which favours the experimentally determined *E*-isomer. The rate-limiting step for the reaction could not be located as the calculation of transition states proved elusive for these bulky compounds. However, the relative stabilities of the intermediates and products determine for this pathway indicate that the mechanism proposed is achievable under the reaction conditions employed.

In conclusion, this study reports the first example of aluminium-catalysed hydrophosphination of alkynes, alkenes and carbodiimides, using a lithium aluminate (pre)-catalyst. A mechanism is proposed, elucidated by stoichiometric reactions, thought to

proceed via formation of the crystallographically characterised lithium aluminium phosphide, **22**.

5.6 Extended Discussion and Future Work

5.6.1 Extension to other substrates

The focus of this project was to study the possible hydrophosphination of alkynes, alkenes and carbodiimides. These unsaturated substrates were chosen as they have previously been hydrophosphinated in the presence of other main group catalysts. However, it was thought it may be fruitful to consider other unsaturated substrate types such as nitriles or isocyanates. One attempt of hydrophosphination of phenyl isocyanate, PhNCO, with catalyst *i*Bu₃AlPPh₂Li(THF)₃, **22**, resulted in the trimerisation of the isocyanate substrate at room temperature. However, Hevia reports the selective trimerisation or hydroamination of isocyanates in the presence of a sodium trialkylmagnesiates catalyst, [NaMg(CH₂SiMe₃)₃].²³² In that study the reaction pathway selectivity was guided by the R group of the isocyanate (RNCO). As such, hydroamination was observed for sterically demanding *tert*-butyl isocyanate, but trimerisation was observed for phenyl isocyanate which has reduced steric bulk. Therefore, further investigations into isocyanates may be worth pursuing with hydrophosphination catalysts. Furthermore, application to the hydrophosphination of nitriles may be possible. As disclosed by Uhl, a P/Al FLP system is capable of stoichiometrically hydrophosphinating heteroatom-substituted nitriles (Scheme 5.4, see page 120).^{301, 302} In these reactions the nitrile is added to the FLP at -78 °C and the reaction is then allowed to warm to room temperature overnight. However, the authors never examined these reactions catalytically.

5.6.2 Structure activity relationships

The solution state structure of *i*Bu₃AlPPh₂Li(THF)₃, **22**, was examined by ¹H DOSY NMR spectroscopy, using 1,2,3,4-tetraphenylnaphthalene as an internal standard (Figure 5.4 and Table 5.2). The predicted molecular weight of 603 g/mol agrees with a monomeric, contacted ion pair structure in C₆D₆ solution with a 7% error.

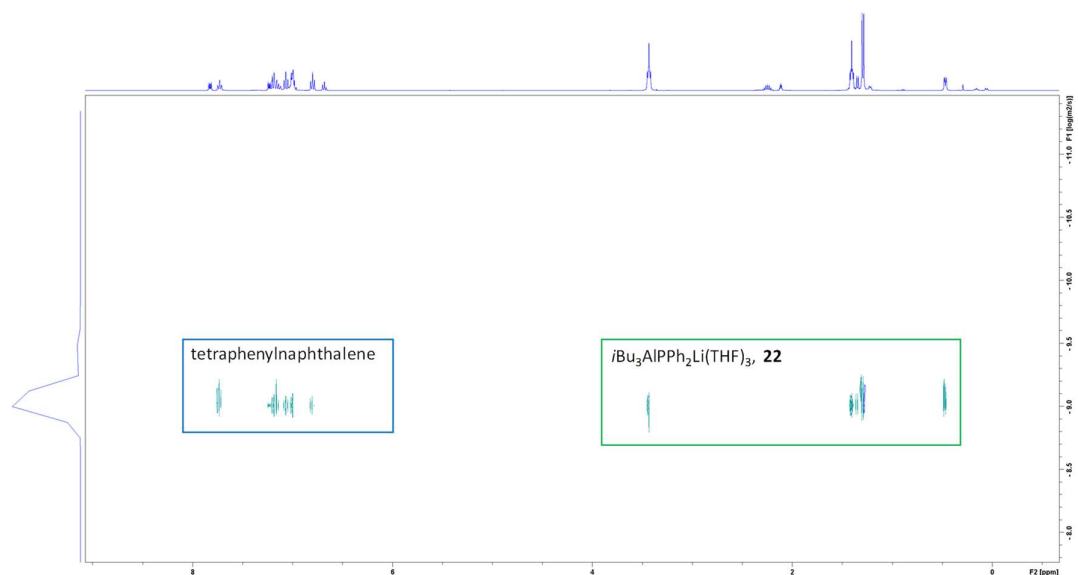


Figure 5.4: ^1H DOSY NMR spectrum for **22**, in d_8 -toluene.

Table 5.2: ^1H DOSY NMR spectrum for **22**, in d_8 -toluene.

Compound	D [m^2s^{-1}]	MW_{calc} [g/mol]	MW_{est} [g/mol]	Error [%]
$i\text{Bu}_3\text{AlPPh}_2\text{Li}(\text{THF})_3$	6.09×10^{-10}	566	603	7
1,2,3,4-Tetraphenyl-naphthalene	6.429×10^{-10}	432	432	0

In Chapter 2 a relationship was observed between the degree of solvation at the lithium centre and the catalytic activity observed for the hydroboration of aldehydes and ketones. In an attempt to further implicate the bimetallic catalytic nature of **22** in this hydrophosphination system a series of Lewis donor additives were added to the hydrophosphination of diphenyl acetylene with $[i\text{Bu}_3\text{AlHLi}]_2$, **11**, employed as the pre-catalyst (Table 5.3). As noted above the addition of three equivalents (30 mol%) of THF to **11** leads to an decrease in the reaction time for the hydrophosphination of diphenylacetylene compared with the donor free experiment (1 hour *versus* 5 hours). This implies that the deaggregation of dimeric $[i\text{Bu}_3\text{AlHLi}]_2$ into postulated $i\text{Bu}_3\text{AlHLi}(\text{THF})_3$ facilitates the deprotonation of HPPh_2 to generate the active lithium aluminium phosphide, **22**. Interestingly, the addition of either one equivalent (10 mol%) of PMDETA, one equivalent of 12-crown-4, or two equivalents (20 mol%) of TMEDA generates the same increase in catalytic activity – all result in

quantitative conversion to the vinyl phosphine product within 1 hour, but with differing *E*:*Z*-isomer ratios. This points to a bimetallic catalytic role as the coordination environment at the lithium centre impacts upon the selectivity observed. However, the addition of one equivalent of Me₆-TREN results in a dramatic drop in catalytic activity, requiring 3 hours to reach quantitative conversion rather than just 1 hour. It is proposed that the increased steric bulk of the Me₆-TREN sequesters the lithium and prevents substrate coordination at the lithium centre thus hindering the catalysis. Similarly, the addition of two equivalents of 1,2-bis(diphenylphosphino)ethane (dppe) also slows the rate of catalysis, which only achieves 95% conversion after 5 hours at 110 °C.

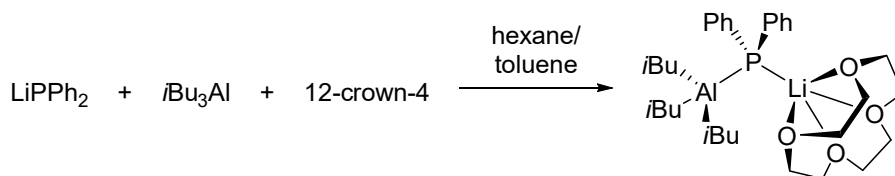
Table 5.3: Lewis donor additive effect on rate of hydrophosphination of diphenylacetylene.

Lewis donor additive	Time (h)	Yield (%)	<i>E</i> : <i>Z</i> ratio
None ([<i>i</i> Bu ₃ AlHLi] ₂ , 11)	5	98	10 : 1
<i>i</i> Bu ₃ AlPPh ₂ Li(THF) ₃ , 22	1	99	10 : 1
11 + 3 eq. THF	1	99	10 : 1
<i>i</i> Bu ₃ AlHLi(PMDETA), 17	1	99	2 : 1
11 + 1 eq. 12-crown-4	1	99	5 : 1
11 + 2 eq. TMEDA	1	99	19 : 1
11 + 1 eq. Me ₆ -TREN	3	99	10 : 1
11 + 2 eq. dppe	5	95	16 : 1

Reaction conditions: 0.5 mmol HPPH₂, 0.6 mmol diphenylacetylene, 10 mol% [Al] (pre)catalyst, d₈-toluene, 110 °C. Yields are reported *versus* hexamethylcyclotrisiloxane internal standard. *E*/*Z*-isomer ratios reported based on ³¹P NMR integration.

In one instance it was possible to crystallise the lithium aluminium phosphide complex from the co-complexation reaction of LiPPh₂, *i*Bu₃Al and 12-crown-4. Slow cooling of a toluene solution to room temperature yielded the expected product *i*Bu₃AlPPh₂Li(12-crown-4), **26** (Scheme 5.7 and Figure 5.5). Unfortunately, the limited quality of the X-ray diffraction data precludes any in-depth discussion of geometrical parameters, but it provides unequivocal proof of atomic connectivity. In the solid state **26** exists as a monomeric, contacted ion pair in which the phosphorus centre bridges both the lithium and aluminium centres. As would

be expected, the lithium centre is capped by the crown ether, bonding *via* all four oxygen donor atoms to the lithium.^{320, 321}



Scheme 5.7: Synthesis of $i\text{Bu}_3\text{AlPPh}_2\text{Li}(12\text{-crown-4})$, **26**.

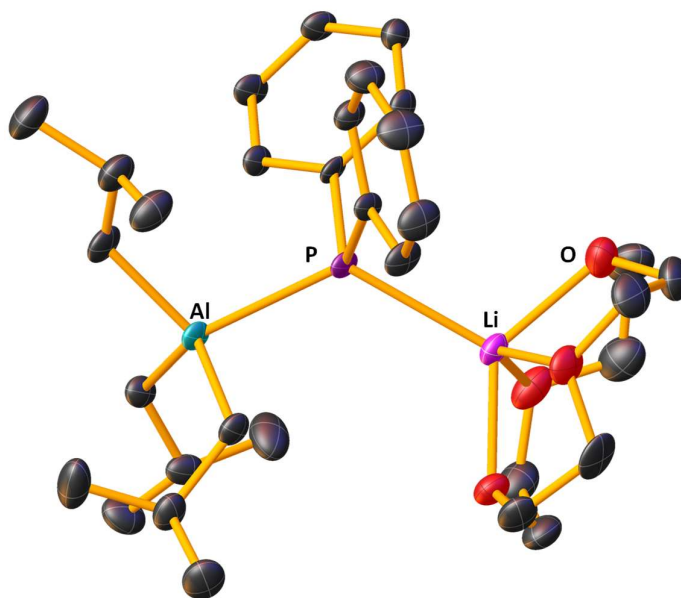


Figure 5.5: Molecular structure of $i\text{Bu}_3\text{AlPPh}_2\text{Li}(12\text{-crown-4})$, **26**. Disordered *i*Bu groups, disordered crown ether and hydrogen atoms have been omitted for clarity. Thermal ellipsoids are drawn at 40% probability.

Further evidence as to the nature (bimetallic or monometallic) of the catalyst could be obtained by preparation of alkali metal analogues of **22**. Thus, the synthesis of the related sodium or potassium aluminium phosphide complex could provide valuable insight into the nature of the catalytically active species. If an alkali metal effect is observed, then clearly

both metals are involved in key steps during the catalytic cycle. Conversely, if the reaction rates, product yields and product isomer ratios remain unchanged on moving from lithium to sodium to potassium it may be that the enhanced catalytic reactivity of **22** over the neutral aluminium (pre)-catalysts is a result of anionic activation.^{233, 322} This activation is observed in Hevia's [NaMg(CH₂SiMe₃)₃] catalysed hydroamination.²³³ In this system, it is proposed that the use of magnesium anionic moieties generates more powerful nucleophilic intermediates than uncharged organomagnesium (pre)-catalysts. It is possible that such anionic activation is in operation in this lithium aluminate catalysed hydrophosphination.

5.6.3 Elucidation of the reaction mechanism by kinetic studies

In an attempt to uncover more information on the reaction mechanism operating in this system a series of kinetic experiments were undertaken. Firstly, a kinetic isotope effect (KIE) study was performed. Thus, heating the reaction of HPPPh₂, diphenylacetylene and 10 mol% **22** at 100 °C and following the reaction by ³¹P NMR spectroscopy provided a *pseudo*-first order reaction profile. A plot of ln[HPPPh₂] against time revealed a straight line which was fitted by conventional linear regression (R² = 0.99987 and 0.99896). From the slopes an average rate constant of (7.2 ± 0.4) × 10⁻⁴ mol s⁻¹ (*k_H*) was obtained over two runs. An example plot is shown in Figure 5.6. An induction period was not observed, which indicates that the catalyst was reactive from the beginning of the process. The same procedure was repeated this time employing DPPPh₂ as the phosphine (Figure 5.7). An average rate constant of (5.2 ± 0.4) × 10⁻⁴ mol s⁻¹ (*k_D*) could be extrapolated from the ln[DPPPh₂] *versus* time plots. From the rates observed a KIE of 1.38 ± 0.13 was obtained by employing Equation 5.1.

$$KIE = \frac{k_H}{k_D}$$

Equation 5.1: Formula for calculating a kinetic isotope effect.

There are limited reports of KIE values arising from H/D substitution at P – H reactive sites, which precludes a detailed discussion of this KIE observed. Waterman observed a KIE of 3.1 in the Cp*₂SnCl₂ catalysed hydrophosphination reaction of styrene.²⁹⁹ However, this value

was obtained as a result of an intermolecular competition reaction between equimolar excesses of HPPH₂ and DPPH₂ and so may not be a true primary KIE.^{323, 324} The small KIE observed in the present lithium aluminate system suggests that the P – H bond has only limited involvement in the rate determining step.

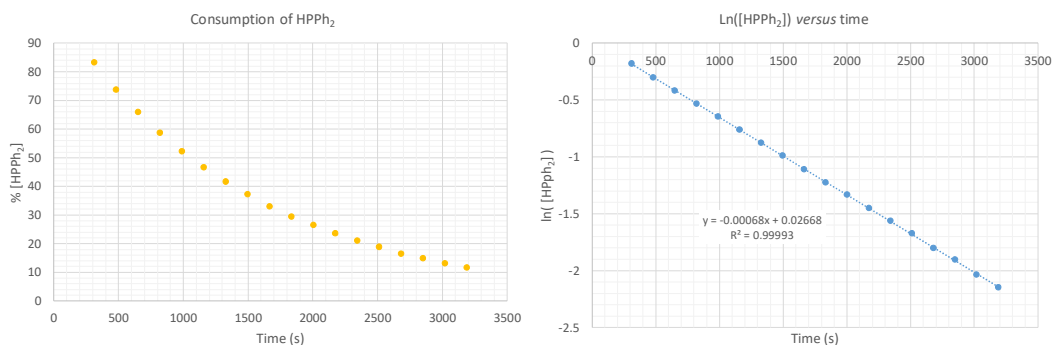


Figure 5.6: Example KIE kinetic data for the hydrophosphination of diphenylacetylene using HPPH₂ catalysed by **22**, at 373 K, for one run.

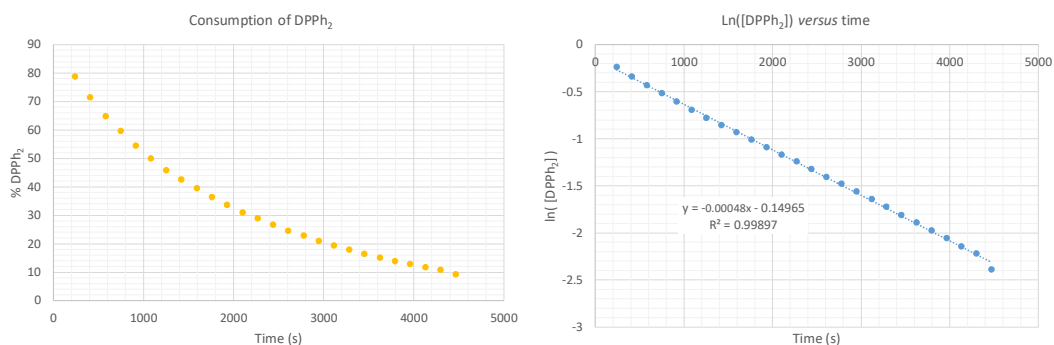


Figure 5.7: Example KIE kinetic data for the hydrophosphination of diphenylacetylene using DPPH₂ catalysed by **22**, at 373 K, for one run.

Next, analysis of the kinetics of the reaction was undertaken by *in situ* NMR spectroscopy monitoring. The dependence of the rate of reaction with respect to catalyst was studied at different initial concentrations of catalyst ([**22**] = 5 – 12.5 mol%). Standard conditions of HPPH₂ (1 M) and diphenylacetylene (1.2 M) in d₈-toluene solution were maintained in a total

reaction volume of 0.5 mL. The reaction rates for the hydrophosphination were followed over time by ^{31}P NMR spectroscopy, monitoring the consumption of HPPH_2 to three half-lives. A plot of observed rate constant k_{obs} against concentration of **22** reveals a linear increase in the reaction rate with catalyst concentration, (Figure 5.8), indicative of a *pseudo*-first order dependence on catalyst.

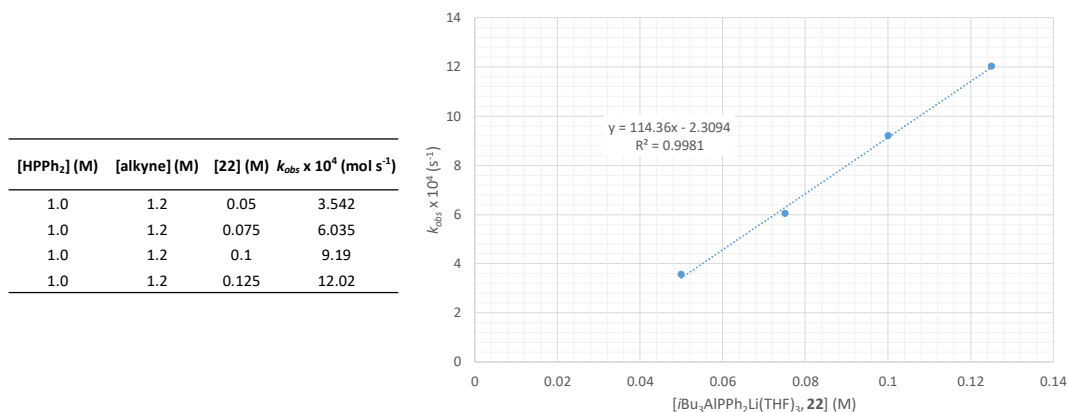


Figure 5.8: Observed reaction rate constants (k_{obs}) versus concentration of [**22**] for the hydrophosphination of diphenylacetylene catalysed by **22** in d_8 -toluene, at 373 K, and at given initial concentrations of HPPH_2 , alkyne, and **22**, showing pseudo-first order dependence in catalyst.

Interrogation of these obtained reaction concentration profiles was then performed using the modern kinetic analysis approach, Variable Time Normalisation Analysis (VTNA), introduced by Burés (Figure 5.9).³²⁵⁻³²⁷ VTNA uses a normalised time scale to adjust entire reaction profiles constructed from concentration data which then allows for visual identification of trends. The profiles of experiments differing in the concentration of one reactant, **A**, will only overlay when the time axis is replaced by the time integral of the concentration of **A** raised to a correct power α . This can be approximated by the trapezoid rule (Equation 5.2). The value of α which provides good plot overlap represents the order for that particular reagent, where t is the time.

$$\int_{t=0}^{t=n} [A]^{\alpha} dt = \sum_{i=1}^n \left(\frac{[A]_i + [A]_{i-1}}{2} \right)^{\alpha} (t_i - t_{i-1}) = \sum [A]^{\alpha} \Delta t$$

Equation 5.2: Trapezoid rule invoked during VTNA visual kinetic analysis.

This method of normalising the time scale for the concentration of each component in the system removes the kinetic effect of that component from the reaction profile. Hence, a benefit of this method is that it allows experiments to be run under synthetically relevant conditions, precluding the requirement for unrealistic “flooding” (*pseudo*-first order) conditions of one of the reaction components. Furthermore, VTNA includes data from the whole reaction profile, rather than data extrapolation from just for the first 10% as used in initial rate approaches. The order in catalyst represents a specific case in which the trapezoid rule in Equation 5.2 can be simplified to $t[cat]^{\alpha}$ provided that the concentration of catalyst does not change over the course of the reaction. Since its introduction the VTNA method has received positive welcome into the reaction profiling community and represents a straightforward and intuitive way to examine kinetic data. This is indicated by the many successful applications of VTNA to metal-catalysed and organo-catalysed reactions.³²⁷ This method is applied here to confirm the order in catalyst in this reaction system. The effect of different orders is shown; the correct order in catalyst is the one which produces an overlay of the concentration profile traces (Figure 5.9). From the graphs presented in Figure 5.9 it is clear that the order which best fits the raw concentration profile data is first order in catalyst (22).

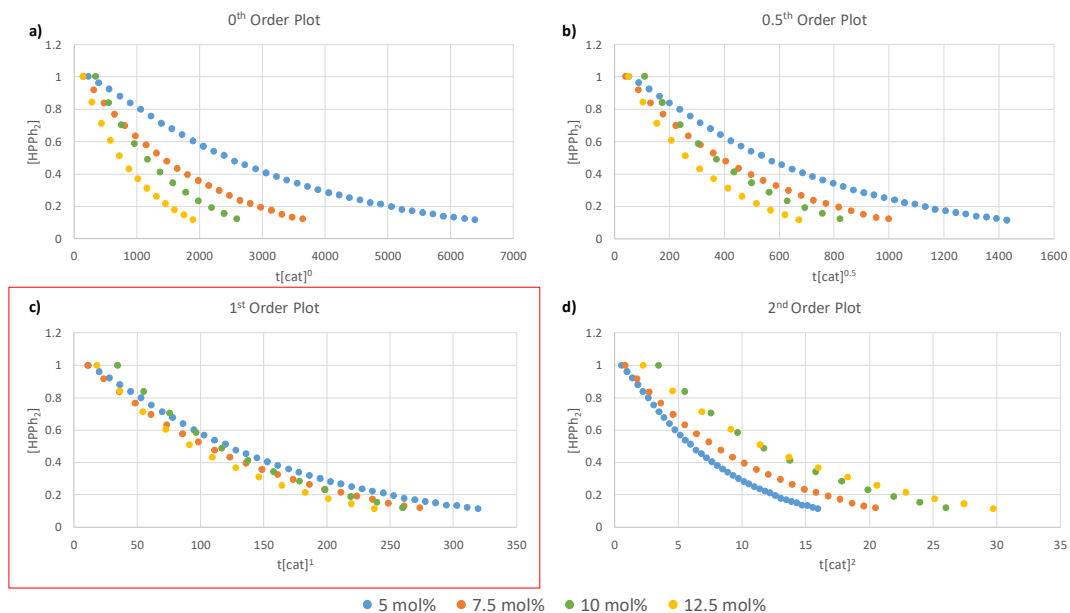


Figure 5.9: VTNA visual kinetic analysis for reaction rate dependence on order in catalyst showing plot for **a) 0th order; b) 0.5th order; c) 1st order, and d) 2nd order.**

Next, the effect of $HPPH_2$ concentration on the rate of the reaction was investigated. Five experiments were carried out varying the concentration of $[HPPH_2]$ in the range 1.1 – 0.7 M, with standard conditions of diphenylacetylene (1.2 M) and catalyst **22** (0.1 M), and a total reaction volume of 0.5 mL in d_8 -toluene solution. From the data obtained it is clear that the presence of phosphine inhibits the reaction; the observed rate constant k_{obs} increases with a decrease in the phosphine concentration in line with an inverse dependence on phosphine (Figure 5.10).

[HPPH ₂] (M)	[alkyne] (M)	[22] (M)	$k_{obs} \times 10^4$ (mol s ⁻¹)
1.1	1.2	0.1	5.34
1.0	1.2	0.1	9.19
0.9	1.2	0.1	10.23
0.8	1.2	0.1	14.70
0.7	1.2	0.1	15.21
0.6	1.2	0.1	16.70

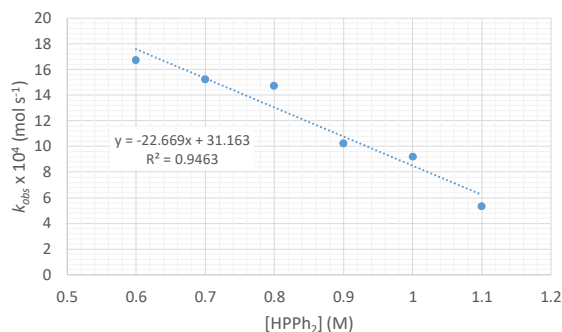


Figure 5.10: Observed reaction rate constants (k_{obs}) *versus* concentration of [HPPH₂] for the hydrophosphination of diphenylacetylene catalysed by **22** in d₈-toluene, at 373 K, and at given initial concentrations of HPPH₂, alkyne, and **22**, showing inverse dependence in HPPH₂.

This result is indicative of substrate inhibition by HPPH₂. Testing this theory, the addition of 0.15 mmol (30 mol%) PPh₃ to the hydrophosphination of diphenylacetylene under otherwise standard conditions results in an increase in the time required to reach quantitative conversion, from less than one hour to 1.5 hours. As was observed in Section 5.6.2 (Table 5.3) the addition of 20 mol% dppe to catalytic run using the pre-catalyst **11** also results in an inhibition of catalyst activity. Taken together, these observations suggest that phosphine inhibits the hydrophosphination reaction by causing an off-cycle process to occur. It should be noted that catalyst poisoning by phosphines is reported in the literature.^{288, 328, 329} Further interrogation of the reaction order of HPPH₂ was performed *via* VTNA visual kinetic interpretation (Figure 5.11). In this instance the best overlay fit was obtained when the order of HPPH₂ was calculated to be inverse first. This suggests that **22** catalysed hydrophosphination is inhibited by phosphine.

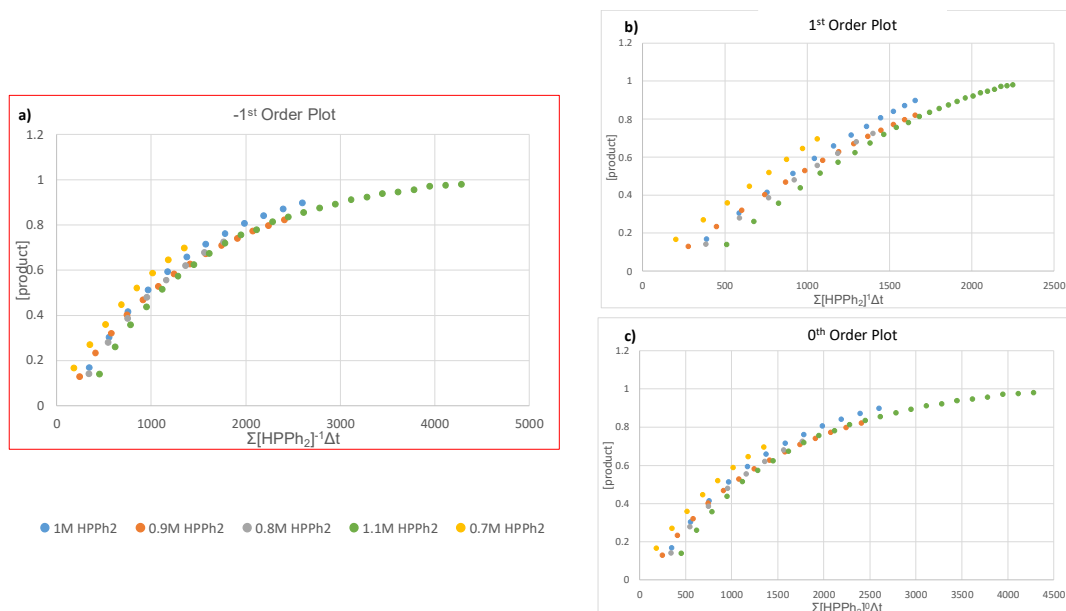


Figure 5.11: VTNA visual kinetic analysis for reaction rate dependence on order in HPPh₂ showing plot for **a)** -1st order; **b)** 1st order, and **c)** 0th order plots.

Lastly, the effect of varying the concentration of diphenylacetylene was examined. Thus, reactions employing diphenylacetylene in a concentration range between 1 – 1.4 M were interrogated. A plot of reaction rate against alkyne concentration provides a linear relationship with a positive gradient (Figure 5.12). This linear relationship implies that the rate of hydrophosphination increases as the concentration of alkyne is increased. For completeness, the concentration profiles for the order in diphenylacetylene were also interrogated by VTNA examination (Figure 5.13). This analysis suggests that the reaction is first order in alkyne.

[HPPh ₂] (M)	[alkyne] (M)	[22] (M)	$k_{obs} \times 10^4$ (mol s ⁻¹)
1.0	1.0	0.1	4.92
1.0	1.2	0.1	9.20
1.0	1.3	0.1	11.47
1.0	1.4	0.1	14.05

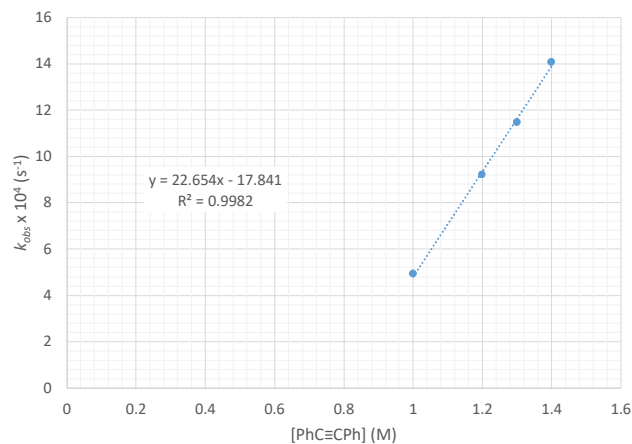


Figure 5.12: Observed reaction rate constants (k_{obs}) versus concentration of [diphenylacetylene] for the hydrophosphination of diphenylacetylene catalysed by **22** in d₈-toluene, at 373 K, and at given initial concentrations of HPPh₂, alkyne, and **22**, showing a positive relationship between alkyne concentration and reaction rate.

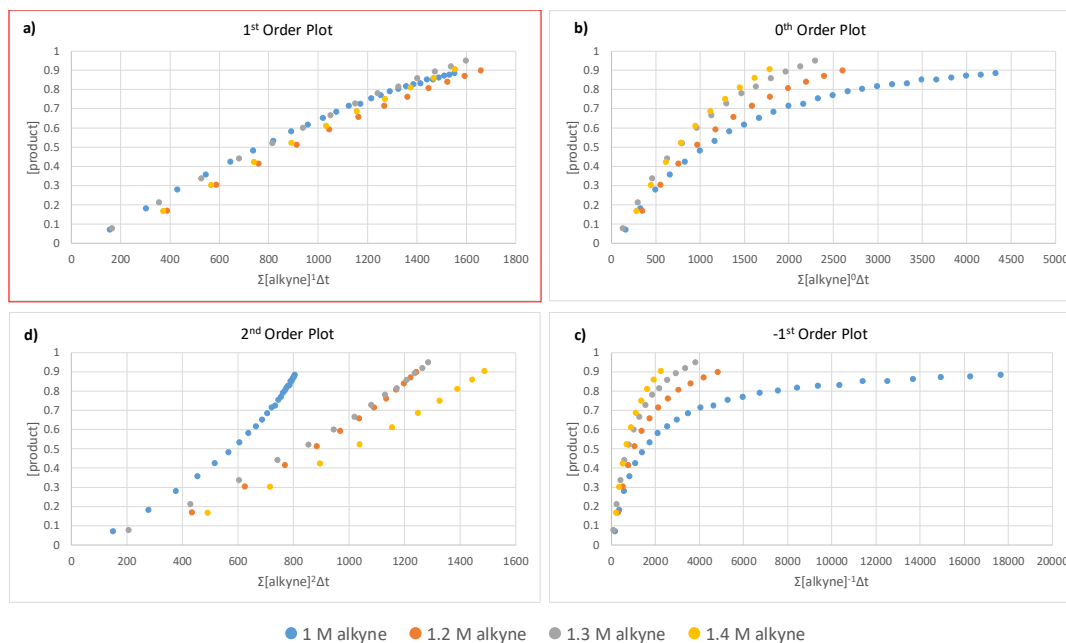


Figure 5.13: VTNA visual kinetic analysis for reaction rate dependence on order in diphenylacetylene showing plot for **a)** 1st order; **b)** 0th order; **c)** 2nd order, and **d)** -1st order plots.

It is possible to draw some general conclusions from the kinetic investigations performed here. Interestingly, HPPH_2 is an essential reagent in the catalytic reaction and also an inhibitor of catalysis. This dual role has further been exemplified by the decrease in the reaction rate of hydrophosphination of diphenylacetylene upon addition of catalytic PPh_3 to the **22**-catalysed reaction. Interrogation by a modern method of kinetic data analysis, VTNA, allows conclusions to be drawn about the order of individual reactants. Thus, the hydrophosphination catalysis has an inverse first order dependence on HPPH_2 , indicative of substrate inhibition. Both catalyst **22** and diphenylacetylene have a positive first order effect on the rate of reaction, which is consistent with the proposed catalytic cycle in Scheme 5.6. Further kinetic analysis *via* the isolation method (holding one reagent in vast excess to force *pseudo*-first order conditions) could be examined to confirm the visual assignment of orders on the basis of VTNA as is presented in this section.³³⁰ However, monitoring of reactions which use excess HPPH_2 may be problematic due to the inhibitory role of the phosphine, resulting in dramatically extended reaction times.

5.6 Conclusions

The aim of this part of the project was to try to expand the concept of lithium aluminates as catalysts for hydroelementation reactions other than hydroboration. Hydrophosphination was selected due in part to the useful and indicative ^{31}P NMR handle, and also because it appears that aluminium-catalysed hydrophosphination has not yet been reported in the literature. Furthermore, the polarity differences between a $\text{B}^{\delta+} - \text{H}^{\delta-}$ bond and a $\text{P}^{\delta-} - \text{H}^{\delta+}$ bond requires an alternative reaction mechanism where the phosphine is initially deprotonated to yield a metal phosphide which is the active species. This new catalytic cycle is therefore different to the hydridic catalytic cycle which has been observed in Chapters 2 and 3 for hydroboration catalysis (see also Chapter 1, section 1.2). Gratifyingly, the lithium aluminate $[\text{iBu}_3\text{AlHLi}]_2$, **11** is observed to be an active (pre)-catalyst for the hydrophosphination of alkynes, alkenes and carbodiimides, albeit under somewhat forcing conditions. By undertaking stoichiometric reactions, the isolation and structural characterisation of $\text{iBu}_3\text{AlPPh}_2\text{Li}(\text{THF})_3$, **22**, was possible, and is proposed to be the *bona fide* active species in the catalytic cycle. Investigation of the reaction mechanism *via* further stoichiometric reactions implies that addition of diphenylacetylene to **22**, and subsequent heating, generates two new

signals in the ^{31}P NMR spectrum which are tentatively assigned to intermediates on the catalytic cycle as a result of Al – P addition across the $\text{C} \equiv \text{C}$ bond. The addition of further HPPH_2 allows for the generation of the expected hydrophosphination products.

Compared to LiPPh_2 , and $i\text{Bu}_3\text{Al}$, $i\text{Bu}_2\text{AlH}$ or $i\text{Bu}_2\text{AlPPh}_2$ (pre)-catalysts, the hydrophosphination reaction times and E/Z isomer stereoselectivities differ when bimetallic $i\text{Bu}_3\text{AlPPh}_2\text{Li}(\text{THF})_3$ **22**, is used as the catalyst. This suggests that the lithium aluminate is acting as a synergistic bimetallic catalyst. Note that a 2019 review article has been published on synergistic effects in polar organometallic chemistry.¹⁰⁹ Preliminary studies into Lewis donor effects show that in the presence of a sterically demanding ligand such as $\text{Me}_6\text{-TREN}$, or in the presence of another phosphine such as triphenylphosphine or dppe, the catalytic reaction takes longer to reach completion than in the example case of diphenylacetylene. Furthermore, in the presence of different Lewis donors the E/Z isomer ratio changes for the hydrophosphination of diphenylacetylene, further implicating the contributing role of the lithium centre in the catalysis.

Attempts to shed light upon the reaction mechanism have been undertaken by employing reaction kinetics techniques. Thus, a small KIE is observed when DPPH_2 is used in place of HPPH_2 , which suggests that the P – H bond is only involved to a minor extent in the rate determining step. Further investigation using VTNA techniques has uncovered an interesting inverse first order dependence of HPPH_2 on the rate of the catalytic reaction, consistent with the reaction rate increasing with decreases in initial phosphine concentration. This is indicative of some type of off-cycle inhibitory process. Comparatively, the reaction kinetics have shown that the hydrophosphination of diphenylacetylene has a first order dependence on both the concentration of alkyne and the concentration of substrate, which is consistent with the proposed reaction mechanism in Scheme 5.6. Furthermore, employing DFT calculations has shown the favourable formation of **22** from **11** in the presence of THF. Whilst transition states have not yet been successfully located, preliminary DFT evidence suggests that the proposed mechanism in Scheme 5.6 is viable.

Chapter 6: Conclusions and Outlook

6.1 Conclusions

Previous exploration by other research groups into aluminium-catalysed hydroelementation chemistry has predominately focused on neutral, monometallic aluminium-hydride complexes. In some instances, examples of Lewis acidic, coordinatively unsaturated aluminium complexes have been employed and shown to be very active in hydrosilylation and hydroamination reactions. Building upon previous experience within the Mulvey group exploiting new metal-metal cooperativity, the aim of this PhD programme was to investigate the applicability of lithium aluminates as pre-catalysts for hydroelementation reactions. It was proposed that the benefit of the second metal might offer catalytic rate enhancements in spite of the more coordinatively saturated aluminium centre. Thus, a series of lithium aluminates have been prepared and extensively characterised by X-ray crystallography and multinuclear NMR studies before being applied as (pre)-catalysts for hydroelementation reactions, namely hydroboration (B – H addition) and hydrophosphination (P – H addition) of unsaturated substrates. These studies were supplemented by stoichiometric reactions aiming to isolate, and thus characterise, possible active species and intermediate species on the catalytic cycles.

Initially, in Chapter 2 a series of heteroleptic, heterometallic diamidodihydrido lithium aluminates were prepared, isolated and characterised in the solid state and solution phase. Bearing different Lewis donor functionalities at the lithium centre, with the general formula $(\text{HMDS})_2\text{Al}(\text{H})_2\text{Li}(\text{donor})_x$ [donor = THF, Et₂O, 12-crown-4, PMDETA, TMEDA, Me₆-TREN], this series was then applied as catalysts for the hydroboration of aldehydes and ketones. From this study it was unequivocally clear that the coordination environment at the lithium influenced the rate of catalysis. Furthermore, on employing a sodium analogue, namely $(\text{HMDS})_2\text{Al}(\text{H})(\mu\text{-H})\text{Na}(\text{THF})_4$, an alkali metal effect was observed, whereby the activity of the lithium system was higher than that of the sodium system, in this particular case. These observations provided the first concrete indication that the catalyst system was acting in a bimetallic fashion. The isolation of a potential catalytic intermediate, namely $(\text{HMDS})_2\text{Al}(\mu\text{-OCH}_2\text{Ph})_2\text{Li}(\text{THF})_2$, **8**, containing both metals provided further credence for this

bimetallic cooperativity. In a subsequent study, Harder reported the LiAlH_4 (pre)-catalysed hydrogenation of imines.⁷⁶ Based on DFT calculations and X-ray crystallography he proposed the active species to be the diamido-dihydrido complex “ $(\text{R}_2\text{N})_2\text{Al}(\text{H})_2\text{Li}$ ”, reminiscent of the (pre)-catalysts employed in Chapter 2. Furthermore, Harder proposed a catalytic cycle in which the lithium centre is involved in key reaction steps such as the coordination/polarisation of H_2 prior to the hydrogenation step. Contrary to this, Cowley and Thomas have reported the LiAlH_4 (pre)-catalysed hydroboration of alkenes.¹⁷⁷ In this instance, the LiAlH_4 pre-catalyst is proposed to deaggregate to AlH_3 and LiH . The authors propose that it is the AlH_3 which is the active species in the hydroboration catalysis, and no role for the LiH was elucidated. However, this catalytic cycle has not been examined by either DFT calculations or reaction kinetics, and no reaction intermediates were structurally characterised.

As a result of these reports, further evidence was required in an attempt to prove or disprove the bimetallic nature of these lithium aluminate (pre)-catalysts. In Chapter 3 the catalytic ability of a range of neutral aluminium compounds was compared to a series of charged lithium aluminate compounds to promote hydroboration for aldehyde, ketone, imine and alkyne substrates. It was observed that in general, the lithium aluminates were the more active systems, but that in the case of sterically demanding substrates it is possible that the neutral aluminium analogue might be better suited to the catalysis. Furthermore, a novel aluminium catalyst initiation process was observed for the neutral aluminium pre-catalyst, $i\text{Bu}_2\text{Al}(\text{TMP})$, as a result of β -hydride transfer from the stabilising $i\text{Bu}$ ligands. Importantly, this represents a method for preparing the proposed active aluminium hydride species *in situ* rather than requiring an Al – H bond to be present in the pre-catalyst.

In Chapter 4, reactivity studies between selected aluminium compounds, previously used as catalysts in Chapter 3, with common hydroboration borane reagents were undertaken. The nature of this reaction chemistry is exceptionally complex, and as a result unanswered questions as to true molecular identities of some products remain. However, analysis of such interactions should be considered with a view to potential catalyst deactivation routes during the hydroboration reactions. Such studies can open the door to the synthesis of more robust and active catalyst systems. A novel aluminium complex was uncovered as a result of cleavage of a B – O bond of HBpin by the neutral dialkyl-monoamido aluminium compounds $i\text{Bu}_2\text{Al}(\text{NR})_2$, whilst the typically more reactive B – H bond is retained

[NR₂ = TMP or HMDS]. For the lithium aluminate system, [*i*Bu₂Al(H)(TMP)Li]₂, studied ligand scrambling was found to occur in generating H₂B(TMP) on the basis of ¹¹B NMR spectroscopy. Thus, a co-product “*i*Bu₂AlLi{OC(Me)₂C(Me)₂O}” species is proposed, but definitive characterisation of this bimetallic species has not yet been achieved.

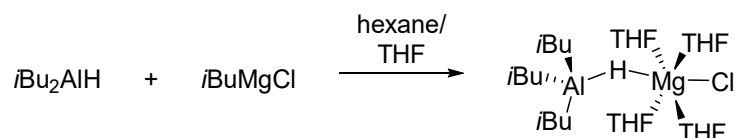
In Chapter 5 the application of lithium aluminate catalysts was extended to hydroelementation reactions other than hydroboration. Crucially, the ability of these catalysts to promote hydroelementation reactions by alternative reaction mechanisms to the hydridic catalytic cycle under operation in hydroboration (see Chapter 1, Section 1.2) would expand the remit of and interest in lithium aluminate catalysis. Thus, an investigation into hydrophosphination was undertaken, leading to the first documented example of aluminium-catalysed hydrophosphination. As was seen with the hydroboration systems, the lithium aluminate system was observed to be more active than the individual, monometallic neutral aluminium or lithium components. Hence, this is an example of a metal-metal synergistic effect, a theme which is gaining momentum but still offers vast scope for development as recently explained in a review article.¹⁰⁹ A lithium aluminium phosphide complex, *i*Bu₃AlPPh₂Li(THF)₃, **22**, was isolated and structurally characterised, and is proposed to be the true active species in this catalysis. This complex is an active catalyst for the hydrophosphination of alkynes, alkenes and carbodiimides. Reaction kinetics monitoring of diphenylacetylene hydrophosphination catalysed by **22** suggests that the reaction has an interesting inverse first order dependence on HPPH₂. Crucially, the work in this Chapter establishes that lithium aluminate catalysts are not solely limited to hydroboration applications and have the potential to become more general hydroelementation catalysts, capable of catalysing a range of different important organic transformations.

6.2 Outlook and Future Perspectives

Further work ideas were discussed at the end of each relevant chapter, which included the hydroelementation catalysis of different substrates, for example the hydroboration of heteroaromatic substrates such as quinolones and pyridines, in Chapter 3. Further investigation into the hydroboration of acetylenes should be undertaken with a view to broadening the substrate scope, as well as extension to alkene substrates. The

hydrophosphination of different substrates such as nitriles or isocyanates could also be examined. Furthermore, employing solvent free reaction conditions could also allow for enhanced catalytic reactivities compared to those observed in solution. However, caution should be employed with a view to ensuring that control of the reaction is maintained (including limiting side reactions, the potential for fast exothermic reactions, or reactions which release high quantities of H₂ gas). The benefit of solvent free conditions is something that is observed fairly routinely in the literature, but has not yet been examined with the lithium aluminate catalyst systems examined in this thesis.^{76, 177, 179, 183} It should be noted that the lack of solvent makes reaction monitoring more challenging, and requires either *in situ* monitoring techniques, removing aliquots from the reaction, or arbitrarily choosing a reaction end-time.

Additionally, detailed analysis of the reaction mechanisms driving hydroelementation catalysis in the presence of lithium aluminates should be examined, either by DFT calculations and/or reaction monitoring kinetic studies. Once the full role of both metals has been unequivocally established, informed systematic modifications (ligand systems/metal combinations) of the catalyst system should lead to more active catalysts. At present it is necessary to choose the main group catalyst carefully, with consideration to the reaction the user wishes to perform. Thus, the generation of a more robust and general aluminium catalyst would be advantageous. To this effect, preliminary studies have been undertaken with a view to modifying the heterobimetallic nature of the aluminate catalysts. One question which could be posed is: what effect do the ligands present at aluminium impart on the catalysis? For example, if the *isobutyl* groups are replaced with methyl groups is the catalysis better or worse? Previously, in Chapter 2 an alkali metal effect was observed on moving from a lithium aluminate to a sodium aluminate. This observation posed questions such as: what would happen if this cationic metal was changed from lithium to potassium? What effect would increasing the charge on the cationic metal have on the rate of catalysis? In a preliminary answer to the latter question, the synthesis of a bimetallic magnesium aluminium hydride complex was undertaken. Reaction of *i*Bu₂AlH and *i*BuMgCl in THF solvent gave the product *i*Bu₃Al(μ-H)MgCl(THF)₄, **27**, as a result of co-complexation between the two organometallic reagents (Scheme 6.1 and Figure 6.1).



Scheme 6.1: Preparation of the magnesium aluminate $i\text{Bu}_3\text{Al}(\mu\text{-H})\text{MgCl}(\text{THF})_4$, **27**.

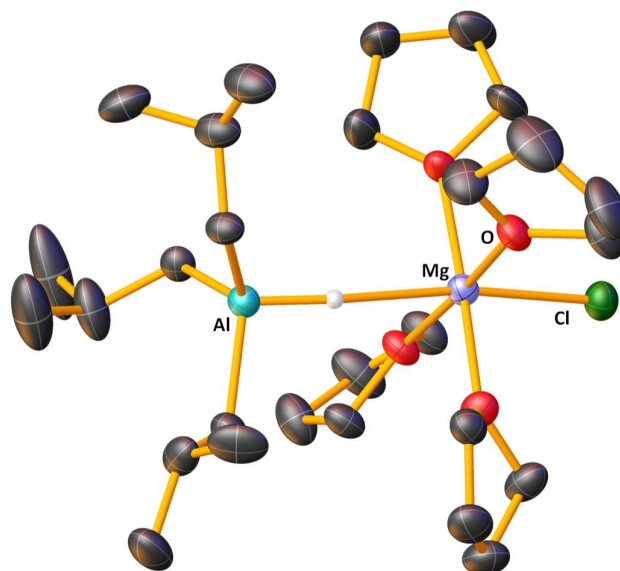


Figure 6.1: Molecular structure of $i\text{Bu}_3\text{Al}(\mu\text{-H})\text{MgCl}(\text{THF})_4$, **27**. Thermal ellipsoids are drawn at 40% probability, and hydrogens except the hydride have been omitted for clarity.

Compound **27** crystallises in an orthorhombic space group ($Pna2_1$) with the hydride bridging between the aluminium and magnesium centres. All three *i*Bu ligands are coordinated to the aluminium centre, while four molecules of THF complete the coordination shell at the magnesium. Unfortunately, the quality of the X-ray crystallographic data precludes any in-depth discussion of the geometric parameters of **27**.

Preliminary investigation into the catalytic proficiency of **27** was undertaken in the hydroboration of benzophenone, in C_6D_6 . Thus, with 5 mol% of **27** after 5 hours at room temperature only 84% of benzophenone had been converted to the hydroborated product: 2,2-diphenylmethoxy pinacolborane. The electronegativity difference between magnesium and aluminium (χ : Mg 1.31; Al 1.61; $\Delta\chi$ 0.30) is not as pronounced as that between alkali

metals and aluminium, (χ : Li 0.98; $\Delta\chi$ 0.63) hence this decreased polarity may be a factor in the poorer catalytic efficiency.²¹ In spite of this poor catalytic performance compared with the lithium aluminates examined in this project, it may be possible to optimise this system. For example, solvent screening was not undertaken, and it may be that moving to more polar solvents, such as THF, or moving to solvent free conditions would drastically alter the rate of catalysis. Furthermore, exchange of the chloride anion for a more weakly coordinating anion (such as BF_4^- or $[\text{B}(3,5\text{-}(\text{CF}_3)_2\text{C}_6\text{H}_2)_4]^-$) might allow the catalysis to proceed more efficiently by allowing the magnesium to more readily coordinate the incoming substrate. Related studies by Arwander on a magnesium aluminate system, $[(\text{THF})_4\text{Mg}\{\mu\text{-H}\text{AlMe}_3\}_2]$, showed that the magnesium aluminate is capable of acting as a magnesium hydride source in reaction with pyridine, forming selectively a magnesium-bis-1,4-dihydropyridide complex.³³¹ Similarly, reaction with 1-hexene formed a $[\text{Mg}(n\text{-hexyl})_2]$ complex, showing the availability of the magnesium-aluminium bridging hydride for reduction reactions. However, no catalytic applications of this magnesium aluminate were investigated.

To conclude, the study of main group compounds as catalysts for hydroelementation reactions is gaining significant prominence within the scientific community driven by the desire to find more environmentally benign reaction processes. In comparison to traditional transition metal catalysis, the field of main group catalysis is still in its infancy. With regards to applications of cooperative polymetallic systems in catalysis Hahn noted that “*the tool box is not even half full*” during the *Organometallics* Roundtable panel in 2011.³³² More work is required to allow such main group systems to compete on a level playing field with the state of the art transition metal catalysts. The application of aluminate compounds for catalysis represents one avenue worth perusing in this hunt for the optimal main group catalyst. The work reported in this thesis represents the first examples of lithium aluminate catalysed hydroboration, and lithium aluminate (and aluminium) catalysed hydrophosphination. Overall, lithium aluminates were observed to generally be superior catalysts to their neutral analogues. This may seem somewhat counterintuitive, given the high coordination number at aluminium for these systems, but it is clear that the cationic alkali metal has a significant role to play. In spite of the studies performed here, further investigation into the reaction mechanisms in operation in these systems is still required. Identification of the best alkali metal/ligand combination should be undertaken to optimise the catalysis in terms reaction conditions (time/temperature), substrate tolerance and product selectivity. In essence, this

thesis should serve as a prelude to future alkali metal aluminate catalysis investigations given the requirement to fill this synthetic chemistry tool box.

Chapter 7: Experimental

7.1 General experimental techniques

7.1.1 Solvent and reagent purification

All reactions and manipulations were performed under a protective argon atmosphere using either standard Schlenk techniques or glove box techniques.³³³ Hexane, THF, diethyl ether and toluene were dried by heating to reflux over sodium benzophenone ketyl and then distilled under nitrogen prior to use.³³⁴ C₆D₆, d₈-toluene and d₈-THF were degassed by freeze-pump-thaw methods and stored over activated 4 Å molecular sieves. All reagents were purchased from commercial sources and used as received, unless stated otherwise. TMEDA, PMDETA and HMDS(H) were distilled and stored over activated 4 Å molecular sieves prior to use.

7.1.2 Analytical techniques

NMR spectra were recorded on a Bruker AV3 or AV 400 MHz, or AV 600 MHz spectrometer operating at 400.13 MHz for ¹H, 155.47 MHz for ⁷Li, 104.2 MHz for ²⁷Al, 128.3 MHz for ¹¹B, 162.0 MHz for ³¹P and 100.62 MHz for ¹³C. All ¹³C spectra were proton decoupled. ¹H, ¹H{²⁷Al}, ¹³C{¹H}, ⁷Li, ²⁷Al, ²⁷Al{¹H}, ¹¹B and ³¹P chemical shifts are expressed in parts per million (δ, ppm) and where appropriate referenced to residual solvent peaks or external references.

Diffusion Ordered Spectroscopy (DOSY) NMR were recorded on an AV400 MHz spectrometer operating at 400.13 MHz, using the pulse program ledbpgp2s. DOSY experiments were performed following the external calibration method introduced by Stalke.^{206, 207} As such, 30mM concentration solutions of the analyte (0.015 mmol) in either C₆D₆, d₈-toluene or d₈-THF (0.5 mL) and either tetramethylsilane (0.015 mmol) or 1,2,3,4-tetraphenylnaphthalene (0.015 mmol) as internal standards.

Kinetic measurements and kinetic isotope effect (KIE) experiment measurements in Chapter 5 were recorded on a Bruker AVII 600 spectrometer operating at 243 MHz for ^{31}P using the pulse program: multi_zgvd2b_noshim.

IR spectra were recorded on a Perkin Elmer Spectrum 100 FTIR spectrometer. Samples were prepared as nujol mulls of the isolated crystalline solids.

Elemental analyses were performed using a Perkin Elmer 2400 elemental analyser.

GC-MS data were acquired on an Agilent Technologies 7890A GC system fitted with a Restek Rxi-5Sil column (30 m, 0.25 mm ID, 0.25 μm) and coupled to an Agilent mass spectrometer using either chemical ionisation (methane) or electron impact ionisation. Helium was used as the carrier gas (1 mL min^{-1}). In all cases, an inlet temperature of 320 $^{\circ}\text{C}$ and the following oven temperature gradient were used: 4 minutes at 40 $^{\circ}\text{C}$; ramp to 320 $^{\circ}\text{C}$ at 20 $^{\circ}\text{C min}^{-1}$; hold for 10 minutes (total run time of 28 min).

X-ray crystallography data for novel complexes reported in this thesis were collected on Oxford Diffraction Gemini S or Xcalibur E instruments with graphite-monochromated Mo $\text{K}\alpha$ ($\lambda = 0.71073 \text{ \AA}$) or Cu $\text{K}\alpha$ ($\lambda = 1.54184 \text{ \AA}$) radiation. Data collection and processing used Rigaku and Bruker software.^{335, 336} All structures were solved and refined to convergence on F^2 for all independent reflections by the full-matrix least squares method using SHELXL-2014/7,^{335, 337} or by the Gauss Newton algorithm using OLEX2.³³⁸

7.2: Experimental data for Chapter 2

The full data set underlying this research can be located online at <http://dx.doi.org/10.15129/2a1e37f8-5fc5-4df2-aaa6-92751990f568>. Selected crystallographic data are shown in Table 7.7.1 and full details for X-ray diffraction in .cif format are available from CCDC (1579613 – 1579620) for compounds **1**, **3** – **9**.

7.2.1: Synthesis of compounds

Synthesis of (HMDS)₂AlH(μ-H)Li(THF)₃, **1**

HMDS(H) (4.2 mL, 20 mmol) in THF (10 mL) was added dropwise to a cooled Schlenk flask containing a THF (10 mL) suspension of LiAlH₄ (0.38 g, 10 mmol) at 0 °C. The resulting suspension was heated to 40 °C for three hours, cooled to room temperature, and then stirred at room temperature overnight. Filtering the suspension via a celite cannula generated a colourless solution. THF was removed under vacuum and the residues dissolved in hexane (20 mL). Cooling to -30 °C generated a crop of colourless crystals (yield 3.50 g, 6.1 mmol, 61 %). Elemental analysis (%) for C₂₄H₅₉AlLiN₂O₃Si₄: calcd: C 50.57, H 10.43, N 4.91; found: C 50.62, H 10.94, N 5.02.

¹H NMR (400.1 MHz, C₆D₆, 300 K): δ 3.49 (t, J = 6.94 Hz, 12H, CH₂), 1.35 (t, J = 6.68 Hz, 12H, CH₂), 0.56 (s, 36H, CH₃) ppm. ¹H{²⁷Al} NMR (400.1 MHz, C₆D₆, 300 K): δ 3.87 (br s, 2H, AlH₂), 3.50 (t, 12H CH₂), 1.35 (s, 12H, CH₂), 0.55 (s, 36H, CH₃) ppm. ¹³C{¹H} NMR (100.6 MHz, C₆D₆, 300 K): δ 68.6 (s, CH₂), 25.4 (s, CH₂), 6.4 (s, CH₃) ppm. ⁷Li NMR (155.5 MHz, C₆D₆, 300 K): δ -0.23 (s) ppm. ²⁷Al{¹H} NMR (104.2 MHz, C₆D₆, 300 K): δ 106.4 (br s) ppm. ²⁷Al NMR (104.2 MHz, C₆D₆, 343 K): δ 106.2 (apparent triplet, J = 160.7 Hz) ppm. IR ν 1752.8 + 1679.3 (br s, Al-H) cm⁻¹.

Synthesis of (HMDS)₂Al(μ-H)₂Li(OEt)₂, **2**

Prepared via a literature method.¹⁹⁵

To a cooled (0 °C) suspension of LiAlH₄ (0.71 g; 18.7 mmol) in Et₂O (30 mL) was added HMDS (8 mL; 38.1 mmol) dropwise. The mixture was allowed to warm to room temperature and then

stirred overnight. The grey precipitate was filtered off and the filtrate was concentrated to the point of crystallisation. Storing the Schlenk flask at -18 °C resulted in the formation of the desired product as colourless crystals.

^1H NMR (400.1 MHz, C_6D_6 , 300 K): δ 0.47 (s, 36H, $\text{N}(\text{Si}(\text{CH}_3)_2)$); 0.94 (t, 12H, OCH_2CH_3); 3.18 (quartet, 8H, OCH_2CH_3) ppm.

Synthesis of $(\text{HMDS})_2\text{Al}(\mu\text{-H})_2\text{Li}(\kappa^4\text{ 12-crown-4})$, **3**

12-crown-4 (0.08 mL, 0.5 mmol) was added dropwise to a Schlenk flask containing a hexane (3 mL) solution of $(\text{HMDS})_2\text{Al}(\mu\text{-H})_2\text{Li}(\text{OEt}_2)_2$, **2** (0.26 g, 0.5 mmol) giving a white precipitate. The reaction was stirred for 1 hour, then toluene (2 mL) was added and the Schlenk flask put in the freezer at -26 °C, which produced colourless crystals (yield 0.20 g, 0.38 mmol, 75 %). Elemental analysis (%) for $\text{C}_{20}\text{H}_{54}\text{AlLiN}_2\text{O}_4\text{Si}_4$: calcd: C 45.08, H 10.21, N 5.26; found: C 45.28, H 9.66, N 5.31.

^1H NMR (400.1 MHz, C_6D_6 , 300 K): δ 2.92 (br s, 16H CH_2), 0.64 (s, 36H, CH_3) ppm. $^1\text{H}\{^{27}\text{Al}\}$ NMR (400.1 MHz, C_6D_6 , 300 K): δ 3.84 (br s, 2H AlH_2), 2.96 (br s, 16H CH_2), 0.64 (s, 36H, CH_3) ppm. $^{13}\text{C}\{^1\text{H}\}$ NMR (100.6 MHz, C_6D_6 , 300 K): δ 66.6 (s, CH_2), 6.6 (s, CH_3) ppm. ^7Li NMR (155.5 MHz, C_6D_6 , 300 K): δ -0.7 ppm. $^{27}\text{Al}\{^1\text{H}\}$ NMR (104.2 MHz, C_6D_6 , 300K): δ 106.4 (br s) ppm. ^{27}Al NMR (104.2 MHz, C_6D_6 , 343K): δ 106.4 (t, $J = 175.70$ Hz) ppm. IR ν 1660.9 (br s, Al-H) cm^{-1} .

Synthesis of $(\text{HMDS})_2\text{AlH}(\mu\text{-H})\text{Li}(\text{PMDETA})$, **4**

PMDETA (0.10 mL, 0.5 mmol) was added dropwise to a Schlenk flask containing a hexane (3 mL) solution of $(\text{HMDS})_2\text{Al}(\mu\text{-H})_2\text{Li}(\text{OEt}_2)_2$, **2** (0.26 g, 0.5 mmol) which instantly formed a white precipitate. The reaction was stirred for 2 hours, then volatiles were removed under vacuum leaving the product as a white solid (yield 0.19 g, 0.36 mmol, 72 %). Colourless crystals suitable for X-ray analysis were grown from a toluene (0.5 mL)/hexane (2 mL) solution at -15 °C. Elemental analysis (%) for $\text{C}_{21}\text{H}_{61}\text{AlLiN}_5\text{Si}_4$: calcd: C 47.59, H 11.60, N 13.21; found: C 47.47, H 11.34, N 12.85.

^1H NMR (600 MHz, C_6D_6 , 300 K): δ 1.96 (s, 15H, PMDETA CH_3), 1.70 (m, 2H, PMDETA CH_2), 1.58 (m, 4H, PMDETA CH_2), 1.50 (m, 2H, PMDETA CH_2), 0.56 (s, 36H, HMDS CH_3) ppm. **$^1\text{H}\{^{27}\text{Al}\}$ NMR (400.1 MHz, C_6D_6 , 300 K):** δ 3.72 (br s, 2H AlH_2), 1.71 (s, 15H, PMDETA CH_3), 1.68 – 1.49 (m, 8H, CH_2), 0.58 (s, 36H, CH_3) ppm. **$^{13}\text{C}\{^1\text{H}\}$ NMR (100.6 MHz, C_6D_6 , 300 K):** δ 56.8 (s, PMDETA CH_2), 53.1 (s, PMDETA CH_2), 45.7 (s, PMDETA CH_3), 45.0 (s, PMDETA CH_3), 6.8 (s, HMDS CH_3). **^7Li NMR (155.5 MHz, C_6D_6 , 300 K):** δ 0.23 ppm. **$^{27}\text{Al}\{^1\text{H}\}$ NMR (104.2 MHz, C_6D_6 , 300K):** δ 106.0 (br s) ppm. **^{27}Al NMR (104.2 MHz, C_6D_6 , 300K):** δ 106.2 (t, $J = 171.86$ Hz) ppm. **IR** ν 1734.4 + 1664.4 (br s, $\text{Al} - \text{H}$) cm^{-1} .

Synthesis of $[(\text{HMDS})_2\text{AlH}_2] [\text{Li}(\text{TMEDA})_2]$, **5**

TMEDA (0.16 mL, 1.0 mmol) was added dropwise to a Schlenk flask containing a hexane (3 mL) solution of $(\text{HMDS})_2\text{Al}(\mu\text{-H})_2\text{Li}(\text{OEt}_2)_2$, **2** (0.26 g, 0.5 mmol) which instantly forms a white precipitate. The reaction was stirred for 1.5 hours, then the volatiles were removed giving the product as a white solid. (yield 0.50 g, 0.85 mmol, 85 %). Addition of toluene (3 mL) and cooling to -15 °C, produced colourless crystals suitable for single crystal X-ray analysis. Elemental analysis (%) for $\text{C}_{24}\text{H}_{70}\text{AlLi}_6\text{Si}_4$: calcd: C 48.93, H 11.98, N 14.27; found: C 49.28, H 12.15, N 13.76.

^1H NMR (400.1 MHz, C_6D_6 , 300.1 K): δ 2.01 (s, 8H, CH_2), 1.98 (s, 24H, CH_3), 0.53 (s, 36H, CH_3) ppm. **$^1\text{H}\{^{27}\text{Al}\}$ NMR (400.1 MHz, C_6D_6 , 300 K):** δ 3.82 (br s, 2H, AlH_2), 1.95 (s, 24H, CH_3), 0.53 (s, 36H, CH_3) ppm. **$^{13}\text{C}\{^1\text{H}\}$ NMR (100.6 MHz, C_6D_6 , 300 K):** δ 57.2 (s, CH_2), 45.6 (s, CH_3), 6.2 (s, CH_2) ppm. **^7Li NMR (155.5 MHz, C_6D_6 , 300 K):** δ 0.29 ppm. **$^{27}\text{Al}\{^1\text{H}\}$ NMR (104.2 MHz, C_6D_6 , 300K):** δ 106.6 (br s) ppm. **^{27}Al NMR (104.2 MHz, d_8 -Tol, 343K):** δ 105.4 (br s) ppm. **IR** ν 1708.7 + 1638.8 (br s, $\text{Al} - \text{H}$) cm^{-1} .

Synthesis of $[(\text{HMDS})_2\text{AlH}_2] [\text{Li}(\text{Me}_6\text{-TREN})_2]$, **6**

$\text{Me}_6\text{-TREN}$ (0.13 mL, 0.5 mmol) was added dropwise to a Schlenk flask containing a hexane (3 mL) solution of $(\text{HMDS})_2\text{Al}(\mu\text{-H})_2\text{Li}(\text{OEt}_2)_2$, **2** (0.26 g, 0.5 mmol). The reaction was stirred for 1 hour, which gave a white precipitate. Removing the volatiles under vacuum gave the product as a white

solid (yield 0.26 g, 0.44 mmol, 89 %). Toluene (5 mL) was added and the Schlenk flask put in the freezer at -26 °C, which produced colourless crystals suitable for X-ray. Elemental analysis (%) for $C_{24}H_{68}AlLiN_6Si_4$: calcd: C 49.10, H 11.67, N 14.31; found: C 49.25, H 11.26, N 14.62.

1H NMR (400.1 MHz, C_6D_6 , 300 K): δ 2.01 (s, 18H, CH_3), 1.99 (t, $J = 5.52$ Hz, 6H, CH_2), 1.77 (t $J = 5.52$ Hz, 6H, CH_2), 0.63 (s, 36H, CH_3) ppm. **$^1H\{^{27}Al\}$ NMR (400.1 MHz, C_6D_6 , 300 K):** δ 3.91 (br s, 2H AlH_2), 2.02 (s, 24H $CH_2 + CH_3$), 1.79 (br s, 6H CH_2), 0.62 (s, 36H, CH_3) ppm. **$^{13}C\{^1H\}$ NMR (100.6 MHz, C_6D_6 , 300 K):** δ 57.1 (s, CH_2), 50.6 (s CH_2), 45.8 (s, CH_3), 6.9 (s, CH_3) ppm. **7Li NMR (155.5 MHz, C_6D_6 , 300 K):** δ 0.09 ppm. **$^{27}Al\{^1H\}$ NMR (104.2 MHz, C_6D_6 , 300K):** δ 107 (br s) ppm. **^{27}Al NMR (104.2 MHz, C_6D_6 , 300K):** δ 107 (t $J = 179.13$ Hz) ppm. **IR ν** 1716.0 + 1649.9 (br s, $Al - H$) cm^{-1} .

Synthesis of $(HMDS)_2AlH(\mu-H)Na(THF)_3$, 7

HMDS(H) (0.84 mL, 4 mmol) in THF (2 mL) was added dropwise to a cooled Schlenk flask containing a THF (2 mL) suspension of $NaAlH_4$ (0.108 g, 2 mmol) at 0 °C. The resulting suspension was heated to 40 °C for three hours, then stirred at room temperature overnight. Filtering the suspension via a celite cannula generated a colourless solution was removed under vacuum and the residues dissolved in hexane (5 mL). Cooling to -30 °C generated a crop of colourless crystals (yield 0.44 g, 0.75 mmol, 38 %). Elemental analysis (%) for $C_{16}H_{45}N_2NaAlOSi_4$: calcd: C 43.30, H 10.22, N 6.31; found: C 42.97, H 9.84, N 5.59. Elemental analysis agrees with 1H NMR data confirming that THF molecules are lost under vacuum.

1H NMR (400.1 MHz, C_6D_6 , 300 K): δ 3.49 (m, 4H, CH_2), 1.37 (m, 4H, CH_2), 0.46 (s, 36H, CH_3) ppm. **$^1H\{^{27}Al\}$ NMR (400.1 MHz, C_6D_6 , 300 K):** δ 3.77 (br s, 2H, AlH_2), 3.51 (t, 4H CH_2), 1.38 (t, 4H, CH_2), 0.48 (s, 36H, CH_3) ppm. 1H NMR are indicative of loss of THF molecules under vacuum, during isolation of the crystalline product. **$^{13}C\{^1H\}$ NMR (100.6 MHz, C_6D_6 , 300 K):** δ 68.2 (s, CH_2), 25.6 (s, CH_2), 6.4 (s, CH_3). **$^{27}Al\{^1H\}$ NMR (104.2 MHz, C_6D_6 , 300K):** δ 104.5 (br s) ppm. **^{27}Al NMR (104.2 MHz, C_6D_6 , 343K):** δ 104.6 (br s) ppm. **IR ν** 1730.7 + 1675.6 + 1627.8 (br s, $Al - H$) cm^{-1} .

Synthesis of (HMDS)₂Al(μ-OCH₂Ph)₂Li(THF)₂, **8**

To a hexane (3 mL) solution of **1** (0.28 g; 0.5 mmol) was added 2 equivalents of benzaldehyde (0.10 mL; 1 mmol). The resulting clear, colourless solution was stirred at room temperature for 1.5 hours then placed in the freezer at -30 °C. Colourless crystals of the product were isolated by cannula filtration. (Yield 0.15 g; 0.21 mmol; 42%). Elemental analysis (%) for C₃₄H₆₄AlLiN₂O₄Si₄: calcd: C 57.42, H 9.0, N 3.94; found: C 57.39, H 9.20, N 4.35.

¹H NMR (400.1 MHz, C₆D₆, 300 K): δ 7.32 (d, J = 6.55 Hz, 4H, CH), 7.01 (t of t, J = 7.26, 1.80 Hz, 4H, CH), 6.94 (t of t, J = 7.32, 1.35 Hz, 2H, CH), 4.93 (s, 4H, CH₂), 2.93 (m, 8H, CH₂), 1.10 (m, 8H, CH₂), 0.56 (s, 36H, CH₃) ppm. **¹³C{¹H} NMR (100.6 MHz, C₆D₆, 300 K):** δ 144.4 (s, CH), 128.6 (s, CH), 128.2 (s, CH), 127.1 (s, CH), 67.6 (s, CH₂), 65.8 (s, CH₂), 25.3 (s, CH₂), 6.5 (s, CH₃) ppm. **⁷Li NMR (155.5 MHz, C₆D₆, 300 K):** δ -0.12 (s) ppm. No signal was observed in the ²⁷Al NMR spectrum.

Synthesis of [(HMDS)AlH(μH)[C₃H₄N₃]Li(THF)], **9**

To hexane (3 mL) was added LiAlH₄ (0.5 mL, 1 mmol, 2M in THF), followed by HMDS(H) (0.84 mL, 4 mmol) and 1-methyl-1,2,4-triazole (0.08 mL, 1 mmol). The colourless solution was stirred for 15 minutes and then cooled to -30 °C. Colourless crystals of the product were isolated by cannula filtration. (Yield 0.186 g; 0.53 mmol, 53 %). Elemental analysis (%) for C₁₃H₃₁AlLiN₄OSi₂: calcd: C 44.67, H 8.94, N 16.03; found: C 44.53, H 8.92, N 15.98.

¹H NMR (400.1 MHz, d₈-THF, 300 K): δ 7.57 (s, 1H, triazole CH), 3.95 (s, 3H, triazole CH₃), 3.61 (m, 4H, CH₂), 1.77 (m, 4H, CH₂), -0.02 (s, 18H, CH₃) ppm. **¹³C{¹H} NMR (100.6 MHz, d₈-THF, 300 K):** δ 149.8 (s, triazole CH), 68.0 (s, CH₂), 37.7 (s, triazole CH₃), 26.2 (s, CH₂), 5.1 (s, CH₃) ppm. **⁷Li NMR (155.5 MHz, d₈-THF, 300 K):** δ 0.68 (s) ppm. **²⁷Al NMR (104.2 MHz, d₈-THF, 300K):** δ 113.4 (br s) ppm.

Synthesis of Me₆-TREN

Prepared via a literature method.³³⁹

To a solution of tris[2-aminoethyl]amine (3 mL; 20 mmol) and acetic acid (125 mL) in acetonitrile (600 mL) was added aqueous formaldehyde (49 mL; 37 wt%, 660 mmol) and the reaction allowed to stir for 1 hour. The reaction was then cooled to 0 °C and sodium borohydride (10 g; 13.4 mmol) was added slowly. The reaction was then stirred at room temperature for 48 hours. Subsequently all solvents were removed using a rotatory evaporator and the residues made strongly basic by the addition of aqueous sodium hydroxide (3 M). The product was then extracted by CH₂Cl₂ (3 x 20 mL). The extracts were combined, dried with MgSO₄ and the solvent was removed by rotatory evaporation. The residues were dissolved in pentane and filtered. The filtrate was reduced to dryness to give the product as a pale yellow oil.

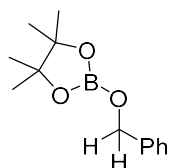
¹H NMR (400.1 MHz, C₆D₆, 300 K): 2.11 (s, 18H, 3xN(CH₃)₂); 2.36 (m, 6H, 3xNCH₂CH₂NMe₂); 2.62 (m, 6H, 3xNCH₂CH₂NMe₂) ppm.

7.2.2 Hydroboration Catalysis

The lithium aluminate (HMDS)₂AlH(μ-H)Li(THF)₃, **1**, (0.005 mmol, i.e. 1 mol%), was added to 0.5 mL of a C₆D₆ solution containing 0.5 mmol of the carbonyl precursor and of pinacolborane (73 μL, 0.5 mmol), as well as 10 mol% of internal standard; hexamethylcyclotrisiloxane. The mixture was transferred to a sealed Young's tap NMR tube and the reaction was regularly monitored by ¹H and ¹¹B NMR until the formation of products was completed. The reactions were performed at room temperature, except for substrates mesitaldehyde and 2,4,6-trimethyl acetophenone which were heated to 70 °C. The yields reported are based on ¹H NMR relative to the internal standard. In all cases, the bulk of the NMR solution can be attributed to either the boronate esters or starting material.

Aldehydes:*Benzaldehyde*

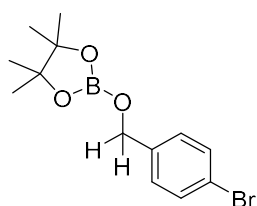
Consistent with characterisation data in the literature.⁵⁴



¹H NMR (400.1 MHz, C₆D₆, 300 K): δ 7.25 – 7.28 (dm, 2H, J = 7.64 Hz, Ar-H), 7.00 – 7.13 (m, 3H, Ar-H), 4.90 (s, 2H, OCH₂), 1.02 (s, 12H, CH₃) ppm. **¹¹B NMR (128.38 MHz, C₆D₆, 300 K):** δ 22.7 (s, O-B) ppm. **¹³C NMR (100.62 MHz, C₆D₆, 300 K):** δ 140.1 (s, ipso Ar CH), 128.6 (s, Ar C), 127.6 (s, Ar C), 127.1 (s, Ar C), 82.8 (s, C(CH₃)₂), 67.0 (s, OCH₂), 24.7 (s, CH₃) ppm.

4-bromobenzaldehyde

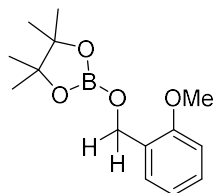
Consistent with characterisation data in the literature.¹⁸⁵



¹H NMR (400.1 MHz, C₆D₆, 300 K): δ 7.22 (m, 2H, J = 8.64 Hz, J = 1.96 Hz, Ar-H), 6.94 (m, 2H, J = 8.64 Hz, J = 1.67 Hz), 4.72 (s, 2H, OCH₂), 1.03 (s, 12H, CH₃) ppm. **¹¹B NMR (128.38 MHz, C₆D₆, 300 K):** δ 22.7 (s, O-B) ppm. **¹³C NMR (100.62 MHz, C₆D₆, 300 K):** δ 138.9 (s, ipso C), 131.6 (s, Ar CH), 128.7 (s, Ar CH), 121.5 (s, Ar CBr), 82.9 (s, C(CH₃)₂), 66.1 (OCH), 24.7 (s, CH₃) ppm.

2-methoxybenzaldehyde

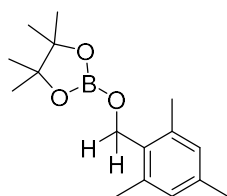
Consistent with characterisation data in the literature.¹⁷²



¹H NMR (400.1 MHz, C₆D₆, 300 K): δ 7.61 (dt, 1H, J = 7.59 Hz, 0.94 Hz, Ar-H), 7.07 (tm, 1H, J = 8.08 Hz, Ar-H), 6.88 (td, 1H, J = 7.49 Hz, J = 0.94 Hz, Ar-H), 6.49 (dd, 1H, J = 8.21 Hz, 0.94 Hz, Ar-H), 5.24 (s, 2H, OCH₂), 3.27 (s, 3H, OCH₃), 1.05 (s, 12H, CH₃) ppm. **¹¹B NMR (128.38 MHz, C₆D₆, 300 K):** δ 22.8 (s, O-B) ppm. **¹³C NMR (100.62 MHz, C₆D₆, 300 K):** δ 156.8 (s, COCH₃), 135.6 (s, Ar CH), 128.5 (s, ipso C), 127.5 (s, Ar CH), 120.7 (s, Ar CH), 110.1 (s, Ar CH), 82.7 (s, C(CH₃)₂), 62.6 (s, OCH₂), 54.8 (s, OCH₃), 24.7 (s, CH₃) ppm.

Mesitaldehyde

Consistent with characterisation data in the literature.⁵⁴

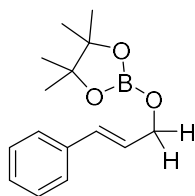


¹H NMR (400.1 MHz, C₆D₆, 300 K): δ 6.71 (s, 2H, Ar), 5.00 (s, 2H, OCH₂), 2.34 (s, 6H, Ar CH₃), 2.11 (s, 3H, Ar CH₃), 1.01 (d, J = 2.75 Hz, 12H CH₃) ppm.

¹¹B NMR (128.38 MHz, C₆D₆, 300 K): δ 22.5 (s, O-B) ppm. **¹³C NMR (100.62 MHz, C₆D₆, 300 K):** δ 137.7 (s, ArCCH₃), 137.4 (s, ArCCH₃), 132.9 (s, Ar ipso C), 130.7 (s, Ph), 82.5 (s, C(CH₃)₂), 61.5 (s, ArCH₂), 24.7 (s, CH₂(CH₃)₂), 21.0 (s, Ar-CH₃), 19.6 (s, Ar-CH₃) ppm.

Cinnamaldehyde

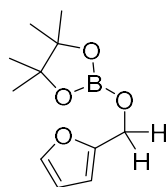
Consistent with characterisation data in the literature.⁷⁹



¹H NMR (400.1 MHz, C₆D₆, 300 K): δ 7.18 (dm, 2H, J = 8.32 Hz, Ar-H), 7.09 (tm, 2H, J = 7.20 Hz, Ar-H), 7.02 (tt, 1H, J = 7.26 Hz, J = 2.40 Hz, Ar-H), 6.59 (tt, 1H, J = 15.9 Hz, J = 1.84 Hz, CHCH), 6.17 (dt, 1H, J = 15.90 Hz, 5.42 Hz, CHCH), 4.52 (dd, 2H, J = 5.47 Hz, J = 1.86 Hz, OCH₂), 1.07 (s, 12H, CH₃) ppm. **¹¹B NMR (128.38 MHz, C₆D₆, 300 K):** δ 22.7 (s, O-B) ppm. **¹³C NMR (100.62 MHz, C₆D₆, 300 K):** δ 137.3 (s, ipso C), 130.9 (s, ArCHC), 128.8 (s, ArCH), 127.7 (s, Ph), 127.50 (s, Ph), 126.8 (s, Ph), 82.8 (s, C(CH₃)₂), 65.5 (s, CH₂), 24.7 (s, CH₃) ppm.

Furfural

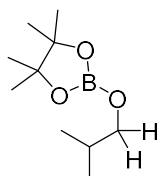
Consistent with characterisation data in the literature.⁷⁹



¹H NMR (400.1 MHz, C₆D₆, 300 K): δ 7.08 (dd, 1H, J = 1.73 Hz, J = 0.99 Hz, CH), 6.13 (dd, 1H, J = 3.35, 0.75, CH), 6.04 (dd, 1H, J = 3.24 Hz, J = 1.77 Hz, CH), 4.81 (s, 2H OCH₂), 1.04 (s, 12H, CH₃) ppm. **¹¹B NMR (128.38 MHz, C₆D₆, 300 K):** δ 22.7 (br s O-B) ppm. **¹³C NMR (100.62 MHz, C₆D₆, 300 K):** δ 153.3, 142.6, 110.5, 108.5 (s, C₄H₃O), 82.8 (C(CH₃)₂), 59.4 (CH₂), 24.7 (CH₃) ppm.

Isobutyraldehyde

Consistent with characterisation data in the literature.⁵⁴



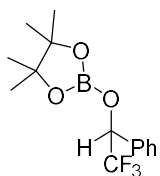
¹H NMR (400.1 MHz, C₆D₆, 300 K): δ 3.67 (d, 2H, J = 6.43 Hz, OCH₂), 1.76 (sep, 1H, J = 6.47 Hz, (CH₃)₂CH), 1.07 (s, 12H, CH₃), 0.82 (d, 6H, J = 6.76 Hz, CH(CH₃)₂) ppm.

¹¹B NMR (128.38 MHz, C₆D₆, 300 K): δ 22.4 (s, O-B) ppm. **¹³C NMR (100.62 MHz, C₆D₆, 300 K):** δ 82.4 (s, C(CH₃)₂), 71.5 (s, CH₂CH₃), 30.3 (s, CH), 24.8 (s, C(CH₃)₂),

18.9 (s, CH₂CH₃) ppm.

Ketones:*2,2,2-trifluoroacetophenone*

Consistent with characterisation data in the literature.¹⁸⁵



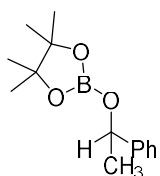
¹H NMR (400.1 MHz, C₆D₆, 300 K): δ 7.38 – 7.36 (m, 2H, Ar CH), 7.04 – 7.02 (m, 3H, Ar CH), 5.53 (q, 1H, J = 6.73 Hz, OCH), 0.99 (s, 6H, CH₃), 0.95 (s, 6H, CH₃) ppm.

¹¹B NMR (128.38 MHz, C₆D₆, 300 K): δ 22.8 (s, O-B) ppm. **¹³C NMR (100.62 MHz, C₆D₆, 300 K):** δ 134.1 (s, ipso C), 129.7 (s, Ar C), 128.8 (s, Ar C), 128.4 (s, Ar CH),

123.4 (q, ¹J_{CF} = 230 Hz, CF₃), 83.9 (s, C(CH₃)₂), 74.9 (q, ²J_{CF} = 33 Hz, CCF₃), 25.1 (s, CH₃), 24.8 (s, CH₃) ppm. **¹⁹F NMR (376 MHz, C₆D₆, 300 K):** δ – 78.1 (d, J = 6.69 Hz) ppm.

Acetophenone

Consistent with characterisation data in the literature.⁵⁴

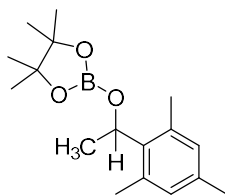


¹H NMR (400.1 MHz, C₆D₆, 300 K): δ 7.35 – 7.32 (m, 2H, Ph), 7.16 – 7.12 (m, 2H, Ph), 7.05 – 7.03 (m, 2H, Ph), 5.30 (q, 1H, J = 6.48 Hz, OCH), 1.43 (d, 3H, J = 6.32 Hz, OCCH₃), 1.01 + 1.00 (two s, 6H each, C(CH₃)₂) ppm. **¹¹B NMR (128.38 MHz, C₆D₆, 300 K):** δ 22.5 (s, O-B) ppm. **¹³C NMR (100.62 MHz, C₆D₆, 300 K):** δ 145.4 (s,

ipso C), 128.5 (s, Ar CH), 127.3 (s, Ar CH), 125.7 (s, Ar CH), 82.5 (s, C(CH₃)₂), 72.9 (s, OCH), 25.7 (s, OCH(CH₃)), 24.7 (s, CH₃), 24.6 (s, CH₃) ppm.

2,4,6-trimethyl acetophenone

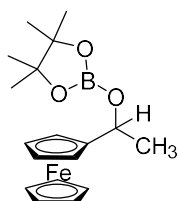
Consistent with characterisation data in the literature.⁵⁴



¹H NMR (400.1 MHz, C₆D₆, 300 K): δ 6.70 (s, 2H, Ph), 5.80 (q, 1H, J = 6.8 Hz, OCH), 2.44 (s, 6H, Ar CH₃), 2.08 (s, 3H, Ar CH₃), 1.49 (d, 3H, J = 6.8 Hz, OCCH₃), 1.00 (s, 6H, C(CH₃)₂), 0.96 (s, 6H, C(CH₃)₂) ppm. **¹¹B NMR (128.38 MHz, C₆D₆, 300 K):** δ 22.3 (s, O-B) ppm. **¹³C NMR (100.62 MHz, C₆D₆, 300 K):** δ 137.4 (s, Ar CMe), 136.1 (s, Ar CMe), 135.7 (s, Ar ipso), 130.3 (s, Ph), 82.4 (s, C(CH₃)₂), 70.2 (s, OCH₂), 25.0 (s, Bpin CH₃), 24.7 (s, Bpin CH₃), 22.0 (s, ArC-CH₃), 20.7 (s, ArC-CH₃) ppm.

Acetyl ferrocene

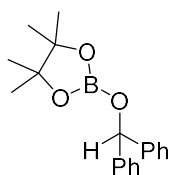
Consistent with characterisation data in the literature.⁶⁵



¹H NMR (400.1 MHz, C₆D₆, 300 K): δ 5.24 (q, 2H, J = 6.48 Hz, OCH₂), 4.32 (m, 1H, Cp H), 4.08 (m, 1H, Cp-H), 4.06 (s, 5H, Cp ring), 3.97 (t, 2H, J = 1.87 Hz, Cp-H), 1.49 (d, 3H, J = 6.28 Hz, OCCH₃), 1.10 (s, 12H, CH₃) ppm. **¹¹B NMR (128.38 MHz, C₆D₆, 300 K):** δ 22.3 (br s, O-B) ppm. **¹³C NMR (100.62 MHz, C₆D₆, 300 K):** δ 92.5 (s, ipso Cp C), 82.5 (s, C(CH₃)₂), 70.0 (s, Cp C), 69.2 (s, OCH), 67.9 (s, Cp C), 67.4 (s, Cp C), 67.5 (s, Cp C), 66.1 (s, Cp C), 24.8 (s, CH₃), 24.0 (s, OCH₃) ppm.

Benzophenone

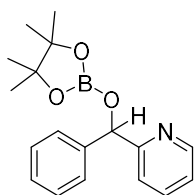
Consistent with characterisation data in the literature.⁵⁴



¹H NMR (400.1 MHz, C₆D₆, 300 K): δ 7.40 (dm, 4H, J = 8.34 Hz, Ar-H), 7.05 – 7.09 (m, 4H, Ar-H), 6.98 (tt, 2H, J = 7.32 Hz, J = 1.39 Hz, Ar-H), 6.37 (s, 1H, OCH), 0.96 (s, 12H, CH₃) ppm. **¹¹B NMR (128.38 MHz, C₆D₆, 300 K):** δ 22.8 (s, O-B) ppm. **¹³C NMR (100.62 MHz, C₆D₆, 300 K):** δ 143.9 (s, ipso-CH), 128.6 (s, Ar CH), 127.5 (s, Ar CH), 127.0 (s, Ar-H), 82.9 (s, C(CH₃)₂), 78.5 (s, OCH), 24.6 (s, CH₃) ppm.

2-benzoyl pyridine

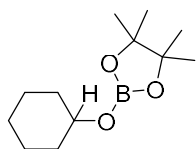
Consistent with characterisation data in the literature.⁶⁵



¹H NMR (400.1 MHz, C₆D₆, 300 K): δ 8.31 (d, 1H, J = 5.22 Hz, Py-H), 7.55 (d, 2H, J = 6.90 Hz, Ar H), 7.08 (t, 2H, J = 7.68 Hz, Ar H), 7.04 – 6.98 (m, 2H, Py-H), 6.90 (d, 1H, J = 7.68 Hz, Py-H), 6.14 (s, 1H, OCH), 1.38 (s, 12H, CH₃) ppm. **¹¹B NMR (128.38 MHz, C₆D₆, 300 K):** δ 16.3 (br s, O-B) ppm. **¹³C NMR (100.62 MHz, C₆D₆, 300 K):** δ 162.3 (s, ipso C), 143.6 (s, Ar CH), 124.9 (s, ipso C), 139.1 (s, Ar CH), 128.7 (s, Ar CH), 128.0 (s, Ar CH), 127.1 (s, Ar CH), 123.2 (s, Ar CH), 120.5 (s, Ar CH), 81.2 (s, C(CH₃)₂), 78.8 (s, OCH), 25.9 (s, CH₃) ppm.

Cyclohexanone

Consistent with characterisation data in the literature.¹⁸⁵



¹H NMR (400.1 MHz, C₆D₆, 300 K): δ 4.15 (m, 1H, J = 3.87 Hz, OCH), 1.87 – 1.83 (m, 2H Cy H), 1.62 – 1.58 (m, 2H, Cy H), 1.48 – 1.39 (m, 2H, Cy H), 1.32 – 1.26 (m, 2H, Cy H), 1.17 – 1.10 (m, 2H, Cy H), 1.07 (s, 12H, CH₃) ppm. **¹¹B NMR (128.38 MHz, C₆D₆, 300 K):** δ 22.3 (br s, O-B) ppm. **¹³C NMR (100.62 MHz, C₆D₆, 300 K):** δ 82.2 (s, C(CH₃)₂), 72.7 (s, OCH), 34.8 (s, cy CH₂), 25.8 (s, cy CH₂), 24.75 (s, CH₃), 24.11 (s, cy CH₂) ppm.

7.3: Experimental data for Chapter 3

The full data set underlying this research can be located online at <https://doi.org/10.15129/9f7efa41-0688-40ea-baf6-c5e4431a4575>. Selected crystallographic data are shown in Table 7.7.2 and full details of X-ray diffraction in .cif format are available from CCDC (1845056 and 1845057).

7.3.1: Synthesis of compounds

Synthesis of [iBu₂Al(TMP)(H)Li]₂, **10**

Prepared via a literature method.²⁰⁹

To a solution of *n*BuLi (3.13 mL; 1.6 M/hexane; 5 mmol) in hexane (20 mL) was added 2,2,6,6-tetramethylpiperidine (0.85 mL; 5 mmol) dropwise and the solution then stirred at room temperature for 1 hour. *i*Bu₂AlH (5 mL; 1 M/hexane; 5 mmol) was then added dropwise and the reaction stirred for 2 hours during which time a colourless precipitate appeared. The solids were filtered and dried under vacuum before being taken into the glove box.

¹H NMR (400.1 MHz, C₆D₆, 300 K): δ 0.38 (dd, J = 13.5 Hz, 8.2 Hz, 2H, *i*Bu CH₂); 0.55 (dd, J = 13.5 Hz, 5.6 Hz, 2H, *i*Bu CH₂); 1.15 (br. s, 4H, TMP β CH₂); 1.32 (m, 24H, *i*Bu 2xCH₃ and TMP 4xCH₃); 1.50 (br. s, 2H, γ CH₂ TMP); 2.21 (sept., 2H, *i*Bu 2xCH); 3.18 (br. s, 1H, Al – H – Li) ppm.

Synthesis of [iBu₃AlHLi]₂, **11**

To a solution of *i*Bu₂AlH (1 M/hexane; 5 mL; 5 mmol) in hexane (5 mL) was added *i*BuLi (1.7 M/heptane; 5 mmol; 2.9 mL). Spontaneous precipitation of the product was observed. The white suspension was stirred at room temperature for 1 hour, then the product isolated by filtration. (0.816 g; 3.96 mmol; 89% yield).

¹H NMR (400.1 MHz, C₆D₆, 300 K): δ -0.03 (d, J = 6.64 Hz, 6H CH₂); 1.17 (d, J = 6.69 Hz, 18H CH₃); 2.01 (sept, J = 6.92 Hz, 3H, CH) ppm. ¹³C{¹H} NMR (100.6 MHz, C₆D₆, 300 K): δ 22.9 (s, CH₂); 27.8 (s, CH); 28.7 (s, CH₃) ppm. ⁷Li NMR (155.5 MHz, C₆D₆, 300 K): δ -2.42 (s) ppm. No signal was observed in the ²⁷Al NMR spectrum.

Synthesis of $i\text{Bu}_2\text{Al}(\text{TMP})$, 12

Prepared via a literature method.¹³⁵

To a solution of 2,2,6,6-tetramethylpiperidine (3.4 mL; 20 mmol) in hexane (25 mL) was added $n\text{BuLi}$ (12.5 mL; 1.6 M/hexane; 20 mmol) dropwise and the reaction was stirred for 1 hour. $i\text{Bu}_2\text{AlCl}$ (3.8 mL; 20 mmol) was then added dropwise and the resulting white suspension stirred for 2 hours. The suspension was then filtered *via* filter stick over celite, washed with hexane (3 x 10 mL) and the solvents then removed *in vacuo* to yield the desired product as a pale yellow oil.

^1H NMR (400.1 MHz, C_6D_6 , 300 K): δ 0.26 (d, $J = 7.19$ Hz, 4H, $i\text{Bu}$ CH_2); 0.97 (d, $J = 6.53$ Hz, 12H, $i\text{Bu}$ CH_3); 1.25 (s, 12H, 4 x CH_3); 1.27 (m, 4H, TMP β CH_2); 1.69 (m, 2H, TMP γ CH_2) 1.95 (sept, $J = 6.68$ Hz, 2H, $i\text{Bu}$ CH_2) ppm.

Synthesis of $(\text{HMDS})_2\text{AlH}$, 13

Prepared via a literature method.³⁴⁰

To a cooled (-35 °C) solution of $(\text{HMDS})_2\text{Al}(\mu\text{-H})_2\text{Li}(\text{OEt})_2$ (0.42 g; 0.98 mmol) in hexane (5 mL) was added a solution of Me_3SiCl (0.12 mL; 0.98 mmol) in hexane (5 mL) dropwise. After addition a white precipitate formed. The reaction was allowed to warm to room temperature and stirred for 2 hours. The suspension was filtered, and the volume of the filtrate reduced *in vacuo*. The solution was then cooled in the freezer (-35 °C) to obtain colourless crystals of the desired compound.

^1H NMR (400.1 MHz, C_6D_6 , 300 K): δ 0.32 (s, 36H, 2xN($\text{Si}(\text{CH}_3)_2$)); 4.55 (br. s, 1H Al – H) ppm.

Synthesis of [(TMP)(Ph₂(H)CO)Al(μ-OC(H)Ph₂)₂], **15**

To a solution of *i*Bu₂Al(TMP) (0.84 g; 3 mmol) in hexane (10 mL) was added benzophenone (0.5462 g; 3 mmol) and the reaction solution turned immediately purple. The reaction was stirred at room temperature for 15 minutes during which time the colour dissipated. Subsequent standing at room temperature overnight yielded a crop of colourless crystals (0.78 g; 0.66 mmol; 45 % yield). Elemental analysis (%) for C₇₀H₈₀Al₂N₂O₄: calc'd C 78.77 H 7.55 N 2.62; found: C 78.25 H 7.58 N 2.85.

¹H NMR (400.1 MHz, C₆D₆, 300 K): δ 0.99 (t, J = 6.65 Hz, 8H, 4 x TMP β-CH₂); 1.29 (s, 24 H 4 x TMP Me); 1.44 (m, 4H, 2 x TMP γ-CH₂); 6.68 + 6.80 (s, 2 H each, 2 x OC(H)Ph₂ each); 6.93 – 6.98 (m, 12H, Ar-CH); 7.08 (t, J = 7.35 Hz, 4 H, Ar-CH); 7.20 – 7.22 (m, 4H Ar-CH); 7.29 (t, J = 7.58 Hz, 8 H, Ar-CH); 7.51 – 7.53 (m, 4 H Ar-CH); 7.88 (d, J = 7.17 Hz, 8 H Ar-CH) ppm. **¹³C{¹H} NMR (100.6 MHz, C₆D₆, 300 K):** δ 17.8 (s, TMP γ-CH₂); 35.0 (s, TMP CH₃); 39.5 (s, TMP β-CH₂); 51.7 (s, TMP C(CH₃)₂); 80.1 (s, OC(H)Ph₂); 81.0 (s, OC(H)Ph₂); 127.5 + 128.0 + 128.7 + 128.9 + 129.0 + 129.5 (s, Ar-CH); 141.1 (s, ipso Ar-C); 142.6 (s, ipso Ar-C) ppm. No signal was observed in the ²⁷Al NMR spectrum.

Synthesis of [*i*Bu₂Al(μ-N(C)Ph₂)₂], **16**

To a solution of *i*Bu₂Al(TMP) (0.84 g; 3 mmol) in hexane (10 mL) was added benzophenone imine (0.55 mL; 3 mmol). The reaction solution turned immediately bright yellow and was stirred for 1 hour. Cooling at -30 °C overnight provided yellow crystal suitable for X-ray diffraction. (0.468 g; 0.73 mmol; 24 % yield).

¹H NMR (400.1 MHz, C₆D₆, 300 K): δ 0.18 (d, J = 6.92 Hz, 8 H, CH₂); 1.01 (d, J = 6.41 Hz, 24 H, CH₃); 1.79 (nonet J = 6.65 Hz, 4 H, CH); 7.04 – 7.12 (m, 12 H, Ar-CH); 7.53 – 7.55 (m, 8 H, Ar-CH) ppm. **¹³C{¹H} NMR (100.6 MHz, C₆D₆, 300 K):** δ 25.6 (s, CH₂); 26.7 (s, CH); 28.7 (s, CH₃); 128.4 + 129.0 + 142.9 (s, Ar-CH); 142.9 (s, ipso Ar-C); 185.8 (s, C=N) ppm. No signal was observed in the ²⁷Al NMR spectrum.

Synthesis of $i\text{Bu}_3\text{AlHLi}(\text{PMDETA})$, **17**

To a solution of $i\text{Bu}_2\text{AlH}$ (2 mL; 1 M/hexane; 2 mmol) in hexane (5 mL) was added $i\text{BuLi}$ (1.18 mL; 1.7 M/hexane; 2 mmol), dropwise. The resulting white suspension was stirred at room temperature for 1 hour. Addition of PMDETA (0.42 mL; 2 mmol) yielded a slightly cloudy solution which was placed in the fridge at 5 °C. Colourless crystals of the desired product were obtained, which were suitable for X-ray diffraction (0.54 g; 1.4 mmol; 71% yield).

^1H NMR (400.1 MHz, C_6D_6 , 300 K): δ 0.39 (d; J = 6.87 Hz, 6H1, $i\text{Bu}$ CH_2); 1.44 (d, J = 6.43Hz, 18H, $i\text{Bu}$ CH_3); 1.52 – 1.61 (m, 11H, PMDETA $4\times\text{CH}_2$ and $1\times\text{CH}_3$); 1.92 (s; 6H, PMDETA CH_3); 2.37 (sept., J = 6.43 Hz, $i\text{Bu}$ CH) ppm. **$^{13}\text{C}\{^1\text{H}\}$ NMR (100.6 MHz, C_6D_6 , 300 K):** δ 29.0 (s, $i\text{Bu}$ CH_2); 29.6 (s, $i\text{Bu}$ CH); 44.4 (s, $i\text{Bu}$ CH_3); 45.5 (br. s, PMDETA CH_3); 53.1 (s, PMDETA CH_2); 56.9 (s, PMDETA CH_2) ppm. **^7Li NMR (155.5 MHz, C_6D_6 , 300 K):** δ 0.56 (s) ppm.

7.3.2: Hydroboration Catalysis

The desired catalyst **1**, **10** – **14** at the desired catalyst loading was added to 0.5 mL of a deuterated NMR solvent (C_6D_6 , or d_8 -toluene as appropriate) solution containing 0.5 mmol of the substrate precursor and of pinacolborane (80 μL , 0.55 mmol), as well as 10 mol% of internal standard; hexamethylcyclotrisiloxane. The mixture was transferred to a sealed J. Young's tap NMR tube and the reaction was regularly monitored by ^1H and ^{11}B NMR until the formation of products was completed. The yields reported are based on ^1H NMR relative to the internal standard. In all cases, the bulk of the NMR solution can be attributed to either the boronate esters or starting material. Aldehydes, ketones and imines required 5 mol% [Al] catalyst and the reactions were performed at room temperature. Acetylenes required 10 mol% [Al] catalyst and were performed in d_8 -toluene and heated to 110 °C.

Ketones:

Benzophenone

For characterisation data see Chapter 7; Section 7.2.2 Experimental for Chapter 2.

Acetophenone

For characterisation data see Chapter 7; Section 7.2.2 Experimental for Chapter 2.

Cyclohexanone

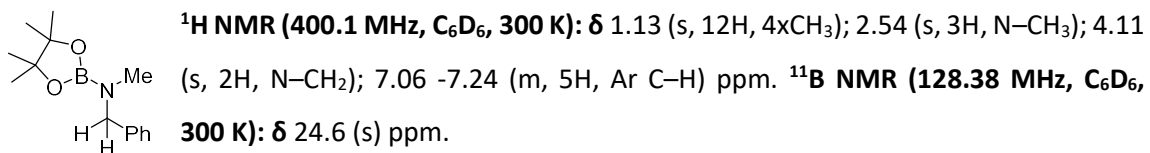
For characterisation data see Chapter 7; Section 7.2.2 Experimental for Chapter 2.

Benzaldehyde

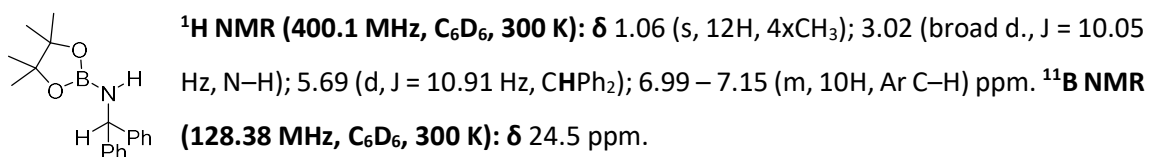
For characterisation data see Chapter 7; Section 7.2.2 Experimental for Chapter 2.

Imines:*N-Benzylidenemethylamine*

Consistent with characterisation data in the literature.¹⁷³

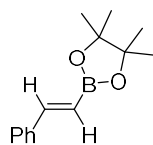
*Benzophenone imine*

Consistent with characterisation data in the literature.²⁰⁸



Alkynes:*Phenylacetylene*

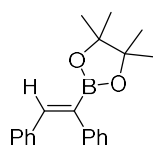
Consistent with characterisation data in the literature.¹⁷⁸



¹H NMR (400.1 MHz, C₆D₆, 300 K): δ 1.14 (s, 12H, 4xCH₃); 6.31 (d, J = 18.40 Hz, (pinB)CH=CH(Ph)); 7.00 – 7.08 (m, 3H Ar C–H); 7.27 – 7.30 (m, 2H, Ar C–H); 7.58 (d, J = 18.40 Hz, (pinB)CH=CH(Ph)) ppm. **¹¹B NMR (128.38 MHz, C₆D₆, 300 K):** δ 30.4 ppm.

Diphenylacetylene

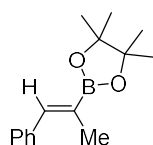
Consistent with characterisation data in the literature.¹⁷⁸



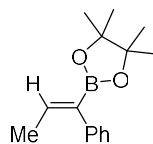
¹H NMR (400.1 MHz, C₆D₆, 300 K): Signals in ¹H NMR spectrum for product and starting materials overlap, due to low yield (10 %) of product it is not possible to assign ¹H NMR accurately. **¹¹B NMR (128.38 MHz, C₆D₆, 300 K):** δ 33.4 ppm.

1-phenyl-1-propyne

Consistent with characterisation data in the literature.³⁴¹



Major isomer: (Z)-4,4,5,5-Tetramethyl-2-(1-phenylprop-1-en-2-yl)-1,3,2-dioxaborolane [Ph(H)C=C(Me)Bpin]: **¹H NMR (400.1 MHz, C₆D₆, 300 K):** δ 1.12 (s, 12H, 4xCH₃); 2.00 (d, J = 1.6 Hz, 1H, C=C(CH₃)); 7.14 – 7.28 (m, 2H, Ar C–H); 7.29 – 7.37 (m, 3H, Ar C–H); 7.54 (d, J = 1.60 Hz, PhC(H)=C) ppm. **¹¹B NMR (128.38 MHz, C₆D₆, 300 K):** δ 30.7 ppm.



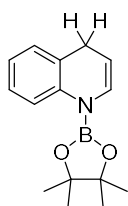
Minor isomer: (Z)-4,4,5,5-Tetramethyl-2-(1-phenylprop-1-en-1-yl)-1,3,2-dioxaborolane: [Ph(pinB)C=C(H)Me] Diagnostic signals: **¹H NMR (400.1 MHz, C₆D₆,**

300 K): δ 1.06 (s, 12H, 4xCH₃); 1.70 (br. s, 3H, CH₃); 6.89 – 6.96 (m, 1H, C=C(H)Me) ppm. **¹¹B NMR (128.38 MHz, C₆D₆, 300 K):** δ 33.9 ppm.

Pyridines:

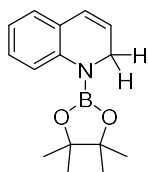
Quinoline

Overlapping signals in the aromatic region arising from 1,2-product, 1,4-product and starting material precluded a full assignment; however diagnostic signals are reported consistent with the literature which confirm the presence of both 1,2- and 1,4-dihydroquinoline products.^{53,342}



N-(Bpin)-1,4-dihydroquinoline

Diagnostic signals: **¹H NMR (400.1 MHz, d₈-toluene, 300 K):** δ 1.02 (s, 12H, 4xCH₃); 3.31 (s, 2H, CH₂); 4.81 (dt, J = 8.07 Hz, 4.07 Hz, 1H, CH); 8.10 (d, J = 8.42 Hz, 1H, CH) ppm. **¹¹B NMR (128.38 MHz, d₈-toluene, 300 K):** δ 24 ppm.



N-(Bpin)-1,2-dihydroquinoline

Diagnostic signals: **¹H NMR (400.1 MHz, d₈-toluene, 300 K):** δ 1.03 (s, 12H, 4xCH₃); 4.14 (dd, J = 4.26 Hz, 1.75 Hz, 2H, CH₂); 5.57 (dt, J = 9.52 Hz, 4.17 Hz, 1H, CH); 6.24 (dt, J = 9.66 Hz, 1.81 Hz, 1H, CH); 7.78 (d, J = 8.13 Hz, 1H, CH) ppm. **¹¹B NMR (128.38 MHz, d₈-toluene, 300 K):** δ 33 ppm.

7.4: Experimental data for Chapter 4

Selected crystallographic data are shown in Table 7.7.3.

7.4.1: Synthesis of compounds

Synthesis of $i\text{Bu}_2\text{Al}(\text{HMDS})$, **18**

To a solution of HMDS(H) (2.13 mL; 10 mmol) in hexane (10 mL) was added $n\text{BuLi}$ (6.40 mL; 1.6 M; 10 mmol) dropwise. The resulting clear solution was stirred at room temperature for 1 hour. Then, $i\text{Bu}_2\text{AlCl}$ (2 mL; 10 mmol) was added dropwise at room temperature which formed a white precipitate. The suspension was stirred at room temperature for 1 hour and then filtered over celite and glass wool using a filter stick, washed with hexane (3 x 5 mL) and then the solvents removed *in vacuo* to yield the desired product as a colourless oil (2.06 g; 6.83 mmol; 68% yield).

$^1\text{H NMR}$ (400.1 MHz, C_6D_6 , 300 K): δ 0.19 (s, 18H, $2x\text{SiMe}_3$); 0.37 (d, $J = 7.03$ Hz, 6H, $i\text{Bu CH}_2$); 1.06 (d, $J = 6.67$ Hz, 12H, $i\text{Bu CH}_3$); 2.01 (sept., $J = 6.72$ Hz, 2H, $i\text{Bu CH}$) ppm. $^{13}\text{C NMR}$ (151 MHz, C_6D_6 , 300 K): δ 4.1 (s, SiMe_3); 26.0 (s, $i\text{Bu CH}_2$); 27.3 (br. s, $i\text{Bu CH}$); 28.2 (s, $i\text{Bu CH}_3$) ppm.

Synthesis of $i\text{Bu}_2\text{Al}(\{\text{OC}(\text{CH}_3)_2\text{C}(\text{CH}_3)_2\text{O}\}_2)\text{B}(\text{H})\text{TMP}$, **19**

To a solution of $i\text{Bu}_2\text{Al}(\text{TMP})$ (0.90 g; 3 mmol) in benzene (3 mL) at room temperature was added HBpin (0.44 mL; 3 mmol) dropwise without stirring. The reaction was left to stand at room temperature overnight after which colourless crystals of the product suitable for X-ray crystallography had formed. (Yield 1.29 g; 1.56 mmol; 56%).

$^1\text{H NMR}$ (400.1 MHz, C_6D_6 , 300 K): δ 0.47 (d, $J = 6.66$ Hz, 4H, $i\text{Bu CH}_2$); 1.18 (d, $J = 6.53$ Hz, 12H, $i\text{Bu CH}_3$); 1.39 (s, 12H, TMP CH_3); 1.39 – 1.47 (m, 6H, TMP CH_2); 1.65 (s, 6H, $\text{C}(\text{CH}_3)_2$); 1.84 (s, 6H, $\text{C}(\text{CH}_3)_2$); 2.14 (sept., $J = 6.55$ Hz, 2H, $i\text{Bu CH}$); 4.75 (br. s, 1H B – H) ppm. $^1\text{H}\{^{11}\text{B}\}$ NMR (400.1 MHz, C_6D_6 , 300 K): δ 4.75 (s, 1H, B – H) ppm. $^{13}\text{C NMR}$ (151 MHz, C_6D_6 , 300 K): δ 25.9 (s, $i\text{Bu CH}_2$); 26.3 (s, $\text{C}(\text{CH}_3)_2$); 27.2 (s, $i\text{Bu CH}$); 28.9 (s, $i\text{Bu CH}_3$); 33.8 (s, TMP CH_3); 40.7 (s, TMP CH_2); 53.4 (s, TMP

$\text{C}(\text{CH}_3)_2$; 79.5 (s, $\text{C}(\text{CH}_3)_2$); 84.7 (s, $\text{C}(\text{CH}_3)_2$) ppm. ^{11}B NMR (128.38 MHz, C_6D_6 , 300 K): δ 30.0 (br. s) ppm. ^{27}Al NMR: No signal was observed.

Synthesis of $i\text{Bu}_2\text{Al}(\{\text{OC}(\text{CH}_3)_2\text{C}(\text{CH}_3)_2\text{O}\}_2)\text{B}(\text{H})\text{HMDS}$, 20

To a solution of $i\text{Bu}_2\text{Al}(\text{HMDS})$ (0.90 g; 3 mmol) in hexane (3 mL) at room temperature was added HBpin (0.44 mL; 3 mmol) dropwise. The reaction was allowed to stir for 2 hours at room temperature and then cooled to $-25\text{ }^\circ\text{C}$ overnight. Left to stand at room temperature overnight after which colourless crystals of the product suitable for X-ray crystallography had formed. (Yield 1.29 g; 1.56 mmol; 56%).

^1H NMR (400.1 MHz, C_6D_6 , 300 K): δ 0.28 (s, 18H, HMDS CH_3); 0.43 (d, $J = 6.64$ Hz, 4H, $i\text{Bu}$ CH_2); 1.15 (d, $J = 6.37$ Hz, 12 H, $i\text{Bu}$ CH_3); 1.61 (s, 6H, $\text{C}(\text{CH}_3)_2$); 1.79 (s, 6H, $\text{C}(\text{CH}_3)_2$); 2.10 (sept., $J = 6.41$ Hz, 2H, $i\text{Bu}$ CH); 4.80 (br. s, 1H, B – H) ppm. $^1\text{H}\{^{11}\text{B}\}$ NMR (400.1 MHz, C_6D_6 , 300 K): δ 4.80 (s, 1H, B – H) ppm. ^{13}C NMR (151 MHz, C_6D_6 , 300 K): δ 4.0 (s, HMDS CH_3); 25.6 (s, $\text{C}(\text{CH}_3)_2$); 26.1 (s, $i\text{Bu}$ CH_2); 26.3 (s, $\text{C}(\text{CH}_3)_2$); 27.1 (s, $i\text{Bu}$ CH); 28.8 (s, $i\text{Bu}$ CH_3); 80.0 (s, $\text{C}(\text{CH}_3)_2$); 84.3 (s, $\text{C}(\text{CH}_3)_2$) ppm. ^{11}B NMR (128.38 MHz, C_6D_6 , 300 K): δ 31.8 (br. s) ppm. ^{27}Al NMR: No signal was observed.

Reaction of $[i\text{Bu}_2\text{Al}(\text{TMP})(\text{H})\text{Li}]_2$ with HBpin, product, 21

In a J. Young's NMR tube, $[i\text{Bu}_2\text{Al}(\text{TMP})(\text{H})\text{Li}]_2$ (0.0362 g; 0.125 mmol) was dissolved in C_6D_6 (0.5 mL) and HBpin (0.02 mL; 0.125 mmol) was added.

^1H NMR (400.1 MHz, C_6D_6 , 300 K): δ 0.21 (br. d, $J = 6.90$ Hz, 4H, $i\text{Bu}$ CH_2); 1.21 (br. s, 12H, $i\text{Bu}_3$ CH_3); 1.29 (s, 12H, pin CH_3); 2.18 (sept., $J = 6.70$ Hz, 2H, $i\text{Bu}$ CH), 5.07 (br. q, $J = 126$ Hz, BH_2) ppm. ^{11}B NMR (128.38 MHz, C_6D_6 , 300 K): δ 37 (t, $J = 126.04$ Hz) ppm. ^7Li NMR (155.5 MHz, C_6D_6 , 300 K): δ 0.59 (s) ppm.

Reaction of $[i\text{Bu}_2\text{Al}(\text{TMP})(\text{H})\text{Li}]_2$ with HBcat

In a J. Young's NMR tube, $[i\text{Bu}_2\text{Al}(\text{TMP})(\text{H})\text{Li}]_2$ (0.072 g; 0.25 mmol) was dissolved in C_6D_6 (0.5 mL) and HBcat (0.033 g; 0.25 mmol) was added.

^1H NMR (400.1 MHz, C_6D_6 , 300 K): δ no obvious diagnostic signals. **^{11}B NMR (128.38 MHz, C_6D_6 , 300 K):** δ 37 (t, $J = 126.69$ Hz) ppm. **$^{11}\text{B}\{^1\text{H}\}$ NMR (128.38 MHz, C_6D_6 , 300 K):** δ 37 (s) ppm.

7.4.2: Hydroboration Catalysis

The desired catalyst at the desired catalyst loading was added to 0.5 mL of a deuterated NMR solvent (C_6D_6) solution containing 0.5 mmol of the substrate precursor and of pinacolborane (80 μL , 0.55 mmol), as well as 10 mol% of internal standard; hexamethylcyclotrisiloxane. The mixture was transferred to a sealed J. Young's tap NMR tube and the reaction was regularly monitored by ^1H and ^{11}B NMR until the formation of products was completed. The yields reported are based on ^1H NMR relative to the internal standard. In all cases, the bulk of the NMR solution can be attributed to either the boronate esters or starting material.

Ketones:*Benzophenone*

For characterisation data see Chapter 7; Section 7.2.2 Experimental for Chapter 2.

7.5: Experimental data for Chapter 5

Selected crystallographic data are shown in Table 7.7.4.

7.5.1: Synthesis of compounds

Synthesis of $i\text{Bu}_3\text{AlPPh}_2\text{Li}(\text{THF})_3$, **22**

Method a): To a stirred solution of $[i\text{Bu}_3\text{AlHLi}]_2$ (0.412 g; 1 mmol) in hexane (10 mL) was added HPPH_2 (0.34 mL; 2 mmol) and the reaction stirred 1 hour. THF (0.5 mL; 6 mmol) was added then the volatiles were removed. The residue was taken up in hexane (5 mL) and toluene (1 mL). Subsequent cooling to $-30\text{ }^\circ\text{C}$ yielded the desired product as pale-yellow crystals. Crystalline yield 0.494 g; 0.82 mmol; 41 %.

Method b): To a stirred solution of HPPH_2 (0.17 mL; 1 mmol) in hexane (5 mL) was added dropwise $n\text{BuLi}$ (0.63 mL; 1.6 M/hexane; 1 mmol) and the resulting bright yellow suspension stirred for 1 hour. Addition of $i\text{Bu}_3\text{Al}$ (1 mL; 1 M/hexane; 1 mmol) generated a clear pale-yellow solution, which was stirred for 1 h. THF (0.3 mL; 3 mmol) was added and the pale-yellow solution cooled at $-30\text{ }^\circ\text{C}$ overnight. Crystalline yield 0.150 g; 0.25 mmol; 24%.

^1H NMR (400.1 MHz, d_8 -toluene, 300 K): δ 0.48 (d of d, $J = 6.93\text{ Hz}, 2.88\text{ Hz}$, 6H, $i\text{Bu CH}_2$); 1.31 (d, $J = 6.29\text{ Hz}$, 18H, $i\text{Bu CH}_3$); 1.41 (m, 12H, THF CH_2); 2.26 (m, 3H, $i\text{Bu CH}$); 3.44 (m, 12H, THF CH_2); 7.00 (m, 2H [overlapping solvent], Ph); 7.17 (m, 4H [overlapping solvent], Ph); 7.14 (m, 4H, Ph) ppm. **^{31}P NMR (104.2 MHz, d_8 -toluene, 300 K):** δ -49.2 ppm. **$^{13}\text{C}\{^1\text{H}\}$ NMR (151 MHz, d_8 -toluene, 300 K):** δ 25.4 (THF CH_2); 25.5 + 25.6 ($i\text{Bu CH}_2$); 28.3 ($i\text{Bu CH}$); 29.5 ($i\text{Bu CH}_3$); 68.6 (THF CH_2); 124.9 (Ar C–H); 127.3 (d, $J = 6.17\text{ Hz}$, Ar C–H); 134.0 (d, $J = 13.04\text{ Hz}$, Ar C–H); 144.1 (d, $J = 13.08\text{ Hz}$, ipso Ar) ppm. **^7Li NMR (155.5 MHz, d_8 -toluene, 300 K):** δ 0.21 (s) ppm. **^{27}Al NMR:** no signal was observed. Elemental analysis failed after multiple attempts due to decomposition during transportation.

Synthesis of LiPPh₂, 23

To a solution of *n*BuLi (0.63 mL; 1.6 M/hexane; 1 mmol) in hexane (5 mL) was added HPPH₂ (0.17 mL; 1 mmol), dropwise at room temperature. The resulting yellow solution was allowed to stir for two hours, and then the mixture allowed to stand at room temperature overnight. The colourless supernatant was removed *via* syringe and the solids washed with hexane (5 mL), and then removed *via* syringe. The yellow solids were dried *in vacuo* and stored in the glove box.

¹H NMR (400.1 MHz, C₆D₆, 300 K): δ 6.87 (br. m, 6H, Ar C-H); 7.32 (br. m, 4H, Ar C-H) ppm.

³¹P NMR (104.2 MHz, C₆D₆, 300 K): δ -52.2 (s) ppm. ⁷Li NMR (155.5 MHz, C₆D₆, 300 K): δ 1.45 (s) ppm.

Synthesis of [iBu₂AlPPh₂]₂, 25

Prepared via a literature method.³⁰⁸

To a solution of *i*Bu₂AlH (2 mL; 1 M/hexane; 2 mmol) in hexane (5 mL) was added HPPH₂ (0.35 mL; 2 mmol) dropwise at room temperature. The reaction was then heated to reflux for 10 hours, and then the reaction was cooled to room temperature. A small amount of solvent was removed *in vacuo* and the Schlenk flask then put in the freezer (-15 °C) upon which colourless crystals were obtained.

¹H NMR (400.1 MHz, C₆D₆, 300 K): δ 0.71 (d, J = 7.28 Hz, 4H, CH₂); 1.02 (d, J = 6.64 Hz, 12H CH₃); 1.96 (sept. J = 6.64 Hz, 2H, CH); 6.95 – 7.03 (m, 6H, Ar C – H); 7.53 – 7.58 (m, 4H, Ar C – H) ppm.

³¹P NMR (104.2 MHz, C₆D₆, 300 K): δ -31.0 ppm.

Synthesis of iBu₃AlPPh₂Li(12-crown-4), 26

To a solution of *n*BuLi (0.63 mL; 1.6M/hexane; 1 mmol) in hexane (5 mL) was added HPPH₂ (0.17 mL; 1 mmol) dropwise at room temperature and the resulting yellow suspension stirred for 1 hour. *i*BuAl₃ (1 mL; 1 M/hexane; 1 mmol) was then added dropwise forming a clear solution, which was stirred for 30 minutes. 12-crown-4 (0.16 mL; 1 mmol) was added which formed a pale

yellow suspension. Solvents were removed *in vacuo* and toluene (4 mL) was added. Gentle heating generated a pale yellow solution. Upon slow cooling a crop of colourless crystals suitable for X-ray diffraction was obtained. (Yield 0.218g; 0.38 mmol; 38 %).

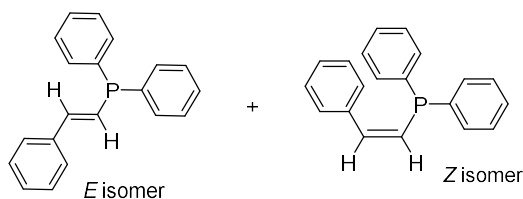
¹H NMR (400.1 MHz, C₆D₆, 300 K): δ 0.59 (dd, J = 6.77 Hz + 2.88 Hz, 6H, *i*Bu CH₂); 1.39 (d, J = 6.46 Hz, 18H, *i*Bu CH₃); 2.40 (sept., J = 6.51 Hz, 3H, *i*Bu CH); 2.87 (br. s., 28H, 12-crown-4 CH₂); 7.01 – 7.08 (m, 2H, Ar CH); 7.24 (br. t, J = 7.49 Hz, 4H, Ar CH); 7.90 (br. t, J = 7.25 Hz, 4H, Ar CH) ppm. **³¹P NMR (104.2 MHz, C₆D₆, 300 K):** δ -48.4 (s) ppm. **¹³C{¹H} NMR (151 MHz, C₆D₆, 300 K):** δ 28.4 (br. s, *i*Bu CH₂); 28.5 (s, *i*Bu CH); 29.8 (s, *i*Bu CH₃); 66.3 (s, 12-crown-4 CH₂); 124.7 (s, Ar CH); 127.7 (d, J = 6.69 Hz, Ar CH); 134.3 (d, J = 12.84 Hz, Ar CH); 144.7 (d, J = 12.57 Hz, ipso C) ppm. **⁷Li NMR (155.5 MHz, C₆D₆, 300 K):** δ -0.10 (br. s) ppm. **²⁷Al NMR:** no signal was observed.

7.5.2: Hydrophosphination Catalysis

The desired catalyst loading was added to 0.5 mL of d₈-toluene solution (unless alternative solvent specified) containing the substrate precursor (0.6 mmol) and HPPH₂ (0.5 mmol, 0.09 mL). The reaction mixture was transferred to a sealed J. Young's tap NMR tube and the reaction was regularly monitored by ¹H and ³¹P until the formation of the products was completed as determined by integration versus an internal capillary standard (hexamethylcyclotrisiloxane). The yields reported are based on ¹H NMR and ³¹P relative to the internal standard. In all cases, the bulk of the NMR solution can be attributed to either product compounds or starting materials. For **alkynes** and **alkenes**, the hydrophosphination catalysis was performed at 110 °C with 10 mol% [Al] catalyst loading. For **carbodiimides** the hydrophosphination catalysis was performed at room temperature with 5 mol% [Al] catalyst loading. Isolated yields are provided for example substrates, isolated *via* either recrystallization methods or column chromatography (EtOAc:hexane 1:19).

Alkynes:*Phenylacetylene*

Consistent with characterisation data in the literature.²⁸⁶



The product was obtained as an intractable mixture of *E*- and *Z*-isomers via column chromatography. Isolated yield 0.112 g; 0.39 mmol; 78 %. Trace amounts of HPPH_2 and phosphine oxides were detected by NMR spectroscopy.

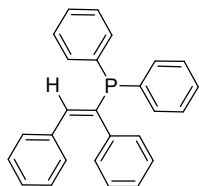
***E*-isomer:** ^1H NMR (600 MHz, CDCl_3 , 300 K): δ 6.95 (d, $J = 10.80$ Hz, 1H, *E*-isomer C(H)-PPh_2); 7.22 – 7.40 (m, 10H, Ar C–H); 7.4 – 7.58 (m, 6H, Ar C–H) ppm.

***Z*-isomer:** ^1H NMR (600 MHz, CDCl_3 , 300 K): δ 6.46 (dd, $J = 2.83$ Hz, 12.73 Hz, 1H, *Z*-isomer C(H)-PPh_2); 7.22 – 7.40 (m, 10H, Ar C–H); 7.4 – 7.58 (m, 6H, Ar C–H) ppm.

^{31}P NMR (243 MHz, CDCl_3 , 300 K): δ – 11.5 (*E*-isomer); – 24.7 (*Z*-isomer) ppm. **^{13}C NMR (151 MHz, CDCl_3 , 300 K):** δ 119.3 (d, $J = 103.7$ Hz, Ar C–H); 126.9 (s, Ar C–H); 128.1 (s, Ar C–H); 128.5 (s, Ar C–H); 128.6 (d, $J = 5.40$ Hz, Ar C–H); 129.5 (d, $J = 13.54$ Hz *E*-isomer CH=C(H)P); 129.6 (d, $J = 8.3$ Hz, *Z*-isomer CH=C(H)P); 132.7 (d, $J = 18.79$ Hz, Ar C–H); 133.1 (d, $J = 19.34$ Hz, Ar C–H); 134.0 (d, $J = 17.68$ Hz, Ar C–H); 137.0 (d, $J = 2.33$ Hz, quat. C); 138.2 (d, $J = 9.61$ Hz, quat. C); 139.3 (d, $J = 9.61$ Hz, quat. C); 143.8 (d, $J = 31.26$ Hz, *E*-isomer C(H)=C(H)P); 144.1 (d, $J = 18.90$ Hz, *Z*-isomer C(H)=C(H)P) ppm. **m/z (GCMS EI):** 287.1 $[\text{M} - \text{H}]^+$.

Diphenylacetylene

Consistent with characterisation data in the literature.²⁸⁶



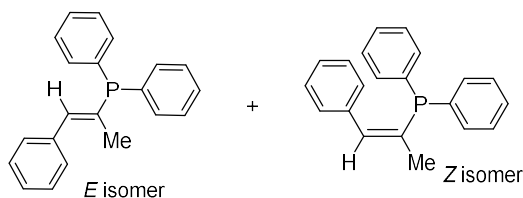
The product was isolated by filtering over a plug of silica and recrystallising from pentane. Isolated crystalline yield 0.146 g; 0.4 mmol; 80 %.

^1H NMR (400 MHz, CDCl_3 , 300 K): δ 6.54 (d, J = 9.29 Hz, 1H, C=C(H)); 6.93 – 6.95 (m, 2H, Ar); 7.09 – 7.10 (m, 3H, Ar); 7.16 – 7.19 (m, 5H, Ar); 7.33 – 7.36 (m, 6H, Ar); 7.46 – 7.50 (m, 4H, Ar) ppm.
 ^{31}P NMR (162.0 MHz, CDCl_3 , 300 K): δ 8.46 (s) ppm.

^{13}C NMR (100 MHz, CDCl_3 , 300 K): δ 127.1 (s, Ar C–H); 127.4 (s, Ar C–H); 128.1 (s, Ar C–H); 128.5 (s, Ar C–H); 128.6 (s, Ar C–H); 129.0 (s, Ar C–H); 129.2 (d, J = 6.17 Hz, Ar C–H); 129.4 (s, Ar C–H); 134.3 (s, J = 20.13 Hz, Ar C–H); 135.5 (d, J = 12.57 Hz, quat. C); 137.0 (d, J = 6.77 Hz, quat. C); 138.1 (d, J = 18.86 Hz, C(H)=C); 140.1 (d, J = 17.02 Hz, quat. C); 141.5 (d, J = 18.91 Hz, quat. C) ppm. **m/z (GCMS EI):** 363.3 [M - H]⁺.

1-phenyl-1-propyne

Consistent with characterisation data in the literature.²⁸⁶

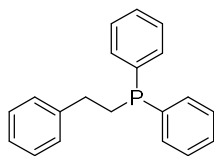


The product was isolated as a mixture of *E*- and *Z*-isomers by column chromatography. Isolated yield 0.119 g; 0.39 mmol; 79 %.

^1H NMR (600 MHz, CDCl_3 , 300 K): δ 1.69 (dd, J = 1.46 Hz, 2.82 Hz, 3H, CH_3 *E*-isomer); 1.90 (dd, J = 1.32 Hz, 9.01 Hz, 3H, CH_3 *Z*-isomer); 6.60 (d, J = 13.36 Hz, 1H C(H)=C *Z*-isomer); 7.10 – 7.12 (td, J = 1.87 Hz, 9.01 Hz, 2H, Ar H); 7.16 – 7.26 (m, 19H, Ar H); 7.28 – 7.31 (m, 4H, Ar H); 7.34 – 7.36 (td, J = 1.75 Hz, 7.73 Hz, 4H, Ar H) ppm. **^1H COSY** correlation assigns C(H)=C *E*-isomer resonance at 7.26 ppm. **^{31}P NMR (243 MHz, CDCl_3 , 300 K):** δ 8.4 (s, *Z*-isomer); -13.2 (s, *E*-isomer) ppm. **^{13}C NMR (151 MHz, CDCl_3 , 300 K):** δ 18.0 (d, J = 17.15 Hz, CH_3 *Z*-isomer); 24.5 (d, J = 3.71 Hz, CH_3 *E*-isomer); 127.1 (s, Ar CH); 127.4 (s, Ar C–H); 127.9 (s, Ar C–H); 128.3 (d, J = 14.27 Hz, Ar C–H); 128.5 (d, J = 6.39 Hz, Ar C–H); 128.6 (d, J = 6.09 Hz, Ar C–H); 128.9 (s, Ar C–H); 129.1 (s, Ar C–H); 129.5 (d, J = 7.30 Hz, Ar C–H); 133.3 (d, J = 18.86 Hz, Ar C–H); 133.9 (d, J = 18.86 Hz, Ar C–H); 136.1 (d, J = 14.20 Hz, quat. C); 136.3 (d, J = 12.07 Hz; quat. C); 137.0 (d, J = 12.36 Hz, quat. C); 137.5 (d, J = 6.54 Hz, quat. C); 137.8 (d, J = 12.18 Hz, quat. C); 139.1 (d, J = 28.39 Hz, C(H)=C *Z*-isomer); 143.4 (d, J = 29.07 Hz, C(H)=C *E*-isomer) ppm. **m/z (GCMS EI):** 301.1 [M - H]⁺

Alkenes:*Styrene*

Consistent with characterisation data in the literature.²⁸⁶

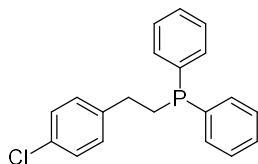


The product was isolated column chromatography. Isolated yield 0.082 g; 0.3 mmol; 60 %

¹H NMR (600 MHz, CDCl₃, 300 K): δ 2.32 – 2.35 (m, 2H, CH₂-PPh₂); 2.68 – 2.72 (m, 2H, Ph-CH₂); 7.12 – 7.15 (m, 3H, Ar C-H); 7.21 – 7.24 (m, 2H, Ar C-H); 7.27 – 7.30 (m, 6H, Ar C-H); 7.41 – 7.44 (m, 4H Ar C-H) ppm. **³¹P NMR (243 MHz, CDCl₃, 300 K):** δ -15.7 ppm. **¹³C NMR (151 MHz, CDCl₃, 300 K):** δ 30.3 (d; J = 13.08 Hz, CH₂-PPh₂); 32.2 (d; J = 17.31 Hz, Ph-CH₂); 126.1 (s, Ar C-H); 128.2 (s, Ar C-H); 128.5 (s, Ar C-H); 128.6 (s, Ar C-H); 128.7 (s, Ar C-H); 132.8 (d, J = 17.51 Hz, Ar C-H); 138.6 (d, J = 13.37 Hz, ipso P-C(Ar)); 142.6 (d, J = 13.54 Hz, ipso Ph) ppm. **m/z (GCMS EI):** 289.1 [M - H]⁺

4-fluoro styrene

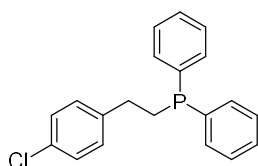
Consistent with characterisation data in the literature.²⁸⁰



¹H NMR (400 MHz, d₈-toluene, 300 K): δ 2.13 – 2.17 (m, 2H, Ph₂PCH₂CH₂); 2.52 – 2.58 (m, 2H, Ph₂PCH₂CH₂); 6.75 -6.76 (m, 5H, Ar C-H); 7.09 – 7.14 (m, 5H, Ar C-H); 7.36 – 7.40 (m, 4H, Ar C-H) ppm. **³¹P NMR (162.0 MHz, d₈-toluene, 300 K):** δ -16.2 ppm. **¹⁹F NMR (376 MHz, d₈-toluene, 300 K):** δ -117.1 ppm.

4-chloro styrene

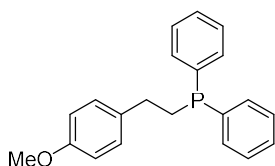
Consistent with characterisation data in the literature.²⁸⁰



¹H NMR (400 MHz, d₈-toluene, 300K): δ 2.13 – 2.17 (m, 2H, Ph₂PCH₂CH₂); 2.50 -2.56 (m, 2H, Ph₂PCH₂CH₂); 6.71 – 6.73 (m, 2H, Ar C–H); 7.05 -7.14 (m, 8H, Ar C–H); 7.37 – 7.41 (m, 4H, Ar C–H) ppm. **³¹P NMR (162.0 MHz, d₈-toluene, 300K):** δ -16.1 ppm.

4-vinyl anisole

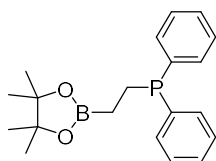
Consistent with characterisation data in the literature.²⁸⁰



¹H NMR (400 MHz, d₈-toluene, 300 K): δ 2.26 – 2.30 (m, 2H, Ph₂PCH₂CH₂); 2.65 – 2.71 (m, 2H, Ph₂PCH₂CH₂); 6.73 -6.76 (m, 2H, Ar C–H); 7.10 -7.16 (m, 6H, Ar C–H); 7.41 – 7.45 (m, 4H, Ar C–H) ppm. **³¹P NMR (162.0 MHz, d₈-toluene, 300 K):** δ -16.0 ppm.

Vinyl boronic acid pinacol ester

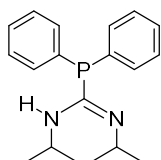
Consistent with characterisation data in the literature.³⁰⁶



¹H NMR (400 MHz, d₈-toluene, 300 K): δ 1.07 (s, 12H, 4xCH₃); 2.19 -2.23 (m, 2H, Ph₂PCH₂CH₂); 3.54 – 3.57 (m, 2H, Ph₂PCH₂CH₂); 7.04 -7.07 (m, 6H, Ar C–H); 7.36 -7.40 (m, 4H, Ar C–H) ppm. **³¹P NMR (162.0 MHz, d₈-toluene, 300 K):** δ -10.3 ppm. **¹¹B NMR (128.0 MHz, d₈-toluene, 300 K):** δ 33.7 ppm.

Carbodiimides:*Diisopropyl carbodiimide*

Consistent with characterisation data in the literature.²⁹⁷

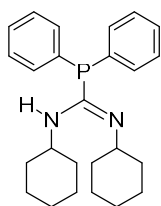


The product was isolated *via* recrystallising from hexane solution. Isolated crystalline yield 0.123 g; 0.4 mmol; 80 %

¹H NMR (400 MHz, C₆D₆, 300 K): δ 0.96 (d, J = 6.51 Hz, 6H, CH(CH₃)₂); 1.27 (d, J = 6.10 Hz, 6H, CH(CH₃)₂); 3.66 (br d, J = 6.75 Hz, 1H, N–H); 4.32 (hept., J = 6.44, 1H, CH(CH₃)₂); 4.42 (hept., J = 6.17 Hz, CH(CH₃)₂); 7.00 – 7.07 (m, 6H, Ar C–H); 7.47 (td, J = 1.65 Hz, 7.67 Hz, 4H, Ar C–H) ppm. **³¹P NMR (162.0 MHz, C₆D₆, 300 K):** δ – 18.7 ppm. **¹³C NMR (100 MHz, C₆D₆, 300 K):** δ 22.5 (s, CH(CH₃)₂); 25.4 (s, CH(CH₃)₂); 43.0 (s, CH(CH₃)₂); 52.2 (d, J = 35.23 Hz, CH(CH₃)₂); 129.1 (d, J = 7.40 Hz, Ar C–H); 129.4 (s, Ar C–H); 134.4 (d, J = 19.52 Hz, Ar C–H); 135.6 (d, J = 13.94 Hz, ipso C); 152.4 (d, J = 32.20 Hz, N=C(PPh₂)–N) ppm.

Dicyclohexyl carbodiimide

Consistent with characterisation data in the literature.²⁹⁷



¹H NMR (400 MHz, d₈-toluene, 300 K): δ 0.93 – 1.91 (m, 20H, Cy CH₂); 3.77 (s, 1H, N–H); 4.04 (d, J = 26.37 Hz, Cy C–H) ppm. **³¹P NMR (162.0 MHz, d₈-toluene, 300 K):** δ -18.4 ppm.

7.5.3: Donor screening reactions

To a solution of [*i*Bu₃AlHLi]₂, **11**, (0.05 mmol), diphenylacetylene (0.6 mmol) and HPPH₂ (0.5 mmol) in d₈-toluene (0.5 mL) was added the desired amount of Lewis donor ligand, and the

reaction mixture loaded into a sealed J Young's NMR tube. The reaction was heated to 110 °C and monitored regularly by ^1H and ^{31}P NMR spectroscopies.

7.5.4: Kinetic Isotope Effect (KIE) measurement

$i\text{Bu}_3\text{AlPPh}_2\text{Li}(\text{THF})_3$ (10 mol%, 0.05 mmol, 0.0302 g) was added to 0.5 mL of d_8 -toluene **or** d_0 -toluene solution containing diphenyl acetylene (0.6 mmol; 0.1069 g) and HPPH_2 **or** DPPH_2 (0.5 mmol, 0.09 mL), as appropriate. This mixture was transferred to a sealed J. Young's tap NMR tube, heated to 373 K, and monitored by ^{31}P NMR spectroscopy every 120 seconds. Spectra were Fourier transformed, phased, and base line corrected using Bruker Topspin software (version 3.57). The reaction rates were determined by monitoring the consumption of diphenyl phosphine and the formation of the vinyl phosphine product(s) over more than three half-lives. Reaction rate constants were derived from the plot of $\ln[\text{diphenyl phosphine}]$ vs time by using linear trend lines generated by Microsoft Excel software.

Rates for HPPH_2 and DPPH_2 used for the calculation of KIE are the average of two runs.

HPPH_2 : average reaction rate $(7.2 \pm 0.4) \times 10^{-4} \text{ s}^{-1}$

DPPH_2 : average reaction rate $(5.2 \pm 0.4) \times 10^{-4} \text{ s}^{-1}$

$$\text{KIE} = \frac{k_{\text{H}}}{k_{\text{D}}} = \frac{7.2 \times 10^{-4}}{5.2 \times 10^{-4}} = 1.38 \pm 0.13$$

Synthesis of DPPH_2

Prepared via a literature method.³⁴³

To a cooled (0 °C) solution of diphenyl phosphine (0.85 mL; 5 mmol) in THF (5 mL) was added $n\text{BuLi}$ (3.44 mL; 1.6 M; 5.5 mmol) dropwise. The reaction was warmed to room temperature and stirred for 1 hour. Degassed D_2O (0.2 mL; from a single use ampoule and degassed *via* freeze-pump-thaw method) was then added and the reaction stirred vigorously for 10 minutes. After this time anhydrous MgSO_4 was added and the solution then filtered *via* cannula. Solvent

was removed *in vacuo* to yield the product as a colourless oil. Resulting in 90% deuterium incorporation.

^1H NMR (400 MHz, d_8 -toluene, 300 K): δ 7.03 – 7.05 (m, 6H, Ar C – H); 7.33 – 7.37 (m, 4H, Ar C – H) ppm. ^{31}P NMR (162.0 MHz, d_8 -toluene, 300 K): δ -42 (t, J = 33.25 Hz) ppm.

7.5.5: Reaction kinetics study

A reaction mixture of the desired concentrations of diphenylacetylene, diphenyl phosphine and catalyst (**22**), with a total volume of 0.5 mL in d_8 -toluene were transferred to a sealed J. Young's tap NMR tube, heated to 373 K, and monitored by ^{31}P NMR spectroscopy every 120 seconds. Spectra were Fourier transformed, phased, and base line corrected using Bruker Topspin software (version 3.57). The reaction rates were determined by monitoring the consumption of diphenyl phosphine and the formation of the vinyl phosphine product(s) over than three half-lives. Reaction rate constants were derived from the plot of $\ln[\text{HPPH}_2]$ versus time by using linear trend lines generated by Microsoft Excel software.

7.5.6: Computational calculations

The DFT calculations carried out in Chapter 4 were performed by collaborators Professor Tell Tuttle and PhD student Allan Young and ran on the whole system. Calculations were performed at the B3LYP-D3/³⁰⁹⁻³¹⁵6-311G(d,p)³¹⁶⁻³¹⁸ level of theory and employed a continuum solvent with the dielectric constant of toluene within the IEFPCM model.³¹⁹ Computational results were obtained using the EPSRC-funded ARCHIE-WeST High Performance Computer (www.archie-west.ac.uk), using Gaussian software. The optimised molecular geometries obtained are presented in Figure 7.1 – Figure 7.4.

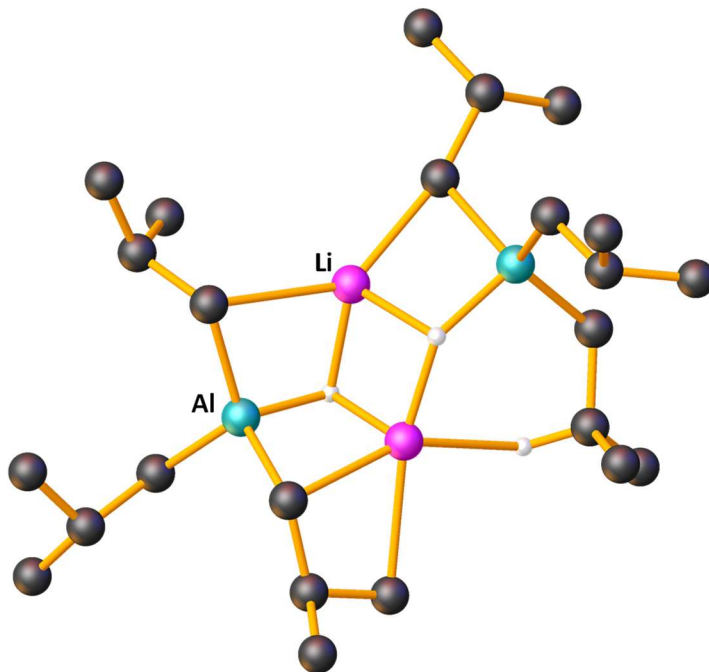


Figure 7.1: Optimised molecular geometry of [iBu₃AlHLi]₂, **11**.

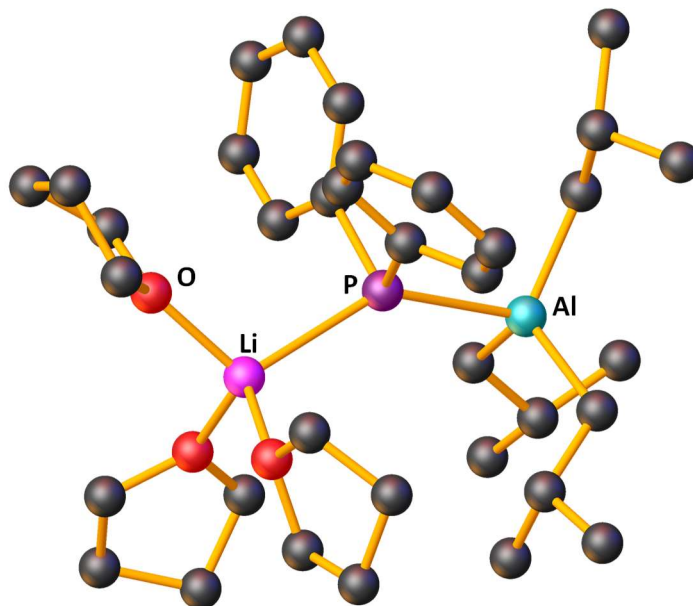


Figure 7.2: Optimised molecular geometry of iBu₃AlPPh₂Li(THF)₃, **22**.

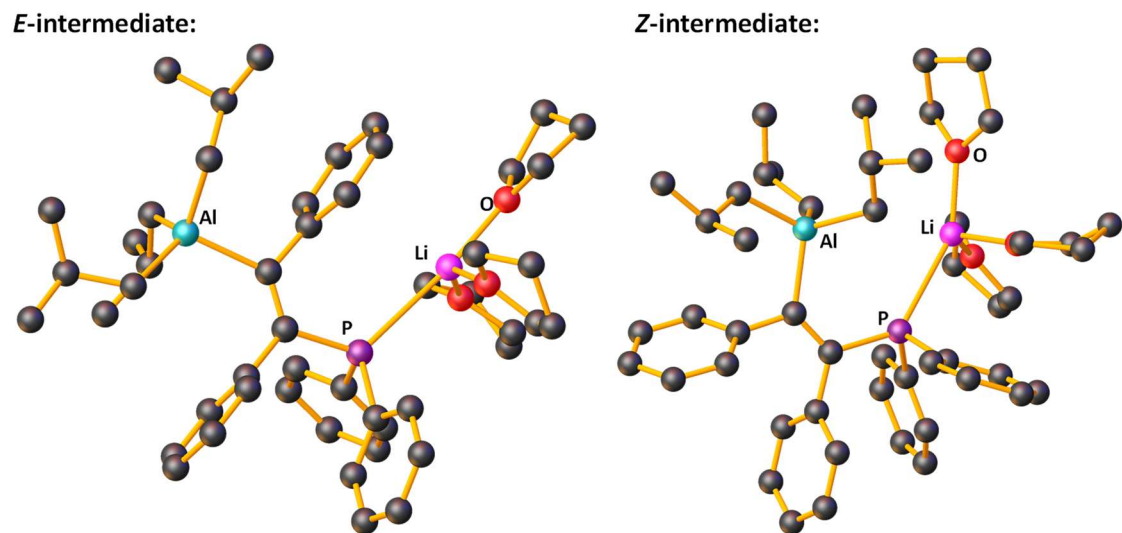


Figure 7.3: Optimised molecular geometry of proposed catalytic intermediates, for both *E*- and *Z*-stereoisomers.

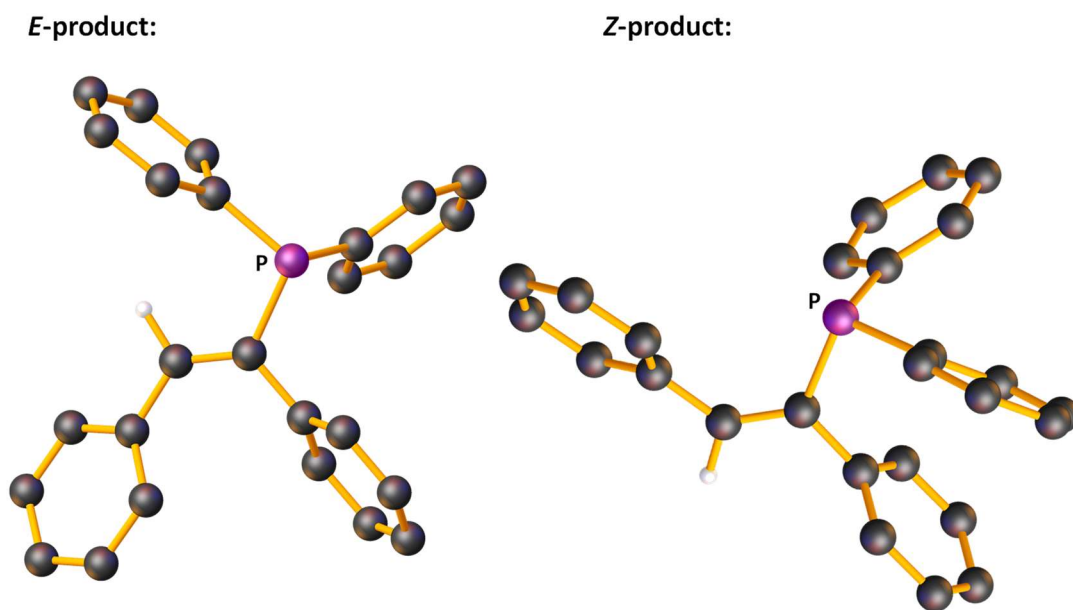


Figure 7.4: Optimised molecular geometry of *E*- and *Z*-stereoisomer products.

7.6: Experimental data for Chapter 6

Selected crystallographic data are shown in Table 7.6.5.

7.6.1: Synthesis of compounds

Synthesis of $i\text{Bu}_3\text{AlHMg}(\text{THF})_4\text{Cl}$, **27**

To a solution of $i\text{Bu}_2\text{AlH}$ (2 mL; 1 M/hexane; 2 mmol) in THF (5 mL) was added $i\text{BuMgCl}$ (1 mL; 2 M/ Et_2O ; 2 mmol) dropwise at room temperature. The resultant yellow solution was stirred at room temperature for 30 minutes and then the solvents were removed *in vacuo*. Hexane (2 mL) and THF (0.2 mL) were added to the residues to generate a clear solution. Cooling to $-15\text{ }^\circ\text{C}$ generated a crop of colourless crystals which were suitable for X-ray diffraction. (0.914 g; 1.68 mmol; 84% yield).

^1H NMR (400.1 MHz, C_6D_6 , 300 K): δ 0.19 (d, $J = 7.22\text{ Hz}$, 6H, $i\text{Bu CH}_2$); 1.24 (d, $J = 6.55\text{ Hz}$, 18H, $i\text{Bu CH}_3$); 1.34 (br. s., 14H, THF CH_2); 2.11 (sept., $J = 6.40\text{ Hz}$, $i\text{Bu CH}$); 3.69 (br. s., 15H, THF CH_2) ppm. **$^{13}\text{C}\{^1\text{H}\}$ NMR (151 MHz, C_6D_6 , 300 K):** δ 23.5 (s, THF CH_2); 25.3 (s, $i\text{Bu CH}_2$); 27.2 (s, $i\text{Bu CH}$); 29.0 (s, $i\text{Bu CH}_3$); 69.6 (s, THF) ppm. **^{27}Al NMR:** no signal was observed.

7.7: Crystal structure data and refinement details for compounds reported in this thesis

Table 7.7.1: Chapter 2 – compounds 1, 3 - 5

Compound	(HMDS) ₂ Al(H)(μ-H)Li(THF) ₃ , 1	(HMDS) ₂ Al(μ-H ₂)Li(12-crown-4), 3	(HMDS) ₂ Al(H)(μ-H)Li(PMDETA), 4	[(HMDS) ₂ AlH ₂][Li(TMEDA) ₂], 5
Empirical formula	C ₂₄ H ₅₂ AlLiN ₂ O ₃ Si ₄	AlLiSi ₄ O ₄ N ₂ C ₂₇ H ₆₂	AlLiSi ₄ N ₅ C ₂₁ H ₆₁	AlLiSi ₄ N ₆ C ₂₄ H ₇₀
Molecular Mass	573.03	625.07	530.02	589.13
Crystal system (space group)	Monoclinic (P2 ₁ /c)	Orthorhombic (P2 ₁ 2 ₁ 2 ₁)	Monoclinic (P2 ₁ /c)	Monoclinic (P2 ₁ /c)
a / Å	19.1211(7)	12.3904(3)	18.2497(3)	17.8785(3)
b / Å	11.6571(5)	14.4124(3)	11.7867(2)	12.5619(2)
c / Å	16.3906(6)	21.2850(5)	16.1366(3)	17.5361(3)
α / °	90	90	90	90
β / °	90.154	90	93.426(2)	90.296(2)
γ / °	90	90	90	90
V / Å³	3653.4(2)	3800.98(15)	3464.84(10)	3938.34(11)
Z	4	4	4	4
λ / Å	Mo Kα 0.7107	Cu Kα 1.54184	Cu Kα 1.54184	Cu Kα 1.54184
Measured reflections	36740	30698	31783	32432
Unique reflections	8703	7551	6868	7818
R_{sigma}	0.0425	0.0328	0.0299	0.0375
R_{int}	0.0391	0.0416	0.0567	0.0523
Observed rflns [I > 2σ(I)]	6410	7190	6189	6487
Goof	1.014	1.022	1.046	1.017
R [on F, obs rflns only]	0.0527	0.0320	0.0365	0.0522
ωR [on F², all data]	0.1345	0.0837	0.1040	0.1458
Largest diff. peak/ hole e/Å⁻³	0.44 / -0.47	0.29/ -0.26	0.40/ -0.26	0.53/ -0.36

Table 7.7.1 cont'd: Chapter 2 – compounds 6 – 9

Compound	[(HMDS) ₂ AlH ₂][Li(Me ₆ -TREN)], 6	(HMDS) ₂ Al(H)(μ-H)Na(THF) ₄ , 7	(HMDS) ₂ Al(μ-OCH ₂ Ph) ₂ Li(THF) ₂ , 8	(HMDS)AlH(μ-H)[C ₃ H ₄ N ₃]Li(THF), 9
Empirical formula	AlLiSi ₄ N ₆ C ₂₄ H ₆₈	AlNaSi ₄ O ₄ N ₂ C ₂₈ H ₇₀	C ₉₉ H ₉₀ N ₉ O ₉ SiAlLi	C ₁₃ H ₃₁ AlLiN ₄ OSi ₂
Molecular Mass	587.11	661.19	1426.35	350.52
Crystal system (space group)	Monoclinic (P2 ₁ /n)	Orthorhombic (P2 ₁ 2 ₁ 2 ₁)	Triclinic (P -1)	Monoclinic (P2 ₁ /c)
a / Å	14.9972(4)	12.8589(2)	11.2443(7)	13.3714(7)
b / Å	12.4262(3)	16.0231(2)	13.0965(8)	14.1997(7)
c / Å	20.9919(6)	19.8745(4)	16.3279(10)	11.4816(7)
α / °	90	90	77.340(5)	90
β / °	105.804(3)	90	72.377(5)	90.332(5)
γ / °	90	90	67.344(6)	90
V / Å³	3764.13(18)	4094.933(12)	2100.4(2)	2166.7(2)
Z	4	4	1	4
λ / Å	Cu Kα 1.54184	Cu Kα 1.54184	Cu Kα 1.54184	Mo Kα 0.7107
Measured reflections	14851	33288	18846	10020
Unique reflections	7378	8122	8238	4611
R_{sigma}	0.0562	0.0161	0.0602	0.0693
R_{int}	0.0400	0.0259	0.0637	0.0390
Observed rflns [I > 2σ(I)]	5456	7995	7082	2713
Goof	1.044	1.081	1.073	1.038
R [on F, obs rflns only]	0.0551	0.0344	0.0500	0.067
ωR [on F², all data]	0.1649	0.0351	0.1539	0.2310
Largest diff. peak/ hole e/Å⁻³	0.64/ -0.33	0.50 / -0.23	0.48/ -0.39	0.46/ -0.47

Table 7.7.2: Chapter 3 – compounds 15 and 16

Compound	[(TMP)(Ph ₂ (H)CO)Al(μ-OC(H)Ph ₂)] ₂ , 15	[<i>i</i> Bu ₂ Al(μ-NCPH ₂)] ₂ , 16	<i>i</i> Bu ₃ AlHLi(PMDETA), 17
Empirical formula	C ₇₀ H ₈₀ Al ₂ N ₂ O ₄	C ₄₂ H ₅₆ Al ₂ N ₂	C ₂₁ H ₅₂ AlLiN ₃
Molecular Mass	1067.32	642.89	379.56
Crystal system (space group)	Monoclinic (P2 ₁ /n)	Triclinic (P -1)	Orthorhombic (Pnma)
a/ Å	14.04490(10)	10.4347(6)	16.6792(5)
b/ Å	17.85020(10)	19.3559(14)	15.6104(5)
c/ Å	23.1821(2)	21.3099(13)	10.2931(3)
α/ °	90	70.236(6)	90
β/ °	92.8660(10)	89.901(5)	90
γ/ °	90	81.826(5)	90
V/ Å ³	5804.58(7)	4004.4(5)	2680.00(14)
Z	4	4	4
λ/ Å	Cu Kα (λ = 1.54184)	Mo Kα (λ = 0.71073)	Cu Kα (λ = 1.54184)
Measured reflections	72409	30347	6327
Unique reflections	11508	15688	2381
R _{int}	0.0736	0.055	0.0574
Observed rflns [I > 2σ(I)]	10297	8801	2773
Goof	1.025	0.994	1.059
R [on F, obs rflns only]	0.0458	0.0678	0.0676
ωR [on F ² , all data]	0.1237	0.1621	0.1906
Largest diff. peak/ hole e/ Å ⁻³	0.409/ -0.263	0.72/ -0.55	0.53/-0.30

7.7.3: Chapter 4 – compounds 19 – 20

Compound	<i>i</i> Bu ₂ Al({OC(CH ₃)C(CH ₃)O} ₂)B(H)(TMP), 19	<i>i</i> Bu ₂ Al({OC(CH ₃)C(CH ₃)O} ₂)B(H)(HMDS), 20
Empirical formula	C ₂₃ H ₄₉ AlBNO ₂	Al ₂ Si ₄ O ₄ N ₂ C ₄₀ B ₂ H ₉₈
Molecular mass	409.46	859.19
Crystal system (space group)	Triclinic (P-1)	Monoclinic (P2 ₁ /c)
a/ Å	9.1582(5)	14.9419(6)
b/ Å	12.6441(7)	15.3025(6)
c/ Å	13.1393(8)	12.7753(5)
α/ °	116.645(6)	90
β/ °	102.254(5)	110.850(5)
γ/ °	94.953(4)	90
V/ Å ³	1299.9(15)	2759.8(2)
Z	2	2
λ/ Å	Cu Kα (λ = 1.54184)	Mo Kα (λ = 0.71073)
Measured reflections	11194	15460
Unique reflections	5101	4365
R _{int}	0.01175	0.0358
Observed rflns [I > 2σ(I)]	4561	5868
GOOF	1.297	1.039
R [on F, obs rflns only]	0.0972	0.0451
ωR [on F ² , all data]	0.2987	0.1175
Largest diff. peak/hole e/Å ⁻³	1.06/-1.13	0.50/-0.39

7.7.4: Chapter 5 – compounds 22, and 26

Compound	<i>i</i> Bu ₃ AlPPh ₂ Li(THF) ₃ , 22	<i>i</i> Bu ₃ AlPPh ₂ Li(12-crown-4), 26
Empirical formula	AlLiPO ₃ C ₃₆ H ₆₁	AlLiPO ₄ C ₃₂ H ₅₃
Molecular mass	606.73	566.63
Crystal system (space group)	Monoclinic (C _c)	Triclinic (P-1)
a/ Å	18.0340(9)	9.1586(6)
b/ Å	11.3773(6)	11.8525(7)
c/ Å	18.6888(10)	16.5468(10)
α/ °	90	97.746(5)
β/ °	98.341(5)	104.970(6)
γ/ °	90	101.162(5)
V/ Å ³	3794.0(3)	1669.74(18)
Z	4	2
λ/ Å	MoKα (λ = 0.71073 Å)	CuKα (λ = 1.54184 Å)
Measured reflections	19956	12010
Unique reflections	7944	6280
R _{int}	0.0402	0.0931
Observed rflns [I > 2σ(I)]	5775	4564
GOOF	1.008	1.244
R [on F, obs rflns only]	0.0525	0.1154
ωR [on F ² , all data]	0.1107	0.3509
Largest diff. peak/hole e/Å ⁻³	0.31/-0.25	1.40/-1.01

7.7.5: Chapter 6 – compound 27

Compound	<i>i</i> Bu ₃ AlHMg(THF) ₄ Cl, 27
Empirical formula	C ₂₈ H ₆₀ AlClMgO ₄
Molecular mass	547.50
Crystal system (space group)	Orthorhombic (Pna2 ₁)
a/ Å	23.6312(10)
b/ Å	14.2446(6)
c/ Å	9.8776(4)
α/ °	90
β/ °	90
γ/ °	90
V/ Å³	3325.0(2)
Z	4
λ/ Å	CuKα (λ = 1.54184 Å)
Measured reflections	5575
Unique reflections	3407
R_{int}	0.0572
Observed rflns [I > 2σ(I)]	2862
GOOF	1.253
R [on F, obs rflns only]	0.0727
ωR [on F², all data]	0.2066
Largest diff. peak/hole e/Å⁻³	0.59/-0.31

References

1. International Year of the Periodic Table, <https://www.iypt2019.org>, (accessed 23rd February 2019).
2. EuChemS Periodic Table, <http://bit.ly/euchems-pt>, (accessed 30th January 2019).
3. P. Atkins, T. Overton, J. Rourke, M. Weller and F. Armstrong, *Shriver and Atkin's Inorganic Chemistry*, Oxford University Press, Fifth edn., 2010.
4. D. Rabinovich, *Nature Chem.*, 2012, **5**, 76.
5. J. J. Eisch, in *Comprehensive Organometallic Chemistry*, eds. F. G. A. Stone and E. W. Abel, Pergamon, Oxford, 1982, DOI: 10.1016/B978-008046518-0.00011-8, pp. 555-682.
6. J. J. Eisch, in *Comprehensive Organometallic Chemistry II*, eds. F. G. A. Stone and G. Wilkinson, Elsevier, Oxford, 1995, DOI: 10.1016/B978-008046519-7.00010-1, pp. 431-502.
7. J. K. Groves, *Chem. Soc. Rev.*, 1972, **1**, 73-97.
8. C. Elschenbroich, *Organometallics*, WILEY-VCH Verlag GmbH & Co. KGaA, third edn., 2006.
9. The Nobel Prize in Chemistry 1963, <https://www.nobelprize.org/prizes/chemistry/1963/summary/>, (accessed 29th January 2019).
10. M. Bochmann, *Organometallics and Catalysis*, Oxford University Press, New York, 2015.
11. *Modern Organoaluminium Reagents*, eds. S. Woodward and S. Dagorne, Springer Berlin Heidelberg, Berlin, Heidelberg, 2013.
12. P. Bag, C. Weetman and S. Inoue, *Angew. Chem. Int. Ed.*, 2018, **57**, 14394-14413.
13. H. W. Roesky, *Inorg. Chem.*, 2004, **43**, 7284-7293.
14. H. W. Roesky and S. S. Kumar, *Chem. Commun.*, 2005, 4027-4038.
15. W. Li, X. Ma, M. G. Walawalkar, Z. Yang and H. W. Roesky, *Coord. Chem. Rev.*, 2017, **350**, 14-29.

16. G. I. Nikonov, *ACS Catal.*, 2017, **7**, 7257-7266.
17. C. Weetman and S. Inoue, *ChemCatChem*, 2018, **10**, 4213-4228.
18. S. Dagherne and R. Wehmschulte, *ChemCatChem*, 2018, **10**, 2509-2520.
19. R. G. Vranka and E. L. Amma, *J. Am. Chem. Soc.*, 1967, **89**, 3121-3126.
20. F. A. Cotton, *Inorg. Chem.*, 1970, **9**, 2804-2804.
21. A. L. Allred, *J. Inorg. Nucl. Chem.*, 1961, **17**, 215-221.
22. K. Wade, in *Electron Deficient Compounds*, Springer US, Boston, MA, 1971, DOI: 10.1007/978-1-4684-6054-4_1, pp. 1-5.
23. M. F. Self, W. T. Pennington and G. H. Robinson, *Inorganica Chim. Acta*, 1990, **175**, 151-153.
24. P. Knochel, T. Blümke, K. Groll and Y.-H. Chen, in *Modern Organoaluminum Reagents: Preparation, Structure, Reactivity and Use*, eds. S. Woodward and S. Dagherne, Springer Berlin Heidelberg, Berlin, Heidelberg, 2013, DOI: 10.1007/3418_2012_36, pp. 173-186.
25. T. Blümke, Y.-H. Chen, Z. Peng and P. Knochel, *Nature Chem.*, 2010, **2**, 313.
26. E.-i. Negishi and S. Baba, *J. Chem. Soc., Chem. Commun.*, 1976, 596b-597b.
27. S. Baba and E. Negishi, *J. Am. Chem. Soc.*, 1976, **98**, 6729-6731.
28. B. Liang, T. Novak, Z. Tan and E.-i. Negishi, *J. Am. Chem. Soc.*, 2006, **128**, 2770-2771.
29. S. Kawamura, R. Agata and M. Nakamura, *Org. Chem. Front.*, 2015, **2**, 1053-1058.
30. S. H. Wunderlich and P. Knochel, *Angew. Chem. Int. Ed.*, 2009, **48**, 1501-1504.
31. W. Uhl, E. Er, O. Hübner and H.-J. Himmel, *Z. Anorg. Allg. Chem.*, 2008, **634**, 2133-2139.
32. H. Schumann, S. Dechert, S. Schutte, J.-Y. Hyeon, M. Hummert, B. C. Wassermann, W. Kaminsky, A. Eisenhardt, K. Köhler and J. Eichhorn, *Organometallics*, 2003, **22**, 1391-1401.
33. S. Kawamura, K. Ishizuka, H. Takaya and M. Nakamura, *Chem. Commun.*, 2010, **46**, 6054-6056.
34. S. Kawamura, T. Kawabata, K. Ishizuka and M. Nakamura, *Chem. Commun.*, 2012, **48**, 9376-9378.
35. H. Minami, T. Saito, C. Wang and M. Uchiyama, *Angew. Chem. Int. Ed.*, 2015, **54**, 4665-4668.

36. C. Dohmeier, C. Robl, M. Tacke and H. Schnöckel, *Angew. Chem. Int. Ed.*, 1991, **30**, 564-565.
37. S. Schulz, H. W. Roesky, H. J. Koch, G. M. Sheldrick, D. Stalke and A. Kuhn, *Angew. Chem. Int. Ed.*, 1993, **32**, 1729-1731.
38. A. Hofmann, T. Tröster, T. Kupfer and H. Braunschweig, *Chem. Sci.*, 2019, **10**, 3421-3428.
39. C. Cui, H. W. Roesky, H.-G. Schmidt, M. Noltemeyer, H. Hao and F. Cimpoesu, *Angew. Chem. Int. Ed.*, 2000, **39**, 4274-4276.
40. G. Coates, B. J. Ward, C. Bakewell, A. J. P. White and M. R. Crimmin, *Chem. -Eur. J.*, 2018, **24**, 16282-16286.
41. C. Bakewell, A. J. P. White and M. R. Crimmin, *Angew. Chem. Int. Ed.*, 2018, **57**, 6638-6642.
42. C. Bakewell, A. J. P. White and M. R. Crimmin, *Chem Sci*, 2019, **10**, 2452-2458.
43. J. Hicks, P. Vasko, J. M. Goicoechea and S. Aldridge, *Nature*, 2018, **557**, 92-95.
44. J. W. Akitt, *Prog. Nucl. Magn. Reson. Spectrosc.*, 1989, **21**, 1-149.
45. M. Haouas, F. Taulelle and C. Martineau, *Prog. Nucl. Magn. Reson. Spectrosc.*, 2016, **94-95**, 11-36.
46. R. Benn, A. Ruffińska, H. Lehmkuhl, E. Janssen and C. Krüger, *Angew. Chem. Int. Ed.*, 1983, **22**, 779-780.
47. J. Gauss, U. Schneider, R. Ahlrichs, C. Dohmeier and H. Schnoekel, *J. Am. Chem. Soc.*, 1993, **115**, 2402-2408.
48. C. Martineau, F. Taulelle and M. Haouas, in *PATAI'S Chemistry of Functional Groups*, 2016, DOI: 10.1002/9780470682531.pat0840, pp. 1-51.
49. M. S. Hill, D. J. Liptrot and C. Weetman, *Chem. Soc. Rev.*, 2016, **45**, 972-988.
50. P. P. Power, *Nature*, 2010, **463**, 171.
51. M. R. Crimmin and M. S. Hill, in *Alkaline-Earth Metal Compounds: Oddities and Applications*, ed. S. Harder, Springer Berlin Heidelberg, Berlin, Heidelberg, 2013, DOI: 10.1007/978-3-642-36270-5_6, pp. 191-241.
52. R. L. Melen, *Chem. Soc. Rev.*, 2016, **45**, 775-788.
53. M. Arrowsmith, M. S. Hill, T. Hadlington, G. Kociok-Köhn and C. Weetman, *Organometallics*, 2011, **30**, 5556-5559.

54. M. Arrowsmith, T. J. Hadlington, M. S. Hill and G. Kociok-Köhn, *Chem. Commun.*, 2012, **48**, 4567-4569.
55. M. Arrowsmith, M. S. Hill and G. Kociok-Köhn, *Chem. -Eur. J.*, 2013, **19**, 2776-2783.
56. C. Weetman, M. S. Hill and M. F. Mahon, *Chem. Commun.*, 2015, **51**, 14477-14480.
57. C. Weetman, M. S. Hill and M. F. Mahon, *Chem. -Eur. J.*, 2016, **22**, 7158-7162.
58. C. Weetman, M. S. Hill and M. F. Mahon, *Polyhedron*, 2016, **103**, Part A, 115-120.
59. M. D. Anker, M. Arrowsmith, P. Bellham, M. S. Hill, G. Kociok-Köhn, D. J. Liptrot, M. F. Mahon and C. Weetman, *Chem. Sci.*, 2014, **5**, 2826-2830.
60. A. G. M. Barrett, I. J. Casely, M. R. Crimmin, M. S. Hill, J. R. Lachs, M. F. Mahon and P. A. Procopiou, *Inorg. Chem.*, 2009, **48**, 4445-4453.
61. M. D. Anker, M. S. Hill, J. P. Lowe and M. F. Mahon, *Angew. Chem. Int. Ed.*, 2015, **54**, 10009-10011.
62. H. Bauer, M. Alonso, C. Färber, H. Elsen, J. Pahl, A. Causero, G. Ballmann, F. De Proft and S. Harder, *Nat. Catal.*, 2018, **1**, 40-47.
63. H. Bauer, M. Alonso, C. Fischer, B. Rösch, H. Elsen and S. Harder, *Angew. Chem. Int. Ed.*, 2018, **57**, 15177-15182.
64. H. Bauer, K. Thum, M. Alonso, C. Fischer and S. Harder, *Angew. Chem. Int. Ed.*, 2019, **58**, 4248-4253.
65. R. McLellan, A. R. Kennedy, R. E. Mulvey, S. A. Orr and S. D. Robertson, *Chem. -Eur. J.*, 2017, **23**, 16853-16861.
66. R. McLellan, A. R. Kennedy, S. A. Orr, S. D. Robertson and R. E. Mulvey, *Angew. Chem. Int. Ed.*, 2017, **56**, 1036-1041.
67. G. C. Welch, R. R. S. Juan, J. D. Masuda and D. W. Stephan, *Science*, 2006, **314**, 1124.
68. L. J. Hounjet and D. W. Stephan, *Org. Proc. Res. Dev.*, 2014, **18**, 385-391.
69. D. W. Stephan, *J. Am. Chem. Soc.*, 2015, **137**, 10018-10032.
70. M. Alcarazo, *Synlett*, 2014, **25**, 1519-1520.
71. J. Lam, K. M. Szkop, E. Mosaferi and D. W. Stephan, *Chem Soc Rev*, 2019, DOI: 10.1039/c8cs00277k.
72. P. A. Chase, T. Jurca and D. W. Stephan, *Chem. Commun.*, 2008, 1701-1703.
73. B. McNerney, B. Whittlesey, D. B. Cordes and C. Krempner, *Chem. -Eur. J.*, 2014, **20**, 14959-14964.

74. J. A. Hatnean, J. W. Thomson, P. A. Chase and D. W. Stephan, *Chem. Commun.*, 2014, **50**, 301-303.
75. J. L. Jezl and A. P. Stuart, *U.S. Patent*, 1960, US 2983770.
76. H. Elsen, C. Färber, G. Ballmann and S. Harder, *Angew. Chem. Int. Ed.*, 2018, **57**, 7156-7160.
77. K. Jakobsson, T. Chu and G. I. Nikonov, *ACS Catal.*, 2016, **6**, 7350-7356.
78. J. Chen and E. Y.-X. Chen, *Angew. Chem. Int. Ed.*, 2015, **54**, 6842-6846.
79. Z. Yang, M. Zhong, X. Ma, S. De, C. Anusha, P. Parameswaran and H. W. Roesky, *Angew. Chem. Int. Ed.*, 2015, **54**, 10225-10229.
80. M. Khandelwal and R. J. Wehmschulte, *Angew. Chem. Int. Ed.*, 2012, **51**, 7323-7326.
81. J. Koller and R. G. Bergman, *Organometallics*, 2012, **31**, 2530-2533.
82. R. J. Wehmschulte, M. Saleh and D. R. Powell, *Organometallics*, 2013, **32**, 6812-6819.
83. J. Koller and R. G. Bergman, *Chem. Commun.*, 2010, **46**, 4577-4579.
84. T. E. Müller, K. C. Hultsch, M. Yus, F. Foubelo and M. Tada, *Chem. Rev.*, 2008, **108**, 3795-3892.
85. J. Koller and R. G. Bergman, *Organometallics*, 2010, **29**, 3350-3356.
86. M. Khandelwal and R. J. Wehmschulte, *J. Organomet. Chem.*, 2012, **696**, 4179-4183.
87. S. Tobisch, *Dalton Trans.*, 2015, **44**, 12169-12179.
88. J. Koller and R. G. Bergman, *Organometallics*, 2010, **29**, 5946-5952.
89. R. J. Less, R. L. Melen and D. S. Wright, *RSC Adv.*, 2012, **2**, 2191-2199.
90. Z. Yang, M. Zhong, X. Ma, K. Nijesh, S. De, P. Parameswaran and H. W. Roesky, *J. Am. Chem. Soc.*, 2016, **138**, 2548-2551.
91. E. A. Romero, J. L. Peltier, R. Jazzar and G. Bertrand, *Chem. Commun.*, 2016, **52**, 10563-10565.
92. C. W. Hamilton, R. T. Baker, A. Staubitz and I. Manners, *Chem. Soc. Rev.*, 2009, **38**, 279-293.
93. A. Staubitz, A. P. M. Robertson, M. E. Sloan and I. Manners, *Chem. Rev.*, 2010, **110**, 4023-4078.
94. A. D. Sutton, A. K. Burrell, D. A. Dixon, E. B. Garner, J. C. Gordon, T. Nakagawa, K. C. Ott, J. P. Robinson and M. Vasiliu, *Science*, 2011, **331**, 1426 - 1429.
95. H. J. Cowley, M. S. Holt, R. L. Melen, J. M. Rawson and D. S. Wright, *Chem. Commun.*, 2011, **47**, 2682-2684.

96. M. M. Hansmann, R. L. Melen and D. S. Wright, *Chem. Sci.*, 2011, **2**, 1554-1559.
97. R. J. Less, H. R. Simmonds, S. B. J. Dane and D. S. Wright, *Dalton Trans.*, 2013, **42**, 6337-6343.
98. R. J. Less, H. R. Simmonds and D. S. Wright, *Dalton Trans.*, 2014, **43**, 5785-5792.
99. W. Schlenk and J. Holtz, *Chem. Ber.*, 1917, **50**, 262-274.
100. T. T. Tidwell, *Angew. Chem. Int. Ed.*, 2001, **40**, 331-337.
101. J. Clayden, *Organolithiums: Selectivity for Synthesis*, Pergamon, Oxford, 2002.
102. M. Schlosser, in *Organometallics in Synthesis*, ed. M. Schlosser, Wiley, New York, 1994, DOI: 10.1002/9781118750407.ch1, pp. 1 - 166.
103. H. W. Gschwend and H. R. Rodriguez, in *Organic Reactions*, John Wiley & Sons, Inc., 2004, DOI: 10.1002/0471264180.or026.01.
104. D. B. Collum, *Acc. Chem. Res.*, 1993, **26**, 227-234.
105. R. E. Mulvey and S. D. Robertson, *Angew. Chem. Int. Ed.*, 2013, **52**, 11470-11487.
106. T. L. Rathman and J. A. Schwindeman, *Org. Proc. Res. Dev.*, 2014, **18**, 1192-1210.
107. R. E. Mulvey and S. D. Robertson, *Top Organomet. Chem.*, 2014, **47**, 129-158.
108. R. E. Mulvey, *Dalton Trans.*, 2013, **42**, 6676-6693.
109. S. D. Robertson, M. Uzelac and R. E. Mulvey, *Chem. Rev.*, 2019, DOI: 10.1021/acs.chemrev.9b00047.
110. R. E. Mulvey, *Acc. Chem. Res.*, 2009, **42**, 743-755.
111. A. E. Finholt, A. C. Bond and H. I. Schlesinger, *J. Am. Chem. Soc.*, 1947, **69**, 1199-1203.
112. J. Magano and J. R. Dunetz, *Org. Proc. Res. Dev.*, 2012, **16**, 1156-1184.
113. W. G. Brown, in *Organic Reactions*, John Wiley and Sons, 2011, DOI: 10.1002/0471264180.or006.10.
114. in *CRC Handbook of Chemistry and Physics*, eds. R. C. Weast and M. J. Astle, Boca Raton, FL, 1982.
115. H. C. Brown and S. Krishnamurthy, *Tetrahedron*, 1979, **35**, 567-607.
116. H. C. Brown, *Angew. Chem.*, 1980, **92**, 675 - 683.
117. J. A. Wanklyn, *Justus Liebigs Annalen der Chemie*, 1858, **108**, 67-79.
118. G. Wittig, *Angew. Chem*, 1958, **70**, 65-71.
119. R. E. Mulvey, F. Mongin, M. Uchiyama and Y. Kondo, *Angew. Chem. Int. Ed.*, 2007, **46**, 3802-3824.
120. L. Lochmann, J. Pospíšil and D. Lím, *Tetrahedron Lett.*, 1966, **7**, 257-262.

121. M. Schlosser, *J. Organomet. Chem.*, 1967, **8**, 9-16.
122. M. Schlosser, H. C. Jung and S. Takagishi, *Tetrahedron*, 1990, **46**, 5633-5648.
123. K. Shen, Y. Fu, J.-N. Li, L. Liu and Q.-X. Guo, *Tetrahedron*, 2007, **63**, 1568-1576.
124. P. Benrath, M. Kaiser, T. Limbach, M. Mondeshki and J. Klett, *Angew. Chem. Int. Ed.*, 2016, **55**, 10886-10889.
125. P. C. Andrikopoulos, D. R. Armstrong, H. R. L. Barley, W. Clegg, S. H. Dale, E. Hevia, G. W. Honeyman, A. R. Kennedy and R. E. Mulvey, *J. Am. Chem. Soc.*, 2005, **127**, 6184-6185.
126. V. Snieckus, *Chem. Rev.*, 1990, **90**, 879-933.
127. M. C. Whisler, S. MacNeil, V. Snieckus and P. Beak, *Angew. Chem. Int. Ed.*, 2004, **43**, 2206-2225.
128. H. Gilman and R. L. Bebb, *J. Am. Chem. Soc.*, 1939, **61**, 109-112.
129. G. Wittig, U. Pockels and H. Dröge, *Ber. Dtsch. Chem. Ges.*, 1938, **71**, 1903-1912.
130. A. J. Martínez-Martínez, A. R. Kennedy, R. E. Mulvey and C. T. O'Hara, *Science*, 2014, **346**, 834-837.
131. A. J. Martínez-Martínez, S. Justice, B. J. Fleming, A. R. Kennedy, I. D. H. Oswald and C. T. O'Hara, *Science Advances*, 2017, **3**, e1700832.
132. M. Uchiyama, H. Naka, Y. Matsumoto and T. Ohwada, *J. Am. Chem. Soc.*, 2004, **126**, 10526-10527.
133. H. Naka, M. Uchiyama, Y. Matsumoto, A. E. H. Wheatley, M. McPartlin, J. V. Morey and Y. Kondo, *J. Am. Chem. Soc.*, 2007, **129**, 1921-1930.
134. R. E. Mulvey, D. R. Armstrong, B. Conway, E. Crosbie, A. R. Kennedy and S. D. Robertson, *Inorg. Chem.*, 2011, **50**, 12241-12251.
135. D. R. Armstrong, E. Crosbie, E. Hevia, R. E. Mulvey, D. L. Ramsay and S. D. Robertson, *Chem. Sci.*, 2014, **5**, 3031-3045.
136. M. Uzelac and R. E. Mulvey, *Chem. -Eur. J.*, 2018, **28**, 7786 - 7793.
137. B. Conway, E. Crosbie, A. R. Kennedy, R. E. Mulvey and S. D. Robertson, *Chem. Commun.*, 2012, **48**, 4674-4676.
138. E. Crosbie, P. García-Álvarez, A. R. Kennedy, J. Klett, R. E. Mulvey and S. D. Robertson, *Angew. Chem. Int. Ed.*, 2010, **49**, 9388-9391.
139. M. Á. Fuentes, A. R. Kennedy, R. E. Mulvey, J. A. Parkinson, T. Rantanen, S. D. Robertson and V. Snieckus, *Chem. -Eur. J.*, 2015, **21**, 14812-14822.

140. R. McLellan, M. Uzelac, A. R. Kennedy, E. Hevia and R. E. Mulvey, *Angew. Chem. Int. Ed.*, 2017, **56**, 9566-9570.
141. W. Clegg, E. Crosbie, S. H. Dale-Black, E. Hevia, G. W. Honeyman, A. R. Kennedy, R. E. Mulvey, D. L. Ramsay and S. D. Robertson, *Organometallics*, 2015, **34**, 2580-2589.
142. J. García-Álvarez, D. V. Graham, A. R. Kennedy, R. E. Mulvey and S. Weatherstone, *Chem. Commun.*, 2006, 3208-3210.
143. B. Conway, P. García-Álvarez, A. R. Kennedy, J. Klett, R. E. Mulvey and S. D. Robertson, *New J. Chem.*, 2010, **34**, 1707-1712.
144. B. Conway, A. R. Kennedy, R. E. Mulvey, S. D. Robertson and J. G. Álvarez, *Angew. Chem. Int. Ed.*, 2010, **49**, 3182-3184.
145. H. C. Brown, H. I. Schlesinger and A. B. Burg, *J. Am. Chem. Soc.*, 1939, **61**, 673-680.
146. H. C. Brown and B. C. S. Rao, *J. Am. Chem. Soc.*, 1956, **78**, 5694-5695.
147. E. R. Burkhardt and K. Matos, *Chem. Rev.*, 2006, **106**, 2617-2650.
148. G. Schmid, T. Fukuyama, K. Akasaka and Y. Kishi, *J. Am. Chem. Soc.*, 1979, **101**, 259-260.
149. M. A. Reichle and B. Breit, *Angew. Chem. Int. Ed.*, 2012, **51**, 5730-5734.
150. R. P. Rucker, A. M. Whittaker, H. Dang and G. Lalic, *J. Am. Chem. Soc.*, 2012, **134**, 6571-6574.
151. A. J. J. Lennox and G. C. Lloyd-Jones, *Chem. Soc. Rev.*, 2014, **43**, 412-443.
152. N. Miyaoura and A. Suzuki, *Chem. Rev.*, 1995, **95**, 2457-2483.
153. A. Suzuki, *Angew. Chem. Int. Ed.*, 2011, **50**, 6722-6737.
154. S. J. Geier, C. M. Vogels and S. A. Westcott, in *Boron Reagents in Synthesis*, American Chemical Society, 2016, vol. 1236, ch. 6, pp. 209-225.
155. The Nobel Prize in Chemistry 1979, http://www.nobelprize.org/nobel_prizes/chemistry/laureates/1979, (accessed 17th January 2019).
156. J. A. Soderquist and H. C. Brown, *J. Org. Chem.*, 1981, **46**, 4599-4600.
157. C. E. Tucker, J. Davidson and P. Knochel, *J. Org. Chem.*, 1992, **57**, 3482-3485.
158. H. C. Brown and S. K. Gupta, *J. Am. Chem. Soc.*, 1971, **93**, 1816-1818.
159. D. Männig and H. Nöth, *Angew. Chem. Int. Ed.*, 1985, **24**, 878-879.
160. A. Harinath, J. Bhattcharjee, K. R. Gorantla, B. S. Mallik and T. K. Panda, *Eur. J. Org. Chem.*, 2018, 3180-3192.

161. S. Pereira and M. Srebnik, *Organometallics*, 1995, **14**, 3127-3128.
162. G. Zhang, H. Zeng, J. Wu, Z. Yin, S. Zheng and J. C. Fettinger, *Angew. Chem. Int. Ed.*, 2016, **55**, 14369-14372.
163. G. Jin, C. G. Werncke, Y. Escudié, S. Sabo-Etienne and S. Bontemps, *J. Am. Chem. Soc.*, 2015, **137**, 9563-9566.
164. L. Zhang, D. Peng, X. Leng and Z. Huang, *Angew. Chem. Int. Ed.*, 2013, **52**, 3676-3680.
165. L. Koren-Selfridge, H. N. Londino, J. K. Vellucci, B. J. Simmons, C. P. Casey and T. B. Clark, *Organometallics*, 2009, **28**, 2085-2090.
166. L. Zhang, Z. Zuo, X. Leng and Z. Huang, *Angew. Chem. Int. Ed.*, 2014, **53**, 2696-2700.
167. R. J. Newland, J. M. Lynam and S. M. Mansell, *Chem. Commun.*, 2018, **54**, 5482-5485.
168. T. Ohmura, Y. Yamamoto and N. Miyaoura, *J. Am. Chem. Soc.*, 2000, **122**, 4990-4991.
169. R. Shintani and K. Nozaki, *Organometallics*, 2013, **32**, 2459-2462.
170. P. A. Lummis, M. R. Momeni, M. W. Lui, R. McDonald, M. J. Ferguson, M. Miskolzie, A. Brown and E. Rivard, *Angew. Chem. Int. Ed.*, 2014, **53**, 9347-9351.
171. C. C. Chong and R. Kinjo, *ACS Catal.*, 2015, **5**, 3238-3259.
172. M. K. Bisai, T. Das, K. Vanka and S. S. Sen, *Chem. Commun.*, 2018, **54**, 6843-6846.
173. Y. Wu, C. Shan, J. Ying, J. Su, J. Zhu, L. L. Liu and Y. Zhao, *Green Chem.*, 2017, **19**, 4169-4175.
174. D. Mukherjee, H. Osseili, T. P. Spaniol and J. Okuda, *J. Am. Chem. Soc.*, 2016, **138**, 10790-10793.
175. J. L. Carden, L. J. Gierlichs, D. F. Wass, D. L. Browne and R. L. Melen, *Chem. Commun.*, 2019, **55**, 318-321.
176. N. W. J. Ang, C. S. Buettner, S. Docherty, A. Bismuto, J. R. Carney, J. H. Docherty, M. J. Cowley and S. P. Thomas, *Synthesis*, 2018, **50**, 803-808.
177. A. Bismuto, M. J. Cowley and S. P. Thomas, *ACS Catal.*, 2018, **8**, 2001-2005.
178. A. Bismuto, S. P. Thomas and M. J. Cowley, *Angew. Chem. Int. Ed.*, 2016, **55**, 15356-15359.
179. V. K. Jakhar, M. K. Barman and S. Nembenna, *Org. Lett.*, 2016, **18**, 4710-4713.
180. D. Franz, L. Sirtl, A. Pöthig and S. Inoue, *Z. Anorg. Allg. Chem.*, 2016, **642**, 1245-1250.
181. B. Prashanth, M. Bhandari, S. Ravi, K. R. Shamasundar and S. Singh, *Chem. -Eur. J.*, 2018, **24**, 4794-4799.

182. G. Zhang, J. Wu, H. Zeng, M. C. Neary, M. Devany, S. Zheng and P. A. Dub, *ACS Catal.*, 2018, **9**, 874-884.
183. A. Harinath, J. Bhattacharjee and T. K. Panda, *Adv. Synth. Catal.*, 2019, **361**, 850-857.
184. M. K. Bisai, S. Pahar, T. Das, K. Vanka and S. S. Sen, *Dalton Trans.*, 2017, **46**, 2420-2424.
185. T. J. Hadlington, M. Hermann, G. Frenking and C. Jones, *J. Am. Chem. Soc.*, 2014, **136**, 3028-3031.
186. C. C. Chong, H. Hirao and R. Kinjo, *Angew. Chem. Int. Ed.*, 2015, **54**, 190-194.
187. D. M. C. Ould and R. L. Melen, *Chem. -Eur. J.*, 2018, **24**, 15201-15204.
188. V. L. Weidner, C. J. Barger, M. Delferro, T. L. Lohr and T. J. Marks, *ACS Catal.*, 2017, **7**, 1244-1247.
189. U. Mayer, V. Gutmann and W. Gerger, *Monatsh Chem.*, 1975, **106**, 1235-1257.
190. M. A. Beckett, G. C. Strickland, J. R. Holland and K. Sukumar Varma, *Polymer*, 1996, **37**, 4629-4631.
191. G. C. Welch, L. Cabrera, P. A. Chase, E. Hollink, J. D. Masuda, P. Wei and D. W. Stephan, *Dalton Trans*, 2007, 3407-3414.
192. M. A. Dureen and D. W. Stephan, *J. Am. Chem. Soc.*, 2009, **131**, 8396-8397.
193. C. Appelt, H. Westenberg, F. Bertini, A. W. Ehlers, J. C. Sloatweg, K. Lammertsma and W. Uhl, *Angew. Chem. Int. Ed.*, 2011, **50**, 3925-3928.
194. G. Ménard and D. W. Stephan, *Angew. Chem. Int. Ed.*, 2011, **50**, 8396-8399.
195. A. Heine and D. Stalke, *Angew. Chem. Int. Ed.*, 1992, **31**, 854-855.
196. H. Osseili, D. Mukherjee, T. P. Spaniol and J. Okuda, *Chem. -Eur. J.*, 2017, **23**, 14292 - 14298.
197. A. R. Kennedy, R. McLellan, G. J. McNeil, R. E. Mulvey and S. D. Robertson, *Polyhedron*, 2016, **103, Part A**, 94-99.
198. S. W. Youn and Y. H. Kim, *Synlett*, 2000, 880 - 882.
199. B. Zeynizadeh and L. Sadighnia, *Synth. Commun.*, 2011, **41**, 637-644.
200. M. Itoh, M. Kobayashi and J. Ishikawa, *Organometallics*, 1997, **16**, 3068-3070.
201. S. Ghose and T. L. Gilchrist, *J. Chem. Soc., Perkin Trans.*, 1991, 775-779.
202. R. Raap, *Can. J. Chem.*, 1971, **49**, 1792-1798.
203. L. Davin, R. McLellan, A. Hernan-Gomez, W. Clegg, A. R. Kennedy, M. Mertens, I. A. Stepek and E. Hevia, *Chem. Commun.*, 2017, **53**, 3653-3656.

204. D. Li, I. Keresztes, R. Hopson and P. G. Williard, *Acc. Chem. Res.*, 2009, **42**, 270-280.
205. P. Pregosin, *Acta Crystallogr. C*, 2013, **69**, 1433-1436.
206. R. Neufeld and D. Stalke, *Chem. Sci.*, 2015, **6**, 3354-3364.
207. A.-K. Kreyenschmidt, S. Bachmann, T. Niklas and D. Stalke, *ChemistrySelect*, 2017, **2**, 6957-6960.
208. H. Stachowiak, J. Kaźmierczak, K. Kuciński and G. Hreczycho, *Green Chem.*, 2018, **20**, 1738-1742.
209. L. E. Lemmerz, R. McLellan, N. R. Judge, A. R. Kennedy, S. A. Orr, M. Uzelac, E. Hevia, S. D. Robertson, J. Okuda and R. E. Mulvey, *Chem. -Eur. J.*, 2018, **24**, 9940-9948.
210. C. Hilf, F. Bosold, K. Harms, M. Marsch and G. Boche, *Chem. Ber.*, 1997, **130**, 1213-1221.
211. S. E. Baillie, V. L. Blair, T. D. Bradley, W. Clegg, J. Cowan, R. W. Harrington, A. Hernán-Gómez, A. R. Kennedy, Z. Livingstone and E. Hevia, *Chem. Sci.*, 2013, **4**, 1895-1905.
212. K. C. Molloy, P. C. Waterfield and M. F. Mahon, *J. Organomet. Chem.*, 1989, **365**, 61-73.
213. M. Uzelac, A. R. Kennedy, E. Hevia and R. E. Mulvey, *Angew. Chem. Int. Ed.*, 2016, **55**, 13147-13150.
214. R. Arévalo, C. M. Vogels, G. A. MacNeil, L. Riera, J. Pérez and S. A. Westcott, *Dalton Trans.*, 2017, **46**, 7750-7757.
215. A. Kaithal, B. Chatterjee and C. Gunanathan, *J. Org. Chem.*, 2016, **81**, 11153-11161.
216. J. Wu, H. Zeng, J. Cheng, S. Zheng, J. A. Golen, D. R. Manke and G. Zhang, *J. Org. Chem.*, 2018, **83**, 9442-9448.
217. A. E. King, S. C. E. Stieber, N. J. Henson, S. A. Kozimor, B. L. Scott, N. C. Smythe, A. D. Sutton and J. C. Gordon, *Eur. J. Inorg. Chem.*, 2016, **2016**, 1635-1640.
218. D. Mukherjee, A.-K. Wiegand, T. P. Spaniol and J. Okuda, *Dalton Trans.*, 2017, **46**, 6183-6186.
219. D. D. Yan, X. L. Wu, J. Xiao, Z. Y. Zhu, X. J. Xu, X. G. Bao, Y. M. Yao, Q. Shen and M. Q. Xue, *Org. Chem. Front.*, 2019, **6**, 648-653.
220. D. Mukherjee, S. Shirase, T. P. Spaniol, K. Mashima and J. Okuda, *Chem. Commun.*, 2016, **52**, 13155-13158.
221. Q. Yin, Y. Soltani, R. L. Melen and M. Oestreich, *Organometallics*, 2017, **36**, 2381-2384.

222. Y.-C. Lin, E. Hatzakis, S. M. McCarthy, K. D. Reichl, T.-Y. Lai, H. P. Yennawar and A. T. Radosevich, *J. Am. Chem. Soc.*, 2017, **139**, 6008-6016.
223. C.-H. Tien, M. R. Adams, M. J. Ferguson, E. R. Johnson and A. W. H. Speed, *Org. Lett.*, 2017, **19**, 5565-5568.
224. O. Tai, R. Hopson and P. G. Williard, *Org. Lett.*, 2017, **19**, 3966-3969.
225. Y. Ding, X. Liu, X. Ma, Y. Liu, M. Zhong, W. Li, Z. Yang and Y. Yang, *J. Organomet. Chem.*, 2018, **868**, 55-60.
226. M. Fleige, J. Möbus, T. vom Stein, F. Glorius and D. W. Stephan, *Chem. Commun.*, 2016, **52**, 10830-10833.
227. R. F. Nystrom and W. G. Brown, *J. Am. Chem. Soc.*, 1947, **69**, 1197-1199.
228. R. F. Nystrom and W. G. Brown, *J. Am. Chem. Soc.*, 1948, **70**, 3738-3740.
229. J. Park and S. Hong, *Chem. Soc. Rev.*, 2012, **41**, 6931-6943.
230. N. P. Mankad, *Chem. -Eur. J.*, 2016, **22**, 5822-5829.
231. C. Glock, H. Görls and M. Westerhausen, *Chem. Commun.*, 2012, **48**, 7094-7096.
232. A. Hernán-Gómez, T. D. Bradley, A. R. Kennedy, Z. Livingstone, S. D. Robertson and E. Hevia, *Chem. Commun.*, 2013, **49**, 8659-8661.
233. M. De Tullio, A. Hernán-Gómez, Z. Livingstone, W. Clegg, A. R. Kennedy, R. W. Harrington, A. Antiñolo, A. Martínez, F. Carrillo-Hermosilla and E. Hevia, *Chem. -Eur. J.*, 2016, **22**, 17646-17656.
234. Y.-F. Liu, D.-D. Zhai, X.-Y. Zhang and B.-T. Guan, *Angew. Chem. Int. Ed.*, 2018, **57**, 8245-8249.
235. Y. Zhang, J. Wei, W.-X. Zhang and Z. Xi, *Inorg. Chem.*, 2015, **54**, 10695-10700.
236. V. A. Pollard, S. A. Orr, R. McLellan, A. R. Kennedy, E. Hevia and R. E. Mulvey, *Chem. Commun.*, 2018, **54**, 1233-1236.
237. P. H. M. Budzelaar and G. Talarico, in *Group 13 Chemistry III: Industrial Applications*, eds. H. W. Roesky and D. A. Atwood, Springer Berlin Heidelberg, Berlin, Heidelberg, 2003, DOI: 10.1007/3-540-46110-8_4, pp. 141-165.
238. H. Haubstock and E. B. Davidson, *J. Org. Chem.*, 1963, **28**, 2772-2775.
239. C. F. de Graauw, J. A. Peters, H. van Bekkum and J. Huskens, *Synthesis*, 1994, 1007-1017.
240. C. R. Graves, E. J. Campbell and S. T. Nguyen, *Tetrahedron: Asymmetry*, 2005, **16**, 3460-3468.

241. C. R. Graves, B.-S. Zeng and S. T. Nguyen, *J. Am. Chem. Soc.*, 2006, **128**, 12596-12597.
242. R. Cohen, C. R. Graves, S. T. Nguyen, J. M. L. Martin and M. A. Ratner, *J. Am. Chem. Soc.*, 2004, **126**, 14796-14803.
243. U. Schümann, J. Kopf and E. Weiss, *Angew. Chem. Int. Ed.*, 1985, **24**, 215-216.
244. T. Tatic, S. Hermann, M. John, A. Loquet, A. Lange and D. Stalke, *Angew. Chem. Int. Ed.*, 2011, **50**, 6666-6669.
245. K. W. Henderson, A. E. Dorigo, Q.-Y. Liu and P. G. Williard, *J. Am. Chem. Soc.*, 1997, **119**, 11855-11863.
246. S. Park and S. Chang, *Angew. Chem. Int. Ed.*, 2017, **56**, 7720-7738.
247. A. Caise, D. Jones, E. L. Kolychev, J. Hicks, J. M. Goicoechea and S. Aldridge, *Chem. - Eur. J.*, 2018, **24**, 13624-13635.
248. K. Knabel, I. Krossing, H. Nöth, H. Schwenk-Kircher, M. Schmidt-Amelunxen and T. Seifert, *Eur. J. Inorg. Chem.*, 1998, 1095-1114.
249. R. A. Snelling, G. Amberchan, A. Resendez, C. L. Murphy, L. Porter and B. Singaram, *Tetrahedron Lett.*, 2017, **58**, 4073-4077.
250. S. Harder and J. Spielmann, *J. Organomet. Chem.*, 2012, **698**, 7-14.
251. K. Burgess and W. A. van der Donk, *Organometallics*, 1994, **13**, 3616-3620.
252. I. P. Query, P. A. Squier, E. M. Larson, N. A. Isley and T. B. Clark, *J. Org. Chem.*, 2011, **76**, 6452-6456.
253. J. H. Docherty, J. Peng, A. P. Dominey and S. P. Thomas, *Nature Chem.*, 2017, **9**, 595.
254. A. Caise, E. L. Kolychev, J. Hicks, M. A. Fuentes, J. M. Goicoechea and S. Aldridge, *Dalton Trans*, 2019, DOI: 10.1039/c9dt00535h.
255. S. Chakraborty, J. Zhang, Y. J. Patel, J. A. Krause and H. Guan, *Inorg. Chem.*, 2013, **52**, 37-47.
256. W. Clegg, A. J. Scott, C. Dai, G. Lesley, T. B. Marder, N. C. Norman and L. J. Farrugia, *Acta Crystallogr. C*, 1996, **52**, 2545-2547.
257. S. W. Hadebe and R. S. Robinson, *Eur. J. Org. Chem.*, 2006, 4898-4904.
258. B. Ghaffari, B. A. Vanchura, G. A. Chotana, R. J. Staples, D. Holmes, R. E. Maleczka and M. R. Smith, *Organometallics*, 2015, **34**, 4732-4740.
259. T. J. Hadlington, T. Szilvási and M. Driess, *Angew. Chem. Int. Ed.*, 2017, **56**, 7470-7474.
260. J. Chu, C. Wang, L. Xiang, X. Leng and Y. Chen, *Organometallics*, 2017, **36**, 4620-4625.

261. M. A. Esteruelas, F. J. Fernández-Alvarez, A. M. López, M. Mora and E. Oñate, *J. Am. Chem. Soc.*, 2010, **132**, 5600-5601.
262. W. Wang, Y. Lv, X. Gou, X. Leng and Y. Chen, *Chin. J. Chem.*, 2014, **32**, 752-756.
263. A. S. Dudnik, V. L. Weidner, A. Motta, M. Delferro and T. J. Marks, *Nature Chem.*, 2014, **6**, 1100.
264. S. A. Westcott, H. P. Blom, T. B. Marder, R. T. Baker and J. C. Calabrese, *Inorg. Chem.*, 1993, **32**, 2175-2182.
265. R. K. Das, E. Barnea, T. Andrea, M. Kapon, N. Fridman, M. Botoshansky and M. S. Eisen, *Organometallics*, 2015, **34**, 742-752.
266. J. Klosin, G. R. Roof, E. Y. X. Chen and K. A. Abboud, *Organometallics*, 2000, **19**, 4684-4686.
267. J. Chen and E. Y. X. Chen, *Dalton Trans.*, 2016, **45**, 6105-6110.
268. V. A. Pollard, M. A. Fuentes, A. R. Kennedy, R. McLellan and R. E. Mulvey, *Angew. Chem. Int. Ed.*, 2018, **57**, 10651-10655.
269. Y. R. Luo, in *Comprehensive Handbook of Chemical Bond Energies*, CRC Press, FL, 2007, ch. 23, pp. 1070 - 1115.
270. W. H. Lam, S. Shimada, A. S. Batsanov, Z. Lin, T. B. Marder, J. A. Cowan, J. A. K. Howard, S. A. Mason and G. J. McIntyre, *Organometallics*, 2003, **22**, 4557-4568.
271. J. Zhu, Z. Lin and T. B. Marder, *Inorg. Chem.*, 2005, **44**, 9384-9390.
272. L. Dang, H. Zhao, Z. Lin and T. B. Marder, *Organometallics*, 2008, **27**, 1178-1186.
273. H. Nöth and H. Vahrenkamp, *Chem. Ber.*, 1967, **100**, 3353-3362.
274. K. B. Dillon, F. Mathey and J. F. Nixon, *Phosphorus: The carbon copy*, John Wiley and Sons, Chichester, 1998.
275. Y. Moglie, M. J. González-Soria, I. Martín-García, G. Radivoy and F. Alonso, *Green Chem.*, 2016, **18**, 4896-4907.
276. D. S. Glueck, in *C-X Bond Formation*, ed. A. Vigalok, Springer Berlin Heidelberg, Berlin, Heidelberg, 2010, DOI: 10.1007/978-3-642-12073-2_4, pp. 65-100.
277. V. Koshti, S. Gaikwad and S. H. Chikkali, *Coord. Chem. Rev.*, 2014, **265**, 52-73.
278. C. A. Bange and R. Waterman, *Chem. -Eur. J.*, 2016, **22**, 12598-12605.
279. D. Chattopadhyay, *Resonance*, 2017, **22**, 79-87.
280. Y. Zhang, L. Qu, Y. Wang, D. Yuan, Y. Yao and Q. Shen, *Inorg. Chem.*, 2018, **57**, 139-149.

281. H. Ohmiya, H. Yorimitsu and K. Oshima, *Angew. Chem. Int. Ed.*, 2005, **44**, 2368-2370.
282. R. Webster, *Inorganics*, 2018, **6**, 120.
283. P. G. Pringle and M. B. Smith, *J. Chem. Soc., Chem. Commun.*, 1990, 1701-1702.
284. M. R. Douglass and T. J. Marks, *J. Am. Chem. Soc.*, 2000, **122**, 1824-1825.
285. B. Liu, T. Roisnel, J.-F. Carpentier and Y. Sarazin, *Chem. -Eur. J.*, 2013, **19**, 13445-13462.
286. H. Hu and C. Cui, *Organometallics*, 2012, **31**, 1208-1211.
287. A. K. King, K. J. Gallagher, M. F. Mahon and R. L. Webster, *Chem. -Eur. J.*, 2017, **23**, 9039-9043.
288. M. Itazaki, S. Katsube, M. Kamitani and H. Nakazawa, *Chem. Commun.*, 2016, **52**, 3163-3166.
289. K. J. Gallagher, M. Espinal-Viguri, M. F. Mahon and R. L. Webster, *Adv. Synth. Catal.*, 2016, **358**, 2460-2468.
290. H. R. Sharpe, A. M. Geer, W. Lewis, A. J. Blake and D. L. Kays, *Angew. Chem. Int. Ed.*, 2017, **56**, 4845-4848.
291. W.-X. Zhang, M. Nishiura and Z. Hou, *Chem. Commun.*, 2006, 3812-3814.
292. N. T. Coles, M. F. Mahon and R. L. Webster, *Chem. Commun.*, 2018, **54**, 10443-10446.
293. J. Pahl, T. E. Stennett, M. Volland, D. M. Guldi and S. Harder, *Chem. -Eur. J.*, 2019, **25**, 2025-2034.
294. M. R. Crimmin, A. G. M. Barrett, M. S. Hill, P. B. Hitchcock and P. A. Procopiou, *Organometallics*, 2007, **26**, 2953-2956.
295. T. M. A. Al-Shboul, H. Görls and M. Westerhausen, *Inorg. Chem. Commun.*, 2008, **11**, 1419-1421.
296. T. M. A. Al-Shboul, V. K. Pálfi, L. Yu, R. Kretschmer, K. Wimmer, R. Fischer, H. Görls, M. Reiher and M. Westerhausen, *J. Organomet. Chem.*, 2011, **696**, 216-227.
297. M. R. Crimmin, A. G. M. Barrett, M. S. Hill, P. B. Hitchcock and P. A. Procopiou, *Organometallics*, 2008, **27**, 497-499.
298. K. A. Erickson, L. S. H. Dixon, D. S. Wright and R. Waterman, *Inorganica Chim. Acta*, 2014, **422**, 141-145.
299. J. P. W. Stelmach, C. A. Bange and R. Waterman, *Dalton Trans.*, 2016, **45**, 6204-6209.
300. L. Liu, C. Chan, J. Zhu, C.-H. Cheng and Y. Zhao, *J. Org. Chem.*, 2015, **80**, 8790-8795.

301. L. Keweloh, H. Klöcker, E.-U. Würthwein and W. Uhl, *Angew. Chem. Int. Ed.*, 2016, **55**, 3212-3215.
302. L. Keweloh, N. Aders, A. Hepp, D. Pleschka, E.-U. Würthwein and W. Uhl, *Dalton Trans.*, 2018, **47**, 8402-8417.
303. G.-Q. Chen, G. Kehr, C. G. Daniliuc, B. Wibbeling and G. Erker, *Chem. -Eur. J.*, 2015, **21**, 12449-12455.
304. P. Moquist, G.-Q. Chen, C. Mück-Lichtenfeld, K. Bussmann, C. G. Daniliuc, G. Kehr and G. Erker, *Chem. Sci.*, 2015, **6**, 816-825.
305. P. Merino, E. Marqués-López and R. P. Herrera, *Adv. Synth. Catal.*, 2008, **350**, 1195-1208.
306. S. G. Thangavelu, K. E. Hocker, S. R. Cooke and C. N. Muhoro, *J. Organomet. Chem.*, 2008, **693**, 562-566.
307. B. R. Nichols, N. G. Akhmedov, J. L. Petersen and B. V. Popp, *Dalton Trans.*, 2018, **47**, 8456-8465.
308. S. A. Sangokoya, W. T. Pennington, G. H. Robinson and D. C. Hrncir, *J. Organomet. Chem.*, 1990, **385**, 23-31.
309. A. D. Becke, *Phys. Rev. A*, 1988, **38**, 3098-3100.
310. A. D. Becke, *J. Chem. Phys.*, 1993, **98**, 5648-5652.
311. C. Lee, W. Yang and R. G. Parr, *Phys. Rev. B*, 1988, **37**, 785-789.
312. S. H. Vosko, L. Wilk and M. Nusair, *Can. J. Phys.*, 1980, **58**, 1200-1211.
313. P. J. Stephens, F. J. Devlin, C. F. Chabalowski and M. J. Frisch, *J. Phys. Chem.*, 1994, **98**, 11623-11627.
314. R. H. Hertwig and W. Koch, *Chem. Phys. Lett.*, 1997, **268**, 345-351.
315. S. Grimme, J. Antony, S. Ehrlich and H. Krieg, *J. Chem. Phys.*, 2010, **132**, 154104.
316. A. D. McLean and G. S. Chandler, *J. Chem. Phys.*, 1980, **72**, 5639-5648.
317. R. Krishnan, J. S. Binkley, R. Seeger and J. A. Pople, *J. Chem. Phys.*, 1980, **72**, 650-654.
318. M. J. Frisch, J. A. Pople and J. S. Binkley, *J. Chem. Phys.*, 1984, **80**, 3265-3269.
319. J. Tomasi, B. Mennucci and R. Cammi, *Chem. Rev.*, 2005, **105**, 2999-3094.
320. P. P. Power and X. Xiaojie, *J. Chem. Soc., Chem. Commun.*, 1984, 358-359.
321. R. A. Bartlett, H. V. Rasika Dias, H. Hope, B. D. Murray, M. M. Olmstead and P. P. Power, *J. Am. Chem. Soc.*, 1986, **108**, 6921-6926.

322. C. Vidal, J. García-Álvarez, A. Hernán-Gómez, A. R. Kennedy and E. Hevia, *Angew. Chem. Int. Ed.*, 2014, **53**, 5969-5973.
323. M. Gómez-Gallego and M. A. Sierra, *Chem. Rev.*, 2011, **111**, 4857-4963.
324. E. M. Simmons and J. F. Hartwig, *Angew. Chem. Int. Ed.*, 2012, **51**, 3066-3072.
325. J. Burés, *Angew. Chem. Int. Ed.*, 2016, **55**, 2028-2031.
326. J. Burés, *Angew. Chem. Int. Ed.*, 2016, **55**, 16084-16087.
327. C. D. T. Nielsen and J. Burés, *Chem. Sci.*, 2019, **10**, 348-353.
328. M. Kamitani, M. Itazaki, C. Tamiya and H. Nakazawa, *J. Am. Chem. Soc.*, 2012, **134**, 11932-11935.
329. I. Kovacic, C. Scriban and D. S. Glueck, *Organometallics*, 2006, **25**, 536-539.
330. B. G. Cox, *Modern Liquid Phase Kinetics*, Oxford University Press, 1996.
331. C. Stuhl, M. M. Katzenmayer, C. Maichle-Mössmer and R. Anwänder, *Dalton Trans.*, 2018, **47**, 15173-15180.
332. J. A. Gladysz, Z. T. Ball, G. Bertrand, S. A. Blum, V. M. Dong, R. Dorta, F. E. Hahn, M. G. Humphrey, W. D. Jones, J. Klosin, I. Manners, T. J. Marks, J. M. Mayer, B. Rieger, J. C. Ritter, A. P. Sattelberger, J. M. Schomaker and V. W.-W. Yam, *Organometallics*, 2012, **31**, 1-18.
333. D. F. Shriver and M. A. Drezdon, *The Manipulation of Air-Sensitive Compounds*, J. Wiley and Sons, New York, 1986.
334. J. Leonard, B. Lygo and G. Procter, *Advanced Practical Organic Chemistry*, CRC Press: Boca Raton, 3rd edn., 2013.
335. G. M. Sheldrick, *Acta Crystallogr.*, 2008, **A64**, 112 - 122.
336. G. M. Sheldrick, *Acta Crystallogr.*, 2015, **C71**, 3 -8
337. A. P. Dove, V. C. Gibson, E. L. Hormnirun, E. L. Marshall, J. A. Segal, A. J. P. White and D. J. Williams, *Dalton Trans.*, 2003, 3088 - 3097.
338. O. V. Dolomanov, L. J. Bourhis, R. J. Gildea, J. A. K. Howard and H. Puschmann, *J. Appl. Crystallogr.*, 2009, **42**, 339 - 341.
339. G. J. P. Britovsek, J. England and A. J. P. White, *Inorg. Chem.*, 2005, **44**, 8125.
340. S. Christoph and A. Reiner, *Eur. J. Inorg. Chem.*, 2013, 3302-3306.
341. S. Mandal, P. K. Verma and K. Geetharani, *Chem. Commun.*, 2018, **54**, 13690-13693.
342. S. R. Tamang, A. Singh, D. K. Unruh and M. Findlater, *ACS Catal.*, 2018, **8**, 6186-6191.
343. A. Schmidt, A. R. Nödling and G. Hilt, *Angew. Chem. Int. Ed.*, 2015, **54**, 801-804.

